

MICROWAVE APPLICATOR OPTIMIZATION THROUGH METAHEURISTIC
ALGORITHMS FOR THE MINING INDUSTRY

Iván Mauricio Amaya Contreras
Ingeniero Mecatrónico

Universidad Industrial de Santander
Facultad de Ingenierías Fisicomecánicas
Escuela de Ingenierías Eléctrica, Electrónica, y de Telecomunicaciones
Bucaramanga, Santander, Colombia
2015

MICROWAVE APPLICATOR OPTIMIZATION THROUGH METAHEURISTIC
ALGORITHMS FOR THE MINING INDUSTRY

Iván Mauricio Amaya Contreras
Ingeniero Mecatrónico

Informe final del trabajo de investigación para optar al título de
Doctor en Ingeniería, área Ingeniería Electrónica

Director
Carlos Rodrigo Correa Cely, Ph.D.
Profesor Titular, Ingeniero Químico

Universidad Industrial de Santander
Facultad de Ingenierías Fisicomecánicas
Escuela de Ingenierías Eléctrica, Electrónica, y de Telecomunicaciones
Bucaramanga, Santander, Colombia

2015

Dedicado a las personas que me acompañaron a lo largo de este proceso, pues más que recordar las buenas experiencias, considero que lo importante en la vida es aprender algo de todas las situaciones (buenas, y malas).

Existen muchas personas que merecen una mención en este espacio. Así, es probable que algunas se me queden en el tintero, por lo que les ofrezco sinceras disculpas...

Es impensable que un proceso como el que culmina hoy pudiera llevarse a cabo sin la guía ni el incansable acompañamiento de un excelente director. Mis más profundos agradecimientos al profesor Rodrigo Correa, quien siempre me motivó a ir más allá y a no dejarme limitar por mínimos establecidos en un reglamento. Nuestras discusiones me permitieron profundizar en el mundo de la producción intelectual y de la academia, ayudándome a crecer como investigador y como persona.

También quiero expresar mi reconocimiento a dos colegas de la investigación, Yuri y Jorge, a quienes considero grandes amigos y con quienes siempre viene bien un café y una discusión de resultados (o, por lo menos, de los problemas que evitan que los alcancemos). Asimismo, a todos mis colegas del grupo CEMOS, por los incontables espressos con los que discutíamos nuestras investigaciones.

Una mención especial también a mi familia, por la motivación y el apoyo incondicional brindado durante estos años.

Asimismo quiero agradecer a mis amigos y amigas (tanto en Colombia como en España), por brindarme espacios de esparcimiento cada vez que los problemas me abrumaban. A esas personas especiales que estuvieron a mi lado estos años y que por uno u otro motivo ya no lo están. Aunque solamente una de ellas quede, cada relación debe enseñar algo valioso para las futuras, por lo que son dignas de recordar. Ello fortalece la actual y logra que se valore más.

Finalmente quiero aprovechar este espacio para reconocer el esfuerzo y la dedicación de los estudiantes con quienes trabajamos en los diferentes temas de investigación.

CONTENTS

	page
INTRODUCTION	25
1. FUNDAMENTALS	33
1.1 AN OVERVIEW OF THE RESEARCH PROBLEM	33
1.2 TYPES OF ORES	35
1.3 OBJECTIVES	36
1.3.1 General objective	36
1.3.2 Specific objectives	36
1.4 ORGANIZATION OF THE CURRENT DISSERTATION	37
REFERENCES	39
2. DESCRIBING THE PROBLEM	42
2.1 THE RECTANGULAR RESONATOR	42
2.2 FITNESS EVALUATION	47
2.3 THE OBJECTIVE FUNCTION	49
2.4 FINAL COMMENTS	50

REFERENCES	52
3. KNOWING THE SAMPLES	53
3.1 SAMPLES CONSIDERED DURING THE RESEARCH	54
3.2 METHODOLOGY	54
3.2.1 Experimental testing	54
3.2.2 Dielectric properties	56
3.3 RESULTS	59
3.3.1 Experimental testing	59
3.3.2 Dielectric properties	62
3.3.3 Further results	69
3.4 DISCUSSION	73
3.5 FINAL COMMENTS	78
REFERENCES	80
4. KNOWING THE ALGORITHMS	84
4.1 HOW DO ALGORITHMS WORK?	85
4.1.1 Original approaches	85
4.1.2 Modifications proposed by our group	89
4.2 WHAT WERE ALGORITHMS USED FOR IN THIS DISSERTATION?	95

4.3	METHODOLOGY	96
4.4	RESULTS	99
4.4.1	Standard test functions	99
4.4.2	Further testing with SFHS	100
4.4.3	Optimization of electromagnetic absorbers	104
4.4.4	Solution of system of equations and other scenarios	107
4.5	DISCUSSION	109
4.6	FINAL COMMENTS	111
	REFERENCES	113
5.	SOLVING THE PROBLEM	122
5.1	AN OVERVIEW OF THE OPTIMIZATION STRATEGY	122
5.2	METHODOLOGY	123
5.3	RESULTS	126
5.3.1	Resonator uniformly filled with a material	126
5.3.2	Resonator filled with multiple lossless materials	128
5.3.3	Resonator filled with lossy materials	137
5.4	FINAL COMMENTS	140
	REFERENCES	141
	BIBLIOGRAPHY	142

LIST OF FIGURES

	page
Figure 1-1. Classification of gold ores and typical recovery with traditional methods	35
Figure 1-2. Most common causes for refractoriness and double refractory ore appearance	36
Figure 2-1. Rectangular resonator split into N blocks	43
Figure 2-2. Frequency response of circuital analysis considering the 1-norm	46
Figure 2-3. PSNR of the solutions provided by commercial software against the analytical solutions, for four different TE01p modes and considering four different values of relative permittivity	48
Figure 2-4. Field distribution yielded by commercial software (left, PSNR=21 dB), by the analytic solution (center), and by the model developed throughout this chapter (right, PSNR=50 dB).	49
Figure 2-5. Overview of the process required for evaluating the objective function for a given set of network heights (ci). fres is a vector containing all resonant frequencies found for the resonator, Etest contains the information of the electric field distribution at each resonant frequency, and fresbest is the resonant frequency that yields the electric field with the highest PSNR	50
Figure 3-1. General procedure for obtaining dielectric properties as a function of temperature. ϵ' and ϵ'' are the real and imaginary part of the complex permittivity (respectively); CC means cylindrical cavity; f means frequency; Q is the quality factor of the resonator; DK stands for dielectric kit.	57
Figure 3-2. R^2 as a function of the order used for the fitting model	58
Figure 3-3. SSE as a function of the order used for the fitting model	58
Figure 3-4. RMSE as a function of the order used for the fitting model	59
Figure 3-5. Pareto chart (a) and normal probability plot (b) for mine “Juan Blanco”	60
Figure 3-6. Pareto chart (a) and residuals plot (b) for mine “Reina de Oro”	60

Figure 3-7. Pareto chart (a) and normal probability plot (b) for mine “Tajo Abierto”	61
Figure 3-8. Effect of sieve size on the complex permittivity for mineral “Juan Blanco” at room temperature	63
Figure 3-9. Real (left) and imaginary (right) components of the complex permittivity for "Juan Blanco" sieve: 100, as a function of temperature and time	64
Figure 3-10. Dielectric properties as a function of temperature for "Juan Blanco", sieve: 100	64
Figure 3-11. Dielectric properties as a function of temperature for "Juan Blanco", sieve: 200	65
Figure 3-12. Dielectric properties as a function of temperature for "Juan Blanco", sieve: -200	65
Figure 3-13. Dielectric properties as a function of temperature for "M9", sieve: 100	66
Figure 3-14. Dielectric properties as a function of temperature for "Carlos Arias", sieve: 100	66
Figure 3-15. Dielectric properties as a function of temperature for "Ismael", sieve: -170	68
Figure 3-16. Dielectric properties as a function of temperature for "Core from El Volcán", sieve: -120	68
Figure 3-17. Dielectric properties as a function of temperature for "Rock from Segovia, Antioquia", sieve: -120	69
Figure 3-18. Effect of cavity reduction on maximum temperature for a water load. Based on [20]	70
Figure 3-19. Experimental setup for temperature measurement. Based on [22]	70
Figure 3-20. Temperature [°C] evolution for different sample holders, with no silicon carbide. Based on [22]	71
Figure 3-21. Temperature ratio evolution for two sample holders, considering silicon carbide. Based on [22]	71

Figure 3-22. Block diagram of the multi-point temperature measurement system. Based on [19]	72
Figure 3-23. Temperature readings of a hot plate after calibration. Based on [19]	73
Figure 3-24. Temperature readings of 60 g of mineral sample, heated at 1000 W for 40 min. Based on [19]	73
Figure 4-1. Adjustment of the search domain. For clarity, only one dimension is labeled	90
Figure 4-2. Mapping stage for avoiding convergence to local optima, allowing for a bigger initial search domain	91
Figure 4-3. Initial distribution of probes, following a normal distribution centered on the best coordinates found by the mapping stage	91
Figure 4-4. General overview of the modifications proposed with ABHS, where DC is the decay counter, j is the current iteration, SatCt is the saturation counter, and SatLim is the saturation limit	92
Figure 4-5. Fretwidth behavior for the ABHSv1 (up) and ABHSv2 (down) modifications, considering that a better answer is found at iterations 24 and 45	93
Figure 4-6. General overview of the modifications proposed with SFHS, , where DC is the decay counter, j is the current iteration, SatCt is the saturation counter, and FWsat is the saturation limit	93
Figure 4-7. Fretwidth behavior for SFHS, considering that a better answer is found at iterations 5, 24, and 27	94
Figure 4-8. General scheme of an optimization problem, where it is required to minimize the total thickness and the reflection coefficient	96
Figure 4-9. Graphical representation of the approach for solving a system of equations through an optimization algorithm	96
Figure 4-10. General scheme of the methodology used with each undergraduate study	97
Figure 4-11. Normalized increment of iterations and run time for Sum of powers function, as a function of the range per dimension	101

Figure 4-12. Normalized increment of iterations and run time for Axis parallel hyper-ellipsoid function, as a function of the range per dimension	101
Figure 4-13. Normalized increment of iterations and run time for Dropwave function, as a function of the range per dimension	102
Figure 4-14. Normalized increment of iterations and run time for Ackley function, as a function of the range per dimension	102
Figure 4-15. Normalized increment of iterations and run time for Rosenbrock function, as a function of the range per dimension	103
Figure 4-16. Normalized increment of iterations and run time for Six hump camel back function, as a function of the range per dimension	103
Figure 4-17. Time and iterations increase (normalized to 2D) as a function of the problem dimensions, for function Sum of Powers	104
Figure 4-18. Time and iterations increase (normalized to 2D) as a function of the problem dimensions, for function Axis Parallel Hyper-ellipsoid	104
Figure 4-19. Increase Ratio (Normalized Time / Normalized Iterations) up to 50 dimensions for five functions: Jong, Axis Parallel Hyper-ellipsoid (APH), Rotated Hyper-ellipsoid (RH), Sum of Powers (SP), and Steps	104
Figure 4-20. Frequency response of the best results found by [2] and of those reported by [96]	106
Figure 4-21. Simple circuit with one non-linear element	107
Figure 4-22. General scheme of the scalable circuit used for testing	108
Figure 4-23. Average function evaluation as iterations progress (15 runs), for Test Function 1 (left) and Jong (right), both in 2D	110
Figure 4-24. Function evaluation ratio as iterations progress, between HS and SFHS, for Jong's function in 2D, 6D, and 10D	110
Figure 5-1. Overview of the procedure for merging objective function and optimization algorithm	123
Figure 5-2. Methodology followed throughout this chapter	124

Figure 5-3. Quality of the answers found with all combinations of UPSO and SFHS (average data for 30 runs), compared against the quality of solutions yielded by commercial software	127
Figure 5-4. Comparison of all algorithms for different widths of search domain, and two scenarios with different relative permittivity (ϵ_r). Average data for 30 runs	128
Figure 5-5. Electric field distribution (normalized) for a resonator of volume $0.1 \times 0.2 \times 1.0$ [m3], 25% filled with $\epsilon_r = 10$. Resonant frequency: (a) 0.72 [GHz] (b) 0.89 [GHz]	129
Figure 5-6. Electric field distribution (normalized) for a resonator of volume $0.1 \times 0.2 \times 1.0$ [m3], 50% filled with $\epsilon_r = 10$	129
Figure 5-7. Electric field distribution (normalized) for a resonator of volume $0.1 \times 0.2 \times 1.0$ [m3], 25% filled with $\epsilon_r = 100$	130
Figure 5-8. Electric field distribution (normalized) for a resonator of volume $0.1 \times 0.2 \times 1.0$ [m3], 50% filled with $\epsilon_r = 50$	130
Figure 5-9. PSNR (average \pm standard deviation) found by all algorithms for different scenarios and 30 runs. A minimum PSNR of 20 dB was demanded in all cases	131
Figure 5-10. Electric field distribution (normalized) for a resonator of volume $0.1 \times 0.2 \times 1.0$ [m3], 33% filled with $\epsilon_r = 10$. Resonant frequency: 0.63 [GHz]	132
Figure 5-11. Electric field distribution (normalized) for a resonator of volume $0.1 \times 0.2 \times 1.0$ [m3], 33% filled with $\epsilon_r = 10$. Resonant frequency: (a) 0.75 [GHz] (b) 1.02 [GHz]	132
Figure 5-12. First 250 function evaluations for the third scenario, using all combinations of the algorithms. Average data for 10 runs	134
Figure 5-13. Electric field distribution (normalized) for a resonator of volume $0.1 \times 0.2 \times 1.0$ [m3], split into three blocks of the same length. Dielectric properties and resonant frequency: (a) $\epsilon_r = [10 \ 1 \ 10]$, $f = 0.75$ [GHz] (b) $\epsilon_r = [1 \ 10 \ 20]$, $f = 1.02$ [GHz]	134
Figure 5-14. Electric field distribution (normalized) for a resonator of volume $0.1 \times 0.2 \times 1.0$ [m3], split into five blocks of the same length. Dielectric properties: $\epsilon_r = [1 \ 10 \ 20 \ 10 \ 1]$. Resonant frequency: (a) $f = 0.24$ [GHz] (b) $f = 0.86$ [GHz]	135

Figure 5-15. Electric field distribution (normalized) for a resonator of volume $0.1 \times 0.2 \times 1.0$ [m³], split into five blocks of the same length. Dielectric properties: $\epsilon_r = [10 \ 1 \ 20 \ 10 \ 1]$. Resonant frequency: (a) $f = 0.26$ [GHz] (b) $f = 0.90$ [GHz] 136

Figure 5-16. Electric field distribution (normalized) for a resonator of volume $0.1 \times 0.2 \times 1.0$ [m³], split into five blocks of the same length. Dielectric properties and resonant frequency: (a) $\epsilon_r = [10 \ 20 \ 1 \ 10 \ 20]$, $f = 0.26$ [GHz] (b) $\epsilon_r = [10 \ 20 \ 1 \ 10 \ 1]$, $f = 0.26$ [GHz] 137

Figure 5-17. Electric field distribution (normalized) for a resonator of volume $0.1 \times 0.2 \times 1.0$ [m³], 33% filled with $\epsilon_r = 10$ and $\sigma = 0.1$. Complex frequency: $0.75+j0.08$ [GHz] 138

Figure 5-18. Electric field distribution for a resonator of volume $0.1 \times 0.2 \times 0.5$ [m³], 33% filled with a mineral sample of Juan Blanco (Sieve 100) at different temperatures. Values are normalized to the maximum field intensity of all five cases 139

LIST OF TABLES

	page
Table 2-1. Resonant frequencies for the first ten TE01p modes, found through the analytic solution and through three different types of matrix norms.....	46
Table 3-1. Summary of samples used during the research, including their starting (St.) and ending (En.) dielectric properties at room temperature	54
Table 3-2. Summary of mineral samples used in experiments with undergraduate students	54
Table 3-3. Factors and levels used with Bernal et al. Exposure time was split into seven minutes intervals, with one additional minute for manual mixing	55
Table 3-4. Factors and levels used with Diaz et al. Exposure time was split into six minutes intervals, with three additional minute for manual mixing	55
Table 3-5. Factors and levels used with Aguirre et al. Exposure time was split into five minutes intervals, with one additional minute for manual mixing	56
Table 3-6. Regression models, order N , used during the research.	57
Table 3-7. Resulting data for the traditional approach and the three experiments carried out. TR stands for time reduction, ER stands for energy reduction, and MR is the maximum gold recovery achieved. The high percentage of the second experiment means that the sample was better roasted by microwaves than through the traditional approach	61
Table 3-8. Mineral composition before and after roasting for “Juan Blanco”, sieve: 170 ..	61
Table 3-9. Five most abundant elements for each sample, where JB: Juan Blanco; IS: Ismael; CA: Carlos Arias; CV: Core from El Volcán; RS: Rock from Segovia, Antioquia. The sieve size is given by the letter S and the number next to it	62
Table 3-10. Mineral composition before and after roasting for “Juan Blanco”, sieve: 100. N.Q.: Not Quantifiable.....	66
Table 3-11. Mineral composition before and after roasting for “M9”, 100. N.Q.: Not Quantifiable.....	67

Table 3-12. Mineral composition before and after roasting for “Carlos Arias”, sieve: 100	67
Table 3-13. Grade [g/ton] and recovery margin (RM) of microwave (MS) and traditionally (TS) smelted samples, using ores with different roasting conditions. Based on [22]	72
Table 3-14. Summary of best fits for the mineral samples. The general expression of each model is shown in Table 3-6 and the starting and ending values of permittivity is given in Table 3-1.	75
Table 4-1. List of standard test functions used during the research	97
Table 4-2. Average number of iterations (Iter.) and fitness, for different algorithms and standard test functions. Global optimum is 837.9658 for Schwefel 26 and 0 for the others	99
Table 4-3. Average results of ABHSv2 for three standard test functions, and their respective reduction of iterations [%] when compared to the best results yielded by HS	99
Table 4-4. Average results of SFHS for nine standard test functions in 2D, and their respective reduction of iterations [%] when compared to the best results yielded by ABHSv2	100
Table 4-5. Materials database. Based on [95]	104
Table 4-6. Results of the one-stage (1-St) and two-stage (2-St) processes when using CFO with AC for three different initial distributions, for the frequency range 0.8-1.9 GHz. Based on [91]	105
Table 4-7. Summary of designs found with CFO+AC, SO, and GSA, for the frequency range 2-8 GHz, and previously reported data	106
Table 4-8. Solutions obtained with PSO and UPSO for a circuit with one non-linear element, considering a swarm size of 10 particles. Theoretical solution: V1 = 9.9080 V and V2 = 0.7125 V	107
Table 4-9. Solutions of each node [V] for the scalable circuit with different number of additional loops. For 10 additional loops, read the first column as FirstNode; SecondNode	108
Table 4-10. Solutions [V] found by UPSO for different number of additional loops in the scalable circuit. For 10 additional loops, read the first column as FirstNode; SecondNode	108

Table 4-11. Ranking of the preselected algorithms, including SFHS, where one is the worst score and five is the best one..... 111

Table 5-1. Scenarios for the second battery of tests..... 125

Table 5-2. Scenarios for the third battery of tests 125

Table 5-3. Scenarios for resonators split into five blocks..... 125

Table 5-4. Scenarios considered for simulations including minerals 126

Table 5-5. Statistical data for all combinations of algorithms and the three scenarios of the first design. Average data for 10 runs. Tests for the third scenario were not run with SFHS/UPSO and SFHS/SFHS since the other alternatives outperformed them in the previous stages 133

Table 5-6. Designs found by UPSO/SFHS for each one of the scenarios considered during this testing phase, including the length of each block (**Li**), the resonant frequency, and the PSNR. In all cases, a theoretical value of 0.33 [m] was assumed for each block..... 135

Table 5-7. Designs found by UPSO/SFHS for each one of the scenarios considered during this testing phase, including the length of each block (**Li**), the resonant frequency, and the PSNR. In all cases, a theoretical value of 0.20 [m] was assumed for each block..... 137

Table 5-8. Designs found by UPSO/SFHS for three mineral samples at different temperatures, including the length of each block (**Li**), the real (**f'**) and imaginary (**f''**) parts of the complex frequency, and the PSNR. In all cases, a theoretical value of 0.166 [m] was assumed for each block 139

LIST OF APPENDICES

	page
A. ELECTROMAGNETIC MODELLING OF THE RESONATOR	162
A.1. COMPLETELY FILLED RECTANGULAR RESONATOR	162
A.2. FIELD VISUALIZATION	164
A.3. PARTIALLY FILLED RECTANGULAR RESONATOR	167
A.4. CIRCUITAL ANALYSIS	169
A.5. ANALYSIS INVOLVING LOSSY MATERIALS	177
B. ANALYTIC RESULTS OF THE SAMPLES	180
C. RESULTS OF THE DESIGN OF EXPERIMENTS	184
C.1. MINE “JUAN BLANCO” (ASSIGNED TO: BERNAL, D; GARNICA, S; RESLEN, Y)	184
C.2. MINE “REINA DE ORO” (ASSIGNED TO: DIAZ, M; RUEDA, M)	185
C.3. MINE “TAJO ABIERTO” (ASSIGNED TO: AGUIRRE, R; BOTERO, W)	186
D. ALGORITHMS BOARDED THROUGHOUT THE DISSERTATION	187
D.1. ARTIFICIAL BEE COLONY (ABC)	187

D.2. BAT-INSPIRED ALGORITHM (BA)	188
D.3. CENTRAL FORCE OPTIMIZATION (CFO)	189
D.4. FIREFLY ALGORITHM (FA)	190
D.5. GRAVITATIONAL SEARCH ALGORITHM (GSA)	190
D.6. HARMONY SEARCH (HS)	191
D.7. INTELLIGENT WATER DROPS (IWD)	192
D.8. PARTICLE SWARM OPTIMIZATION (PSO)	193
D.9. QUANTUM-INSPIRED EVOLUTIONARY ALGORITHM (QEA)	194
D.10. SIMULATED ANNEALING (SA)	194
D.11. SPIRAL OPTIMIZATION (SO)	195
D.12. UNIFIED PARTICLE SWARM OPTIMIZATION (UPSO)	196
E. ANALYSIS OF HYBRID MODES IN A PARTIALLY-FILLED WAVEGUIDE	197

RESUMEN

TÍTULO: OPTIMIZACIÓN DE APLICADORES MICROONDAS, A TRAVÉS DE ALGORITMOS METAHEURÍSTICOS, PARA LA INDUSTRIA MINERA¹.

AUTOR: IVÁN MAURICIO AMAYA CONTRERAS²

PALABRAS CLAVE: MICROONDAS, ANÁLISIS CIRCUITAL, OPTIMIZACIÓN MODERNA, MINERALES, PROPIEDADES DIELECTRICAS.

DESCRIPCIÓN:

Esta tesis se enfoca al desarrollo de una estrategia de optimización que permita encontrar las dimensiones y frecuencia de resonancia de un aplicador microondas, tal que su distribución de campo corresponda a una definida por el usuario. Se reservan tres capítulos a discutir los pilares principales para establecer dicha estrategia: el modelo matemático de resonadores microondas analizados a través de análisis circuital, las propiedades dieléctricas experimentales de diferentes muestras minerales que cambian con la temperatura, y la formulación de diferentes técnicas de optimización moderna. Luego, se realizó la sinergia de esta información (es decir, el modelo, las propiedades, y los algoritmos de optimización). Se inicia por ejecutar algunas pruebas simples con los algoritmos, para determinar la mejor combinación de ellos. Posteriormente, se abordan algunos escenarios de diseño que incluyen materiales con y sin pérdidas. Se encontraron varias cosas de interés. Pero, la más relevante se refiere a la factibilidad de utilizar la estrategia propuesta. En algunos escenarios (especialmente a altas frecuencias) fue posible lograr un nivel de ajuste mayor a 50 [dB]. Sin embargo, en otros escenarios este valor cayó hasta 20 [dB] (especialmente, cerca del modo fundamental del aplicador). Esto significa que el modelo matemático debe ser refinado. Aun así, luego de comparar los datos respecto a software comercial (CST), se encontró que incluso en los casos donde CST sobrepasó a la estrategia propuesta en esta tesis, la segunda generó una distribución de campo más uniforme. Por tanto, se considera como exitosa la propuesta, así que se recomienda su uso y se sugiere que se trabaje en expandir el modelo a las direcciones restantes y a otros sistemas de coordenadas. Además, se sugiere incluir una métrica que considere el factor de forma de las distribuciones de campo, quizás a través de una suma ponderada.

¹ Trabajo de grado de doctorado.

² Facultad de ingenierías fisiscomecánicas. Escuela de ingenierías eléctrica, electrónica, y de telecomunicaciones (E3T). Director: Carlos Rodrigo Correa Cely, Ph.D. Ingeniero Químico.

ABSTRACT

TITLE: MICROWAVE APPLICATOR OPTIMIZATION THROUGH METAHEURISTIC ALGORITHMS FOR THE MINING INDUSTRY³.

AUTHOR: IVÁN MAURICIO AMAYA CONTRERAS⁴

KEYWORDS: MICROWAVES, CIRCUITAL ANALYSIS, MODERN OPTIMIZATION, MINERAL ORES, DIELECTRIC PROPERTIES.

DESCRIPTION:

The current dissertation aims at developing an optimization strategy able to find the dimensions and resonant frequency of a microwave applicator, such that the field distribution matches a user-defined one. Three chapters are reserved to discuss the main pillars required for establishing such strategy: the Mathematical model of microwave resonators analyzed through circuitual analysis, the experimental dielectric properties of different mineral samples that change with temperature, and the formulation of different modern optimization techniques. Afterwards, some design scenarios that include lossless and lossy materials were boarded. Several things of interest were found. But, the most relevant one relates to the feasibility of the proposed strategy. A level of agreement as good as over 50 [dB] was possible in some scenarios (especially for higher frequencies). However, in other scenarios this value dropped to 20 [dB] (especially near the fundamental mode of the applicator), meaning that the Mathematical model needs to be improved. Even so, after a comparison with commercial software (CST), it was found that even in those cases where CST outperformed the strategy proposed in this dissertation, the latter yielded more uniform field distribution. Hence, the approach is deemed as successful. So, its use is recommended, as well as suggestion is made to work on expanding the model to the remaining directions and to other coordinate systems. Also, the inclusion of a metric that considers the form factor of the field distributions, perhaps through a weighted sum approach, is suggested.

³ Doctoral dissertation: Ph.D. on Engineering

⁴ Facultad de ingenierías fisiscomecánicas. Escuela de ingenierías eléctrica, electrónica, y de telecomunicaciones (E3T). Advisor: Carlos Rodrigo Correa Cely, Ph.D. Chemical engineer.

INTRODUCTION

Within this document, the theoretical foundation of my dissertation is discussed. We delve into three cornerstones: the Mathematical model of microwave resonators analyzed through circuitual analysis, the experimental dielectric properties of different mineral samples that change with temperature, and the formulation of different modern optimization techniques. But, for now, we summarize the main results.

MAIN CONTRIBUTIONS OF THIS WORK

Considering that the topic of this dissertation is interdisciplinary by nature, I strived to generate contributions on its different fields. Furthermore, and since it is a formative process, I deemed important to strengthen the formation of new potential researchers, especially those at the undergraduate level, and to disseminate the results of this work. Hence, the main contributions can be summarized as follows:

- Regarding mineral samples and processing, we gathered and analyzed experimental data of dielectric properties as a function of temperature. This information was not previously available and we selected different Colombian pyritic and non-pyritic mineral ore samples. Also, we generated a set of correlations that can be used to easily calculate the dielectric properties at a given temperature.
- Regarding the Mathematical model of circuitual analysis, I proposed the use of the *norm* instead of the *determinant*, as a metric for identifying the resonant frequencies. By doing so, I was able to analyze the family of TE_{mnp} modes given by $m = 0, n = 1$. This was impossible to calculate through the determinant because of the appearance of rows and columns completely filled with zeros.
- Regarding optimization, I proposed a strategy that allows finding the optimum dimensions of a microwave resonator and its operating frequency. This strategy implies two optimization loops, one in charge of finding the dimensions, and one that finds the operating frequency for each test design.
- Regarding modern optimization techniques, two new variants of the traditional Harmony Search (HS) algorithm were presented. The first one, called ABHS, proposed that one of the fixed parameters of HS became variable, and that it changed exponentially throughout the iterations. The second one, called SFHS, was a natural evolution of the first proposal, where the now varying parameter became self-tuned.
- Regarding the formation of new researchers, we proposed and advised more than 30 undergraduate theses (about 55 students), and one master thesis.

- Regarding dissemination of results, we published 17 articles in national and international peer-reviewed Journals, and recognized by COLCIENCIAS, and three international conference papers. Also, we submitted five articles and some more are currently in the works.

MAIN CONCLUSION OF THIS WORK

Several things can be concluded. The first one is that both of the proposed modifications for the Harmony Search algorithm (HS), represent good improvements. Through them, it was possible not only to enhance the precision, but also the convergence speed of the strategy. Nonetheless, and regarding the particular problem we boarded in this dissertation, we found that the Unified Particle Swarm Optimization algorithm (UPSO) was best suited to search for the optimum dimensions of a resonator. Our proposed modification of HS (SFHS), on the other hand, was best suited to identify the proper resonant frequency. Their combination led to a strategy able to find appropriate designs for different test scenarios.

Dielectric properties of the mineral samples boarded in this dissertation also revealed important information. We found that gold ores with high sulfur content interact more easily with microwaves, due to their higher complex permittivity. Furthermore, and at least for one of the minerals considered in this study, microwave smelting seems feasible. On this regard, the required processing time was about only 8% of the required by a traditional furnace, with recovery margins between 95% and 100%. This could impact heavily on gold processing, as long as a vapor collection system is implemented, to avoid unloading sulfur-based vapors to the environment.

In spite of the good results that our algorithm was able to achieve at some frequencies (especially high order modes), in some cases there was some error margin at the first modes. This level of error can be reduced to some extent by increasing the number of elements assumed for each of the incident fields. But, this also increases the computational cost of evaluating the objective function, so special care must be taken to find an appropriate balance.

All of these features point at the same conclusion: it is possible to use a modern optimization technique to optimize the dimensions of a microwave resonator, such that the electric field distribution matches a desired one, and obtain results that, in some cases, surpass 50 [dB]. Hence, we recommend using this approach and expanding the Mathematical model of circuit analysis to the remaining directions, and to other coordinate systems.

ACADEMIC PRODUCTION RELATED TO THIS WORK

Published articles

- [1] R. Correa, I. Amaya, A. Araque-Herrera, Uso de algoritmos metaheurísticos híbridos para la minimización de entropía en problemas de transferencia de calor en circuitos electrónicos, *Rev. Ing. Y Univ.* 15 (2011) 403–421.
- [2] I. Amaya, J. Cruz, R. Correa, Real Roots of Nonlinear Systems of Equations Through a Metaheuristic Algorithm, *Rev. Dyna.* 78 (2011) 15–23.
- [3] C. Gómez, I. Amaya, R. Correa, An Alternative Method for the Design of Time-varying Feedback Control Systems, *Rev. Dyna.* 79 (2012) 168–174.
- [4] I. Amaya, J. Cruz, R. Correa, Solution of the Mathematical Model of a Nonlinear Direct Current Circuit Using Particle Swarm Optimization, *Rev. Dyna.* 79 (2012) 77–84.
- [5] J. Rincón, I. Amaya, R. Correa, Assymetrical Capacitors: Experiments and Modelling, *Rev. Ing. Univ. Medellín.* 11 (2012) 227–238.
- [6] I. Amaya, R. Correa, Electromagnetic heating as a way of cutting costs while saving energy: Time evolution, *Rev. Ing. Univ. Medellín.* 11 (2012) 215–226.
- [7] S. Vanegas, I. Amaya, R. Correa, Virtual bat algorithm for the computation of Duhamel's Integral applied to structural systems with one degree of freedom, *Rev. Ing. Construcción.* 28 (2013) 278–289.
- [8] J. Cruz, I. Amaya, C. Correa, Algoritmo de optimización para el cálculo de múltiples raíces de sistemas de ecuaciones no lineales, *Inge CUC.* 9 (2013) 197–208.
- [9] O. Pérez, I. Amaya, R. Correa, Numerical solution of certain exponential and non-linear Diophantine systems of equations by using a discrete particle swarm optimization algorithm, *Appl. Math. Comput.* 225 (2013) 737–746. doi:10.1016/j.amc.2013.10.007.
- [10] I. Amaya, R. Correa, Optimal Design of Multilayer EMAs for Frequencies between 0.85 GHz and 5.4 GHz, *Rev. Ing.* 38 (2013) 33–37.
- [11] I. Amaya, D. Bernal, S. Garnica, M. Reslen, R. Correa, Improved Roasting of Some Colombian Gold Ores, *Rev. Dyna.* 80 (2013) 70–77.
- [12] I. Amaya, J. Cruz, R. Correa, A modified firefly-inspired algorithm for global computational optimization, *Dyna.* 81 (2014) 85–90. doi:http://dx.doi.org/10.15446/dyna.v81n187.34594.
- [13] I. Amaya, L.A. Gómez, R. Correa, Discrete Particle Swarm Optimization in the numerical solution of a system of linear Diophantine equations, *Dyna.* 81 (2014) 139–144.

[14] J. Contreras, I. Amaya, R. Correa, An improved variant of the conventional Harmony Search algorithm, *Appl. Math. Comput.* 227 (2014) 821–830. doi:10.1016/j.amc.2013.11.050.

[15] I. Amaya, W. Botero, R. Correa, Microwave Assisted Roasting for Enhanced Processing of A Mineral Gold Ore, *Rev. Ing. Univ. Medellín* InPress. (2015).

[16] I. Amaya, R. Correa, Finding resonant frequencies of microwave cavities through a Modified Harmony Search algorithm, *Int. J. Bio-Inspired Comput.* InPress. (2015).

[17] J. Cruz, I. Amaya, R. Correa, Optimal rectangular microchannel design, using simulated annealing, unified particle swarm and spiral algorithms, in the presence of spreading resistance, *Appl. Therm. Eng.* 84 (2015) 126–137. doi:10.1016/j.applthermaleng.2015.03.049.

Submitted articles

[1] I. Amaya, F. Peñaranda, R. Correa, Dielectric Properties of some Colombian Pyritic Mineral Samples as a Function of Temperature, *Int. J. Min. Proc.* 2014.

[2] I. Amaya, J. Cruz, R. Correa, Harmony Search algorithm: A Variant with Self-Regulated Fretwidth, *Appl. Math. Comput.* 2014.

[3] M. Diaz, I. Amaya, R. Correa, Microwave Enhanced Roasting for Pyrite Ore Samples with Dielectric Properties Strongly Dependent on Temperature, *Rev. Ing. Univ.* 2014.

Conference papers

[1] J. Cruz, I. Amaya, and R. Correa, “Solution of the mathematical model of a DC nonlinear electronic circuit using an optimization strategy: Application of the original and unified Particle Swarm Metaheuristics,” in *2012 IEEE 4th Colombian Workshop on Circuits and Systems (CWCAS)*, 2012, pp. 1–6.

[2] O. Roa, I. Amaya, F. Ramirez, and R. Correa, “Solution of nonlinear circuits with the Central Force Optimization algorithm,” in *2012 IEEE 4th Colombian Workshop on Circuits and Systems (CWCAS)*, 2012, pp. 1–6.

[3] J. E. González, I. Amaya, and R. Correa, “Design of an Optimal Multi-layered Electromagnetic Absorber through the Central Force Optimization Algorithm,” in *PIERS Proceedings*, 2013, vol. 1, no. 1, pp. 1082–1086.

Undergraduate theses (finished)

- [1] H. Castro, M. Otero, El Algoritmo del Murciélago Virtual (Bat Algorithm) como Estrategia para el Diseño Óptimo de Filtros Pasa-Bajas, Undergraduate Thesis, Universidad Industrial de Santander, 2014.
- [2] A. Rodríguez, K. Gaona, Diseño Óptimo de Filtros Electrónicos (Chebyshev) Mediante el Algoritmo de la Luciérnaga Virtual (Firefly), Undergraduate Thesis, Universidad Industrial de Santander, 2014.
- [3] D. Jurado, M. Ortiz, Implementación de un Sistema de Medición y Control de la Temperatura en una Cavidad Electromagnética, Undergraduate Thesis, Universidad Industrial de Santander, 2013.
- [4] E. Farfán, J. Fontecha, Obtención de Las Curvas de Dispersión de Modos Híbridos para Guías de Onda de Sección Transversal Rectangular Parcialmente Llena con un Dieléctrico, Mediante Optimización por Enjambre de Partículas Unificado UPSO, Undergraduate Thesis, Universidad Industrial de Santander, 2013.
- [5] C. Gómez, O. Pérez, Implementación de un Algoritmo de Optimización para Sistemas Discretos Fundamentado en la Técnica de Enjambre de Partículas, Undergraduate Thesis, Universidad Industrial de Santander, 2012.
- [6] C. Pinzón, E. Ardila, Evaluación y Comparación de los Métodos UPSO y Newton Raphson para el Análisis de Flujo de Cargas en un Sistema de Potencia, Undergraduate Thesis, Universidad Industrial de Santander, 2013.
- [7] J. Celis, F. Rincón, Evaluación y Comparación entre los Métodos Newton Raphson y Artificial Bee Colony (ABC) para el Análisis del Flujo de Carga de un Sistema de Potencia, Undergraduate Thesis, Universidad Industrial de Santander, 2013.
- [8] E. Petro, R. Fuentes, Mantenimiento Preventivo Básico de un Desfibrilador Monofásico Mediante los Métodos de Enjambre de Partículas Mejorado y Colonia Artificial de Abejas, Undergraduate Thesis, Universidad Industrial de Santander, 2013.
- [9] J. Arias, M. Mogollón, Algoritmo de Optimización Gotas de Agua Virtuales Inteligentes Aplicado a la Planeación de Ruta Óptima de un Robot Móvil, Undergraduate Thesis, Universidad Industrial de Santander, 2013.
- [10] D. Dávila, A. Rutto, Identificación de Sistemas No Lineales Mediante el Método de Optimización de la Gota de Agua Virtual Inteligente, Undergraduate Thesis, Universidad Industrial de Santander, 2014.

- [11] J. Ávila, O. Navarro, El Método de Colonia Artificial de Abejas y el Criterio de Mínima Entropía para el Diseño Óptimo de un Disipador de Calor, Undergraduate Thesis, Universidad Industrial de Santander, 2014.
- [12] M. Hernandez, Inteligencia Computacional Inspirada en la Cuántica, Aplicada a la Optimización de la Producción de Petróleo en el Modelo de un Pozo Inteligente, Undergraduate Thesis, Universidad Industrial de Santander, 2013.
- [13] A. Miranda, J. Ruiz, Implementacion del Algoritmo de Busqueda Gravitacional (GSA) para el Diseño de un Absorbedor Electromagnetico Óptimo, Undergraduate Thesis, Universidad Industrial de Santander, 2014.
- [14] J. Garcia, D. Corredor, Algoritmo Híbrido del Simplex con la Estrategia de Optimizacion de Fuerza Central (CFO) Aplicado a la Solucion de Sistemas de Ecuaciones No Lineales, Undergraduate Thesis, Universidad Industrial de Santander, 2013.
- [15] S. Gonzalez, O. Trasladino, Análisis de la Eficiencia del Algoritmo Harmony Search en la Solución de un Circuito Electrónico No Lineal, Undergraduate Thesis, Universidad Industrial de Santander, 2013.
- [16] K. Barreto, Evaluación del Método Optimizador de Fuerza Central Frente al Optimizador por Enjambre de Partículas Unificado en la Solución de Ecuaciones No Lineales, Undergraduate Thesis, Universidad Industrial de Santander, 2014.
- [17] J. Portilla, Solución de las Ecuaciones que Modelan un Circuito No Lineal de Corriente Directa Mediante el Método de Espiral, Undergraduate Thesis, Universidad Industrial de Santander, 2012.
- [18] R. Ortiz, E. García, Diseño de un Absorbedor Electromagnético Multicapa Mediante el Método de la Espiral, Undergraduate Thesis, Universidad Industrial de Santander, 2013.
- [19] J. Suarez, J. Romero, Solución de las Ecuaciones que Describe el Comportamiento de los Modos Híbridos en una Guía de Onda Rectangular Parcialmente Llena Mediante el Método de Optimización Recocido Simulado (Simulated Annealing), Undergraduate Thesis, Universidad Industrial de Santander, 2013.
- [20] M. Díaz, M. Rueda, Uso de las Microondas en el Proceso de Recuperación de Trazas de Oro, Undergraduate Thesis, Universidad Industrial de Santander, 2012.
- [21] D. Bernal, S. Garnica, Y. Reslen, Irradiacion con Microondas a Minerales Ricos en Oro en Muestras Provenientes de la Zona del Sur de Bolivar, Undergraduate Thesis, Universidad Industrial de Santander, 2012.

- [22] J. Ramirez, F. Osorio, Algoritmo de Enjambre de Partículas Unificado para la Solución de Ecuaciones Diofánticas Lineales Comúnmente Encontradas en Problemas de Ingeniería Electrónica, Undergraduate Thesis, Universidad Industrial de Santander, 2013.
- [23] J.S. Abril, J.A. Gomez, Ingeniería Conceptual de un Proceso de Recuperación de Oro con Microondas a Partir de Muestras Provenientes de los Municipios de Vetas y California (Santander), Undergraduate Thesis, Universidad Industrial de Santander, 2012.
- [24] J. González, C. Bayona, Aplicación del Método de Optimización por Fuerza Central (CFO), al Diseño de un Absorbedor Electromagnético Óptimo, Undergraduate Thesis, Universidad Industrial de Santander, 2013.
- [25] J. Contreras, C. Villanueva, Solución de un Sistema de Ecuaciones No Lineales, Utilizando una Estrategia Basada en el Algoritmo de Harmony Search, Undergraduate Thesis, Universidad Industrial de Santander, 2013.
- [26] J. Cruz, Solución del Modelo Matemático de un Circuito Electrónico D.C. No Lineal Mediante una Estrategia de Optimización, Undergraduate Thesis, Universidad Industrial de Santander, 2012.
- [27] F. Ramírez, O. Roa, Solución de las Ecuaciones que Describen el Modelo Matemático de un Circuito Electrónico Compuesto de Elementos No Lineales Mediante el Optimizador de Fuerza Central, Undergraduate Thesis, Universidad Industrial de Santander, 2012.
- [28] R.D. Aguirre, W. Botero, Interacción de las Microondas con Trazas de Oro en Muestras Provenientes del Municipio de Vetas (Santander), Undergraduate Thesis, Universidad Industrial de Santander, 2012.
- [29] A. Hinojosa, K. Espinosa, El Método de Enjambre de Partículas y el Criterio de Mínima Entropía en el Diseño Óptimo de un Disipador de Calor, Tesis de Pregrado, Universidad Industrial de Santander, 2011.
- [30] E. Barrios, D. Barrios, Ingeniería Conceptual de un Proceso de Fabricación de un Material vía Microondas (2450 mhz), Undergraduate Thesis, Universidad Industrial de Santander, 2009.

Undergraduate theses (ongoing)

- [1] J. Angel, Estrategia Numérica para la Solución del Modelo Circuital de una Guía de Onda Circular Totalmente Llena con un Dieléctrico, Undergraduate Thesis, Universidad Industrial de Santander, 2015.

[2] D. Franco, J. Jaimes, Cálculo de las Frecuencias de Resonancia en un Aplicador Circular Cilíndrico a través de Técnicas de Análisis Circuital, Undergraduate Thesis, Universidad Industrial de Santander, 2015.

Master thesis

[1] J. Cruz, El criterio de la Mínima Generación de Entropía (MGE) para el Diseño Óptimo de Disipadores de Calor y su Solución Mediante Algoritmos de Optimización Global, Master Thesis, Universidad Industrial de Santander, 2015.

FUTURE RESEARCH LINES

Several research lines can be derived from this work. One of the most obvious ones could be to keep working on SFHS to improve its precision and convergence speed. But, this is not the only alternative. A really interesting approach implies delving further into the use of the norm to identify the resonant frequencies of circuital analysis, or, even, propose a new approach to identify them altogether. Also, working on circuital analysis to study the microwave resonator with ports entering and exiting along the other directions, is worth investing time and having dedication. This kind of commitment will allow for more complex designs that can be optimized through the proposed strategy. Moreover, the study shown in this dissertation can be extended to other coordinate systems, such as the cylindrical and spherical ones.

1. FUNDAMENTALS

The current dissertation aims at developing an optimization approach able to design a microwave applicator with a desired field distribution. The process includes boarding the problem through modern optimization techniques, and the author hopes that the mining industry will be able to use said design in the near future, for processing gold ores with lower environmental impact. Even so, the application selected for this dissertation does not hinder the generality of the developed optimization approach.

1.1 AN OVERVIEW OF THE RESEARCH PROBLEM

Microwaves have multiple and varied uses. During this dissertation, microwave heating was of special interest, since it does not limit to the interaction between electromagnetic energy and food. In fact, microwaves can be used to assist several industrial processes, e.g. mineral processing [1–7], coal coking [8], and material manufacturing [9] and sintering [10,11]. The use of microwaves also expands to other fields, such as polymer curing [12], oil production [13,14], and agricultural product preservation [15], amongst others [16].

Incorporating microwaves in a given scenario is, alas, no easy task. The efficiency of the process is governed by the interaction between electromagnetic field and materials. The former requires the application of Maxwell equations and vary due to several factors [17,18]. The operating frequency of the electromagnetic source is, of course, a main variable since the number of solutions that can manifest depend upon it. Other relevant variables are those directly affecting the dielectric properties of the sample, as well as its spatial location inside the applicator. Some representative examples include humidity, chemical composition, and temperature. Moreover, the material can be highly anisotropic, exhibiting different values of permittivity in each direction, thus increasing the complexity of the mathematical model.

Knowing the dielectric properties of a given material is not enough for properly implementing microwaves; knowing how to modify the process is also required. Traditional processing of gold incorporates several chemicals, most of which are hazardous to humans. Besides, some minerals do not yield high recovery margins, although heating the ore generally solves this problem (at least partly). In order to assess the grade of a mineral gold ore (i.e. the amount of gold it contains per ton of ore), several approaches can be used. These range from simple, experimental methods, to more complex, analytical tests. A fire assay is a rather simple technique that can quickly yield an estimate over a sample's grade. The process involves grinding the ore, roasting it inside an electric furnace, mixing it with some reagents, smelting the mixture, and separating the gold with the help of an acid. The remaining gold lump is weighted and the grade is calculated via a linear relation.

In spite of the process being simple, stabilizing the electric furnace at the temperature required for roasting (about 700°C) and smelting (about 1000°C) may take up to two and four hours, respectively. Moreover, traditional heating transfers energy through conduction, convection, and radiation phenomena, thus creating a direct heating profile. Here, the surface of the heated sample is hotter than its core, so energy needs to travel inward.

Microwaves can come in handy in this scenario, since the interaction between electromagnetic energy and matter is volumetric in nature, leading to an inverse heating profile where the core is hotter than the surface (as long as appropriate circumstances are present). Whenever a traveling wave makes contact with the surface of a sample, some energy is reflected, but the remaining one is transmitted and begins traveling throughout the object. Should there be no losses associated to this sample, the wave would travel all the way to the other side, generating new reflected and transmitted waves when it reaches the boundary. In the remaining case (i.e. lossy sample), the magnitude of the traveling wave would diminish as it travels, and it may or may not reach the other end. The energy lost is transformed into heat, and so the wave leaves a temperature rise in its wake.

Mineral gold ores usually manifest a lossy behavior, so it is only natural to deem as worthy an exploration of microwave-assisted heating for fire assay. If successful, this scope could be broadened to include roasting of minerals prior to traditional processing, and, even, smelting. But, in order to make this process environmentally friendly, the microwave applicator must be optimized to minimize energy losses (i.e. energy wasted by not heating the sample). This optimization, however, needs to consider the factors that may alter the electromagnetic field distribution (as mentioned above).

Traditional optimization techniques, such as Newton's, base their strategy on a deterministic search, guided by the calculation of gradients, Jacobians, and/or Hessians, that ultimately become matrices with highly complicated operations. This increases the computational cost of the process and the time taken to implement the process.

Modern optimization techniques, however, usually base their strategy on a stochastic search, where only simple calculations are required. They have been around for some time now, but their use escalated thanks to the proposal presented by Eberhart and Kennedy in 1995 [19,20]. Back then, they proposed an algorithm that strived to replicate the behavior of birds and fish when looking for sources of food. This strategy included the use of random numbers and was designed to use the information of all search agents for improving the objective function. Hence, it was a collaborative process that only required simple algebraic operations. The results were so outstanding that more and more people began using it, as well as designing new strategies inspired in nature. Nowadays, it is common to find optimization strategies

inspired on gravitational kinematics [21], on music composition [22], and on bee colonies [23], just to name a few.

Based on the aforementioned paragraphs, this dissertation proposes the use of a modern optimization technique for optimizing a microwave applicator, specifically tailored for processing gold ores. In order to do so, a proper mathematical model must be derived, information about the dielectric properties of local mineral samples and about appropriate exposure conditions needs to be collected, and a study of different optimization techniques needs to be carried out.

1.2 TYPES OF ORES

Gold mineral ores can be divided, from a metallurgical point of view, into two big groups: free-milling and refractory. The latter can be further divided into three groups, depending on how difficult it is to separate gold particles from the ore. Hence, four groups appear (Figure 1-1): free-milling (a.k.a. not refractory, recoveries over 95% can be easily achieved), mildly refractory (recovery between 80-95%), moderately refractory (recovery between 50-80%) and highly refractory (recovery below 50%). Some studies have been carried out to try and determine the causes for refractoriness, and Vaughan synthesized most of them [24]. He found that the main cause is submicroscopic gold, located especially inside pyrite and arsenopyrite, which increases an ore grade, but which is also hard to separate due to its small size. One solution for this case is to grind the ore to a finer size. However, this increases waste product due to slime generation. High levels of Au-Ag tellurides, which has poor solubility in cyanide, as well as very fine grained gold inside sulfides, also contribute to making the ore refractory. In these cases, it is said that the gold is "locked" because it cannot be accessed by cyanide.

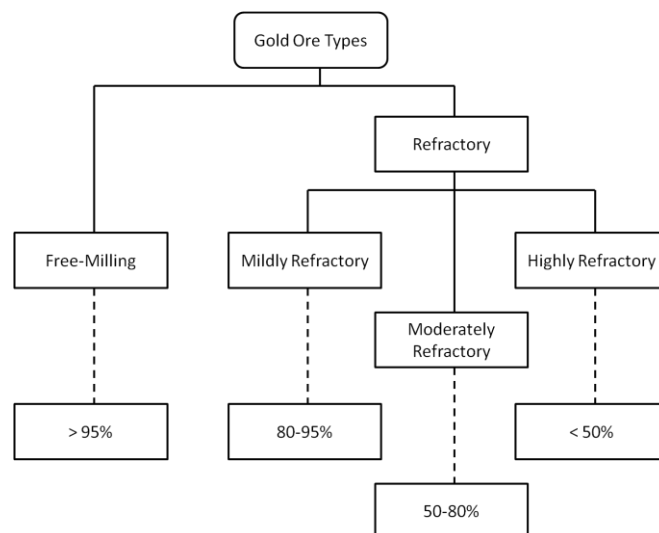


Figure 1-1. Classification of gold ores and typical recovery with traditional methods

Besides physical or chemical locking inside the ore, Vaughan also summarized two types of ores, difficult to treat, but due to the gangue minerals. They are known as carbonaceous and complex ores. Within these, gold particles are free and big enough to be easily recovered. However, in the first case, particles are re-adsorbed by the minerals that compose the gangue (process known as preg-robbing), thus reducing the recovery efficiency. In the second case, composites such as pyrrhotite, as well as some secondary copper sulfides, adsorb the leaching solution (leach-robbes), thus increasing the consumption of reagents. This group generally contain elements such as Copper (Cu), Cobalt (Co), Bismuth (Bi) and Uranium (U). Copper is the most common and abundant element, so the ore is known as copper-gold ore [24]. Should both types of obstacles be present in the ore (i.e. locking and gangue related), it is catalogued as a double refractory ore, which is even harder to process [25]. This information is summarized in Figure 1-2.

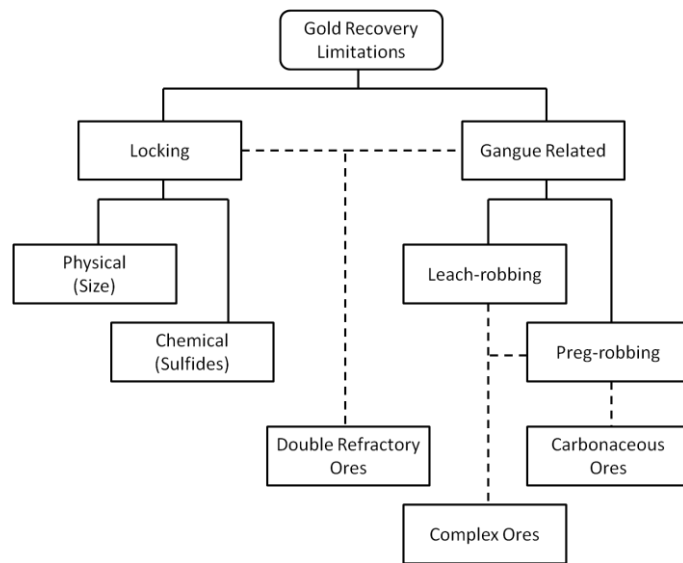


Figure 1-2. Most common causes for refractoriness and double refractory ore appearance

1.3 OBJECTIVES

1.3.1 General objective

To design an optimum applicator through a metaheuristic algorithm, that can be later used by the mining industry, where electromagnetic energy provides an increased benefit (economical, environmental, or both).

1.3.2 Specific objectives

In order to accomplish this objective, several specific ones were proposed:

1. Determine, experimentally, the dielectric properties of some local mineral samples.
2. Determine the conditions (exposure time, power, etc.) required so the microwaves are able to enhance processing of the mineral, through a statistically designed experiment.
3. Model the applicator in simulation software, combining it with a metaheuristic algorithm that optimizes its dimensions.

1.4 ORGANIZATION OF THE CURRENT DISSERTATION

Striving to simplify things for the reader, we organized this dissertation into five chapters and one appendix. Each one of these units was written with a clear purpose in mind. Moreover, each chapter was structured considering the subject area they related to, as described below.

Chapter 2 deals with the mathematical formulation of the electromagnetic problem, i.e. the objective function of this dissertation. We begin with Maxwell equations and end with a circuit analysis that allows interaction between network blocks of differing electromagnetic properties. These blocks can be either lossless or lossy.

After having a general formulation, assessing the electromagnetic properties of the samples covered by this dissertation is required. Hence, Chapter 3 shows a general procedure for measuring dielectric properties of mineral ores as a function of temperature, as well as some of the most relevant data. We focus on samples with high concentration of sulphur-based compounds, and we also show that samples with low sulphur content fail to heat beyond a couple hundred Celsius degrees. Towards the end, general representations for the data are laid out.

Chapter 4 assess different alternatives vastly available for modern numerical optimization. A summary of some of them is presented, and a special discussion is given about a couple variants we proposed to improve one of the algorithms. Striving not to make this chapter excessively long, only some of the most relevant results are shown. We focus on our data for standard test functions, as well as for two applications: optimization of electromagnetic absorbers, and solution of hybrid modes in a partially-filled waveguide. Even so, we also briefly discuss the solution of electronic circuits and mention other scenarios that we worked on.

These three areas (i.e. the model, the application, and the algorithms) are merged during Chapter 5. We begin this chapter by analysing the performance of our approach for resonator uniformly filled with a material. Then, we study the effect of filling the resonator with different materials, including lossy ones. Towards the end of the chapter, we include the

dielectric properties of the samples and analyse the performance of our strategy under different conditions.

The final chapter presents an appendix detailing the mineral composition of the samples considered throughout the dissertation.

REFERENCES

- [1] I. Amaya, D. Bernal, S. Garnica, M. Reslen, R. Correa, Improved Roasting of Some Colombian Gold Ores, *Rev. Dyna.* 80 (2013) 70–77.
- [2] R.K. Amankwah, G. Ofori-Sarpong, Microwave Heating of Gold Ores for Enhanced Grindability and Cyanide Amenability, *Miner. Eng.* 24 (2011) 541–544. doi:10.1016/j.mineng.2010.12.002.
- [3] V.G. Harris, A. Geiler, Y. Chen, S.D. Yoon, M. Wu, A. Yang, et al., Recent advances in processing and applications of microwave ferrites, *J. Magn. Magn. Mater.* 321 (2009) 2035–2047. doi:10.1016/j.jmmm.2009.01.004.
- [4] W. Vorster, The Effect of Microwave Radiation on Mineral Processing, Ph.D. Thesis, The University of Birmingham, 2001.
- [5] S. Kingman, K. Jackson, A. Cumbane, S.M. Bradshaw, N.A. Rowson, R. Greenwood, Recent developments in microwave-assisted comminution, *Int. J. Miner. Process.* 74 (2004) 71–83. doi:10.1016/j.minpro.2003.09.006.
- [6] M. Al-Harashseh, S.W. Kingman, Microwave-assisted leaching—a review, *Hydrometallurgy.* 73 (2004) 189–203. doi:10.1016/j.hydromet.2003.10.006.
- [7] M. Al-Harashseh, S. Kingman, L. Al-Makhadmah, I.E. Hamilton, Microwave treatment of electric arc furnace dust with PVC: dielectric characterization and pyrolysis-leaching., *J. Hazard. Mater.* 274 (2014) 87–97. doi:10.1016/j.jhazmat.2014.03.019.
- [8] E. Binner, M. Mediero-Munoyerro, T. Huddle, S. Kingman, C. Dodds, G. Dimitrakis, et al., Factors affecting the microwave coking of coals and the implications on microwave cavity design, *Fuel Process. Technol.* 125 (2014) 8–17. doi:10.1016/j.fuproc.2014.03.006.
- [9] H.J. Kitchen, S.R. Vallance, J.L. Kennedy, N. Tapia-Ruiz, L. Carassiti, A. Harrison, et al., Modern microwave methods in solid-state inorganic materials chemistry: from fundamentals to manufacturing., *Chem. Rev.* 114 (2014) 1170–206. doi:10.1021/cr4002353.
- [10] A. Borrell, M.D. Salvador, F.L. Peñaranda-Foix, J.M. Cátala-Civera, Microwave Sintering of Zirconia Materials: Mechanical and Microstructural Properties, *Int. J. Appl. Ceram. Technol.* 10 (2013) 313–320. doi:10.1111/j.1744-7402.2011.02741.x.
- [11] D. Agrawal, J. Cheng, H. Peng, L. Hurt, K. Cherian, Microwave Energy Applied to Processing of High-Temperature Materials, *Am. Ceram. Soc. Bull.* 87 (2008) 39–44.

- [12] K. Tanaka, S. Ann, B. Allen, P.A. Kohl, Variable Frequency Microwave Curing of Amide-Epoxy Based Polymers, *IEEE Trans. Components Packag. Technol.* 30 (2007) 472–477.
- [13] B. Hascakir, S. Akin, Recovery of Turkish Oil Shales by Electromagnetic Heating and Determination of the Dielectric Properties of Oil Shales by an Analytical Method, *Energy & Fuels.* 24 (2010) 503–509. doi:10.1021/ef900868w.
- [14] J. Robinson, E. Binner, A. Saeid, M. Al-Harashsheh, S. Kingman, Microwave processing of Oil Sands and contribution of clay minerals, *Fuel.* 135 (2014) 153–161. doi:10.1016/j.fuel.2014.06.057.
- [15] S.O. Nelson, Fundamentals of Dielectric Properties Measurements and Agricultural Applications, *J. Microw. Power Electromagn. Energy.* 44 (2010) 98–113.
- [16] I. Amaya, R. Correa, Electromagnetic heating as a way of cutting costs while saving energy: Time evolution, *Rev. Ing. Univ. Medellín.* 11 (2012) 215–226.
- [17] A.C. Metaxas, R. Meredith, *Industrial Microwave Heating*, The Institution of Electrical Engineers, London, 1983.
- [18] R. Meredith, *Engineers' Handbook of Industrial Microwave Heating*, The Institution of Electrical Engineers, London, 1998.
- [19] R. Eberhart, J. Kennedy, A new optimizer using particle swarm theory, in: *MHS'95. Proc. Sixth Int. Symp. Micro Mach. Hum. Sci., IEEE*, 1995: pp. 39–43. doi:10.1109/MHS.1995.494215.
- [20] J. Kennedy, R. Eberhart, Particle Swarm Optimization, in: *Proc. ICNN'95 - Int. Conf. Neural Networks, IEEE, Perth, Australia*, 1995: pp. 1942–1948. doi:10.1109/ICNN.1995.488968.
- [21] R.A. Formato, Central force optimization: A new metaheuristic with application in applied, *Prog. Electromagn. Res. PIER* 77, 425–491, 2007. (2007) 425–491.
- [22] Z.W. Geem, J.H. Kim, G.V. Loganathan, A New Heuristic Optimization Algorithm: Harmony Search, *Simulation.* 76 (2001) 60–68. doi:10.1177/003754970107600201.
- [23] D. Karaboga, B. Basturk, A powerful and efficient algorithm for numerical function optimization: artificial bee colony (ABC) algorithm, *J. Glob. Optim.* 39 (2007) 459–471. doi:10.1007/s10898-007-9149-x.
- [24] J.P. Vaughan, The process mineralogy of gold: The classification of ore types, *J. Miner. Met. Mater. Soc.* 56 (2004) 46–48. doi:10.1007/s11837-004-0092-8.

- [25] B. Nanthakumar, C. Pickles, S. Kelebek, Microwave Pretreatment of a Double Refractory Gold Ore, *Miner. Eng.* 20 (2007) 1109–1119. doi:10.1016/j.mineng.2007.04.003.

2. DESCRIBING THE PROBLEM

Solving an electromagnetic problem involves dealing with Maxwell equations. This, in turn, requires solving the wave equation, which can be dealt with through a separation of variables. The resulting wave function must comply with Helmholtz equation. Hence, these functions depend on geometry and boundary conditions. During this chapter, some basic resonant structures (networks) will be discussed, focusing on their solution and creating building blocks that can be used in forthcoming chapters (please refer to the appendix for details about the process). Also, the appendix shows a procedure for evaluating the fields inside these networks. Towards the end of this chapter, we will summarize the objective function that will be used in the next chapters, as well as the process associated to its evaluation.

2.1 THE RECTANGULAR RESONATOR

Solving Maxwell equations in rectangular coordinates is perhaps one of the simplest scenarios that can be found, since the solution can be separated into transversal electric (TE) and transversal magnetic (TM) modes [1]. This nullifies some field components and the analytic solution can be easily found. However, if the guide is partially filled with a given material, the problem becomes more complicated. This is due to the fact that each change of material implies continuity conditions that must be satisfied.

Circuitual analysis can be a useful tool in this kind of situations. Even though the segmentation technique has been around for some time (it was first attributed to Harrington in 1961), it has been widely used up to our days [1,2]. The idea behind this approach is to split the nonhomogeneous volume into homogeneous ones (called blocks or networks), calculate the admittance and scattering matrices, and then connect them through a series of ports. For example, consider the rectangular resonator shown in Figure 2-1. Here, the resonator has been split along the z-axis, into N blocks. The interface of each pair of blocks is located at a distance, d_i , from the origin. In the broadest scenario (under these conditions), each block would have different dielectric properties. Using circuitual analysis, we are only required to analyze each type of block (or network), and not each independent block. This means that, based on our configuration, it is only necessary to analyze three structures: one with a port at the bottom, one with the port at the top, and one with one port at each end. Furthermore, this last kind of network shares some common calculations with the other two, so it is only necessary to analyze half of the elements (i.e. the cross-relations between the ports).

The appendix details the calculations required to find the admittance matrix of each kind of network. Hence, this chapter will just summarize the expressions, for the sake of space. The

admittance matrix of the network at the bottom, i.e. the one with a port located at $z = c$, is made up of four items, as shown in eq. (2.1), where $Y^{ss}, Y^{sc}, Y^{cs}, Y^{cc}$ are submatrices composed by q, m elements, as shown by eq. (2.2).

$$[Y] = \begin{bmatrix} Y^{ss} & Y^{sc} \\ Y^{cs} & Y^{cc} \end{bmatrix} \quad (2.1)$$

$$\begin{aligned} Y_{qm}^{ss} &= \frac{-4\gamma}{\omega\mu b^2 \tan(j\gamma c)} \frac{1}{I_q^s I_m^s} & Y_{qm}^{sc} &= \frac{-4\gamma}{\omega\mu b^2 \tan(j\gamma c)} \frac{1}{I_q^s I_m^c} \\ Y_{qm}^{cs} &= \frac{-4\gamma\chi_q}{\omega\mu b^2 \tan(j\gamma c)} \frac{1}{I_q^c I_m^s} & Y_{qm}^{cc} &= \frac{-4\gamma\chi_q}{\omega\mu b^2 \tan(j\gamma c)} \frac{1}{I_q^c I_m^c} \end{aligned} \quad (2.2)$$

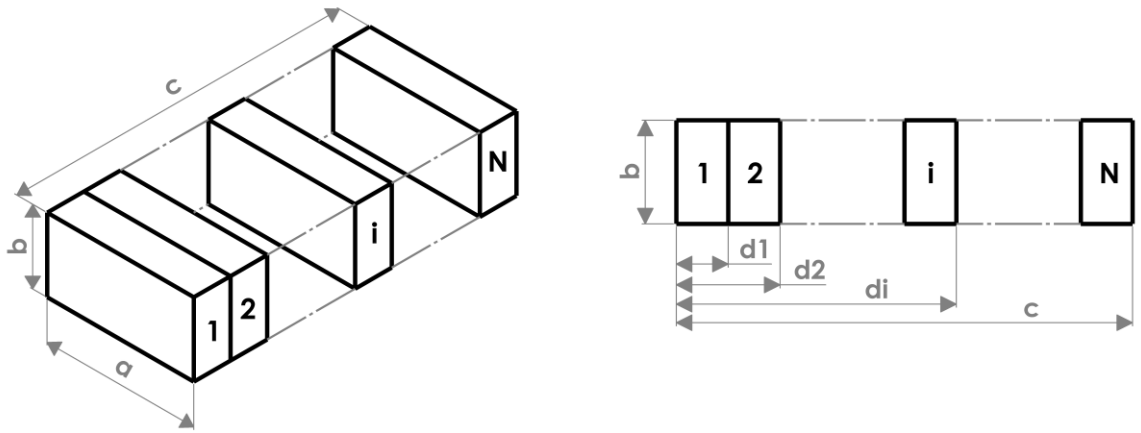


Figure 2-1. Rectangular resonator split into N blocks

It is now important to observe the influence of the integrals over the results. For a given n , they can be calculated as shown in eq. (2.3). Hence, any cross product between sine and cosine components (i.e. $I_q^s I_m^c$ and $I_q^c I_m^s$) yield zero, so $Y^{sc} = Y^{cs} = 0$ for all n . Moreover, $[Y] = [Y^{ss}]$ if $2m = 2q = n$ and $[Y] = [Y^{cc}]$ if n is odd.

$$\begin{aligned}
I_m^s &= \int_0^b \sin\left(\frac{2\pi my}{b}\right) \sin\left(\frac{n\pi y}{b}\right) dy = \begin{cases} b/2 & 2m = n \\ 0 & 2m \neq n \end{cases} \\
I_m^c &= \int_0^b \cos\left(\frac{2\pi my}{b}\right) \sin\left(\frac{n\pi y}{b}\right) dy \\
&= \begin{cases} 0 & 2m = n \text{ OR } n = \text{even} \\ \frac{-2bn}{\pi(4m^2 - n^2)} & n = \text{odd} \end{cases} \\
I_q^s &= \int_0^b \sin\left(\frac{2\pi qy}{b}\right) \sin\left(\frac{n\pi y}{b}\right) dy = \begin{cases} b/2 & 2q = n \\ 0 & 2q \neq n \end{cases} \\
I_q^c &= \int_0^b \cos\left(\frac{2\pi qy}{b}\right) \sin\left(\frac{n\pi y}{b}\right) dy \\
&= \begin{cases} 0 & 2q = n \text{ OR } n = \text{even} \\ \frac{-2bn}{\pi(4q^2 - n^2)} & n = \text{odd} \end{cases}
\end{aligned} \tag{2.3}$$

The top network, i.e. the one with a port at $z = 0$, has an admittance matrix of the same form as its counterpart, but each element of the submatrices are given by eq. (2.4). The remaining network, i.e. the one with two ports, has an admittance matrix made of four sets of submatrices, one for each combination of ports. Hence, this network has 16 submatrices, as shown in eq. (2.5). The elements filling submatrices $[Y_{11}]$ and $[Y_{22}]$ represent the already discussed scenarios, so they not need to be reformulated. The remaining submatrices, on the other hand, are comprised of the elements given in eq. (2.6), $[Y_{12}]$, and in eq. (2.7), $[Y_{21}]$. As it was mentioned above, please refer to the appendix in order to find details about the calculations required for arriving at the aforementioned equations. The calculations for transforming these matrices into the scattering ones, as well as the procedure for connecting them, are also discussed on the appendix.

$$\begin{aligned}
Y_{qm}^{ss} &= \frac{4\gamma}{\omega\mu b^2} \frac{1}{\tan(j\gamma c)} I_q^s I_m^s & Y_{qm}^{sc} &= 0 \\
Y_{qm}^{cs} &= 0 & Y_{qm}^{cc} &= \frac{4\gamma\chi_q}{\omega\mu b^2} \frac{1}{\tan(j\gamma c)} I_q^c I_m^c
\end{aligned} \tag{2.4}$$

$$[Y] = \begin{bmatrix} [Y_{11}] & [Y_{12}] \\ [Y_{21}] & [Y_{22}] \end{bmatrix} = \begin{bmatrix} \begin{bmatrix} [Y^{ss} & Y^{sc}] \\ [Y^{cs} & Y^{cc}] \end{bmatrix}_{11} & \begin{bmatrix} [Y^{ss} & Y^{sc}] \\ [Y^{cs} & Y^{cc}] \end{bmatrix}_{12} \\ \begin{bmatrix} [Y^{ss} & Y^{sc}] \\ [Y^{cs} & Y^{cc}] \end{bmatrix}_{21} & \begin{bmatrix} [Y^{ss} & Y^{sc}] \\ [Y^{cs} & Y^{cc}] \end{bmatrix}_{22} \end{bmatrix} \tag{2.5}$$

$$\left[\begin{aligned} Y_{qm}^{ss} &= \frac{4\gamma}{\omega\mu b^2} \frac{1}{\sin(j\gamma c)} I_q^s I_m^s & Y_{qm}^{sc} &= 0 \\ Y_{qm}^{cs} &= 0 & Y_{qm}^{cc} &= \frac{4\gamma\chi_q}{\omega\mu b^2} \frac{1}{\sin(j\gamma c)} I_q^c I_m^c \end{aligned} \right]_{12} \tag{2.6}$$

$$\left[\begin{array}{l} Y_{qm}^{ss} = \frac{-4\gamma}{\omega\mu b^2} \frac{1}{\sin(j\gamma c)} I_q^s I_m^s \quad Y_{qm}^{sc} = 0 \\ Y_{qm}^{cs} = 0 \quad Y_{qm}^{cc} = \frac{-4\gamma\chi_q}{\omega\mu b^2} \frac{1}{\sin(j\gamma c)} I_q^c I_m^c \end{array} \right]_{21} \quad (2.7)$$

After connecting the networks, a system of two elements remains. In this sense, traditional circuitual analysis theory dictates that the resonant frequency are calculated via eq. (2.8) [3]. Even so, matrix theory states that if all elements of at least one row or column are zero, then the determinant of a matrix becomes zero. This impacts directly our model, since there are always rows or columns full of zero elements for a given n (see the appendix). Hence, an alternative operation must be sought.

$$|\det(\overline{\overline{S_1 S_2}} - I)| = 0 \quad (2.8)$$

In this research work, we considered that the norm function may provide a valid approach at finding the resonant frequencies. Hence, we considered three types of matrix norms. The first one is the 1-norm, and it represents the maximum absolute column sum as shown in eq. (2.9). The second one is the 2-norm, or spectral norm, representing the square root of the maximum eigenvalue of the product of the matrix and its conjugate transpose, as shown in eq. (2.10). The final one is Inf-norm, and it represents the maximum absolute row sum as shown in eq. (2.11).

$$\|A\|_1 = \max_j \left(\sum_{i=1}^n |a_{ij}| \right) \quad (2.9)$$

$$\|A\|_2 = \sqrt{\max(\text{eig}(A^H A))} \quad (2.10)$$

$$\|A\|_\infty = \max_i \left(\sum_{j=1}^n |a_{ij}| \right) \quad (2.11)$$

The process for evaluating the performance of the matrix norms is illustrated as follows. We analyzed the first ten TE_{01p} modes, calculating the error between the analytic solution and the one yielded by different types of norms. We found that all norms allowed finding the resonant frequencies with error levels below 0.01% (Table 2-1). Even so, the 1-norm seems to perform better, though there is only a slight difference with respect to the other two. Still, the 1-norm will be used during the remainder of this dissertation. The frequency response of this approach is shown in Figure 2-2, where it can be seen that even if not all resonant

frequencies yield a value of zero norm, they do correspond with a local minima of the function and so, this approach can be used.

Table 2-1. Resonant frequencies for the first ten TE_{01p} modes, found through the analytic solution and through three different types of matrix norms

p	Analytical 1-Norm				2-Norm			Inf-Norm		
	Frequenc y (GHz)	Frequenc y (GHz)	Error (kHz)	Error (%)	Frequenc y (GHz)	Error (kHz)	Error (%)	Frequenc y (GHz)	Error (kHz)	Error (%)
1	0.7598	0.7599	28.5440	0.0038	0.7599	28.5450	0.0038	0.7599	28.5450	0.0038
2	0.7900	0.7900	55.7820	0.0071	0.7900	55.7880	0.0071	0.7900	55.7860	0.0071
3	0.8380	0.8380	14.1170	0.0017	0.8380	14.8290	0.0018	0.8380	16.6420	0.0020
4	0.9008	0.9009	101.920	0.0113	0.9009	101.920	0.0113	0.9009	101.930	0.0113
5	0.9756	0.9755	120.900	0.0124	0.9755	120.900	0.0124	0.9755	120.890	0.0124
6	1.0599	1.0599	20.6650	0.0019	1.0599	20.9020	0.0020	1.0599	20.0300	0.0019
7	1.1516	1.1518	146.520	0.0127	1.1518	146.530	0.0127	1.1518	146.520	0.0127
8	1.2491	1.2490	157.820	0.0126	1.2490	157.820	0.0126	1.2490	157.820	0.0126
9	1.3511	1.3512	43.8620	0.0032	1.3512	44.6950	0.0033	1.3512	44.8250	0.0033
10	1.4567	1.4569	163.770	0.0112	1.4569	163.780	0.0112	1.4569	163.830	0.0112
Average:			85.3900	0.0078		85.5709	0.0078		85.6818	0.0078
			0		2			3		

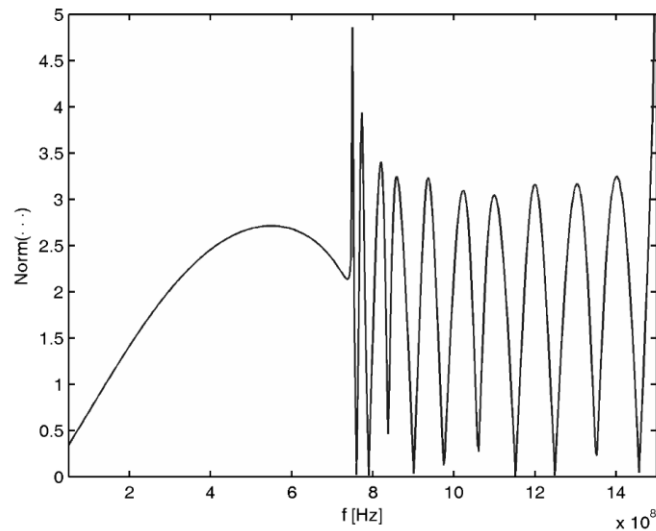


Figure 2-2. Frequency response of circuitual analysis considering the 1-norm

Thus far, lossless materials have been considered. But, a broader scenario requires accommodating the effect of the conductivity that each block may have. The admittance matrices derived from circuital analysis are, hence, modified in the following way: the bottom network is now ruled by eq. (2.12), the top network is now ruled by eq. (2.13) and the middle networks are now ruled by eq. (2.14). The expressions for each integral remain, however, unchanged. It is important to note that eq. (2.14) only shows the formulae for A at each port, and that each one of them has a set of associated admittance matrices (i.e. there is a set of $Y^{ss}, Y^{sc}, Y^{cs}, Y^{cc}$ per each A)

$$A = -\frac{4\gamma_z}{j\omega\mu b^2 \tanh(\gamma_z c)} \quad (2.12)$$

$$\begin{aligned} Y^{ss} &= A I_q^s I_m^s & Y^{sc} &= 0 \\ Y^{cs} &= 0 & Y^{cc} &= A \chi_q I_q^c I_m^c \\ A &= \frac{4\gamma_z}{j\omega\mu b^2 \tanh(\gamma_z c)} \end{aligned} \quad (2.13)$$

$$\begin{aligned} Y^{ss} &= A I_q^s I_m^s & Y^{sc} &= 0 \\ Y^{cs} &= 0 & Y^{cc} &= A \chi_q I_q^c I_m^c \\ A &= \frac{4\gamma_z}{j\omega\mu b^2} \end{aligned}$$

$$\begin{aligned} A_{11} &= -\frac{A}{\tanh(\gamma_z c)} & A_{12} &= \frac{A}{\sinh(\gamma_z c)} \\ A_{21} &= -\frac{A}{\sinh(\gamma_z c)} & A_{22} &= \frac{A}{\tanh(\gamma_z c)} \end{aligned} \quad (2.14)$$

2.2 FITNESS EVALUATION

Every objective function needs the means for assessing its performance. In this case, efforts are focused on establishing a comparison between two field distributions. To achieve this, we used the Peak Signal-to-Noise Ratio (PSNR), which is a technique commonly used for the comparison of images [4]. PSNR is based on the mean squared error, and it can be easily calculated through eq. (2.15), where I is the reference image, i.e. the field distribution we desire to achieve, and K is the test image, i.e. the field distribution generated by the algorithm.

$$\begin{aligned} \text{PSNR}(I, K) &= 10 \log_{10} \left(\frac{\max(I^2)}{\text{SE}} \right) \\ \text{SE} &= \frac{1}{M \cdot N} \sum_{i=0}^{M-1} \sum_{j=0}^{N-1} [I(i, j) - K(i, j)]^2 \end{aligned} \quad (2.15)$$

We now comment on how the PSNR can be used for comparison purposes. Consider a rectangular resonant cavity with a volume of $0.1 \times 0.2 \times 1.2$ [m³]. This resonator is first analyzed assuming that it is uniformly filled with air, i.e. the resonator is empty. Afterwards, the effect of filling it with different materials is boarded, whose relative permittivity are 10, 50, and 100, and focusing on modes TE_{011} , TE_{013} , TE_{016} , TE_{0110} . Finding the resonant frequencies of these modes through commercial software yields valid answers and field distributions that can be easily related to what is expected. But, when the PSNR is calculated against the analytical solution, it is found that the quality of the solutions diminishes for higher modes (Figure 2-3). The cause of this lowered PSNR is shown in Figure 2-4, where a distortion in the field distribution yielded by the commercial software (left) can be easily observed, when compared to the analytic solution (center). The solution provided by the model developed throughout this chapter is plotted in the right. For this example, the TE_{0110} mode is plotted for an empty resonator, and the commercial solution has a PSNR of 21 [dB], whilst the solution found with the model of the dissertation has a PSNR of 50 [dB].

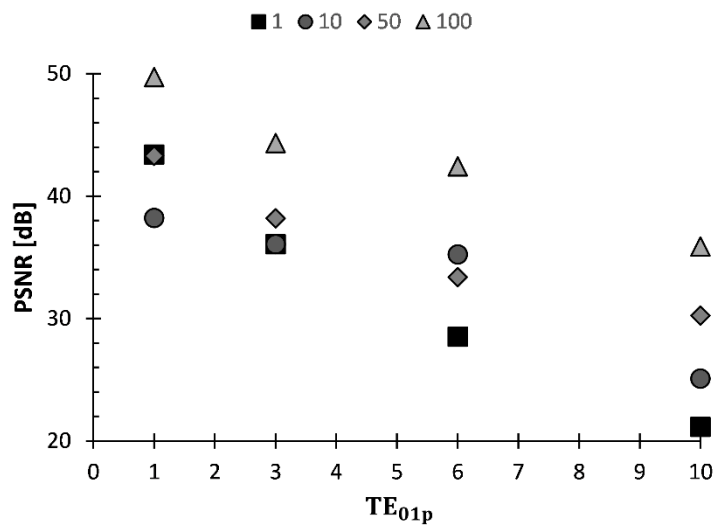


Figure 2-3. PSNR of the solutions provided by commercial software against the analytical solutions, for four different TE_{01p} modes and considering four different values of relative permittivity

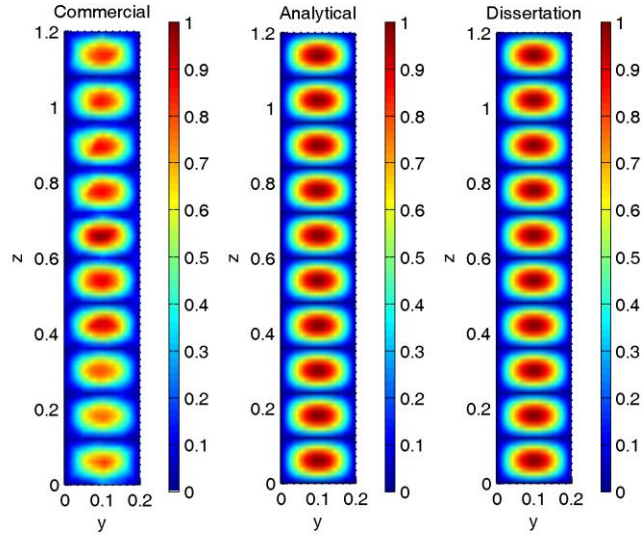


Figure 2-4. Field distribution yielded by commercial software (left, PSNR=21 dB), by the analytic solution (center), and by the model developed throughout this chapter (right, PSNR=50 dB).

2.3 THE OBJECTIVE FUNCTION

As a summary of this chapter, it can be said that the objective function for this dissertation is the one given by eq. (2.16), that depends on the operating frequency (f), and on the height of each one of the N blocks (d_i , see Figure 2-1),

$$\begin{aligned} & \text{Maximize: } F_{\text{obj}}(f, d_i) \\ F_{\text{obj}}(f, d_i) &= \text{PSNR}(E_{\text{desired}}, E_{\text{test}}); i = 1, 2, \dots, N \end{aligned} \quad (2.16)$$

Moreover, E_{desired} represents the desired electric field distribution, which must comply with boundary conditions, whilst E_{test} is the electric field distribution of a given test design (i.e. a given configuration of frequency and block heights). The former, is an input given by the user, and it represents the optimum field distribution. The latter, corresponds to the field distribution inside a test resonator, i.e. inside a design with a given frequency (f) and block heights (c_i), and in order to calculate it the process discussed in the appendix must be followed. It is worth remarking that each one of these blocks require an amplitude parameter whose definition varies according to the number of blocks. The separation equation implies that k_{z_i} depends on the operating frequency and on the mode number considered in the x and y direction. Nonetheless, the latter are the same for all blocks, so k_{z_i} only depends on the operating frequency (f) for a given resonator.

Finding the appropriate operating frequency for a given resonance is rather easy if the resonator is uniformly filled with the same material. However, as discussed in the appendix, whenever it is partially filled, the resonant frequency shifts. Hence, it must be found by other

means, e.g. circuital analysis. The appendix presents details about the stages that must be carried out in order to do so. Nevertheless, this kind of analysis provides multiple solutions, each one of which represents a different resonant mode. So, a strategy must be set into place, such that for any given design, it is able to find as many solutions as possible, generating multiple E_{test} that must be compared against the desired solution (E_{desired}). Figure 2-5 shows an overview of the process that must be followed in order to evaluate the objective function for a particular resonator.

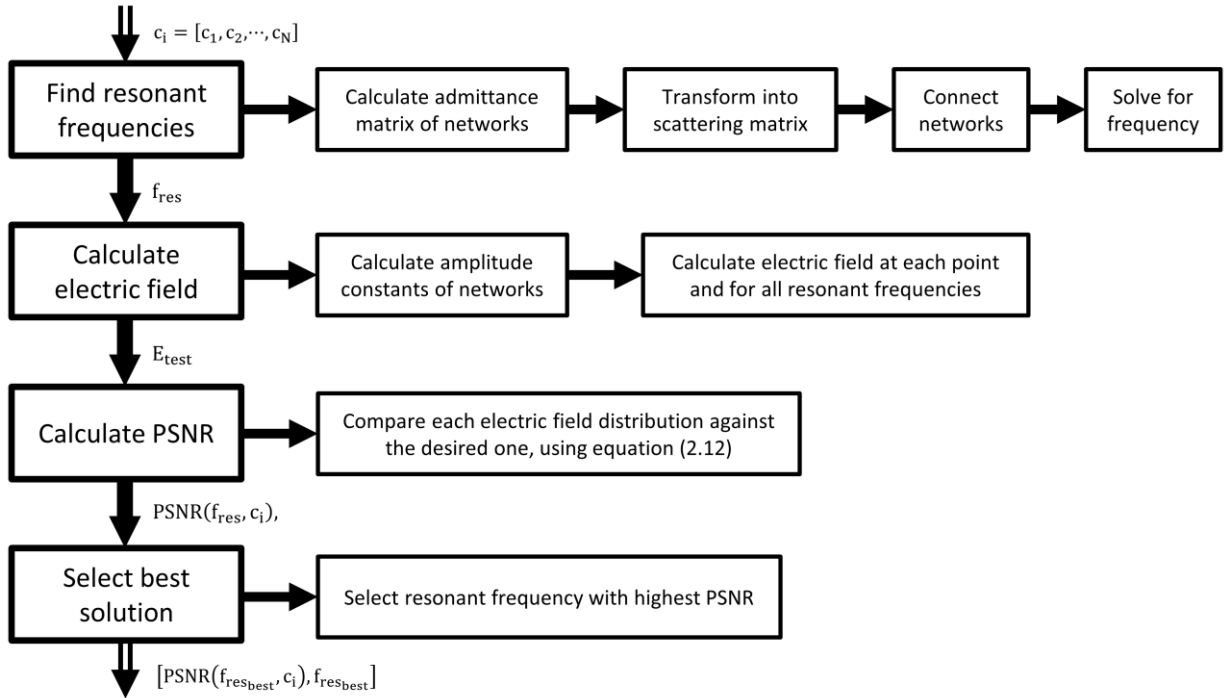


Figure 2-5. Overview of the process required for evaluating the objective function for a given set of network heights (c_i). f_{res} is a vector containing all resonant frequencies found for the resonator, E_{test} contains the information of the electric field distribution at each resonant frequency, and $f_{\text{res}_{\text{best}}}$ is the resonant frequency that yields the electric field with the highest PSNR

2.4 FINAL COMMENTS

Throughout this chapter, the mathematical models related to the dissertation were discussed. An overview of the problem was given, and it was mentioned that more detail can be found in the appendix. We used circuital analysis to study the electromagnetic problem, taking advantage of the segmentation already present in the structure. Furthermore, we established the mathematical model of the admittance matrix for networks with one port at the top face, one at the bottom face, and one at each of them, considering a given transversal mode (i.e. for a fixed value of m and n). The appendix shows the way in which this admittance matrices can be transformed into scattering matrices, and details how to connect them.

We showed that traditional determination of the resonant frequencies was not valid for our case, since it yielded zero for all frequency values (due to rows and columns of the matrix being zero). Hence, we explored an alternative for determining the resonant frequencies through different types of norms, and we found that the 1-norm can be regarded as a valid approach.

Afterwards, we mentioned a strategy for estimating the agreement between the desired electric field distribution, which must comply with boundary conditions, and the electric field distribution of a test design. We selected an approach based on the Peak Signal-to-Noise Ratio (PSNR), since it is traditionally used in imaging. A comparison of the analytic field distribution with the one yielded by commercial software and by the model developed throughout this chapter showed that our approach seems to perform better, reaching a PSNR 29 [dB] higher. Finally, we laid out the objective function that will be used in this dissertation, and summarized the overall process for evaluating it.

The tools for estimating the field distribution for a given scenario have been laid out, and now it is deemed necessary to identify the dielectric properties and the optimization strategy that will be used. This is done in forthcoming chapters.

REFERENCES

- [1] R.F. Harrington, Time-Harmonic Electromagnetic Fields, John Wiley & Sons, Inc., 1961.
- [2] F.L. Penaranda-Foix, J.M. Catala-Civera, Circuital Analysis of Cylindrical Structures Applied to the Electromagnetic Resolution of Resonant Cavities, in: Passiv. Microw. Components Antennas, InTech, 2010: pp. 141–168. doi:10.5772/226.
- [3] F.L. Peñaranda-Foix, Aplicación de la teoría de análisis circuital generalizado a la resolución de problemas de difracción electromagnética, Ph.D. Thesis, Universidad Politécnica de Valencia, 2001. doi:hdl.handle.net/10251/7121.
- [4] Q. Huynh-Thu, M. Ghanbari, Scope of validity of PSNR in image/video quality assessment, Electron. Lett. 44 (2008) 800. doi:10.1049/el:20080522.

3. KNOWING THE SAMPLES

This chapter deals with the experimental component of the dissertation. It relates to the mineral samples (i.e. ores) we considered throughout our research work. Whether it is general information, dielectric properties or exploratory results, it can be found here. The results herein, as well as in most sections of the document, were obtained through a joint work with undergraduate students, who carried out their research under our advisory, so the respective citations are included when appropriate. Moreover, these studies were supported by Vicerrectoría de Investigación y Extensión-UIS, in the framework of Project 5551.

Microwaves can enhance a given process [1–15]. However, their modelling requires solving Maxwell's Equations, which depend on the dielectric properties of the media. Moreover, these properties are not static, so they can vary depending on humidity levels, composition, operating frequency, and temperature [16,17]. This chapter summarizes the evolution of dielectric properties as a function of temperature, for several Colombian samples, so that they can be easily included in simulations. Also, we present data about conditions required for interaction between microwaves and ores, focusing on variables such as exposure time, microwave power, and sieve size. These data were acquired through statistically designed experiments, whose goal was to analyze the effect of different factors (and levels) on gold recovery.

During this chapter, and pursuing a well-defined objectives that are part of the main research objectives described in this dissertation, we selected the following students to join our group as research assistants and complete their undergraduate theses:

Juan Abril and Julián Gómez [18]

Roy Aguirre and William Botero
[19]

Danilo Bernal, Sergio Garnica and Yamit Reslen
[20]

Manuel Díaz and Marcelo Rueda
[22]

Marly Ortiz and Dirney Jurado [21]

We want to declare our deepest appreciation to them, for their dedication and effort in contributing to some of the results discussed in this chapter. Also, to Professor Dr. Felipe Peñaranda, for his help and guidance during the internship, and to Mr. Ambrosio Carrillo, for all his help regarding traditional processing of the samples.

3.1 SAMPLES CONSIDERED DURING THE RESEARCH

Before delving into any details, it is important to summarize the minerals we used. We created one group for measuring dielectric properties (Table 3-1) and one for experimental testing (Table 3-2). The former consisted of six different samples, and one of them was analyzed for three different sieves since they were visually different (please refer to Appendix A for a full description of the samples, including X-ray diffraction and fluorescence). The latter considered minerals from southern Bolivar (“Juan Blanco”) and from Santander (the remaining ones), and it was done to obtain exploratory results about the feasibility of using microwaves for treating local samples. It was supported by undergraduate students whose research was advised, and included a research about conceptual engineering [18].

Table 3-1. Summary of samples used during the research, including their starting (St.) and ending (En.) dielectric properties at room temperature

#	Sample's Name	Sieve	Grade [g/ton]	Iron [%]	Sulfur [%]	St. ϵ'	St. ϵ''	En. ϵ'	En. ϵ''
1	Juan Blanco	100	0	18.35	10.72	5.19	0.8818	7.92	1.0925
		200	--	14.03	6.57	2.61	0.0512	2.46	0.0298
		-200	1	9.17	4.27	2.11	0.0239	1.83	0.0117
2	M9	100	4	30.67	23.51	6.97	1.4388	7.77	1.6692
3	Ismael	-170	3	13.09	0.01	2.19	0.0405	1.99	0.0303
4	Carlos Arias	100	17	24.09	17.11	4.46	0.4068	5.37	0.5499
5	Core from El Volcán	-120	3	8.37	0.45	2.78	0.0345	2.50	0.0266
6	Rock from Segovia, Antioquia	-120	1	2.06	0.95	2.81	0.0272	2.54	0.0190

Table 3-2. Summary of mineral samples used in experiments with undergraduate students

#	Name	Sieve	Grade [g/ton]	Students	Reference
7	Juan Blanco	170	5.0	Bernal, D.; Garnica, S.; Reslen, Y.	[20]
8	Reina de Oro	100	46.0	Diaz, M; Rueda, M.	[22]
9	Tajo Abierto	100	3.3	Aguirre, R; Botero, W.	[19]

3.2 METHODOLOGY

3.2.1 Experimental testing

We began by running these experiments, based on the equipment and funding available at the moment (internal project 5551). We performed three different trials to observe the feasibility of using microwaves for treating local minerals, as well as for identifying the effect of certain factors on gold recovery. In all cases, the general procedure was: determine

appropriate levels for each factor (through preliminary tests), run the experiments (using domestic microwave ovens), and analyze the resulting data.

Factorial design of experiments was carried out for all minerals, considering the grade of the ore (i.e. the amount of gold recovered per ton of ore) as the response variable. Samples seven and nine considered three factors and two levels. Additionally, sample eight considered a multilevel design, comprised of two factors with two levels and a factor with four levels. Each study was carried out for mineral samples of different mines, using three replicates. They considered diverse factors, but they all included exposure time. Data were then analyzed using an evaluation license of Statgraphics.

3.2.1.1 Mine “Juan Blanco” (Assigned to: Bernal, D.; Garnica, S. and Reslen, Y.) [20]

Samples from a mine known as “Juan Blanco”, were considered during this DOE. Three replicates of a 2^3 factorial experiment, with three factors and two levels, was carried out (Table 3-3). It is worth mentioning that the levels shown for the second factor (i.e. grade) correspond to the gold concentration at the outer zone (low level) and at the vein (high level). Also, microwaves were applied in intervals of seven minutes, allowing an extra minute for manual mixing in order to avoid sintering, and striving to oxygenate the sample while avoiding hot spots. Each test was run with 40 grams of mineral and in random order.

Table 3-3. Factors and levels used with Bernal et al. Exposure time was split into seven minutes intervals, with one additional minute for manual mixing

Factor	Low Level	High Level
Exposure Time [min]	28	42
Grade [g/ton]	3	5
Sieve	50	170

3.2.1.2 Mine “Reina de Oro” (Assigned to: Diaz, M. and Rueda, M.) [22]

A concentrated ore from a mine known as "Reina de Oro", with a grade of 46 grams of gold per ton of ore, was used during this research. Again, we considered three factors, but this time one of them had four levels (Table 3-4), so we considered a multilevel factorial DOE (with tests ran in random order). Microwaves were applied in intervals of six minutes, with three additional minutes for manual mixing, and a firebrick was included to reduce heat losses on the sample. Moreover, a preliminary smelting test was carried out, using one sample roasted traditionally, and two samples roasted by microwaves.

Table 3-4. Factors and levels used with Diaz et al. Exposure time was split into six minutes intervals, with three additional minute for manual mixing

Factor	Level 1	Level 2	Level 3	Level 4
SiC [g]	0	12	--	--
Exposure Time [min]	24	36	--	--
Sample Holder	Clay 1	Clay 2	SiC	Graphite

3.2.1.3 Mine “Tajo Abierto”, (Assigned to: Aguirre, R. and Botero, W.) [19]

In a similar fashion as with Bernal et al., three replicates of a 2^3 factorial experiment, with three factors and two levels per factor, was used in this research (Table 3-5). Tests were run randomly and microwaves were applied, in five minutes intervals, to a sample from a mine known as “Tajo Abierto”. The output power of the microwave oven was varied using its internal controller.

Table 3-5. Factors and levels used with Aguirre et al. Exposure time was split into five minutes intervals, with one additional minute for manual mixing

Factor	Low Level	High Level
Sample’s Mass [g]	30	60
Output Power [W]	600	1000
Exposure Time [min]	25	40

3.2.2 Dielectric properties

Based on the good results achieved during the prior stage, it was required to analyze the evolution of the complex permittivity as temperature increased. For this, and considering that the University does not have the required labs for this task, we did a joint work at the ITACA institute (Universitat Politècnica de València, Spain) through an internship and under the guidance of Professor Dr. Felipe Peñaranda. We followed the procedure laid out in Figure 3-1 to obtain values for the complex permittivity as a function of temperature, using a dielectric kit (DK) and a cylindrical cavity (CC), both developed at the ITACA institute. The first one is able to calculate the complex permittivity of a sample located inside a vial, at a given temperature, and can be used for measuring powders, liquids and solids (provided they are machined to match the vial's shape) [23]. The second one is able to measure the resonant frequency (f) and the quality factor (Q) of a cylindrical cavity in real time, while heating the sample, and it is similar to the one developed in [24]. Combining this information, and using resonant frequency and quality factor readings for air, interpolations can be calculated and plots can be generated for each mineral. But, for the sake of space we only report the final plots and the frequency and quality factor regression models.

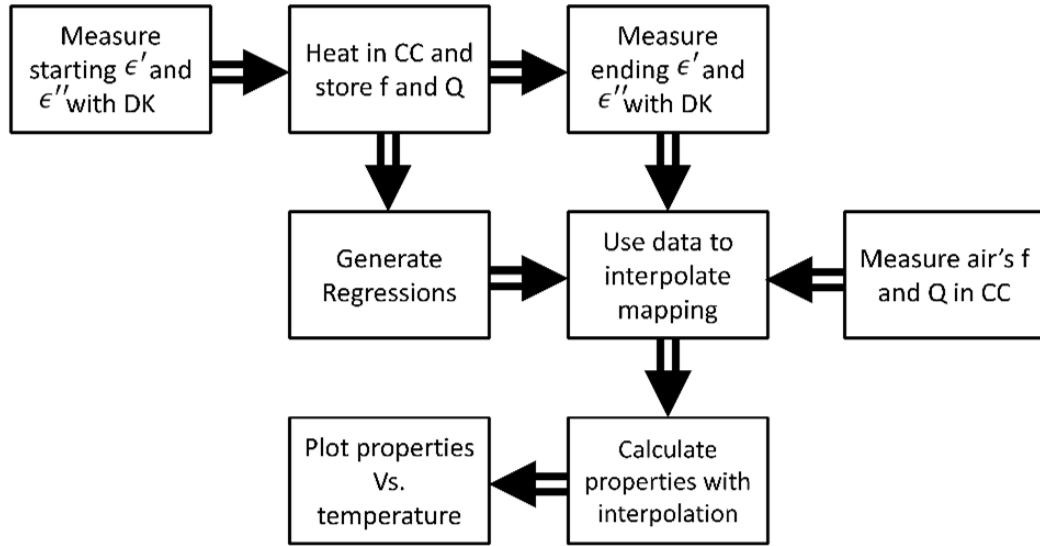


Figure 3-1. General procedure for obtaining dielectric properties as a function of temperature. ϵ' and ϵ'' are the real and imaginary part of the complex permittivity (respectively); CC means cylindrical cavity; f means frequency; Q is the quality factor of the resonator; DK stands for dielectric kit.

Different models with variable orders were tested for each data set (Table 3-6). We looked for the order where the R-Square (R^2), sum of squares due to error (SSE), and the root mean squared error (RMSE) values stabilized. As an example consider the data shown from Figure 3-2 to Figure 3-4. In the case of the Fourier fit all responses tend to stabilize at the sixth and fifth orders (for heating and cooling, respectively) while the Gaussian fit stabilizes at the fifth and fourth ones. Small improvements could be obtained by increasing the orders further, but we decided to discard them in order to keep the fits as simple as possible.

Table 3-6. Regression models, order N , used during the research.

Fit Name	General Expression
Fourier	$a_0 + \sum_{i=1}^N a_i \cdot \cos(i \cdot x \cdot w) + b_i \cdot \sin(i \cdot x \cdot w) \quad (1)$
Gaussian	$\sum_{i=1}^N a_i \cdot e^{-\left(\frac{x-b_i}{c_i}\right)^2} \quad (2)$
Polynomial	$\sum_{i=1}^{N+1} p_i \cdot x^{N+1-i} \quad (3)$
Exponential	$\sum_{i=1}^N a_i \cdot e^{b_i \cdot x} \quad (4)$

Fit Name	General Expression
Sum of Sin	$\sum_{i=1}^N a_i \cdot \sin(b_i \cdot x + c_i) \quad (5)$

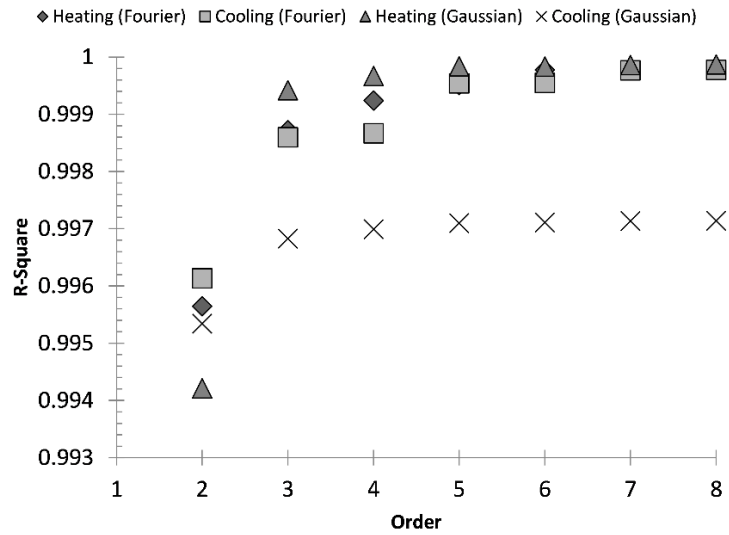


Figure 3-2. R² as a function of the order used for the fitting model

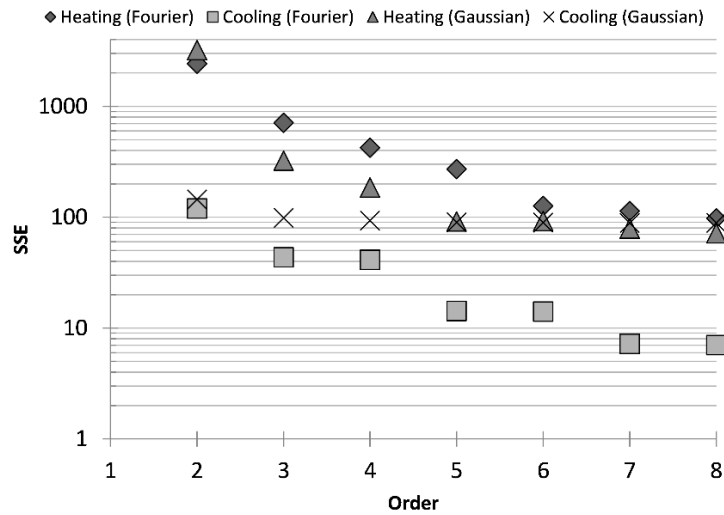


Figure 3-3. SSE as a function of the order used for the fitting model

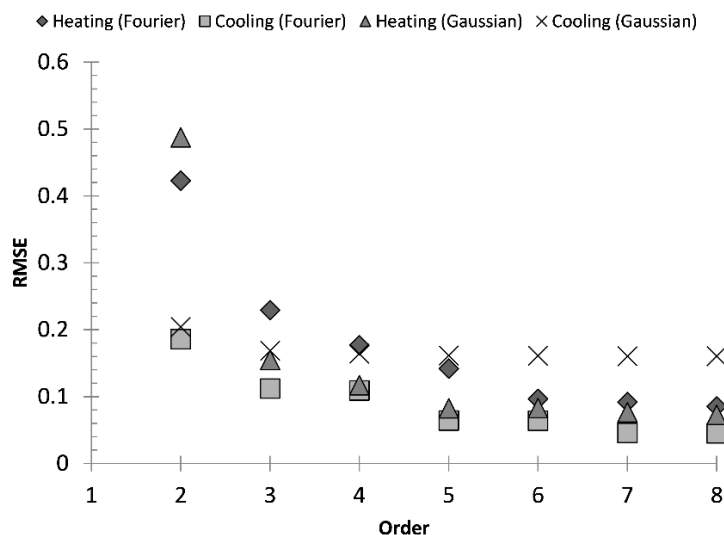


Figure 3-4. RMSE as a function of the order used for the fitting model

3.3 RESULTS

3.3.1 Experimental testing

A brief comment is now made about the experiments carried out with each mineral sample. In a general sense, data report interesting information. In all cases, exposure time had a positive effect on gold recovery. Likewise, the remaining factors also affected the experiments positively (i.e. more gold was recovered when using the high levels of the factors). Furthermore, normal probability and residual plots revealed no problems with normality assumption or with residuals variance (Figure 3-5 – Figure 3-7). The appendix shows the aforementioned information, as well as detailed plots of the main effects and of those due to the interaction between factors. Also, the reader will find ANOVA tables of the data.

Regarding “Juan Blanco”, we found that all three factors significantly affect gold recovery (Figure 3-5). Moreover, there is an important interaction between the type of mineral and sieve size. The remaining two-factor interactions do not yield enough information as to consider their effect significant. The three factor interaction can be safely disregarded for this mineral. Data reveal that the mean absolute error (MAE), i.e. the average value of the residuals, was 0.32. Moreover, the P-value of the Durbin-Watson (DW) statistic test was of 22.6%, indicating no significant correlation of the residuals, at the 5% significance level.

In the case of “Reina de Oro”, we found that all factors and their interactions exhibit a significant effect on gold recovery. Still, the one that yielded the highest relation, by far, was the interaction between Silicon Carbide and the Sample Holder used (Figure 3-6). For these

tests, MAE was 3.11 and the DW statistic test reported a P-value of 73%. Hence, there is no significant correlation of the residuals, at the 5% significance level.

The final mineral sample, “Tajo Abierto”, revealed that the chosen factors affect gold recovery almost independently, for a significance level of 5% (Figure 3-7). Nonetheless, mass yielded the highest effect, while microwave power yielded the lowest one. This time, MAE was 0.46. Once again, the DW statistic test was way above (80.7%) the limit of the significance level. Hence, there is no significant correlation of the residuals, for the tested minerals, at the 5% significance level.

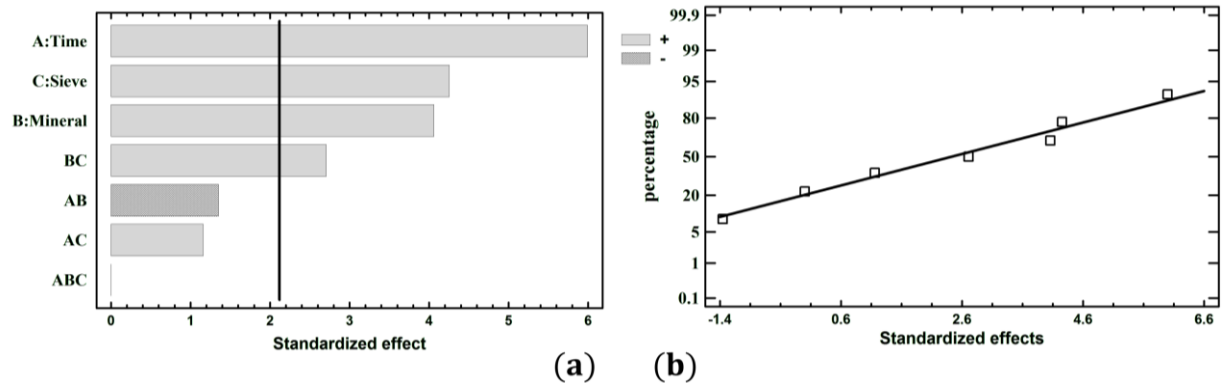


Figure 3-5. Pareto chart (a) and normal probability plot (b) for mine “Juan Blanco”

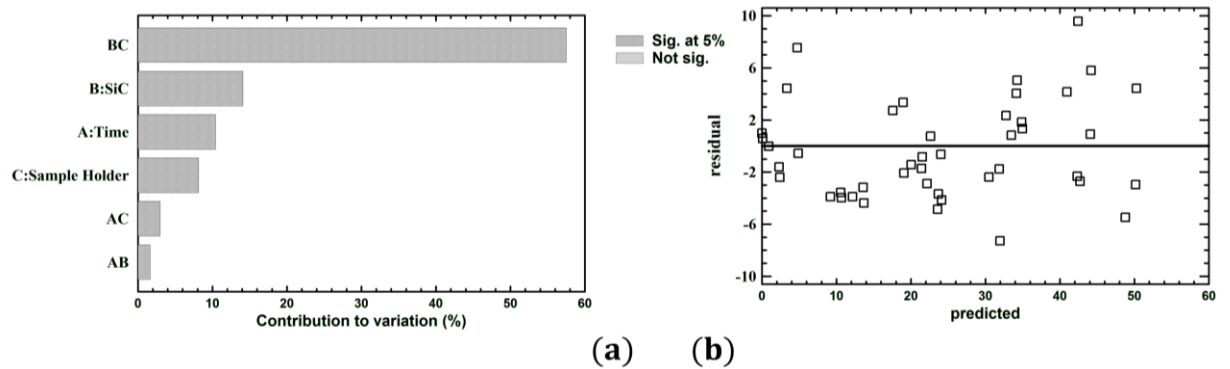


Figure 3-6. Pareto chart (a) and residuals plot (b) for mine “Reina de Oro”

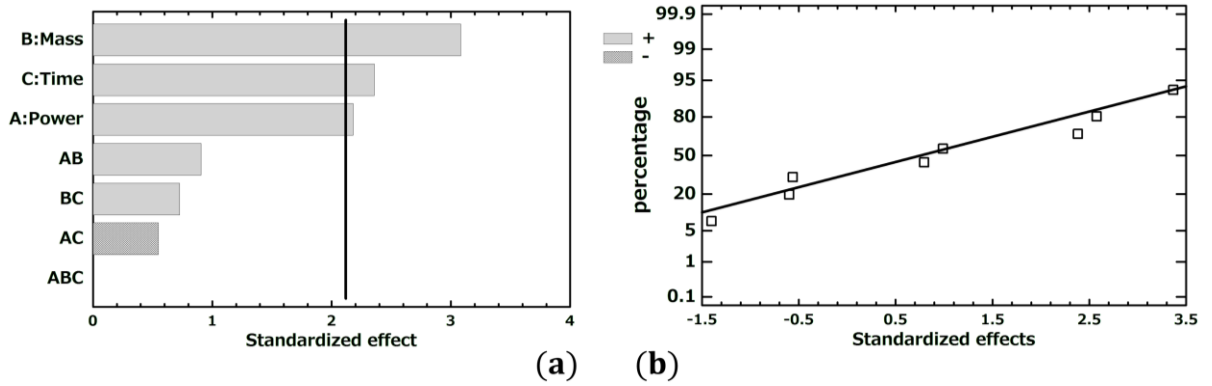


Figure 3-7. Pareto chart (a) and normal probability plot (b) for mine “Tajo Abierto”

Microwaves hold a great potential in terms of processing time and energy consumption, since reductions over 68% (for time) and over 81% (for energy) were always possible (Table 3-7). It is worth noting that during the work with Diaz and Rueda, a recovery margin of 119% was achieved, but this simply means that the sample was better roasted by microwaves than by the traditional approach. An additional argument for this is the fact that during this work we used silicon carbide as a thermal enhancer, thus making it easier to increase the temperature in the sample. Moreover, we verified that microwaves successfully roasted the mineral, removing all the pyrite and allowing the formation of hematite (Table 3-8).

Table 3-7. Resulting data for the traditional approach and the three experiments carried out. TR stands for time reduction, ER stands for energy reduction, and MR is the maximum gold recovery achieved. The high percentage of the second experiment means that the sample was better roasted by microwaves than through the traditional approach

Approach	Time [min]	Energy [kWh]	TR	ER	MR
Traditional	160	5.20	--	--	--
Bernal et al.	47	0.62	71%	88%	90%
Diaz and Rueda	51	1.00	68%	81%	119%
Aguirre and Botero	47	0.95	71%	82%	90%

Table 3-8. Mineral composition before and after roasting for “Juan Blanco”, sieve: 170

Compound	Before	After
Quartz (SiO ₂)	41.9%	24.6%
Moscovite (KAl ₂ (Si, Al) ₄ O ₁₀ (OH) ₂)	15.9%	--
Pyrite (FeS ₂)	29.1%	--
Diaoyudaoite (Na ₂ Al ₂₂ O ₃₄)	3.8%	3.0%
Magnetite (Fe ₃ O ₄)	0.3%	--
Erdite (NaFeS ₂ ·H ₂ O)	0.2%	--
Arsenolite (As ₄ O ₆)	0.6%	--
Hematite (Fe ₂ O ₃)	--	47.7%
Others	8.2%	24.7%

3.3.2 Dielectric properties

The grade (i.e. gold concentration), the iron and sulfur content, and the dielectric properties (at room temperature) of each sample are given in Table 3-1. Please note that sample three has virtually no sulfur, and that samples five and six have low sulfur content compared to the others. As an additional detail, and striving to establish differences between the minerals, we show the five most abundant elements for each sample (Table 3-9). Here, it is worth noting too that iron, silicon and aluminum are present in all the samples, and that the sulfur content in samples three, five and six is so low that it is not among the top five elements (this also applies to sieve: -200 of sample number one, and in the case of sieve: 200 it is the least abundant of the five elements).

Table 3-9. Five most abundant elements for each sample, where JB: Juan Blanco; IS: Ismael; CA: Carlos Arias; CV: Core from El Volcán; RS: Rock from Segovia, Antioquia. The sieve size is given by the letter S and the number next to it

Element	JB S100	JB S200	JB S-200	M9 S100	IS S-170	CA S100	CV S-120	RS S-120
Fe	18.35%	14.03%	9.17%	30.67%	13.09%	24.09%	8.37%	2.06%
Si	14.87%	18.57%	17.98%	14.29%	20.26%	23.43%	22.03%	22.56%
Al	11.02%	14.38%	13.69%	0.60%	11.15%	2.84%	8.56%	9.10%
S	10.72%	6.57%	--	23.51%	--	17.11%	--	--
Pb	6.50%	--	5.72%	--	--	--	--	--
K	--	7.87%	8.94%	--	4.75%	2.04%	7.29%	5.06%
Cu	--	--	--	0.48%	--	--	--	--
As	--	--	--	--	1.55%	--	--	--
Ti	--	--	--	--	--	--	--	--
Mg	--	--	--	--	--	--	1.04%	--
Ca	--	--	--	--	--	--	--	6.46%
Na	--	--	--	--	--	--	--	--
Zn	--	--	--	--	--	--	--	--

We measured the complex permittivity of the three sieves of sample number one, using ITACA's dielectric kit. The dielectric constant decreased about 80% and the loss factor did so in about 97% (Figure 3-8). This relates to the change in composition (Table 3-9), which in turn affects heating (see below).

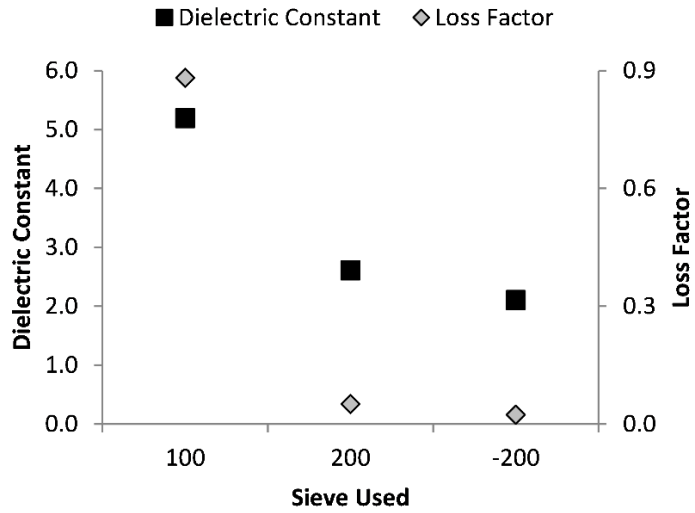


Figure 3-8. Effect of sieve size on the complex permittivity for mineral “Juan Blanco” at room temperature

At some temperatures, complex permittivity remain stable (e.g. between 500 °C and 600 °C) unless the applied power is increased, so it actually depends on time and temperature (Figure 3-9). However, this kind of plot can become awkward and perspective can be easily lost. Nevertheless, the information can be projected into a 2D view without loss of generality, where only the variation as a function of temperature is shown (Figure 3-10). So, from this point onwards, that will be the kind of plot used.

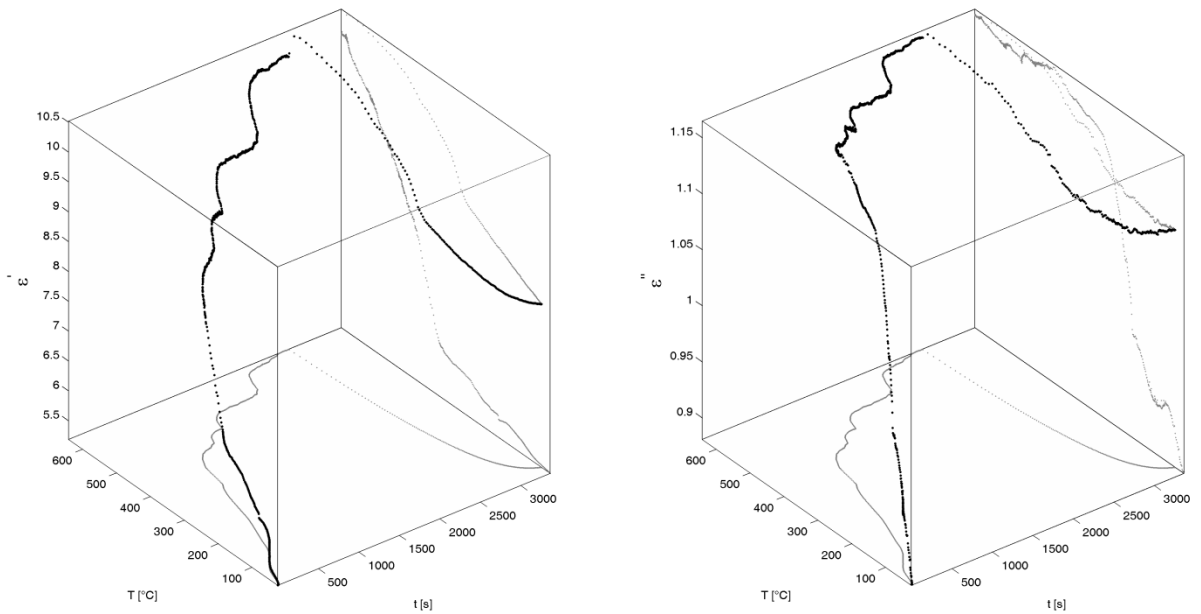


Figure 3-9. Real (left) and imaginary (right) components of the complex permittivity for "Juan Blanco" sieve: 100, as a function of temperature and time

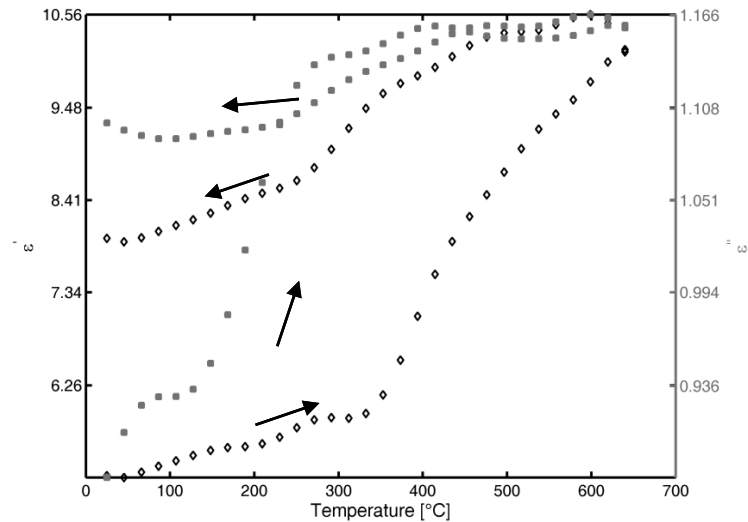


Figure 3-10. Dielectric properties as a function of temperature for "Juan Blanco", sieve: 100

A visual inspection of the three sieves from "Juan Blanco" revealed that the first one (sieve: 100) successfully roasted during the test and varied with temperature in a direct manner. Its dielectric constant and loss factor increased by 52% and 24%, respectively. Moreover, there was a boom for dielectric constant around 350°C and for loss factor around 120°C (Figure 3-10). The second one (sieve: 200), however, slightly changed color and its dielectric constant and loss factor decreased by 6% and 42%, respectively (Figure 3-11). The final one (sieve: -200), remained almost the same (the only change was due to evaporation of the sample's humidity) and the dielectric constant and loss factor decreased by 13% and 51%, respectively (Figure 3-12). Thus, and considering the data given in Table 3-1, we think this reduction in the affinity of the sample to microwaves may be associated with the decreasing concentration of sulfur as the mineral is ground more finely.

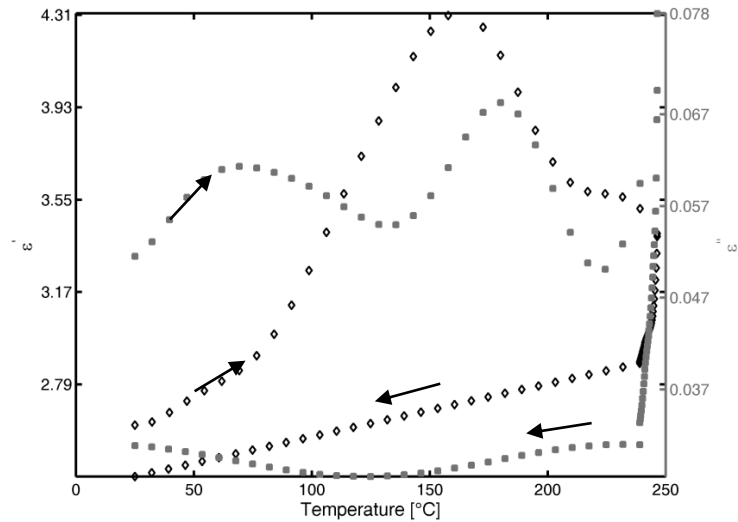


Figure 3-11. Dielectric properties as a function of temperature for "Juan Blanco", sieve: 200

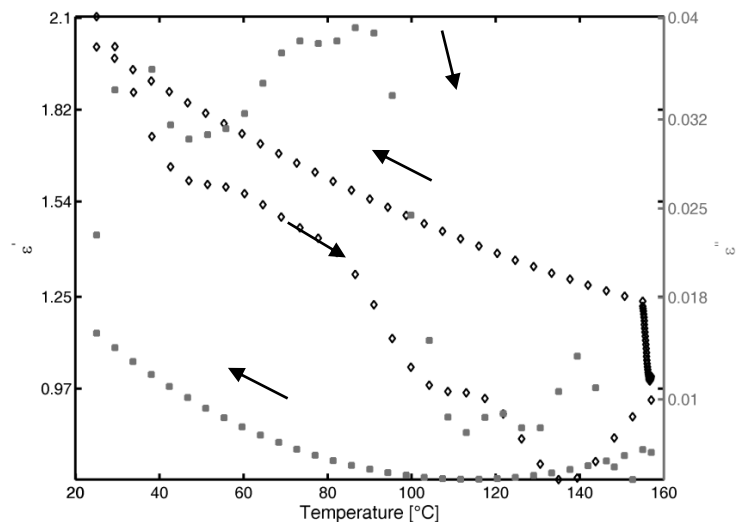


Figure 3-12. Dielectric properties as a function of temperature for "Juan Blanco", sieve: -200

Samples two and four (i.e. "M9" and "Carlos Arias", respectively) successfully roasted, and their dielectric constants and loss factors increased by 12% and 16%, and by 21% and 35%, respectively. However, in the first case roasting occurred around 400°C and in the second case it was around 500°C. After the temperature increased further, the properties of the remaining compounds in both samples changed behavior, quickly decaying and thus reducing the affinity to microwaves (Figure 3-13 and Figure 3-14). A comparison of the compounds in the sample verified that these three minerals roasted to some extent, as can be seen from the comparison shown in Table 3-10, Table 3-11, and Table 3-12, where in all cases the sulfur-based compounds diminished.

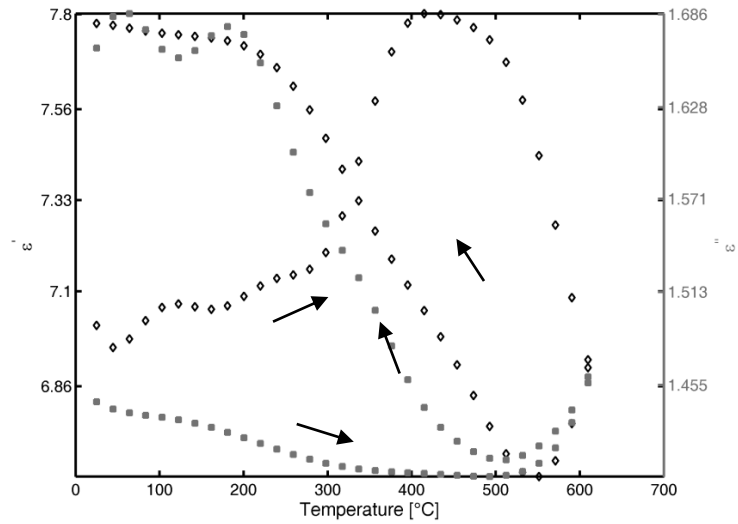


Figure 3-13. Dielectric properties as a function of temperature for "M9", sieve: 100

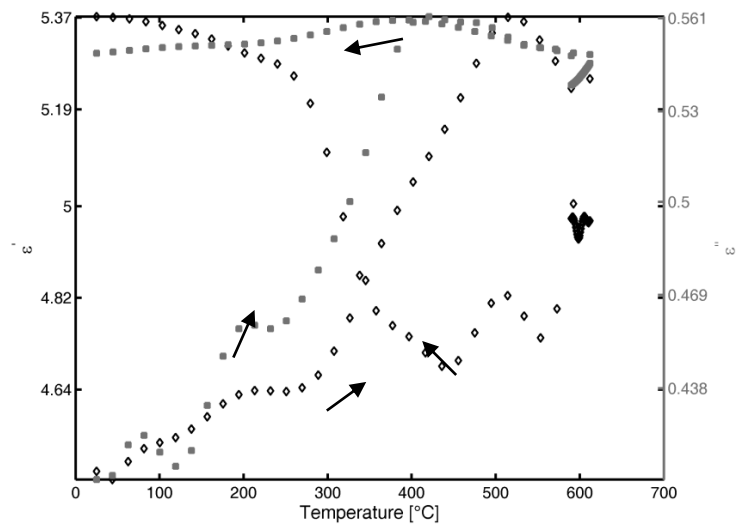


Figure 3-14. Dielectric properties as a function of temperature for "Carlos Arias", sieve: 100

Table 3-10. Mineral composition before and after roasting for "Juan Blanco", sieve: 100. N.Q.: Not Quantifiable

Compound	Before	After
Quartz (SiO ₂)	18.1%	14.0%
Moscovite (KAl ₂ (Si, Al) ₄ O ₁₀ (OH) ₂)	17.5%	20.1%
Pyrite (FeS ₂)	26.7%	12.8%
Mackinawita (FeS)	2.2%	1.5%
Galena (PbS)	<1.0%	<1.0%
Arsenopyrite (FeAsS)	N.Q.	--
Anglesite (Pb(SO ₄))	3.1%	--
Sphalerite (ZnO)	--	<1.0%

Pyrrhotite ($\text{Fe}_{0.95}\text{S}_{1.05}$)	--	1.4%
Spinel ($\text{Mg}_{1.01}\text{Fe}_{1.77}\text{Al}_{2.22}\text{O}_4$)	--	1.9%
Melanterite ($(\text{Fe}, \text{Cu}, \text{Zn})\text{SO}_4 \cdot 7\text{H}_2\text{O}$)	--	1.9%
Zincocopiapite ($\text{ZnFe}_4(\text{SO}_4)_6(\text{OH})_2 \cdot 18\text{H}_2\text{O}$)	--	N.Q.
Anatase (TiO_2)	--	<1.0%
Others	31.6%	44.3%

Table 3-11. Mineral composition before and after roasting for “M9”, 100. N.Q.: Not Quantifiable

Compound	Before	After
Quartz (SiO_2)	38.7%	27.1%
Moscovite ($\text{KAl}_2(\text{Si}, \text{Al})_4\text{O}_{10}(\text{OH})_2$)	9.8%	--
Pyrite (FeS_2)	31.2%	25.0%
Sphalerite (ZnO)	N.Q.	--
Pyrrhotite (Fe_7S_8)	--	16.0%
Others	20.3%	31.9%

Table 3-12. Mineral composition before and after roasting for “Carlos Arias”, sieve: 100

Compound	Before	After
Quartz (SiO_2)	46.1%	47.0%
Moscovite ($\text{KAl}_2(\text{Si}, \text{Al})_4\text{O}_{10}(\text{OH})_2$)	10.9%	6.8%
Pyrite (FeS_2)	17.2%	13.9%
Calcite ($\text{Ca}(\text{CO}_3)$)	1.3%	2.0%
Microcline (KAlSi_3O_8)	2.1%	6.9%
Pyrrhotite ($\text{Fe}_{0.95}\text{S}_{1.05}$)	--	9.1%
Others	22.4%	14.3%

The remaining samples have lower dielectric properties and, thus, temperature did not increase over 230°C, so they did not roast. The dielectric constants and the loss factors respectively decreased by 9% and 25% ("Ismael", Figure 3-15), by 10% and 23% ("Core from El Volcán", Figure 3-16), and by 10% and 30% ("Rock from Segovia, Antioquia", Figure 3-17).

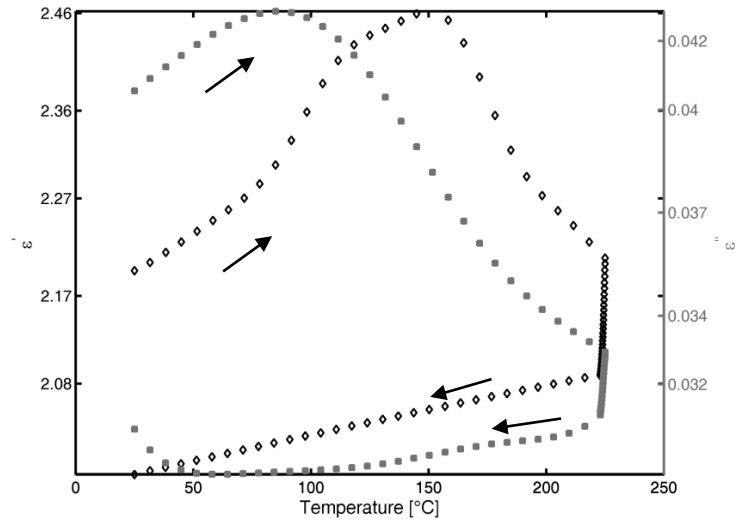


Figure 3-15. Dielectric properties as a function of temperature for "Ismael", sieve: -170

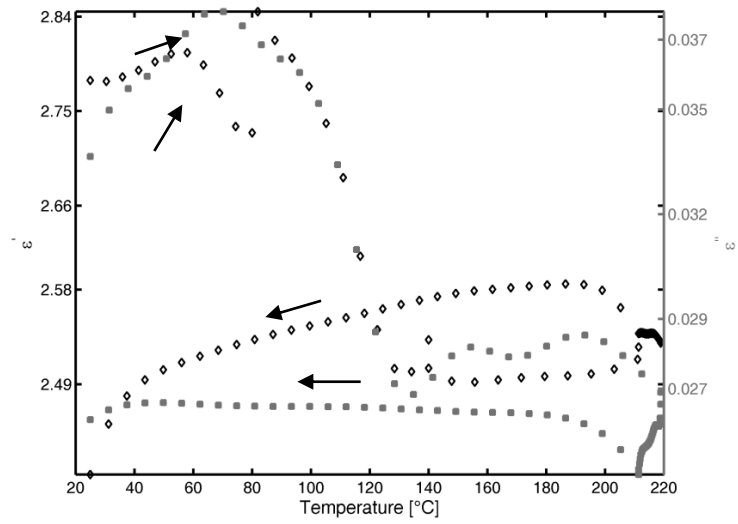


Figure 3-16. Dielectric properties as a function of temperature for "Core from El Volcán", sieve: -120

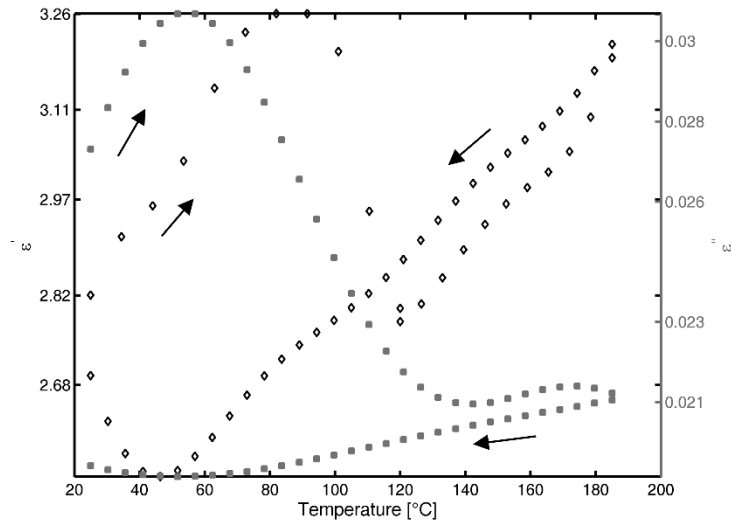


Figure 3-17. Dielectric properties as a function of temperature for "Rock from Segovia, Antioquia", sieve: -120

3.3.3 Further results

Besides the basic feasibility experiments shown above, we analyzed different aspects of microwave processing. Here, only some of the most relevant data is shown, for the sake of space, but the reader is encouraged to consult the full reports of each undergraduate experimental research. Bernal et al. explored the effect of reducing the microwave applicator, on the maximum temperature achieved by a water load. We found temperature increments of up to 12°C after an exposure of 1 minute, but reductions over 18 cm led to a quick decrease in maximum temperature, mainly due to the electromagnetic field being unable to propagate at those dimensions (Figure 3-18). Moreover, care must be taken when diminishing an applicator, since the higher energy concentration facilitate the formation of electric arcs [20].

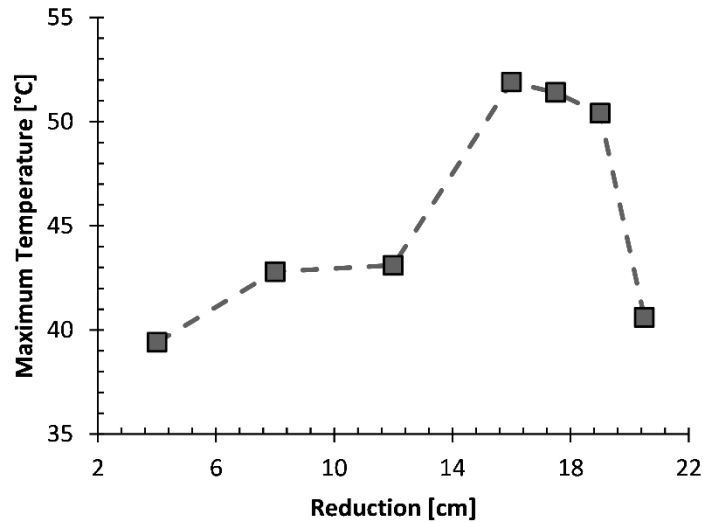


Figure 3-18. Effect of cavity reduction on maximum temperature for a water load. Based on [20]

Diaz and Rueda focused on measuring the temperature inside the sample, and on exploring the feasibility of smelting the sample with microwaves [22]. On the first regard, we considered a setup using a firebrick and the temperature system of a standard electric furnace (Figure 3-19), and we analyzed the effect of adding silicon carbide (SiC) to the sample. We observed that if no carbide is added, the sample holders made of graphite and SiC allow for higher temperatures inside the ore (Figure 3-20). But, if added, the carbide begins competing with the sample holders, neglecting any improvement. However, this hindrance was not present for the clay-based sample holders, due to their lesser natural affinity to microwaves, and thus temperature increased almost twice (Figure 3-21).

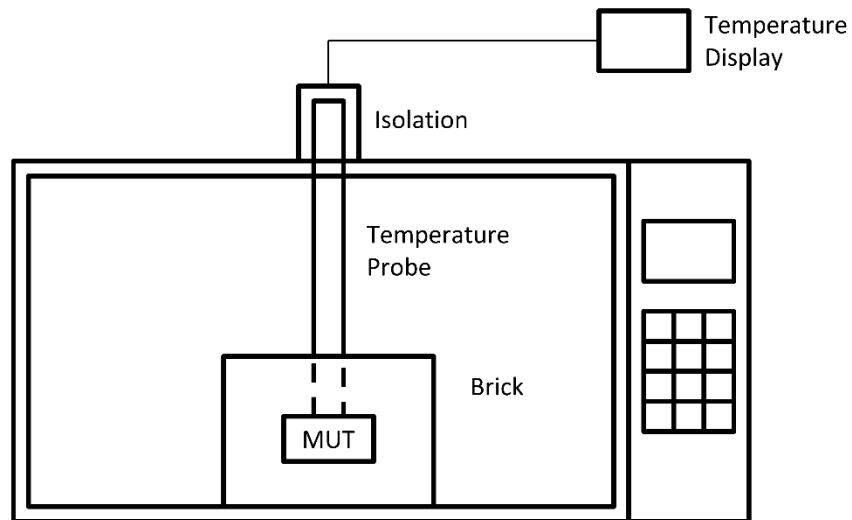


Figure 3-19. Experimental setup for temperature measurement. Based on [22]

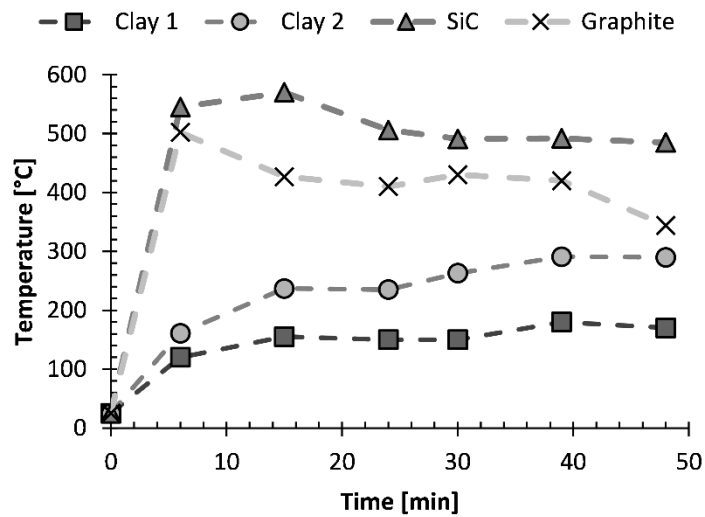


Figure 3-20. Temperature [°C] evolution for different sample holders, with no silicon carbide. Based on [22]

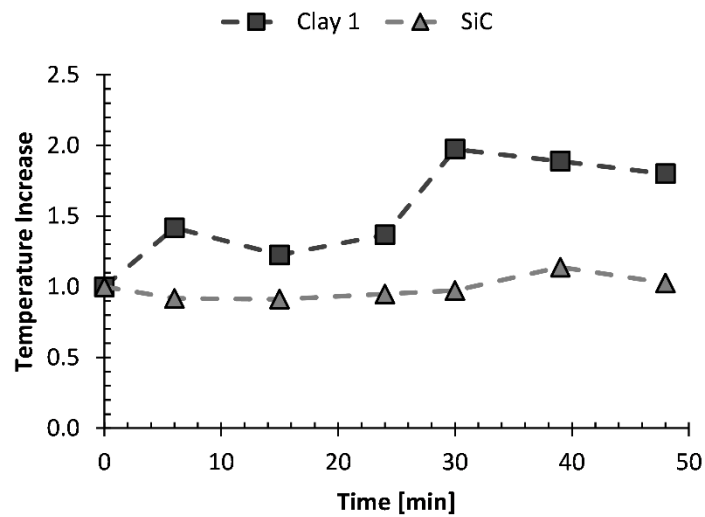


Figure 3-21. Temperature ratio evolution for two sample holders, considering silicon carbide. Based on [22]

An exploratory test was carried out regarding microwave smelting. We chose three samples, one roasted by traditional means and two by microwaves, and at least for this mineral, results were satisfactory (Table 3-13). Two things are worth mentioning here. The first one is that reagents are still used to facilitate the smelting process, so there is not really a gain in this sense. However, the second remark is that the whole smelting process (starting at room temperature) only took 20 minutes, as opposed to 240 minutes required in an electric furnace, so a processing time reduction of about 92% can be easily achieved, thus leading to possible economic and environmental benefits. Even though an energy reading was not registered for the smelting (mainly due to the exploratory mean of the tests), it is fairly obvious that an

energy reduction in the order of the one achieved for roasting (or even greater) can be easily achieved.

Table 3-13. Grade [g/ton] and recovery margin (RM) of microwave (MS) and traditionally (TS) smelted samples, using ores with different roasting conditions. Based on [22]

Sample	MS [g/ton]	TS [g/ton]	RM
Traditionally roasted	43.7	46.0	95%
Roasted using SiC sample-holder and thermal enhancer	36.7	36.7	100%
Roasted using graphite sample-holder and no thermal enhancer	40.0	40.0	100%

Aguirre and Botero strived to improve a temperature measurement system that allowed readings at five different points in the sample [19], whose block diagram is shown in Figure 3-22. The PC runs a graphical user interface (GUI), that allows modification of the parameters (e.g. heating cycle, sensing time, etc.), and that is also in charge of controlling the system. The information goes through a DAQ and some protections for keeping out any current that could be induced during the process. Finally, the PCB enables the magnetron or the thermocouples (but never both, for safety reasons). Thus, temperature is read only when the magnetron is disabled and the data go to a signal conditioning stage, that defines the sensing range and that also filters noise. This information is then gathered by the PCB and sent to the computer via the DAQ. A visualization stage shows the current thermocouple, and indicates if there is an error on the device. The system was calibrated using a hot plate, with a maximum temperature of 300 °C (Figure 3-23), and it was used to register the temperature evolution at five different points during the tests (Figure 3-24).

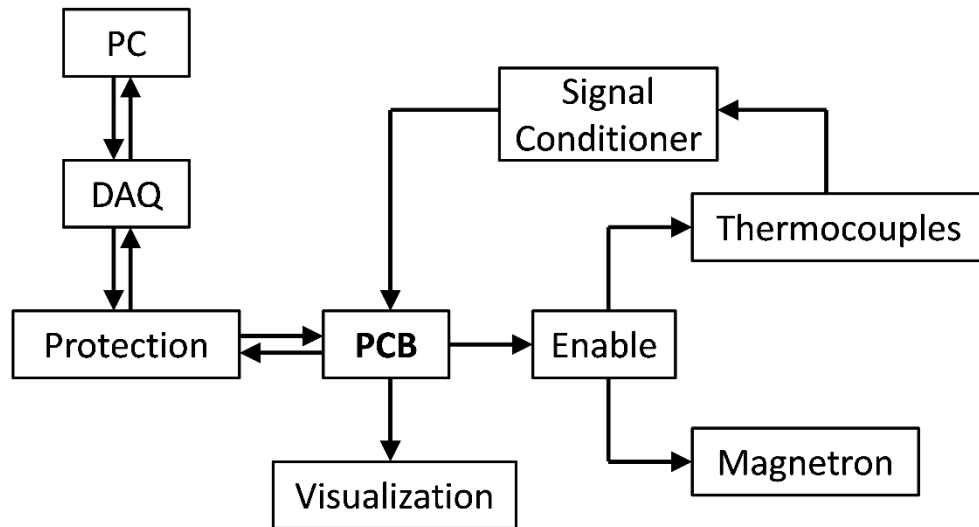


Figure 3-22. Block diagram of the multi-point temperature measurement system. Based on [19]

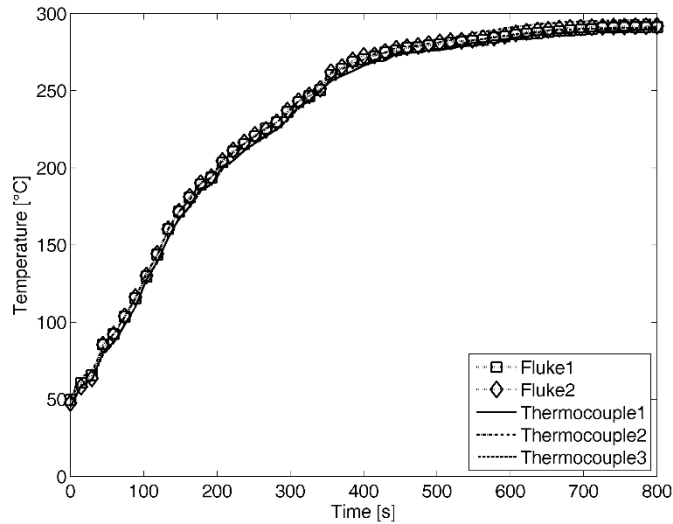


Figure 3-23. Temperature readings of a hot plate after calibration. Based on [19]

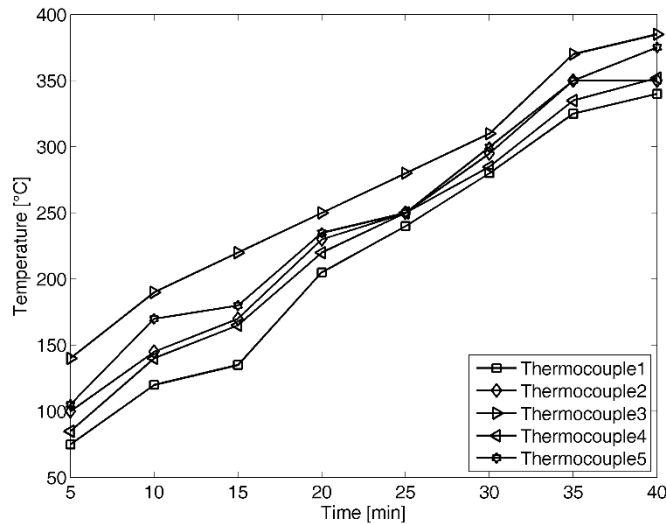


Figure 3-24. Temperature readings of 60 g of mineral sample, heated at 1000 W for 40 min. Based on [19]

3.4 DISCUSSION

Along the lines of this chapter, we have shown two approaches for identifying the mineral samples, both of them important for successfully creating an algorithm able to optimize a waveguide for this particular application. Moreover, we summarized some of the key extra results achieved with each undergraduate experimental research, mainly focused on reducing the microwave applicator, on measuring the temperature in the sample (adapting a standard temperature system and creating one), and on exploring the feasibility of microwave smelting.

We found that microwaves are a good choice for mineral roasting (at least at lab level), since processing time can be reduced between 68% and 71%, and energy consumption between 81% and 88%, while achieving recovery margins of at least 90% of the traditional approach. Even more, one of the studies boasted a recovery of 119%, meaning that the sample was better roasted by microwaves than with the electric furnace. The exposure conditions for this process imply: a mass between 30 and 60 grams, enough for not modifying the following steps of traditional recovery; an exposure between 36 and 42 minutes, split in intervals for allowing oxygenation of the sample; a clay sample holder; a mixture of ore and some silicon carbide; a sieve size between 100 and 170; and a magnetron with one kilowatt of power. Note that since a domestic oven was used during these studies, it is possible to reduce the amount of power required, by designing an appropriate applicator (in a similar way to the equipment used for measuring dielectric properties).

In a similar fashion, measuring the complex permittivity of mineral samples through a resonance-based method yielded good results. The rapid temperature increase, the uniformity of microwave heating, and the equipment's speed, allowed tracking the changes in resonant frequency and quality factor, even when the sample began roasting—changing its internal structure and compounds. However, we also found that variables such as particle size (sieve) must be chosen carefully, since they can drastically alter the complex permittivity of a mineral, as shown for "Juan Blanco" (see Figure 3-8).

Table 3-14 summarizes the best models found for all six minerals (including the three different sieves of "Juan Blanco"), as well as their order and coefficients (please refer to Table 3-6 for the general expressions). In some cases, properties vary so much that a single model cannot be used to properly represent the data and thus it needs to be split into ranges (see, for example, "El Volcán"). Also, please note that the data is given for resonant frequency and quality factor, so different types of interpolations can be easily implemented by the reader (if desired), and that a measurement of air returned a resonant frequency of 2124.9 MHz and a quality factor of 10076. In any case, please refer to Table 3-1 for the starting and ending dielectric properties of each sample at room temperature.

Further studies showed that it is possible to adapt the temperature measurement system of an electric furnace, or even create one from scratch, to simultaneously heat the sample and read its temperature at different locations. This opens the possibility for a more controlled environment, and the eventual economic and environmental benefits of using microwaves at this scale are evident. Thus, their study should be extended, but bear in mind that due to the sulfur vapors released during roasting, a research at pilot plant level must incorporate an additional stage for disposing them (e.g. collecting them as sulfur). Finally, we observed that, at least for one sample, microwave smelting is possible with processing time reductions of about 92%, so we also recommend further exploration of this alternative.

Table 3-14. Summary of best fits for the mineral samples. The general expression of each model is shown in Table 3-6 and the starting and ending values of permittivity is given in Table 3-1.

Sample	Sieve	Process	Suggested Fit	Coefficients
Juan Blanco	100	Heating	Frequency: Gaussian $N=5$	ai = [2137, -9.92, -91632.63, 91623.18, -2.84] bi = [-6074, 647, 525.30, 525.30, 409.90] ci = [54221.56, 49.13, 69.19, 69.19, 39.37]
		Cooling	Gaussian $N=5$	ai = [2100, 40611.59, 4.96, 0.74] bi = [-7.17, 1272, 578.20, 458] ci = [6733, 216.20, 90.81, 458]
		Heating	Quality Factor: Gaussian $N=4$	ai = [1956, 2116, -224.20, 541.90] bi = [10.83, 121.80, 135, 355.40] ci = [51.03, 89.29, 25.28, 713.90]
		Cooling	Gaussian $N=5$	ai = [-96.23, -41157.72, 41281.25, -93.43, 1568] bi = [-10.24, 168.90, 168.90, 456.90, -587.80] ci = [115.60, 74.05, 74.24, 83.89, 1040]
Juan Blanco	200	Heating	Frequency: Gaussian $N=3$	ai = [2115, 1.90, 1.82] bi = [19.33, 263.60, 224.40] ci = [5801, 27.54, 46.92]
		Hold	Gaussian $N=2$	ai = [2115, 0.39] bi = [238.60, 246.40] ci = [437.40, 3.31]
		Cooling	Gaussian $N=1$	ai = 2158 bi = -6.22E+04 ci = 4.42E+05
		Heating	Quality Factor: Fourier $N=4$	a0 = 4023 ai = [-288.60, -59.13, 253.30, 162] bi = [324.20, 397.50, 400, -34.56] w = 0.01989
		Hold	Gaussian $N=4$	ai = [6228, 3189, 1379, 772.70] bi = [229.90, 241.60, 245, 246.20] ci = [10.08, 5.76, 2.60, 1.16]
		Cooling	Fourier $N=1$	a0 = 5588 ai = -88.31 bi = -32.16 w = 0.02851
Juan Blanco	-200	Heating	Frequency: Gaussian $N=6$	ai = [2239, 3.54e-02, 0.45, 3.33e-02, 0.84, 0.20] bi = [-2.06e+04, 157.8, 163.4, 148.2, 140.6, 74.56] ci = [8.77e+04, 1.53, 16.37, 2.22, 53.11, 26.99]
		Hold	Gaussian $N=2$	a0 = 2118 ai = -0.01488

Sample	Sieve	Process	Suggested Fit	Coefficients
M9	100	Cooling	Gaussian $N=2$	bi = -0.03218
				w = 1.51310
		Heating	Quality Factor: Gaussian $N=7$	ai = [2125, 2.44]
				bi = [-1573, 300.60]
		Cooling	Polynomial $N=2$	ci = [2.65e+04, 236]
				ai = [1339, 5187, -117.80, 2.67e+04, 49.71, 2414, 573.1]
		Heating	Frequency: Fourier $N=5$	bi = [158, 119.60, 24.24, -38.78, 28.96, 47.73, 73.47]
				ci = [15.04, 67.54, 1.53, 44.09, 0.42, 22.50, 13.42]
		Cooling	Fourier $N=3$	pi = [-3.54E-02, 8.07, 4795]
				a0 = 2098
Heating	Quality Factor: Fourier $N=5$	ai = [1.32, 2.55, 1.85, 0.14, 0.38]		
		bi = [9.93, 1.18, 0.21, -0.29, 0.04]		
Cooling	Exponential $N=2$	w = 0.00779		
		a0 = 2090		
Heating	Frequency: Gaussian $N=3$	ai = [3.53, 0.88, 0.16]		
		bi = [3.48, -0.55, -0.60]		
Cooling	Polynomial $N=1$	w = 0.00798		
		a0 = 652.3		
Heating	Quality Factor: Fourier $N=5$	ai = [124.50, 26.52, 42.23, 22.91, -12.64]		
		bi = [440.10, 55.03, 30.57, 44.64, 16.73]		
Ismael	-170	Cooling	Exponential $N=2$	w = 0.00925
				ai = [336.40, 1.84e-04]
		Heating	Frequency: Gaussian $N=3$	bi = [-1.33e-03, 2.29e-02]
				ai = [2115, 1.03, 1.35]
		Hold	Gaussian $N=1$	bi = [-20.84, 238.40, 208.30]
				ci = [7966, 22.85, 43.04]
		Cooling	Polynomial $N=1$	ai = 2115
				bi = 222.60
		Heating	Quality Factor: Fourier $N=3$	ci = 191.60
				pi = [-1.46e-03, 2116]
Hold	Gaussian $N=1$	a0 = 5122		
		ai = [-908.50, -96.17, -79.89]		
Cooling	Gaussian $N=3$	bi = [-2318, -162.60, 252.30]		
		w = 0.01538		
Hold	Gaussian $N=1$	ai = 7089		
		bi = 222.50		
Cooling	Gaussian $N=3$	ci = 7.90		
		ai = [2138, 5242, 6856]		

Sample	Sieve	Process	Suggested Fit	Coefficients
Carlos Arias	100	Heating	Frequency: Gaussian $N=3$	bi = [17.49, 64.71, 215.40]
				ci = [44.17, 91.28, 131.10]
		Hold	Fourier $N=2$	ai = [2068, 3.56, 730.5]
				bi = [-632.10, 599.70, 1098]
				ci = [2237, 30.81, 965]
		Cooling	Fourier $N=6$	a0 = 2088
				ai = [-8.56e-02, 5.52e-02]
		Heating	Quality Factor: Fourier $N=6$	bi = [0.15, 0.12]
				w = 0.27120
				a0 = 2091
ai = [5.63, 1.38, 0.83, -0.69, -0.59, -0.17]				
Cooling	Polynomial $N=2$ Fourier $N=3$	bi = [2.57, -1.62, -1.40, -0.84, -0.24, 0.34]		
		w = 0.00862		
Core from El Volcán	-120	Heating ($T \leq 80$)	Frequency: Gaussian $N=3$	a0 = 642.4
				ai = [165, -107.20, 102.50, 96.01, 172, 124.10, 66.14]
		Heating ($82 \leq T \leq 140$)	Gaussian $N=6$	bi = [779.70, 358.90, 362.40, 171, 67.52, 20.01, 15.75]
				w = 0.00820
				pi = [-5.42e-02, 61.97, -1.73e+04]
		Heating ($T \geq 140$)	Fourier $N=3$	a0 = 224.4
				ai = [47.49, -5.01, 1.75]
		Hold	Gaussian $N=3$	bi = [10.56, -16.74, 2.21]
				w = 0.00920
		Cooling	Gaussian $N=3$	ai = [2112, 65.35, 5.24]
bi = [92.33, -20.75, 40.27]				
ci = [552.70, 49.70, 32.04]				
Heating ($82 \leq T \leq 140$)	Gaussian $N=6$	ai = [2114, -7534, -5.31, -0.45, -210.20, 7714]		
		bi = [131.80, 90.32, 83.20, 102.10, 93.43, 90.40]		
Heating ($T \geq 140$)	Fourier $N=3$	ci = [1660, 7.77, 5.95, 5.12, 7.43, 7.80]		
		a0 = -5.00E+04		
Hold	Gaussian $N=3$	ai = [6.39e+04, -1.05e+04, -1416]		
		bi = [-4.51e+04, 2.95e+04, -5031]		
Cooling	Gaussian $N=3$	w = -0.00306		
		ai = [2114, 0.14, 0.02]		
		bi = [223, 208, 214.10]		
Cooling	Gaussian $N=3$	ci = [1657, 4.50, 2.16]		
		ai = [2114, 2.55e+10, 0.40]		
		bi = [-364.10, 575.60, 312.90]		
Cooling	Gaussian $N=3$	ci = [2.98e+04, 71.18, 158.30]		

Sample	Sieve	Process	Suggested Fit	Coefficients
Rock from Segovia	-120	Heating	Quality Factor: Fourier $N=6$	ai = [89.40, 707.90, 3.96e+14, 42.62] bi = [128.70, 290.70, -1.02e+04, 162.30] ci = [19.62, 219.10, 1965, 21.43]
		Hold	Sum of Sin $N=4$	ai = [1392, 599.70, 32.20, 64.77] bi = [0.27, 0.52, 1.05, 1.20] ci = [12.83, 32.20, 64.77, 181.20]
		Cooling	Fourier $N=3$	a0 = 3.60E+09 ai = [-5.38e+09, 2.13e+09, -3.47e+08] bi = [-5.00e+08, 3.99e+08-9.91e+07] w = 0.00082
		Heating ($T \leq 120$)	Frequency: Gaussian $N=4$	ai = [2012, 92.11, 1608, 1] bi = [175.30, 59.46, -69.65, 93.37] ci = [186.80, 68.26, 136.10, 26.58]
		Heating ($T \geq 120$)	Gaussian $N=2$	ai = [2116, 1.31] bi = [102.70, 223.60] ci = [3899, 60.39]
		Cooling	Gaussian $N=2$	ai = [2168, 11.07] bi = [-6842, 570.60] ci = [4.23e+04, 619]
		Heating	Quality Factor: Gaussian $N=4$	ai = [247.80, 3664, 1430, 116.20] bi = [123, 175.40, -1.36, 87.06] ci = [17.01, 207.50, 41.63, 16.59]
		Cooling	Gaussian $N=2$	ai = [3859, 178.80] bi = [44.09, 203.60] ci = [463.30, 52.02]

3.5 FINAL COMMENTS

In this chapter we developed the first two specific objectives of the dissertation, i.e. determination of the dielectric properties and of the exposure conditions of the gold ore samples selected from the beginning. We found that gold ores with high sulfur content interact more easily with microwaves, due to their higher complex permittivity. Using equipment developed at the ITACA institute (Universitat Politècnica de València, Spain), we were able to interpolate the complex permittivity as temperature increased and, even, during the roasting phase. Based on our data, a Gaussian fit was better 59.1% of the time, followed by a Fourier fit in 29.5% of the cases, and scarcely using polynomial, exponential and sinusoidal fits (the remaining 11.4%).

The exposure conditions studied here reported that a mass between 30 and 60 grams, an exposure time between 36 and 42 minutes, a clay sample holder, a mixture of ore and silicon carbide, a sieve size between 100 and 170, and a magnetron with one kilowatt of power, were appropriate conditions for microwave interaction. The amount of power, however, can be reduced if the field distribution is optimized. Furthermore, an exploratory experiment showed that, at least for one type of ore, microwave smelting is possible in a fraction of the time (about 8%), with recovery margins between 95% and 100%. A more extensive research work is needed due to the novelty of this application.

Furthermore, our findings mean that, for the studied minerals, temperature-dependence of the complex permittivity can be now included in simulations, allowing better prediction of internal field distribution or better simulation of heating profiles. Now, the discussion migrates to the third specific objective, related to the use of modern optimization algorithms (also known as metaheuristic algorithms), so the data reported here can be used to design an optimal microwave applicator.

REFERENCES

- [1] R. Amankwah, C. Pickles, W. Yen, Gold recovery by microwave augmented ashing of waste activated carbon, *Miner. Eng.* 18 (2005) 517–526. doi:10.1016/j.mineng.2004.08.015.
- [2] R.K. Amankwah, G. Ofori-Sarpong, Microwave Heating of Gold Ores for Enhanced Grindability and Cyanide Amenability, *Miner. Eng.* 24 (2011) 541–544. doi:10.1016/j.mineng.2010.12.002.
- [3] R.K. Amankwah, A.U. Khan, C.A. Pickles, W.T. Yen, Improved Grindability and Gold Liberation by Microwave Pretreatment of a Free-Milling Gold Ore, *Miner. Process. Extr. Metall.* 114 (2005) 30–36. doi:10.1179/037195505X28447.
- [4] R.K. Amankwah, C.A. Pickles, Microwave roasting of a carbonaceous sulphidic gold concentrate, *Miner. Eng.* 22 (2009) 1095–1101. doi:10.1016/j.mineng.2009.02.012.
- [5] C.A. Pickles, Microwave Heating Behaviour of Nickeliferous Limonitic Laterite Ores, *Miner. Eng.* 17 (2004) 775–784. doi:10.1016/j.mineng.2004.01.007.
- [6] S. Visentin, C. Medana, A. Barge, V. Giancotti, G. Cravotto, Microwave-assisted Maillard reactions for the preparation of advanced glycation end products (AGEs), *Org. Biomol. Chem.* 8 (2010) 2473–7. doi:10.1039/c000789g.
- [7] J. Monzó-Cabrera, J.M. Catalá-Civera, P. Plaza-Gonzalez, D. Sánchez-Hernández, A Model for Microwave-Assisted Drying of Leather: Development and Validation, *J. Microw. Power Electromagn. Energy.* 39 (2004) 53–64.
- [8] S. Marland, B. Han, A. Merchant, N. Rowson, The effect of microwave radiation on coal grindability, *Fuel.* 79 (2000) 1283–1288. doi:10.1016/S0016-2361(99)00285-9.
- [9] M. Willert-Porada, ed., *Advances in Microwave and Radio Frequency Processing*, Springer Berlin Heidelberg, Berlin, Heidelberg, 2006. doi:10.1007/978-3-540-32944-2.
- [10] G. Qin, D. Gong, Pretreatment of petroleum refinery wastewater by microwave-enhanced Fe⁰/GAC micro-electrolysis, *Desalin. Water Treat.* 52 (2013) 2512–2518. doi:10.1080/19443994.2013.811120.
- [11] Y. Zhang, J. Zou, C. Cheuh, H. Yip, A.K.-Y. Jen, Significant Improved Performance of Photovoltaic Cells Made from a Partially Fluorinated Cyclopentadithiophene/Benzothiadiazole Conjugated Polymer, *Macromolecules.* 45 (2012) 5427–5435. doi:10.1021/ma3009178.

- [12] A. Davoodnia, Microwave Assisted Synthesis of Fused Benzimidazoles, *Asian J. Chem.* 22 (2010) 1591–1594.
- [13] M. Darvekar, B. Ghorpade, P.S. Vankar, Microwave Assisted Improved Syntheses of Indigoid and Anthraquinoid Dyes, *Asian J. Chem.* 16 (2004) 965–970.
- [14] C.-W. Hsu, P. Chen, J.-M. Ting, Microwave-Assisted Hydrothermal Synthesis of TiO₂ Mesoporous Beads Having C and/or N Doping for Use in High Efficiency All-Plastic Flexible Dye-Sensitized Solar Cells, *J. Electrochem. Soc.* 160 (2013) H160–H165. doi:10.1149/2.048303jes.
- [15] J. Li, J. Huang, J. Wu, L. Cao, Q. Li, K. Yanagisawa, Microwave-assisted growth of WO₃·0.33H₂O micro/nanostructures with enhanced visible light photocatalytic properties, *CrystEngComm.* 15 (2013) 7904–7913. doi:10.1039/c3ce41005f.
- [16] A.C. Metaxas, R. Meredith, *Industrial Microwave Heating*, The Institution of Electrical Engineers, London, 1983.
- [17] R. Meredith, *Engineers' Handbook of Industrial Microwave Heating*, The Institution of Electrical Engineers, London, 1998.
- [18] J.S. Abril, J.A. Gomez, *Ingeniería Conceptual de un Proceso de Recuperación de Oro con Microondas a Partir de Muestras Provenientes de los Municipios de Vetas y California (Santander)*, Undergraduate Thesis, Universidad Industrial de Santander, 2012.
- [19] R.D. Aguirre, W. Botero, *Interacción de las Microondas con Trazas de Oro en Muestras Provenientes del Municipio de Vetas (Santander)*, Undergraduate Thesis, Universidad Industrial de Santander, 2012.
- [20] D. Bernal, S. Garnica, Y. Reslen, *Irradiación con Microondas a Minerales Ricos en Oro en Muestras Provenientes de la Zona del Sur de Bolívar*, Undergraduate Thesis, Universidad Industrial de Santander, 2012.
- [21] D. Jurado, M. Ortiz, *Implementación de un Sistema de Medición y Control de la Temperatura en una Cavidad Electromagnética*, Undergraduate Thesis, Universidad Industrial de Santander, 2013.
- [22] M. Díaz, M. Rueda, *Uso de las Microondas en el Proceso de Recuperación de Trazas de Oro*, Undergraduate Thesis, Universidad Industrial de Santander, 2012.
- [23] J.M. Catalá Civera, J.D. Gutiérrez Cano, F.L. Peñaranda-Foix, B. Garcia-Baños, *Portable System for Dielectric Characterization of Materials at Microwave*

Frequencies, in: 13th Int. Conf. Microw. RF Heating, AMPERE 2011, Ampere, Toulouse, 2011: pp. 137–140.

- [24] A.J. Canos, F.L. Penaranda-Foix, J.M. Catala-Civera, B. Garcia-Banos, Measurement of dielectric properties at high-temperatures in real-time with cylindrical cavity, in: 2010 IEEE MTT-S Int. Microw. Symp., IEEE, 2010: pp. 1044–1047. doi:10.1109/MWSYM.2010.5515877.

4. KNOWING THE ALGORITHMS

Modern optimization algorithms can be used in a wide array of situations. Since they are not hindered by complex mathematics, they are quite straightforward to implement. During this dissertation, we tested several algorithms under different scenarios that can be broadly classified into optimization problems per se, and solution problems, where the objective function is built from a system of equations (including nonlinear elements).

This kind of optimization strategies have become quite popular during the last couple decades and there currently are a vast number of options available. This chapter is devoted to assessing some of these options and selecting two of them. They will be used in the following chapters, for the development of an optimization strategy for microwave applicators.

Similarly as it was stated in the last chapter, and in pursuing a well-defined objectives that are part of the main research objectives described in this dissertation, we selected a new group of students to join our group as research assistants and complete their undergraduate theses:

Jhonatan Contreras and Carlos Villanueva [1]	Jorge González and Carlos Bayona [2]
Rafael Ortiz and Edgar García [3]	Alejandro Miranda and Juan Ruiz [4]
Alberto Hinojosa and Katherine Espinosa [5]	Julián Ávila and Orlando Navarro [6]
Juan Arias and Moisés Mogollón [7]	Andrés Rodríguez and Kildar Gaona [8]
Héctor Castro and Marco Otero [9]	Marisol Hernandez [10]
Jorge Portilla [11]	Francisco Ramírez and Oscar Roa [12]
Jorge Cruz [13]	Saúl González and Oscar Trasladino [14]
José García and Diego Corredor [15]	Kristian Barreto [16]
Carlos Gómez and Oscar Pérez [17]	Jonathan Ramírez and Fausto Osorio [18]
Julieth Celis and Francis Rincón [19]	Camilo Pinzón and Edwin Ardila [20]
Elkin Petro and Rafael Fuentes [21]	Daniel Dávila and Alejandro Rutto [22]
Edwin Farfán and Jimmy Fontecha [23]	Jhon Suarez and Jorge Romero [24]

We want to declare our deepest appreciation to them, for their dedication and effort in contributing to some of the results discussed in this chapter.

4.1 HOW DO ALGORITHMS WORK?

Throughout this phase of the dissertation, 12 different algorithms were studied. They represent nature-inspired iterative strategies to improve a solution during a number of iterations. But, due to space restrictions, only the six most important approaches will be discussed below. Still, an extended list of the algorithms can be found in the appendices, where each strategy is explained.

The easiest and most simple logic for improving a solution using this kind of algorithms is to keep iterating for a fixed number of cycles. However, most often than not, one of two things happen: a valid answer is not found, or it was found a long time ago. In the first case, the process would have to begin anew allowing for more iterations, while in the second scenario the answer could have been achieved with fewer iterations. In both cases, precious computational resources are wasted. Even so, the algorithms are described as originally conceived, but in this dissertation some convergence criteria are implemented, basically analyzing if the error at a given stage is within a tolerable range. Next, a description of the most relevant strategies is provided.

4.1.1 Original approaches

4.1.1.1 *Central Force Optimization (CFO)*

CFO was proposed by Formato in 2007 [25], and it was inspired by gravitational kinematics. As opposed to other approaches, the inner logic of CFO is deterministic in nature. This means that if the same starting points and parameters are used, the algorithm will always find the same answer. However, Formato also shows that random starting points can be used. In a general sense, CFO creates a set of probes that fly throughout the search domain, constantly attracting themselves while looking for a maximum. Some of the works related to this algorithm can be found in [26–38].

In CFO, the mass (M) represents the fitness, and the gravitational pull (G) is one of the parameters that, as with other metaheuristics, varies for each problem. However, and as posed by Formato, a value of two seems to provide good results. CFO's evolution is governed by eq. (4.1) and eq. (4.2), where the velocity (V) and the time difference (Δt) can be arbitrarily set to zero and one, respectively, in order to simplify calculations (this also following Formato's suggestion). Therefore, the only two relevant parameters that remain from the

physical domain are the position (R) and acceleration (a) of each probe. There are a couple more parameters, i.e. exponents α and β , that usually take a value of two and that do not relate to any physical parameters [39].

$$a_{j-1}^p = G \sum_{\substack{k=1 \\ k \neq p}}^{N_p} U(M_{j-1}^k - M_{j-1}^p) \cdot (M_{j-1}^k - M_{j-1}^p)^\alpha \frac{R_{j-1}^k - R_{j-1}^p}{|R_{j-1}^k - R_{j-1}^p|^\beta} \quad (4.1)$$

$$R_j^p = R_{j-1}^p + V_{j-1}^p \Delta t + \frac{1}{2} a_{j-1}^p \Delta t^2, \quad j \geq 1 \quad (4.2)$$

It is important to note that CFO maximizes a problem, as opposed to other metaheuristics. It also forces the probes to remain inside the search domain, using a factor (F_{rep}) that indicates the loss of energy against the boundary. A general algorithm can be written as:

Algorithm I: Original Central Force Optimization

1. Define an initial position, and zero acceleration, for each probe.
 2. Calculate the mass (M) for each probe, and choose the position with the highest M.
 3. Calculate the new position of the probes, R_j^p , using eq. (4.2), and adjust the ones outside the search domain through F_{rep} .
 4. Update M and find the probe with maximum value.
 5. Update the acceleration of each probe, using eq. (4.1).
 6. Evaluate the convergence criteria. If it does not comply, return to 3.
-

4.1.1.2 Firefly Algorithm (FA)

FA was proposed by Yang in 2010 [40,41], and it is based on the attraction of artificial fireflies via the light they emit. Yang considers that any artificial firefly can attract, or be attracted, to any other one (i.e. they are unisex). Also, that the attractiveness is proportional to the brightness, where the latter is affected by the landscape of the objective function [42]. This implies, however, that the only function of light-emission in fireflies is mating, while it could also be used for attracting preys or for intimidating foes, as appears to be the case for real fireflies.

Regarding the algorithm itself, Yang proposes the use of a fixed pair of constants, α and γ . The former relates to the randomness in the movement of an artificial firefly (between zero and one), while the latter relates to the dimming of emitted light as it travels through the search domain (usually between 0.01 and 100). The algorithm can be briefly described as:

Algorithm II: Original Firefly

1. Initialize fireflies.
 2. Calculate the light emitted by each firefly (i.e. evaluate the objective function for each firefly).
 3. Sort fireflies by light intensity (in ascending order).
 4. Update the position of each firefly (i.e. adjust each firefly according to eq. (4.3) and to the light intensity).
 5. Check for convergence. If it complies, exit. If not, go to step 2.
-

$$\begin{aligned}x_i^{k+1} &= x_i^k(1 - \beta) + x_j^k\beta + \alpha(R_1 - 0.5) \\ \beta &= \beta_0 e^{-\gamma r_{ij}^2}\end{aligned}\tag{4.3}$$

It is important to point out that in eq. (4.3), subscripts i, j relate to the firefly under analysis, and to the other fireflies, respectively. Also, superscript k relates to the time lapse, β_0 to the attractiveness at distance zero, R_1 is a random number such that $R_1 \in [0,1]$, α and γ are the previously mentioned constants and r_{ij} is the Cartesian distance between fireflies.

4.1.1.3 Harmony Search (HS)

HS was proposed by Geem et al. in 2001, and it is the first approach based on the process that musicians carry out when composing music [43]. The general idea is that in a similar fashion that a musician uses his knowledge of music for composing melodies, HS uses the knowledge of solutions stored in its memory in tandem with some random alterations (akin to improvisation), to find a good solution. One of the special things about HS is that it improves the candidate solution (x') one coordinate at a time (x'_i), using a rather simple equation. Since its creation, HS has been continuously used by its creators [43–49] as well as by other authors [50–64]. The procedure can be described as follows:

Algorithm III: Original Harmony Search (HS)

6. Define the execution parameters: memory size (HMS), memory considering rate (HMCR, usually performs better for values between 0.8 and 0.9), pitch adjusting rate (PAR, usually performs better for values around 0.1), and maximum number of iterations (NI).
 7. Generate a random initial matrix, HM, of size $HMS \times N$, where N represents the number of dimensions.
 8. Generate a random number. If it is lower than HMCR, go to step 4. Otherwise, take a random value from the search domain and go to step 6.
 9. Pick the value located at a random row of HM, and at the column corresponding to the component being updated.
 10. Generate a random number. If it is lower than PAR, adjust the pitch using eq. (4.4), where r is a random number in the interval $[-1,1]$.
 11. Repeat steps 3 to 5 for the remaining dimensions.
 12. Evaluate the new candidate solution. If it is better than the worst solution stored in HM, replace it and discard the worst.
 13. Repeat for NI iterations.
 14. Report results and end the process.
-

$$x'_i = x_i + r \cdot BW\tag{4.4}$$

4.1.1.4 Particle Swarm Optimization (PSO)

PSO may have been the strategy that revolutionized optimization approaches and that ignited the spark in bio-inspired computation developments. This technique, proposed by Eberhart and Kennedy almost two decades ago, mimics the collaborative intelligence exhibited by swarms when looking for sources of food [65,66]. PSO was not the first approach based on naturally occurring processes, but it has certainly inspired a great deal of work throughout the years [54,67–83]. Broadly speaking, PSO generates a swarm that transverse the search

domain, communicating the best solutions found by each particle and working together to find a minimum. A general layout of its algorithm can be given as:

Algorithm IV: Original Particle Swarm Optimization

1. Assign a random initial position and zero speed for each particle.
 2. Evaluate the objective function, f , and calculate the best position each particle has found, P_{Best_i} , and the best position of all the swarm G_{Best} .
 3. Update position and speed for each particle with eq. (4.5) and (4.6), where i, j represent pointers for each position and time step, respectively; X is a particle's position, V its speed, w an inertia factor to limit the effect of its previous speed, C_1, C_2 are the self and swarm trust factors (default value: $C_1, C_2 = 2.05$), and R_1, R_2 are random numbers (uniformly distributed) between zero and one.
 4. Evaluate the objective function.
 5. Compare, for each particle, the evaluated value and P_{Best_i} . If it is lower, then update P_{Best_i} .
 6. Select the best particle and compare it to G_{Best} . If it is lower, then update G_{Best} .
 7. Compare G_{Best} with convergence criteria. If it does not comply, return to 3.
-

$$X_i^{j+1} = X_i^j + V_i^{j+1} \quad (4.5)$$

$$V_i^{j+1} = wV_i^j + C_1R_1(P_{Best_i} - X_i^j) + C_2R_2(G_{Best} - X_i^j) \quad (4.6)$$

4.1.1.5 Spiral Optimization (SO)

SO was proposed by Tamura and Yasuda in 2011, mimicking the path followed by a given number of logarithmic spirals [84,85]. Akin to an eagle stalking a prey, each spiral closes in on the minimum through inward traveling loops, changing their target (convergence point) each time a spiral detects a better solution. SO requires defining the rotation angle, θ (default value: $\pi/2$), and the distance rate, r (default value can be either 0.95 or 0.99), at each step. The combination of these two effects (i.e. changing the convergence point and the free definition of rotation angle and distances) may generate paths that resemble anything but a logarithmic spiral, even though the mathematical model is appropriate. Some of the recent work related to SO can be found in [86,87] and a general algorithm can be defined as:

Algorithm V: Original Spiral Optimization

1. Define the number of spirals, m , as well as r and θ .
 2. Assign a random initial position inside the search domain.
 3. Find the starting convergence point, x^* , such as $f(x^*) = \min(f(x^1), f(x^2), \dots, f(x^m))$.
 4. Update position of each spiral, x^k , using eq. (4.7) and eq. (4.8), where t indicates the current iteration, I_n is the identity matrix, and the index n represents the number of dimensions of the problem. Each element of the rotation matrix, $R^n(\theta)$, is given by eq. (4.9), where $a_{i,j}$ is the corresponding element of the identity matrix.
 5. Evaluate the objective function.
 6. Update the convergence point, x^* .
 7. Compare with convergence criteria. If it does not comply, return to 4.
-

$$x^k(t+1) = S_n(r, \theta) \cdot x^k(t) - (S_n(r, \theta) - I_n) \cdot x^* \quad (4.7)$$

$$S_n(r, \theta) = r \cdot R^n(\theta) = r \prod_{i=1}^{n-1} \prod_{j=1}^i R_{n-i, n+1-j}^n(\theta_{n-i, n+1-j}) \quad (4.8)$$

$$Y_{p,q} = \begin{cases} \cos \theta_{i,j} & p = i \wedge q = i \\ -\sin \theta_{i,j} & p = i \wedge q = j \\ \sin \theta_{i,j} & p = j \wedge q = i \\ \cos \theta_{i,j} & p = j \wedge q = j \\ a_{i,j} & \text{otherwise} \end{cases} \quad (4.9)$$

4.1.1.6 Unified Particle Swarm Optimization (UPSO)

UPSO was proposed by Parsopoulos and Vrahatis in 2004 and appeared as a strain of PSO variants [88]. However, we include it in this section since we are leaving the next one just for the modifications proposed during this dissertation. This modification defines a local and global behavior for each particle of the swarm (L_p, G_p respectively), calculated through eq. (4.10) and eq. (4.11), where χ stands for the constriction factor. Default values of $c_p = c_g = 2.05$ are commonly used. Afterwards, the data is merged into a single update of velocity—eq. (4.12)—via the unification factor (default value: $u = 0.5$). The position of each particle, however, is updated in the same fashion as in PSO, i.e. through eq. (4.13).

$$L_p^{t+1} = \chi \cdot [V_p^t + c_p r_3 (P_p - X_p^t) + c_g r_4 (P_{gp} - X_p^t)] \quad (4.10)$$

$$G_p^{t+1} = \chi \cdot [V_p^t + c_p r_1 (P_p - X_p^t) + c_g r_2 (P_g - X_p^t)] \quad (4.11)$$

$$V_p^{t+1} = (1 - u) \cdot L_p^{t+1} + u \cdot G_p^{t+1} \quad (4.12)$$

$$X_p^{t+1} = X_p^t + V_p^{t+1} \quad (4.13)$$

A general algorithm can be laid out as:

Algorithm VI: Unified Particle Swarm Optimization

15. Define UPSO parameters, including the size of the swarm (Ψ).
 16. Randomly initialize the position of each particle and their speed.
 17. Evaluate each candidate solution, and determine the best coordinate of each particle (P_p), of each neighbourhood (P_{gp}), and of all the swarm (P_g).
 18. Update the velocity and position of each particle, using eq. (4.12) and eq. (4.13), respectively.
 19. Evaluate each new position and update P_p, P_{gp}, P_g .
 20. Check convergence criteria. If it complies, stop the process. Otherwise, return to step 4.
-

4.1.2 Modifications proposed by our group

During some of the studies with our undergraduate students, we made an extra effort to propose improvements, and the most important ones relate to CFO and to HS. In the first case, we implemented a mapping stage to identify a good search zone, and a normal distribution of probes around the best point to improve exploitation of the solution. In the second case, we established two possible behaviors for updating the fretwidth (previously known as bandwidth). Similarly, and after the work with our undergraduate students was finished, we proposed some new elements. This time, we kept improving HS and began experimenting with FA.

4.1.2.1 CFO

During 2010, Formato proposed three modifications for improving the original CFO algorithm [39]. One of them is the adjustment of the search domain, whilst the other one relates to the initial probe distribution and the way the repetition factor, F_{rep} , is handled. The first one strives to achieve quicker convergence, while the second one is used to reduce the risk of converging to a local optimum and the latter is used to avoid trapping of the probes. Formato proposes to adjust the search domain every 20 iterations, even though it is an arbitrarily chosen value. Also, he proposes to reduce the search domain around the best probe, creating a new one whose boundaries are located halfway between the best particle's position, and the initial boundary. This can be more easily seen in Figure 4-1, where the best probe is represented by the dot, and j relates to the current time step. In order to keep the figure as simple as possible, only one dimension is labeled, but the other one must be adjusted in the same manner.

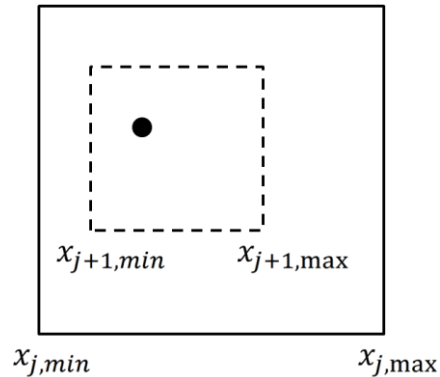


Figure 4-1. Adjustment of the search domain. For clarity, only one dimension is labeled

Another way in which the original algorithm has been modified is by using a variable repetition factor. For the case of antenna optimization, Formato proposes a saw tooth behavior, that is restarted to the value of the increment (ΔF_{rep}) when $F_{rep} > 1$. During this research, we proposed to use a different change for the reposition factor. This was based on results delivered by some preliminary tests, where it was observed that a smaller F_{rep} provided a more accurate answer. This variable also follows a linear behavior, being different to Formato's in the sense that this one is decreasing. After reaching a given value, the behavior changes to an exponentially decaying one, allowing the probes to intensify their search.

As Formato states, the initial distribution is quite important for CFO, and considering the drawback of deterministic algorithms that he comments, it was decided to incorporate a couple modifications to CFO. The first one is an initial, random mapping of the search domain, so CFO is able to begin in a region where it is less likely to converge to a local optimum. The second one is to initialize the probes following a normal probability

distribution, centered around the best point found by the mapping stage. The first process can be seen in Figure 4-2, whilst the initial distribution is shown in Figure 4-3, assuming that the best fitness of the mapping stage was found at (5,5).

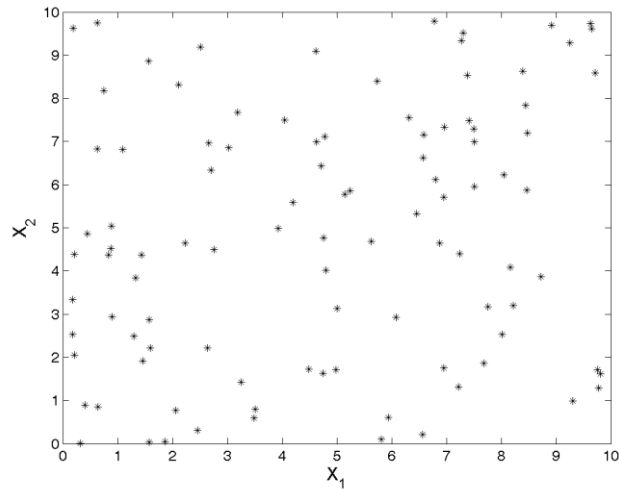


Figure 4-2. Mapping stage for avoiding convergence to local optima, allowing for a bigger initial search domain

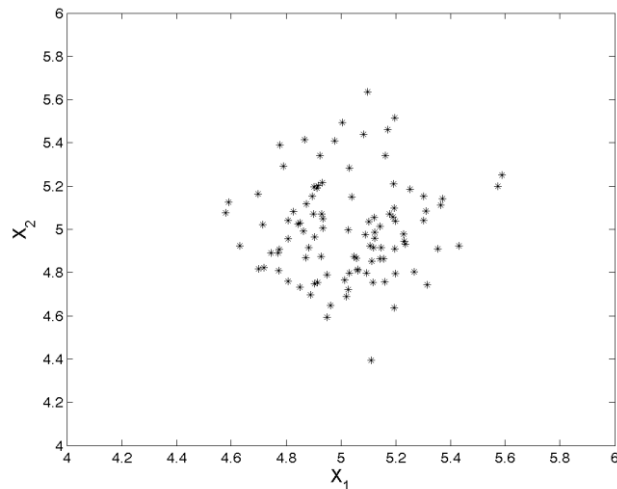


Figure 4-3. Initial distribution of probes, following a normal distribution centered on the best coordinates found by the mapping stage

4.1.2.2 ABHS

With the support yielded by the work of Contreras and Villanueva [1], we noticed that a lot of effort was being put into improving HS's performance and decided that perhaps we could arrive at a worthwhile idea. We focused on IHS, an approach proposed by Mahdavi et al. in 2007 [57], and determined that its drawback was that it required knowing, or at least having an idea, of the total number of iterations that the algorithm was going to execute. Now, this

may not seem detrimental during controlled testing, but in a standalone scenario, where the algorithm should be able to determine when to stop, it becomes paramount. Moreover, the authors assumed that the parameter should always decrease, but this may not always be true since each optimization problem is different. Thus, we decided to adapt the idea and tweak it so the algorithm uses information from its improvement.

We came up with two enticing ideas, ABHSv1 and ABHSv2, and similarly to IHS, our approach does not represent a big overhaul of HS. In fact, it only adds an updating stage for the fretwidth that resets after several non-successful iterations (SatLim). Both approaches decrease exponentially as iterations progress, but after finding a better solution ABHSv1 resets to the original fretwidth (FW), whilst ABHSv2 fixates at the last value. A general flow diagram of these proposals is shown in Figure 4-4, assuming that point one begins after updating the harmony memory (HM) in the original algorithm (i.e. HS), and that point two leads to the next iteration. Also, in Figure 4-5 we present a sample variation of the fretwidth with both proposals, assuming that a better solution is found at iterations 24 and 45.

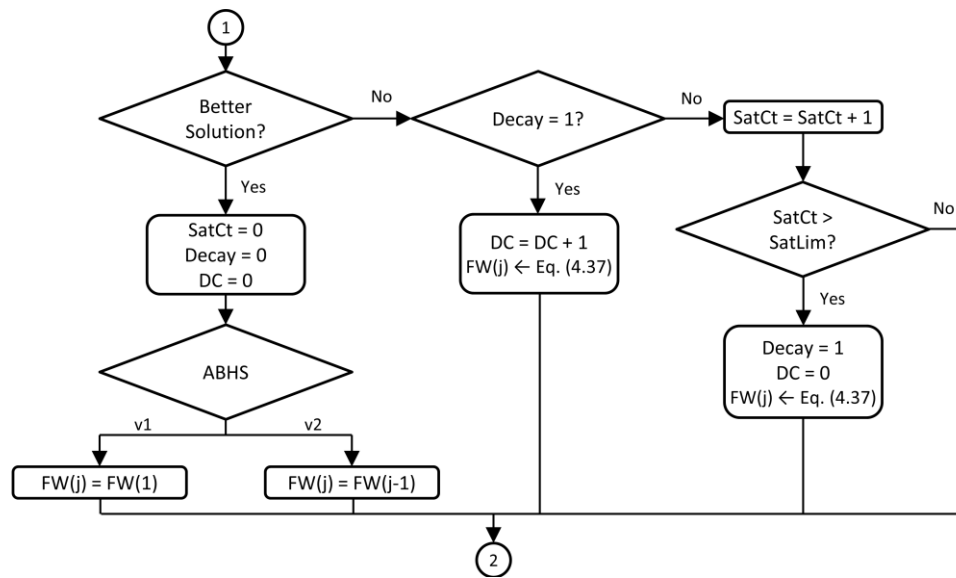


Figure 4-4. General overview of the modifications proposed with ABHS, where DC is the decay counter, j is the current iteration, SatCt is the saturation counter, and SatLim is the saturation limit

$$FW = FW_{\max} \cdot e^{\left(\frac{DC}{DC_{\max}} \cdot \log\left(\frac{FW_{\min}}{FW_{\max}}\right)\right)} \quad (4.14)$$

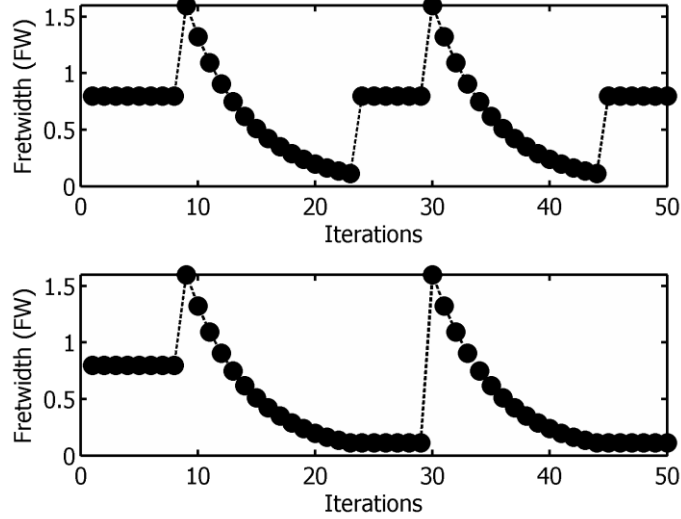


Figure 4-5. Fretwidth behavior for the ABHSv1 (up) and ABHSv2 (down) modifications, considering that a better answer is found at iterations 24 and 45

4.1.2.3 SFHS

Based on the good results achieved with ABHS [52], we strived to improve the results even further. To do so, we designed an approach able to self-adapt as the problem evolved. The general idea is the same: decrease exponentially, but now whenever a new solution is found, the fretwidth updates to a random value around the current one. Again, a general diagram is shown in Figure 4-6, and Figure 4-7 shows a sample variation assuming improvements at iterations 5, 24 and 27.

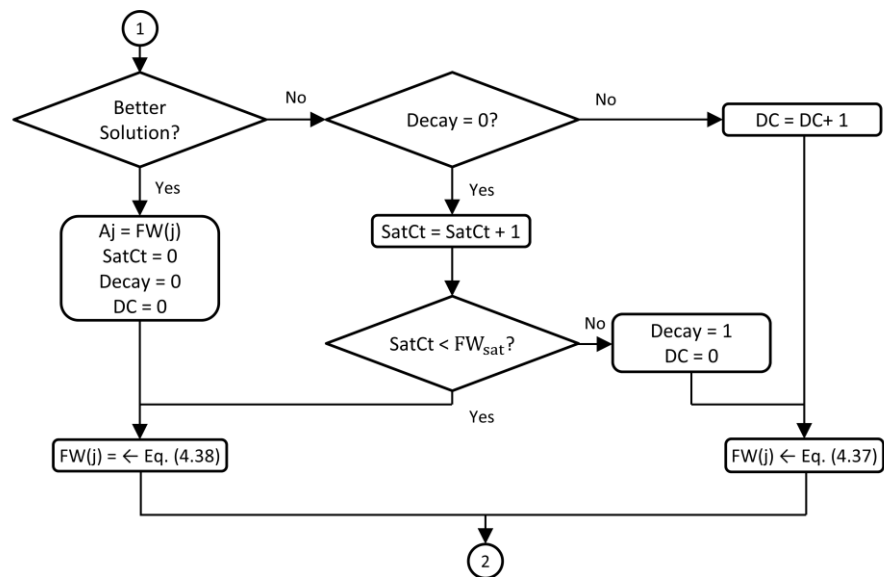


Figure 4-6. General overview of the modifications proposed with SFHS, where DC is the decay counter, j is the current iteration, SatCt is the saturation counter, and FW_{sat} is the saturation limit

$$FW = A_j + (r_{FW} - 0.5) \cdot C_{FW} \cdot A_j \quad (4.15)$$

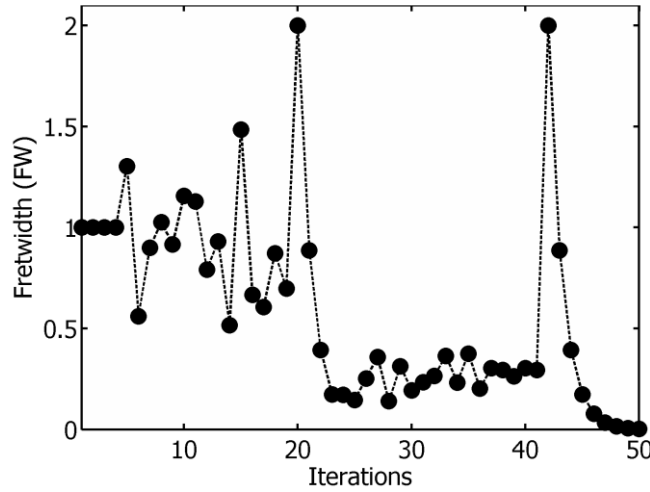


Figure 4-7. Fretwidth behavior for SFHS, considering that a better answer is found at iterations 5, 24, and 27

4.1.2.4 FA

Considering that FA is able to provide good results for test functions [40], but only when α and γ are chosen properly, we decided to explore the behavior of the algorithm after implementing some modifications. The first one allows the constants to vary as the search progresses, and we chose a stochastic behavior that decreases as iterations go by, since a smaller α allows random movement in a smaller area, and because a smaller γ avoids trapping of artificial fireflies in local optima. The behavior is given by eq. (4.16), where Var represents each factor (α, γ), k_{var} is a proportionality constant that defines how much can α or γ be reduced in one iteration, and R is a random number (uniformly distributed between zero and one). Should any factor decrease below a given limit, it is restarted to a random number (also uniformly distributed) between zero and a maximum value, so the procedure begins at different points, thus making it more stochastic. During this research, an inferior limit of 10^{-10} and 10^{-7} was used for α and γ , respectively.

$$\text{Var} = \text{Var} \cdot (1 - k_{\text{var}} \cdot R) \quad (4.16)$$

The second modification alters the way in which artificial fireflies travel through the search domain. We propose that a firefly (x_i) is automatically attracted to the vicinity of another one (x_j), by means of eq. (4.17), striving to speed up the optimization process.

$$x_i^{k+1} = x_j^k + \alpha(R_1 - 0.5) \quad (4.17)$$

The last change consists of dividing α by the index of the attracting firefly, as shown by eq. (4.18). Since the information of x_j is sorted in an ascending order of $f(x_j)$, then the best fireflies (i.e. the ones with higher light emission) have a higher j index. This means that the fireflies attracted to the best solution found so far, would be located in a smaller region, thus favoring intensification of the search.

$$x_i^{k+1} = x_j^k + \frac{\alpha}{j}(R_1 - 0.5) \quad (4.18)$$

4.2 WHAT WERE ALGORITHMS USED FOR IN THIS DISSERTATION?

During this dissertation, we analyzed two types of problems: optimization and solution of a system of equations. The first one, i.e. optimization, represents the classical application of both, traditional and modern optimization algorithms. A direct example is the design of an optimum multilayered electromagnetic absorber, Figure 4-8, that should have minimum thickness and reflection [2–4]. In this case, factors such as the number of layers, as well as their materials and thickness, became design variables for the problem. Other scenarios for the use of optimization algorithms were found in the design of microchannel heat sinks [5,6], route planning [7], filter design [8,9], and oil production [10].

Awareness about the usage of optimization algorithms in the second kind of situations is, alas, less widespread (to our knowledge), and so, we briefly explain the process here. Imagine there is a system of two equations, $f_1(x)$ and $f_2(x)$, and that you need to calculate its solution, x^* . If we analyze each equation separately, we notice there is a total of three different points where at least one equation becomes zero. But, there is only one at which both equations nullify, and that is at the solution to our problem (Figure 4-9). Now, if we build a new equation, made up of the summation of each equation in the system, squared, we only get one point where the equation nullifies, and that is at x^* (again, our solution). This equation can be used as an objective function and thus optimization algorithms can be applied straightaway. In our work, we used this strategy to solve nonlinear equations and circuits [1,11–16], discrete systems [17], and linear Diophantine systems [18]. Also, we used it in the analysis of electrical power flowing throughout a loaded network [19,20], in the identification of nonlinear systems [21,22], and in the solution of the hybrid modes in a partially filled waveguide [23,24]. A more detailed description of the aforementioned process can be found in [69], and a full description of each situation (optimization or solution) is given in their respective reports [1–24].

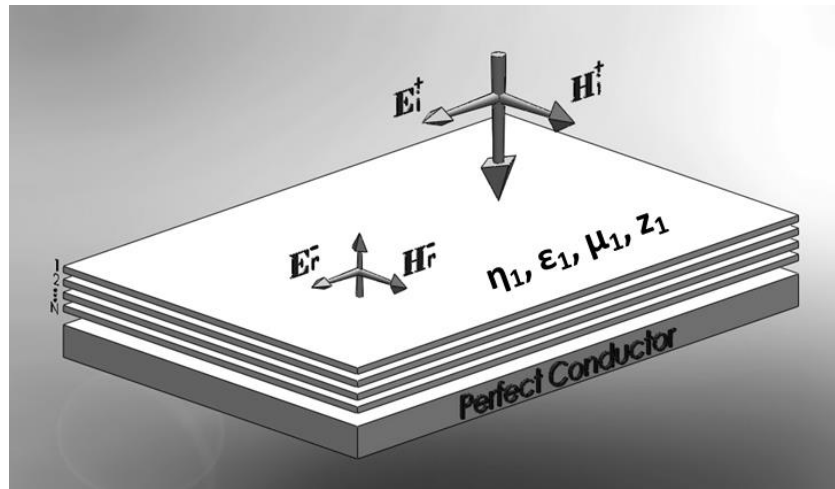


Figure 4-8. General scheme of an optimization problem, where it is required to minimize the total thickness and the reflection coefficient

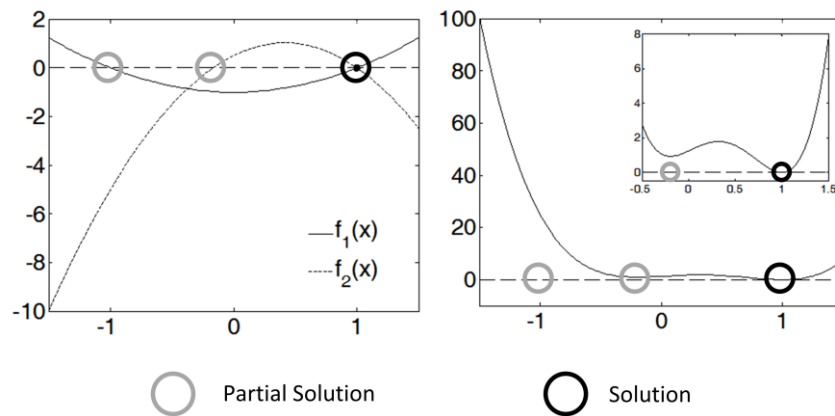


Figure 4-9. Graphical representation of the approach for solving a system of equations through an optimization algorithm

4.3 METHODOLOGY

A straightforward scheme was followed with each undergraduate study (Figure 4-10): define an algorithm, its variant (if possible) and an optimization problem; run some standard tests; apply the algorithm to the research problem; compare and analyze the data against previously reported one; and draw conclusions. Even so, we decided for each group to be free enough as to define the standard test functions they were going to use. More often than not, this decision was based on the test functions used by the creators of the optimization strategy.

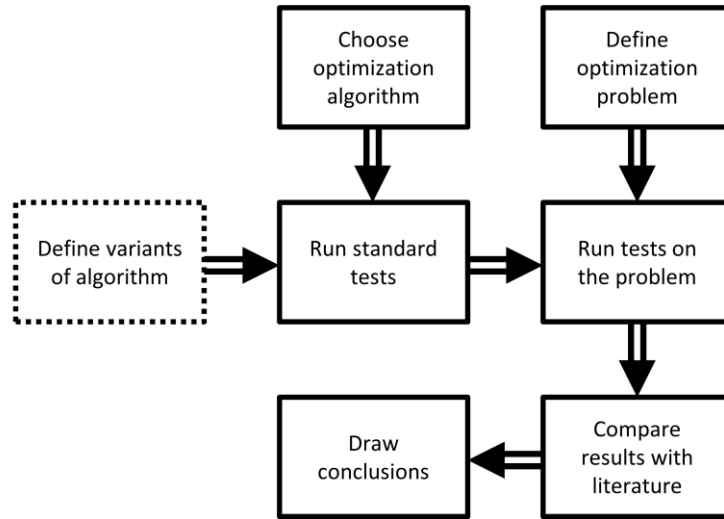


Figure 4-10. General scheme of the methodology used with each undergraduate study

This freedom, however, generated a wide diversity of results, and it would be impractical to include them all in this dissertation. Thus, Table 4-1 presents a summary of the standard test functions used during the different studies, and more information can be found in the respective reports [1–24] and articles [52,67–73,89–94]. Please bear in mind that this list is, by no means, exhaustive since this kind of functions is continuously growing.

Table 4-1. List of standard test functions used during the research

Name	Function	
Test Function 1	$F(x_1, x_2) = x_1^2 + 2x_2^2 - 0.3 \cos(3\pi x_1) - 0.4 \cos(4\pi x_2) + 0.7$	(4.19)
Test Function 2	$F(x_1, x_2) = e^{-0.1\sqrt{x_1^2+x_2^2}}$	(4.20)
Booth	$F(x_1, x_2) = (x_1 + 2x_2 - 7)^2 + (2x_1 + x_2 - 5)^2$	(4.21)
Himmelblau	$F(x_1, x_2) = (x_1^2 + x_2 - 11)^2 + (x_1 + x_2^2 - 7)^2$	(4.22)
Schubert	$F(x_1, x_2) = \sum_{i=1}^5 i \cos(i + x_1(i + 1)) \sum_{i=1}^5 i \cos(i + x_2(i + 1))$	(4.23)
Branin	$F(x_1, x_2) = a(x_2 - bx_1^2 + cx_1 - d)^2 + e(1 - f) \cos(x_1) + e$ $a = 1; b = \frac{5.1}{4\pi^2}; c = \frac{5}{\pi}; d = 6; e = 10; f = \frac{1}{8\pi}$	(4.24)
Six Hump Camel Back	$F(x_1, x_2) = \left(4 - 2.1x_1^2 + \frac{x_1^4}{3}\right)x_1^2 + x_1x_2 + (-4 + 4x_2^2)x_2^2$	(4.25)
Dropwave	$F(x) = -\frac{1 + \cos 12\sqrt{x_1^2 + x_2^2}}{0.5(x_1^2 + x_2^2) + 2}$	(4.26)

Name	Function
Wood	$F(x_1, x_2, x_3, x_4) = (10(x_2 - x_1^2))^2 + (1 - x_1)^2 + (\sqrt{90} \cdot (x_4 - x_3^2))^2 + (1 - x_3)^2 + (\sqrt{10} \cdot (x_2 + x_4 - 2))^2 + \left(\frac{x_2 - x_4}{\sqrt{10}}\right)^2$ (4.27)
Jong (Sphere)	$F(x) = \sum_{i=1}^N x_i^2$ (4.28)
Rastrigin	$F(x) = \sum_{i=1}^N x_i^2 - 10 \cos(2\pi x_i) + 10$ (4.29)
Rosenbrock	$F(x) = \sum_{i=1}^{N-1} 100(x_{i+1} - x_i^2)^2 + (1 - x_i)^2$ (4.30)
Griewank	$F(x) = 1 + \frac{1}{4000} \sum_{i=1}^N x_i^2 - \prod_{i=1}^N \cos\left(\frac{x_i}{\sqrt{i}}\right)$ (4.31)
Schwefel 2	$F(x) = \sum_{i=1}^N \left(\sum_{j=1}^i x_j \right)^2$ (4.32)
Schwefel 26	$F(x) = - \sum_{i=1}^N x_i \sin(\sqrt{ x_i })$ (4.33)
2 ⁿ minima	$F(x) = \sum_{i=1}^N x_i^4 - 16x_i^2 + 5x_i$ (4.34)
Ackley	$F(x) = 20 + e - 20e^{-0.2 \sqrt{\frac{1}{N} \sum_{i=1}^N x_i^2}} - e^{\frac{1}{N} \sum_{i=1}^N \cos(2\pi x_i)}$ (4.35)
Michalewicz	$F(x) = - \sum_{i=1}^N \sin(x_i) \sin^{2m}\left(\frac{ix_i^2}{\pi}\right)$ (4.36)
Schaffer	$F(x) = \sum_{i=1}^{N-1} (x_i^2 + x_{i+1}^2)^{0.25} (\sin^2(50(x_i^2 + x_{i+1}^2)^{0.10}) + 1)$ (4.37)
Sum of Powers	$F(x) = \sum_{i=1}^N x_i^2 ^{i+1}$ (4.38)
Axis Parallel Hyper-ellipsoid	$F(x) = \sum_{i=1}^N i \cdot x_i^2$ (4.39)
Rotated Hyper-ellipsoid	$F(x) = \sum_{i=1}^N \sum_{j=1}^i x_j^2$ (4.40)
Steps	$F(x) = \sum_{i=1}^N [(x_i + 0.5)]^2$ (4.41)

4.4 RESULTS

4.4.1 Standard test functions

Table 4-2 summarizes some of the results achieved with four original optimization strategies (CFO, HS, SO, and UPSO). Considering space restrictions, please refer to the undergraduate reports [1–24] and to the articles [52,67–73,89–94] for more data regarding optimization strategies and test functions.

Table 4-2. Average number of iterations (Iter.) and fitness, for different algorithms and standard test functions. Global optimum is 837.9658 for Schwefel 26 and 0 for the others

Test Function	CFO		HS		SO		UPSO	
	Iter.	Fitness	Iter.	Fitness	Iter.	Fitness	Iter.	Fitness
Jong 2D	334	4.81E-06	32849	4.59E-08	667	9.47E-08	24	4.74E-07
Schwefel 26 2D	276	7.98E+0 2	11554	8.38E+0 2	334	8.38E+0 2	91	8.38E+0 2
Rastrigin 2D	97	2.11E-06	61965	3.71E-08	420	0.00E+0 0	44	4.53E-07
Rastrigin 30D	20210 0	3.13E-03	169737 9	1.54E+0 2	336	3.97E+0 1	969	4.73E+0 1
Rosenbrock 2D	410	7.55E-05	44833	3.43E-07	272	9.56E-11	51	4.14E-07
Rosenbrock 3D	--	--	189771	9.88E-05	188	9.88E-07	384	8.84E-07
Rosenbrock 4D	--	--	563178	9.84E-05	2000 0	5.75E-17	733	9.80E-07
Rosenbrock 10D	20130 0	4.75E-04	897653	1.00E-04	--	--	936600	9.95E-11
Rosenbrock 30D	20120 0	4.73E+0 1	146541 0	1.00E-04	--	--	122370 0	9.92E-11

Some things are worth mentioning from Table 4-2. The first one is that HS required the highest number of iterations, even though it yielded good results, so we decided to explore the effect of adding some improvements (please refer to items 4.1.2.2 and 4.1.2.3 in section 4.1.2 for information on how the improvements work). We analyzed the modification known as ABHS and found that the second version (i.e. ABHSv2) performed better than the first one. Moreover, ABHSv2 greatly improved the performance of the original strategy, reducing the number of iterations up to 92.13% (Table 4-3). Then, we tested the second modification (i.e. SFHS) and found that it further improved ABHSv2 achievements. This time, reductions ranging from 34.41% to 91.19% were possible (

Table 4-4).

Table 4-3. Average results of ABHSv2 for three standard test functions, and their respective reduction of iterations [%] when compared to the best results yielded by HS

Test Function	HS	ABHSv2	Reduction
---------------	----	--------	-----------

	Iterations	Fitness	Iterations	Fitness	
Test Function 1	421454	2.24E-01	33166	4.35E-11	92.13%
Jong 6D	193002	3.65E+00	34304	8.38E-11	82.23%
Rastrigin 10D	649627	9.14E-10	143705	6.86E-10	77.88%

Table 4-4. Average results of SFHS for nine standard test functions in 2D, and their respective reduction of iterations [%] when compared to the best results yielded by ABHSv2

Test Function	HMCR	Fitness	Iterations	Reduction
Axis Parallel Hyper-ellipsoid	0.80	5.37E-11	2.79E+03	53.85%
	0.90	5.33E-11	2.28E+03	62.31%
Rotated Hyper-ellipsoid	0.80	5.39E-11	3.79E+03	39.47%
	0.90	5.35E-11	3.20E+03	48.91%
Rastrigin	0.80	5.32E-11	2.83E+03	79.09%
	0.90	5.32E-11	2.64E+03	80.49%
Schwefel	0.80	7.12E-12	3.84E+03	73.24%
	0.90	6.75E-12	3.64E+03	74.64%
Sum of Powers	0.80	4.36E-11	2.51E+03	34.41%
	0.90	4.31E-11	2.07E+03	45.85%
Ackley	0.80	7.03E-11	4.86E+03	66.83%
	0.90	6.92E-11	4.26E+03	70.90%
Langermann	0.80	5.22E-11	3.27E+03	90.98%
	0.90	5.13E-11	3.19E+03	91.19%
Six Hump Camel Back	0.80	5.42E-11	2.25E+03	80.41%
	0.90	5.35E-11	1.90E+03	83.44%
Dropwave	0.80	5.31E-11	4.01E+03	68.46%
	0.90	5.31E-11	3.74E+03	70.52%

The second important fact about Table 4-2 is that CFO is easily trapped by local optima geometrically distant from the optimum, even though they have similar fitness. For example, Schwefel's function in 2D has a global optimum of 837 located at (421, 421), and several local optimum throughout the search domain, one of which has a value of 719 and is located at (421, -302). Data for this function shows an average fitness of 798, meaning that some of the runs effectively converged to the global optimum but others were trapped by local optima.

As a final remark, Table 4-2 shows, in general, that CFO was unable to find an answer as good as the one found by HS, SO, and UPSO. In fact, CFO was only able to find a better answer for Rastrigin's function in 30D.

4.4.2 Further testing with SFHS

Since SHFS yielded good results, and considering that

Table 4-4 only shows information for standard search domains in 2D, we studied the effect of widening the domain and increasing the number of dimensions.

In the first case, we found some differences depending on the type of test function. For example, monomode functions (Figure 4-11 and Figure 4-12), or multimode functions with a defined global behavior (Figure 4-13), tended to stabilize for wider ranges per dimension. But, functions with planar regions (Figure 4-14, Figure 4-15 and Figure 4-16) tended to increase linearly as the range per dimension went up. Even so, in all cases, the increment for iterations and run time was virtually the same.

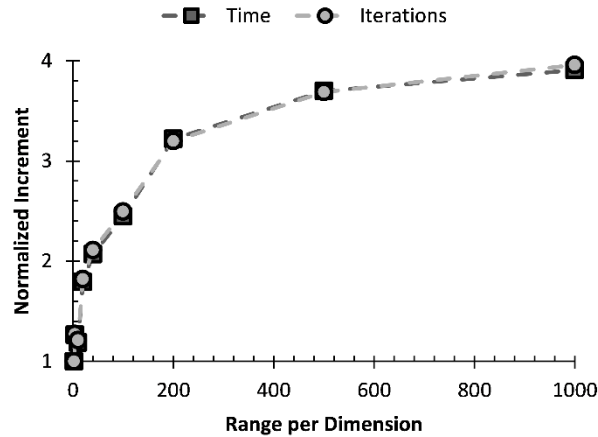


Figure 4-11. Normalized increment of iterations and run time for Sum of powers function, as a function of the range per dimension

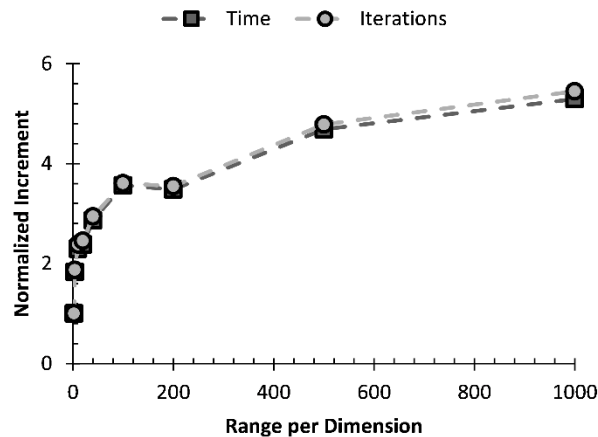


Figure 4-12. Normalized increment of iterations and run time for Axis parallel hyper-ellipsoid function, as a function of the range per dimension

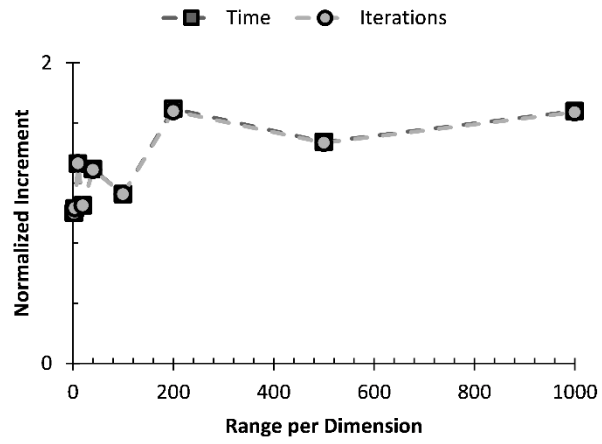


Figure 4-13. Normalized increment of iterations and run time for Dropwave function, as a function of the range per dimension

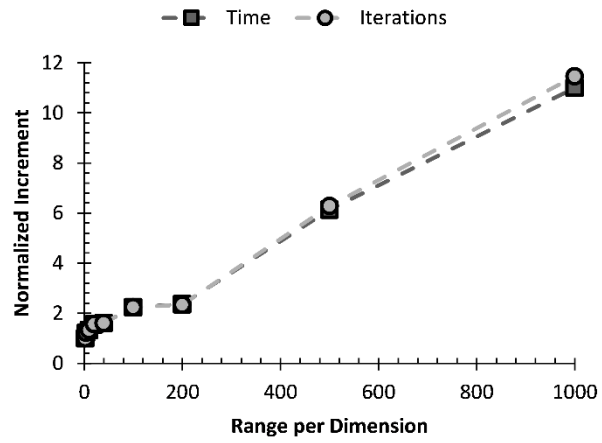


Figure 4-14. Normalized increment of iterations and run time for Ackley function, as a function of the range per dimension

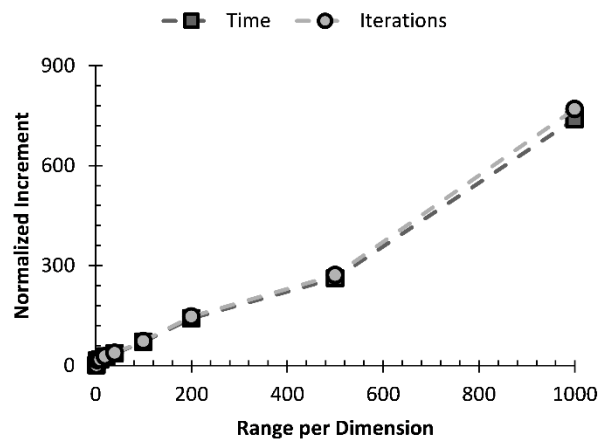


Figure 4-15. Normalized increment of iterations and run time for Rosenbrock function, as a function of the range per dimension

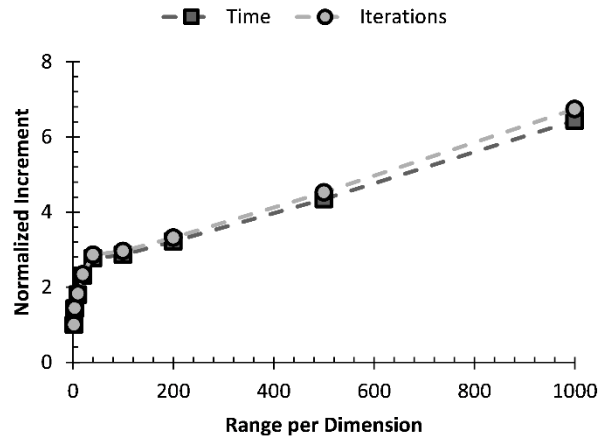


Figure 4-16. Normalized increment of iterations and run time for Six hump camel back function, as a function of the range per dimension

Pushing the algorithm further, we tested the scalability of SFHS with the following functions in up to 50D: Jong, Axis Parallel Hyper-ellipsoid, Rotated Hyper-ellipsoid, Sum of Powers, and Steps. SFHS was able to converge with better precision than $1e^{-7}$, and a 100% rate in virtually all cases (the only difficulty was in 50D for the Steps and Axis Parallel Hyper-ellipsoid functions with convergence rates of 96.97% and 9.09%, respectively). As expected, convergence time and iterations escalate exponentially, so we analyzed the increment normalized to the values required for two dimensions. This way, values tended to stabilize, but in some cases they required almost 100 times of those in two dimensions (Figure 4-17), while in others required more than 10000 (Figure 4-18). Even so, our data shows that the increment in the relation between normalized time and normalized iterations is linear for all tested functions (Figure 4-19).

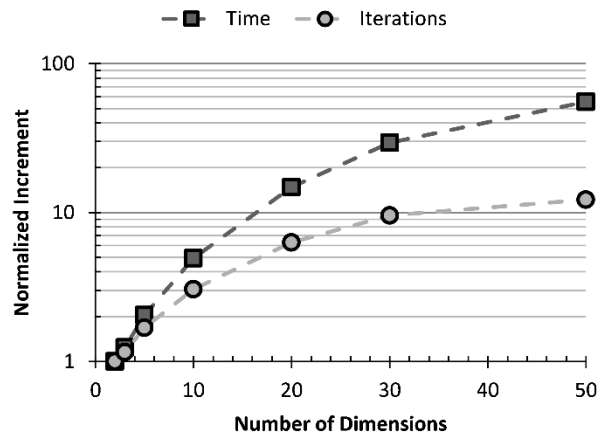


Figure 4-17. Time and iterations increase (normalized to 2D) as a function of the problem dimensions, for function Sum of Powers

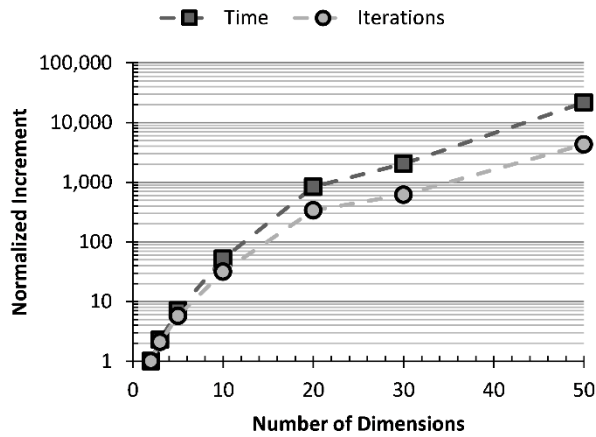


Figure 4-18. Time and iterations increase (normalized to 2D) as a function of the problem dimensions, for function Axis Parallel Hyper-ellipsoid

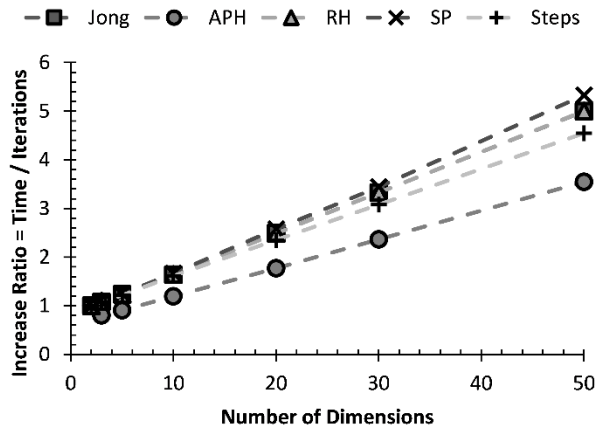


Figure 4-19. Increase Ratio (Normalized Time / Normalized Iterations) up to 50 dimensions for five functions: Jong, Axis Parallel Hyper-ellipsoid (APH), Rotated Hyper-ellipsoid (RH), Sum of Powers (SP), and Steps

4.4.3 Optimization of electromagnetic absorbers

We focused three undergraduate studies on solving this optimization problem through CFO, SO, and GSA [2–4]. In all cases, we considered the materials database shown in Table 4-5, widely available in literature [95].

Table 4-5. Materials database. Based on [95]

Lossless dielectric materials ($\mu_r = 1$)		Relaxed magnetic materials ($\epsilon_r = 15$)		
		$\mu_r = \mu' - j\mu''$	$\mu'(f) = \frac{\mu_m f_m^2}{f^2 + f_m^2}$	$\mu''(f) = \frac{\mu_m f_m f}{f^2 + f_m^2}$
Id	ϵ_r	Id	μ_m	f_m

1	10	9	35	0.8
2	50	10	35	0.5
Lossy magnetic materials ($\epsilon_r = 15$)		11	30	1.0
$\mu_r = \mu' - j\mu''$		12	18	0.5
$\mu'(f) = \frac{\mu'}{f^a}$		13	20	1.5
$\mu''(f) = \frac{\mu''}{f^b}$		14	30	2.5
Id	μ'	a	μ''	b
3	5	0.974	10	0.961
4	3	1.000	15	0.957
5	7	1.000	12	1.000
Lossy dielectric materials ($\mu_r = 1$)		15	30	2.0
$\epsilon_r = \epsilon' - j\epsilon''$		16	25	3.5
$\epsilon'(f) = \frac{\epsilon'}{f^a}$				
$\epsilon''(f) = \frac{\epsilon''}{f^b}$				
Id	ϵ'	a	ϵ''	b
6	5	0.861	8	0.569
7	8	0.778	10	0.682
8	10	0.778	6	0.861

As an example, we delve into different designs achieved by [2]. González and Bayona used a variant of CFO, known as acceleration clipping (AC) that limits the maximum acceleration of a probe. After some testing, it was found that a variable AC improved the results, so we used a maximum acceleration as shown by eq. (4.42).

$$A_{\max} = 0.49e^{-0.003t} + 0.01 \quad (4.42)$$

Moreover, and considering that the material of each layer is a discrete variable, we explored the effect of using a totally random initial distribution, a totally uniform one, and a mixed one (with uniformly distributed materials and randomly distributed thicknesses). We also implemented a two-stage process, striving to simplify the optimization problem. In the first stage, CFO optimizes the whole problem (i.e. materials and thicknesses) and returns the best solution. In the second stage, materials are fixed to the best ones previously found, and CFO only improves the thickness of each layer. A totally random initial distribution performs better, and the benefit of including the second stage is evident, since in all cases the maximum reflection coefficient improved while finding a thinner absorber (Table 4-6). Also, a frequency sweep (Figure 4-20) shows that this benefit extends along the operating range, and that a variable AC makes the response more stable (homogeneous).

Table 4-6. Results of the one-stage (1-St) and two-stage (2-St) processes when using CFO with AC for three different initial distributions, for the frequency range 0.8-1.9 GHz. Based on [91]

Initial Distribution		First Layer	Second Layer	Third Layer	Total	Max Γ [dB]
Random	Material	16	4	4		
	1-St Thickness [mm]	0.85	1.75	1.30	3.90	-27.11
	2-St Thickness [mm]	0.76	1.52	1.46	3.74	-28.76
Uniform	Material	4	5	1		
	1-St Thickness [mm]	1.53	1.34	1.59	4.46	-21.75
	2-St Thickness [mm]	1.65	1.17	1.53	4.36	-21.94

Mixed	Material	4	5	8		
	1-St Thickness [mm]	1.76	1.02	1.68	4.46	-22.00
	2-St Thickness [mm]	1.79	0.98	1.59	4.36	-22.01

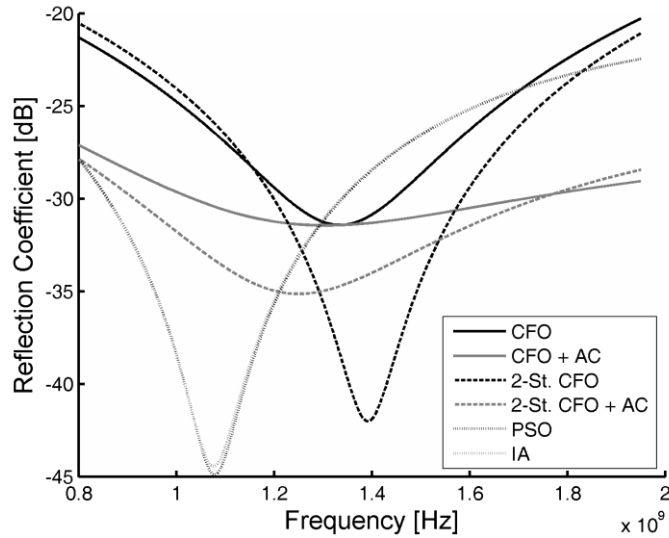


Figure 4-20. Frequency response of the best results found by [2] and of those reported by [96]

As a quick glance at the studies carried out, we present the final designs achieved with CFO+AC (2-Stages) [2], SO [3], and GSA [4], for an electromagnetic absorber in the frequency range between 2-8 GHz. These data do not cover the full scope of each undergraduate study, so please refer to each report if desired. We found that SO yielded the best results (Table 4-7), improving over previously reported data with a slightly thicker absorber (0.17 mm more than the best result). Also, we found that the two-stage CFO considering AC provided a good result in spite of having been designed with three layers. In fact, it performed better than the design previously reported with GSA, and it was also 0.62 mm thinner.

Table 4-7. Summary of designs found with CFO+AC, SO, and GSA, for the frequency range 2-8 GHz, and previously reported data

Algorithm		L1	L2	L3	L4	L5	Total	Max Γ [dB]
2-Stages CFO+AC [2]	Material	16	6	9	--	--		
	Thickness [mm]	0.39	1.96	1.87	--	--	4.23	-22.54
SO [3]	Material	16	6	6	14	11		
	Thickness [mm]	0.36	1.13	1.93	1.11	0.46	4.94	-25.94
GSA [4]	Material	16	6	6	16	5		
	Thickness [mm]	0.37	1.92	1.39	1.13	1.14	5.94	-25.20
CFO [34]	Material	16	6	6	6	15		
	Thickness [mm]	0.38	1.57	0.99	0.38	1.43	4.77	-25.70
SADE [34]	Material	16	6	6	6	15		
	Thickness [mm]	0.38	0.43	1.14	1.45	1.45	4.86	-25.49
GSA [34]	Material	16	6	8	13	4		

Algorithm		L1	L2	L3	L4	L5	Total	Max Γ [dB]
PSO [34]	Thickness [mm]	0.42	1.59	0.49	1.37	0.99	4.85	-21.96
	Material	14	6	8	5	11		
	Thickness [mm]	0.46	2.00	0.32	0.99	1.13	4.89	-23.89

4.4.4 Solution of system of equations and other scenarios

A second application tackled through modern optimization algorithms related to solving electronic circuits. We carried out four undergraduate studies directly related to this application [11–14], but we only show some of the results, for the sake of brevity. The studies began by analyzing the rather simple circuit shown in Figure 4-21, with only one non-linear element. We found that UPSO was able to solve the model appropriately, but PSO was not (Table 4-8) [13].

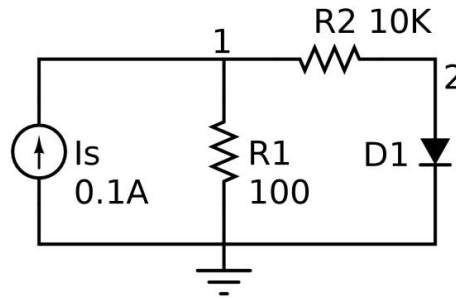


Figure 4-21. Simple circuit with one non-linear element

Table 4-8. Solutions obtained with PSO and UPSO for a circuit with one non-linear element, considering a swarm size of 10 particles. Theoretical solution: $V1 = 9.9080$ V and $V2 = 0.7125$ V

	PSO	UPSO
V1 [V]	10.0000	9.9080
V2 [V]	0.0000	0.7128
Fitness	2.00E-06	7.61E-22
Time [s]	0.28	0.06
Iterations	433	98

A more complex circuit is shown in Figure 4-22, inspired on a Buck converter. We defined a load represented by a number of identical additional loops so the performance of UPSO could be addressed (PSO results are not shown since it was already established that it did not perform well). During the tests, we considered $V_{in} = V_{pwm} = 5$ V, $R1 = 10$ Ω , $R2 = 0.1$ Ω , and $R3 = R(i + 1) = 500$ k Ω . Table 4-9 shows the solution found with simulation software up to 10 additional loops. We found that UPSO was able to get close to the answer (Table 4-10), but still had an average error of 0.42 V for 5 and 10 additional loops.

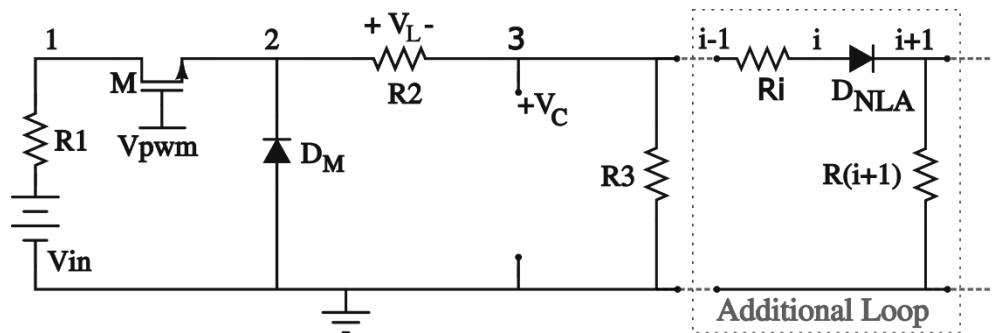


Figure 4-22. General scheme of the scalable circuit used for testing

Table 4-9. Solutions of each node [V] for the scalable circuit with different number of additional loops. For 10 additional loops, read the first column as FirstNode; SecondNode

Additional Loops	0	1	5	10	
Nodes	1 - 3	1 - 5	1 - 13	1 - 13 ...	14 - 23
1; 14	4.9999	4.9999	4.9999	4.9999	3.2382
2; 15	3.3675	3.3037	3.3054	3.3620	3.1889
3; 16	3.3675	3.3037	3.3054	3.3620	3.1889
4; 17		3.3036	3.3053	3.3619	3.1844
5; 18		3.2532	3.2556	3.3519	3.1844
6; 19			3.2556	3.3519	3.1351
7; 20			3.2510	3.3025	3.1351
8; 21			3.2510	3.3025	3.1328
9; 22			3.2012	3.2941	3.1327
10; 23			3.2012	3.2941	3.0835
11			3.1989	3.2448	
12			3.1988	3.2448	
13			3.1491	3.2383	

Table 4-10. Solutions [V] found by UPSO for different number of additional loops in the scalable circuit. For 10 additional loops, read the first column as FirstNode; SecondNode

Additional Loops	0	1	5	10	
Nodes	1 - 3	1 - 5	1 - 13	1 - 13 ...	14 - 23
1; 14	4.9999	5.0000	5.0000	5.0000	3.6665
2; 15	3.4227	3.8168	3.6492	3.4796	3.5591
3; 16	3.4227	3.8168	3.6492	3.4796	3.5595
4; 17		3.8168	3.6490	3.4793	3.9556
5; 18		3.7637	3.5692	3.3838	3.9549
6; 19			3.5693	3.3838	3.8333
7; 20			3.6747	3.2958	3.8337
8; 21			3.6747	3.2959	3.7632
9; 22			3.8814	3.6039	3.7633
10; 23			3.8812	3.6039	4.9572
11			3.7887	3.7729	
12			3.7889	3.7725	
13			3.8121	3.6666	

As a third example, consider the solution of hybrid modes within a waveguide. Homogeneously filled rectangular waveguides can be easily studied by analytical means,

since the problem can be decoupled into modes where one component in the travelling direction is zero. However, if there is a discontinuity (i.e. change of material), perpendicular to wave propagation, the solution cannot be decoupled and hybrid modes appear. This leads to a nonlinear system of equations whose analytic solution is difficult to achieve. Furthermore, as the number of materials (and hence, discontinuities) increase, the electromagnetic problem becomes more complex. Because of that, and considering that the optimization problem of this dissertation is also of the electromagnetic kind, we decided to assess the feasibility of using modern techniques to find some frequency responses of the waveguide. Striving not to expand too much, it will only be said that the data can be found in the appendix.

So far, we have commented on three applications more closely related to the objectives laid out in this dissertation: optimization of electromagnetic absorbers, solution of electronic circuits, and analysis of hybrid modes. As was mentioned in section 4.2 there are other applications, but in order to keep this section as brief as possible, they will not be commented, so we invite the reader to consult the appropriate references (see section 4.2 for more information).

4.5 DISCUSSION

Modern optimization algorithms are almost as diverse as test functions. Similarly, each one has its pros and cons. It is possible to tune a given algorithm to perform well under some scenario, but as Wolpert and Macready concluded, there is no algorithm that will be the best for every situation [97]. Thus, there is a need to rank them.

Several metrics can be carried out to determine if an algorithm will work under given circumstances. One of the more direct approaches is to run tests and compare the convergence rate of a set of algorithms for different test functions (e.g. monomode functions and multimode functions). Additional information can also be compared, such as the number of iterations, the run time, or the number of function evaluations.

We have shown some of the results that were achieved during this dissertation and, in some cases, with the assistance of undergraduate students. Most often than not, it was possible to adapt any given strategy for a particular problem, but their performance varied. For example, based on the work carried out with Cruz [13], we found that UPSO can solve the nonlinear mathematical model of an electronic circuit far more precisely than PSO. On the other hand, work carried out with Ramírez and Roa showed that CFO does not seem good for solving this type of problem [12], even though it worked well with standard test functions and in other applications (e.g. optimization of multilayered electromagnetic absorbers).

As examples of the improvements that can be made to an algorithm, consider the ABHS (both v1 and v2) and SFHS variants. In both cases, we were able to improve the performance of the original idea (i.e. HS), reducing the number of required iterations (up to 92.13% for ABHS, with an additional 91.19% for SFHS) while enhancing the fitness level of the answers. Regarding the latter, consider the plots shown in Figure 4-23, where a steep descent can be observed after 1000 iterations. Even if there is a region, roughly between 10 and 1000, where HS outperforms SFHS, we found that its effect diminishes for higher dimensions (Figure 4-24).

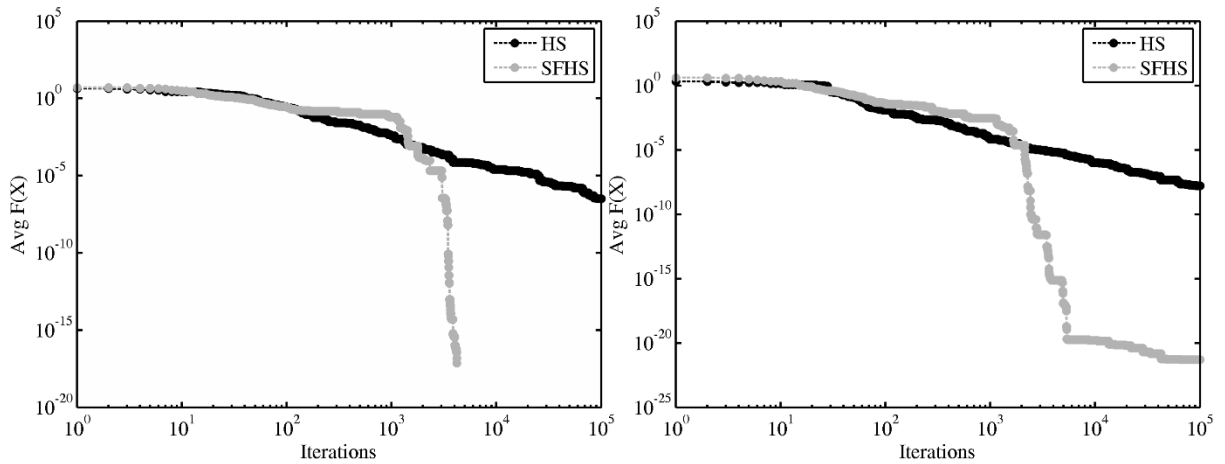


Figure 4-23. Average function evaluation as iterations progress (15 runs), for Test Function 1 (left) and Jong (right), both in 2D

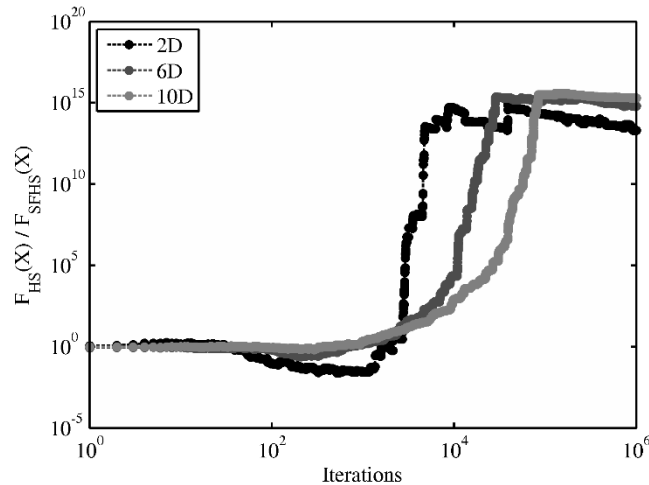


Figure 4-24. Function evaluation ratio as iterations progress, between HS and SFHS, for Jong's function in 2D, 6D, and 10D

After analyzing our data, we preselected four algorithms: CFO, HS, SO, and UPSO. We ranked them using the properties given in Table 4-11, and considering our prior experiences. We found that the best options came to be UPSO and HS. However, one of the main

drawbacks of HS is the elevated number of iterations (and thus, function evaluations) it requires, so we also included SFHS into the ranking. As a result, we obtained the matrix given in Table 4-11, and it is clear that SFHS and UPSO are the best options, so they will be used in the following chapters.

Table 4-11. Ranking of the preselected algorithms, including SFHS, where one is the worst score and five is the best one

Property	CFO	HS	SO	UPSO	SFHS
1. Simple to program	1	5	2	3	4
2. Required iterations	2	1	3	5	4
3. Extra calculations per iteration	1	5	2	3	4
4. Local trapping avoidance	1	2	3	5	4
5. Fitness improvement	1	2	3	4	5
6. Easy to parallelize	1	5	2	3	4
Total	7	20	15	23	25

4.6 FINAL COMMENTS

Throughout this chapter we focused on different modern optimization techniques used in the dissertation (including the undergraduate studies). We explained the general idea behind each approach, as well as a couple modifications made to some of the algorithms. We then commented on different scenarios the algorithms were used in (both, to optimize and to solve a system of nonlinear equations), and on the general methodology used with each undergraduate study. Regarding results, we summarized some of the most relevant data. We found that, in general, each algorithm can be tuned up to a given fitness value for a particular situation and that there is no particular approach that would be the best option for every single case. Moreover, we observed some of the drawbacks that a fixed optimization strategy may have for some kind of functions. For example, at 30 dimensions, CFO performed better than HS, SO, and UPSO for Rastrigin's function, while UPSO outperformed CFO for Rosenbrock's function. This chapter also condensed relevant performance data for SFHS. This modification (derived from ABHS, another modification we proposed), enhanced the fitness level and the required iterations of HS, without increasing the number of function evaluations.

From the vast amount of modern optimization techniques available, we conclude that Self-regulated Fretwidth Harmony Search (SFHS) and Unified Particle Swarm Optimization (UPSO) are the best candidates to keep working with. This decision is supported on a ranking according to six characteristics, for four algorithms that were preselected based on our experiences during the development of this doctoral thesis (see Table 4-12).

Thus, we will use SFHS and UPSO in the following chapters, to develop an optimization strategy for microwave applicators as laid out in the objectives of this dissertation.

REFERENCES

- [1] J. Contreras, C. Villanueva, Solución de un Sistema de Ecuaciones No Lineales, Utilizando una Estrategia Basada en el Algoritmo de Harmony Search, Undergraduate Thesis, Universidad Industrial de Santander, 2013.
- [2] J. González, C. Bayona, Aplicación del Método de Optimización por Fuerza Central (CFO), al Diseño de un Absorbedor Electromagnético Óptimo, Undergraduate Thesis, Universidad Industrial de Santander, 2013.
- [3] R. Ortiz, E. García, Diseño de un Absorbedor Electromagnético Multicapa Mediante el Método de la Espiral, Undergraduate Thesis, Universidad Industrial de Santander, 2013.
- [4] A. Miranda, J. Ruiz, Implementacion del Algoritmo de Búsqueda Gravitacional (GSA) para el Diseño de un Absorbedor Electromagnetico Óptimo, Undergraduate Thesis, Universidad Industrial de Santander, 2014.
- [5] A. Hinojosa, K. Espinosa, El Método de Enjambre de Partículas y el Criterio de Mínima Entropía en el Diseño Óptimo de un Disipador de Calor, Tesis de Pregrado, Universidad Industrial de Santander, 2011.
- [6] J. Ávila, O. Navarro, El Método de Colonia Artificial de Abejas y el Criterio de Mínima Entropía para el Diseño Óptimo de un Disipador de Calor, Undergraduate Thesis, Universidad Industrial de Santander, 2014.
- [7] J. Arias, M. Mogollón, Algoritmo de Optimización Gotas de Agua Virtuales Inteligentes Aplicado a la Planeación de Ruta Óptima de un Robot Móvil, Undergraduate Thesis, Universidad Industrial de Santander, 2013.
- [8] A. Rodríguez, K. Gaona, Diseño Óptimo de Filtros Electrónicos (Chebyshev) Mediante el Algoritmo de la Luciérnaga Virtual (Firefly), Undergraduate Thesis, Universidad Industrial de Santander, 2014.
- [9] H. Castro, M. Otero, El Algoritmo del Murciélago Virtual (Bat Algorithm) como Estrategia para el Diseño Óptimo de Filtros Pasa-Bajas, Undergraduate Thesis, Universidad Industrial de Santander, 2014.
- [10] M. Hernandez, Inteligencia Computacional Inspirada en la Cuántica, Aplicada a la Optimización de la Producción de Petróleo en el Modelo de un Pozo Inteligente, Undergraduate Thesis, Universidad Industrial de Santander, 2013.

- [11] J. Portilla, Solución de las Ecuaciones que Modelan un Circuito No Lineal de Corriente Directa Mediante el Método de Espiral, Undergraduate Thesis, Universidad Industrial de Santander, 2012.
- [12] F. Ramírez, O. Roa, Solución de las Ecuaciones que Describen el Modelo Matemático de un Circuito Electrónico Compuesto de Elementos No Lineales Mediante el Optimizador de Fuerza Central, Undergraduate Thesis, Universidad Industrial de Santander, 2012.
- [13] J. Cruz, Solución del Modelo Matemático de un Circuito Electronico D.C. No Lineal Mediante una Estrategia de Optimización, Undergraduate Thesis, Universidad Industrial de Santander, 2012.
- [14] S. Gonzalez, O. Trasladino, Análisis de la Eficiencia del Algoritmo Harmony Search en la Solución de un Circuito Electrónico No Lineal, Undergraduate Thesis, Universidad Industrial de Santander, 2013.
- [15] J. Garcia, D. Corredor, Algoritmo Hibrido del Simplex con la Estrategia de Optimizacion de Fuerza Central (CFO) Aplicado a la Solucion de Sistemas de Ecuaciones No Lineales, Undergraduate Thesis, Universidad Industrial de Santander, 2013.
- [16] K. Barreto, Evaluación del Método Optimizador de Fuerza Central Frente al Optimizador por Enjambre de Partículas Unificado en la Solución de Ecuaciones No Lineales, Undergraduate Thesis, Universidad Industrial de Santander, 2014.
- [17] C. Gómez, O. Pérez, Implementación de un Algoritmo de Optimización para Sistemas Discretos Fundamentado en la Técnica de Enjambre de Partículas, Undergraduate Thesis, Universidad Industrial de Santander, 2012.
- [18] J. Ramirez, F. Osorio, Algoritmo de Enjambre de Partículas Unificado para la Solución de Ecuaciones Diofánticas Lineales Comúnmente Encontradas en Problemas de Ingeniería Electrónica, Undergraduate Thesis, Universidad Industrial de Santander, 2013.
- [19] J. Celis, F. Rincón, Evaluación y Comparación entre los Métodos Newton Raphson y Artificial Bee Colony (ABC) para el Análisis del Flujo de Carga de un Sistema de Potencia, Undergraduate Thesis, Universidad Industrial de Santander, 2013.
- [20] C. Pinzón, E. Ardila, Evaluación y Comparación de los Métodos UPSO y Newton Raphson para el Análisis de Flujo de Cargas en un Sistema de Potencia, Undergraduate Thesis, Universidad Industrial de Santander, 2013.

- [21] E. Petro, R. Fuentes, *Mantenimiento Preventivo Básico de un Desfibrilador Monofásico Mediante los Métodos de Enjambre de Partículas Mejorado y Colonia Artificial de Abejas*, Undergraduate Thesis, Universidad Industrial de Santander, 2013.
- [22] D. Dávila, A. Rutto, *Identificación de Sistemas No Lineales Mediante el Método de Optimización de la Gota de Agua Virtual Inteligente*, Undergraduate Thesis, Universidad Industrial de Santander, 2014.
- [23] E. Farfán, J. Fontecha, *Obtención de Las Curvas de Dispersión de Modos Híbridos para Guías de Onda de Sección Transversal Rectangular Parcialmente Llena con un Dieléctrico, Mediante Optimización por Enjambre de Partículas Unificado UPSO*, Undergraduate Thesis, Universidad Industrial de Santander, 2013.
- [24] J. Suarez, J. Romero, *Solución de las Ecuaciones que Describe el Comportamiento de los Modos Híbridos en una Guía de Onda Rectangular Parcialmente Llena Mediante el Método de Optimización Recocido Simulado (Simulated Annealing)*, Undergraduate Thesis, Universidad Industrial de Santander, 2013.
- [25] R.A. Formato, *Central Force Optimization: a New Metaheuristic With Applications in Applied Electromagnetics*, *Prog. Electromagn. Res.* 77 (2007) 425–491. doi:10.2528/PIER07082403.
- [26] R.C. Green, L. Wang, M. Alam, *Training neural networks using Central Force Optimization and Particle Swarm Optimization: Insights and comparisons*, *Expert Syst. Appl.* 39 (2012) 555–563. doi:10.1016/j.eswa.2011.07.046.
- [27] R.C. Green, L. Wang, M. Alam, R. a. Formato, *Central force optimization on a GPU: a case study in high performance metaheuristics*, *J. Supercomput.* 62 (2012) 378–398. doi:10.1007/s11227-011-0725-y.
- [28] N.F. Shaikh, D.D. Doye, *A Novel Iris Recognition System Based on Central Force Optimization*, *Int. J. Tomogr. Simul.* 27 (2014) 23–34.
- [29] R.A. Formato, *Central force optimisation: a new gradient-like metaheuristic for multidimensional search and optimisation*, *Int. J. Bio-Inspired Comput.* 1 (2009) 217. doi:10.1504/IJBIC.2009.024721.
- [30] A.M. Montaser, K.R. Mahmoud, H.A. Elmikati, *B15. Tri-band slotted bow-tie antenna design for RFID reader using hybrid CFO-NM algorithm*, in: *2012 29th Natl. Radio Sci. Conf., IEEE, 2012*: pp. 119–126. doi:10.1109/NRSC.2012.6208515.
- [31] A.B. Abdel-Rahman, A.M. Montaser, H.A. Elmikati, *Design a novel bandpass filter with microstrip resonator loaded capacitors using CFO-HC algorithm*, in: *2nd Middle*

- East Conf. Antennas Propag., IEEE, 2012: pp. 1–6. doi:10.1109/MECAP.2012.6618188.
- [32] G.M. Qubati, N.I. Dib, Microstrip Patch Antenna Optimization Using Modified Central Force Optimization, *Prog. Electromagn. Res. B.* 21 (2010) 281–298.
- [33] R.A. Formato, Improved CFO Algorithm for Antenna Optimization, *Prog. Electromagn. Res. B*, Vol. 19, 405–425, 2010. 19 (2010) 405–425.
- [34] A. M.J., D. N.I., Design of Multilayer Microwave Broadband Absorbers Using Central Force Optimization, *Prog. Electromagn. Res. B.* 26 (2010) 101–113.
- [35] R.A. Formato, UWB Array Design Using Variable Zo Technology and Central Force Optimization, *ArXiv.* 0901 (2011) 1–97. <http://arxiv.org/abs/1108.0901> (accessed September 16, 2014).
- [36] R.A. Formato, A novel methodology for antenna design and optimization: Variable Zo, (2011) 1–97. <http://arxiv.org/abs/1107.1437> (accessed December 21, 2011).
- [37] R.A. Formato, Issues in Antenna Optimization - A Monopole Case Study, (2011) 1–82. <http://arxiv.org/abs/1103.5629> (accessed December 21, 2011).
- [38] R.C. Green, L. Wang, M. Alam, R.A. Formato, Central Force Optimization on a GPU: A case study in high performance metaheuristics using multiple topologies, in: 2011 IEEE Congr. Evol. Comput., IEEE, 2011: pp. 550–557. doi:10.1109/CEC.2011.5949667.
- [39] R.A. Formato, Improved CFO Algorithm for Antenna Optimization, *Prog. Electromagn. Res.* 19 (2010) 405–425.
- [40] X. Yang, Firefly Algorithm, Stochastic Test Functions and Design Optimisation, *Int. J. Bio-Inspired Comput.* 2 (2010) 78–84. <http://arxiv.org/abs/1003.1409> (accessed September 21, 2012).
- [41] X.-S. Yang, *Engineering Optimization: An Introduction*, 1st ed., John Wiley & Sons, New Jersey, 2010.
- [42] X. Yang, Firefly Algorithms for Multimodal Optimization, *Stoch. Algorithms Found. Appl.* 5792 (2010) 169–178. <http://arxiv.org/abs/1003.1466> (accessed August 17, 2012).
- [43] Z.W. Geem, J.H. Kim, G.V. Loganathan, A New Heuristic Optimization Algorithm: Harmony Search, *Simulation.* 76 (2001) 60–68. doi:10.1177/003754970107600201.

- [44] Z.W. Geem, State-of-the-Art in the Structure of Harmony Search Algorithm, in: *Recent Adv. Harmon. Search Algorithm*, Springer Berlin Heidelberg, 2010: pp. 1–11. doi:10.1007/978-3-642-04317-8_1.
- [45] Z.W. Geem, *Music-Inspired Harmony Search Algorithm*, 1 th, Springer, 2009.
- [46] Z.W. Geem, Novel derivative of harmony search algorithm for discrete design variables, *Appl. Math. Comput.* 199 (2008) 223–230. doi:10.1016/j.amc.2007.09.049.
- [47] Z.W. Geem, M. Fesanghary, J. Choi, M.P. Saka, J.C. Williams, M.T. Ayvaz, et al., Recent Advances in Harmony Search, in: *Adv. Evol. Algorithms*, InTech, 2008: pp. 127–142.
http://www.intechopen.com/books/advances_in_evolutionary_algorithms/recent_advances_in_harmony_searc.
- [48] Z.W. Geem, H. Hwangbo, Application of Harmony Search to Multi-Objective Optimization for Satellite Heat Pipe Design, (2006) 2–4.
- [49] K.S. Lee, Z.W. Geem, A new meta-heuristic algorithm for continuous engineering optimization: harmony search theory and practice, *Comput. Methods Appl. Mech. Eng.* 194 (2005) 3902–3933. doi:10.1016/j.cma.2004.09.007.
- [50] M. Aghaie, T. Nazari, a. Zolfaghari, a. Minuchehr, a. Shirani, Investigation of PWR core optimization using harmony search algorithms, *Ann. Nucl. Energy.* 57 (2013) 1–15. doi:10.1016/j.anucene.2013.01.046.
- [51] O.M. Alia, R. Mandava, The Variants of the Harmony Search Algorithm: An Overview, *Artif. Intell. Rev.* 36 (2011) 49–68. doi:10.1007/s10462-010-9201-y.
- [52] J. Contreras, I. Amaya, R. Correa, An improved variant of the conventional Harmony Search algorithm, *Appl. Math. Comput.* 227 (2014) 821–830. doi:10.1016/j.amc.2013.11.050.
- [53] C. Hong, G. Xing-sheng, Multi-HM Adaptive Harmony Search Algorithm and its Application to Continuous Function Optimization, *Res. J. Appl. Sci. Eng. Technol.* 4 (2012) 100–103.
- [54] A. Kaveh, A. Nasrollahi, Engineering design optimization using a hybrid PSO and HS algorithm, *Asian J. Civ. Eng.* 14 (2013) 201–223.
- [55] I. Landa-Torres, D. Manjarres, S. Salcedo-Sanz, J. Del Ser, S. Gil-Lopez, A multi-objective grouping Harmony Search algorithm for the optimal distribution of 24-hour medical emergency units, *Expert Syst. Appl.* 40 (2013) 2343–2349. doi:10.1016/j.eswa.2012.10.051.

- [56] M. Mahdavi, M.H. Chehreghani, H. Abolhassani, R. Forsati, Novel meta-heuristic algorithms for clustering web documents, *Appl. Math. Comput.* 201 (2008) 441–451. doi:10.1016/j.amc.2007.12.058.
- [57] M. Mahdavi, M. Fesanghary, E. Damangir, An improved harmony search algorithm for solving optimization problems, *Appl. Math. Comput.* 188 (2007) 1567–1579. doi:10.1016/j.amc.2006.11.033.
- [58] K. Nekooei, M.M. Farsangi, H. Nezamabadi-Pour, K.Y. Lee, An Improved Multi-Objective Harmony Search for Optimal Placement of DGs in Distribution Systems, *IEEE Trans. Smart Grid.* 4 (2013) 557–567. doi:10.1109/TSG.2012.2237420.
- [59] C.C.O. Ramos, A.N. Souza, G. Chiachia, A.X. Falcão, J.P. Papa, A Novel Algorithm for Feature Selection Using Harmony Search and its Application for Non-Technical Losses Detection, *Comput. Electr. Eng.* 37 (2011) 886–894. doi:10.1016/j.compeleceng.2011.09.013.
- [60] S. Salcedo-Sanz, D. Manjarrés, Á. Pastor-Sánchez, J. Del Ser, J. a. Portilla-Figueras, S. Gil-López, One-way urban traffic reconfiguration using a multi-objective harmony search approach, *Expert Syst. Appl.* 40 (2013) 3341–3350. doi:10.1016/j.eswa.2012.12.043.
- [61] W. Sun, J. Wang, J. Chen, Harmony Search Based Optimization GM (1, 1) Model for Power Generation Forecasting, *Int. J. Adv. Inf. Sci. Serv. Sci.* 5 (2013) 500–506. doi:10.4156/aiss.vol5.issue4.62.
- [62] A.A. Taleizadeh, S.T.A. Niaki, F. Barzinpour, Multiple-buyer multiple-vendor multi-product multi-constraint supply chain problem with stochastic demand and variable lead-time: A harmony search algorithm, *Appl. Math. Comput.* 217 (2011) 9234–9253. doi:10.1016/j.amc.2011.04.001.
- [63] E. Valian, S. Tavakoli, S. Mohanna, An intelligent global harmony search approach to continuous optimization problems, *Appl. Math. Comput.* 232 (2014) 670–684. doi:10.1016/j.amc.2014.01.086.
- [64] R.A. Vural, U. Bozkurt, T. Yildirim, Analog active filter component selection with nature inspired metaheuristics, *AEU - Int. J. Electron. Commun.* 67 (2013) 197–205. doi:10.1016/j.aeue.2012.07.009.
- [65] J. Kennedy, R. Eberhart, Particle Swarm Optimization, in: *Proc. ICNN'95 - Int. Conf. Neural Networks*, IEEE, Perth, Australia, 1995: pp. 1942–1948. doi:10.1109/ICNN.1995.488968.

- [66] R. Eberhart, J. Kennedy, A new optimizer using particle swarm theory, in: MHS'95. Proc. Sixth Int. Symp. Micro Mach. Hum. Sci., IEEE, 1995: pp. 39–43. doi:10.1109/MHS.1995.494215.
- [67] I. Amaya, L.A. Gómez, R. Correa, Discrete Particle Swarm Optimization in the numerical solution of a system of linear Diophantine equations, *Dyna*. 81 (2014) 139–144.
- [68] I. Amaya, J. Cruz, R. Correa, Solution of the Mathematical Model of a Nonlinear Direct Current Circuit Using Particle Swarm Optimization, *Dyna*. 79 (2012) 77–84.
- [69] I. Amaya, J. Cruz, R. Correa, Real Roots of Nonlinear Systems of Equations Through a Metaheuristic Algorithm, *Dyna*. 78 (2011) 15–23.
- [70] O. Pérez, I. Amaya, R. Correa, Numerical solution of certain exponential and non-linear Diophantine systems of equations by using a discrete particle swarm optimization algorithm, *Appl. Math. Comput.* 225 (2013) 737–746. doi:10.1016/j.amc.2013.10.007.
- [71] J. Cruz, I. Amaya, C. Correa, Algoritmo de optimización para el cálculo de múltiples raíces de sistemas de ecuaciones no lineales, *Inge CUC*. 9 (2013) 197–208.
- [72] J. Cruz, I. Amaya, R. Correa, Solution of the mathematical model of a DC nonlinear electronic circuit using an optimization strategy: Application of the original and unified Particle Swarm Metaheuristics, in: 2012 IEEE 4th Colomb. Work. Circuits Syst., IEEE, 2012: pp. 1–6. doi:10.1109/CWCAS.2012.6404080.
- [73] C. Gómez, I. Amaya, R. Correa, An Alternative Method for the Design of Time-varying Feedback Control Systems, *Dyna*. 79 (2012) 168–174.
- [74] H. Zhu, Y. Wang, K. Wang, Y. Chen, Particle Swarm Optimization (PSO) for the constrained portfolio optimization problem, *Expert Syst. Appl.* 38 (2011) 10161–10169. doi:10.1016/j.eswa.2011.02.075.
- [75] A. Subramanian, G. Ravi, D. Arun Gopal, Loss Minimization and Voltage Profile Improvement Incorporating Multiple SVC using PSO Algorithm, *Int. J. Comput. Appl.* 46 (2012) 15–20.
- [76] H.K. Verma, C. Jain, A. Rathore, P. Gupta, A Comparative Study of GA, PSO and Big Bang-Big Crunch Optimization Techniques for Optimal Placement of SVC 's, *Int. J. Electron. Commun. Comput. Eng.* 3 (2012) 263–269.

- [77] I. Fister, X.-S. Yang, K. Ljubič, D. Fister, J. Brest, Towards the novel reasoning among particles in PSO by the use of RDF and SPARQL., *Sci. World J.* 2014 (2014) 1–10. doi:10.1155/2014/121782.
- [78] J.J. Liang, A.K. Qin, P.N. Suganthan, S. Baskar, Comprehensive learning particle swarm optimizer for global optimization of multimodal functions, *IEEE Trans. Evol. Comput.* 10 (2006) 281–295. doi:10.1109/TEVC.2005.857610.
- [79] A. Ratnaweera, S.K. Halgamuge, H.C. Watson, Self-Organizing Hierarchical Particle Swarm Optimizer With Time-Varying Acceleration Coefficients, *IEEE Trans. Evol. Comput.* 8 (2004) 240–255. doi:10.1109/TEVC.2004.826071.
- [80] J. Robinson, Y. Rahmat-Samii, Particle Swarm Optimization in Electromagnetics, *IEEE Trans. Antennas Propag.* 52 (2004) 397–407. doi:10.1109/TAP.2004.823969.
- [81] Y. Shi, R. Eberhart, A modified particle swarm optimizer, 1998 *IEEE Int. Conf. Evol. Comput. Proceedings. IEEE World Congr. Comput. Intell.* (Cat. No.98TH8360). (n.d.) 69–73. doi:10.1109/ICEC.1998.699146.
- [82] M. Clerc, J. Kennedy, The particle swarm - explosion, stability, and convergence in a multidimensional complex space, *IEEE Trans. Evol. Comput.* 6 (2002) 58–73. doi:10.1109/4235.985692.
- [83] J. Kennedy, R.C. Eberhart, A Discrete Binary Version of the Particle Swarm Algorithm, in: 1997 *IEEE Int. Conf. Syst. Man, Cybern. Comput. Cybern. Simul.*, IEEE, 1997: pp. 4104–4108. doi:10.1109/ICSMC.1997.637339.
- [84] K. Tamura, K. Yasuda, Primary study of spiral dynamics inspired optimization, *IEEJ Trans. Electr. Electron. Eng.* 6 (2011) S98–S100. doi:10.1002/tee.20628.
- [85] K. Tamura, K. Yasuda, Spiral optimization -A new multipoint search method, in: 2011 *IEEE Int. Conf. Syst. Man, Cybern.*, IEEE, 2011: pp. 1759–1764. doi:10.1109/ICSMC.2011.6083926.
- [86] L. Benasla, A. Belmadani, M. Rahli, Spiral Optimization Algorithm for solving Combined Economic and Emission Dispatch, *Int. J. Electr. Power Energy Syst.* 62 (2014) 163–174. doi:10.1016/j.ijepes.2014.04.037.
- [87] A.N.K. Nasir, M.O. Tokhi, O. Sayidmarie, R.M.T. Raja Ismail, A novel adaptive spiral dynamic algorithm for global optimization, 2013 13th *UK Work. Comput. Intell.* (2013) 334–341. doi:10.1109/UKCI.2013.6651325.
- [88] K.E. Parsopoulos, M.N. Vrahatis, UPSO: A unified particle swarm optimization scheme, *Lect. Ser. Comput. Comput. Sci.* 1 (2004) 868–873.

- [89] O. Roa, F. Ramirez, I. Amaya, R. Correa, Solution of nonlinear circuits with the Central Force Optimization algorithm, in: 2012 IEEE 4th Colomb. Work. Circuits Syst., IEEE, Barranquilla, 2012: pp. 1–6. doi:10.1109/CWCAS.2012.6404079.
- [90] I. Amaya, J. Cruz, R. Correa, A modified firefly-inspired algorithm for global computational optimization, *Dyna.* 81 (2014) 85–90. doi:http://dx.doi.org/10.15446/dyna.v81n187.34594.
- [91] J.E. González, I. Amaya, R. Correa, Design of an Optimal Multi-layered Electromagnetic Absorber through the Central Force Optimization Algorithm, in: PIERS Proc., Stockholm, 2013: pp. 1082–1086.
- [92] I. Amaya, R. Correa, Optimal Design of Multilayer EMAs for Frequencies between 0.85 GHz and 5.4 GHz, *Rev. Ing.* 38 (2013) 33–37.
- [93] S. Vanegas, I. Amaya, R. Correa, Virtual bat algorithm for the computation of Duhamel ' s Integral applied to structural systems with one degree of freedom, *Rev. Ing. Construcción.* 28 (2013) 278–289.
- [94] R. Correa, I. Amaya, A. Araque-Herrera, Uso de algoritmos metaheurísticos híbridos para la minimización de entropía en problemas de transferencia de calor en circuitos electrónicos, *Rev. Ing. Y Univ.* 15 (2011) 403–421.
- [95] H. Liu, L. Zhang, Y. Gao, Y. Shen, D. Shi, Electromagnetic Wave Absorber Optimal Design Based on Improved Particle Swarm Optimization, EMC 2009, IEICE. (2009) 797–800.
- [96] E. Salazar, J. Mora, Diseño de Absorbedores Electromagnéticos Óptimos Utilizando Optimización por Enjambre de Partículas y Análisis de Intervalos, Undergraduate Thesis, Universidad Industrial de Santander, 2011.
- [97] D.H. Wolpert, W.G. Macready, No free lunch theorems for optimization, *IEEE Trans. Evol. Comput.* 1 (1997) 67–82. doi:10.1109/4235.585893.

5. SOLVING THE PROBLEM

Throughout earlier chapters we developed a mathematical model for estimating the field distribution of a test resonator, and for evaluating its similarity to a desired field (Chapter 2). Such procedure was based on the general formulation shown in [1,2], and was applied to circuitual analysis following [3]. We also measured the dielectric properties of different mineral ores as a function of temperature (Chapter 3). Finally, we assessed different modern optimization strategies, based on different approaches (Chapter 4). Now, we have the tools for establishing an optimization strategy that finds the dimensions and operating frequency of a microwave resonator, such that the field distribution matches a desired one, for a given load. Hence, in this chapter we present a general layout of said strategy, and evaluate its validity.

5.1 AN OVERVIEW OF THE OPTIMIZATION STRATEGY

Towards the end of Chapter 2, an overview of the process required for evaluating the objective function was laid out. This included the definition and calculation of the PSNR, which is based on the mean squared error between the images representing the desired and test field distributions.

Figure 5-1 shows a similar layout, but this time it spans to the interaction between the optimization algorithm and the objective function. Briefly speaking, the algorithm (UPSO or SFHS for this dissertation) generates a set of possible solutions (particles for UPSO, and harmonies for SFHS) that must be evaluated in the objective function. This information is used to update the position of each solution. The whole process must be repeated until a solution (i.e. a design) that complies with the convergence criteria is found (i.e. a minimum value of PSNR must be reached before the algorithm stops).

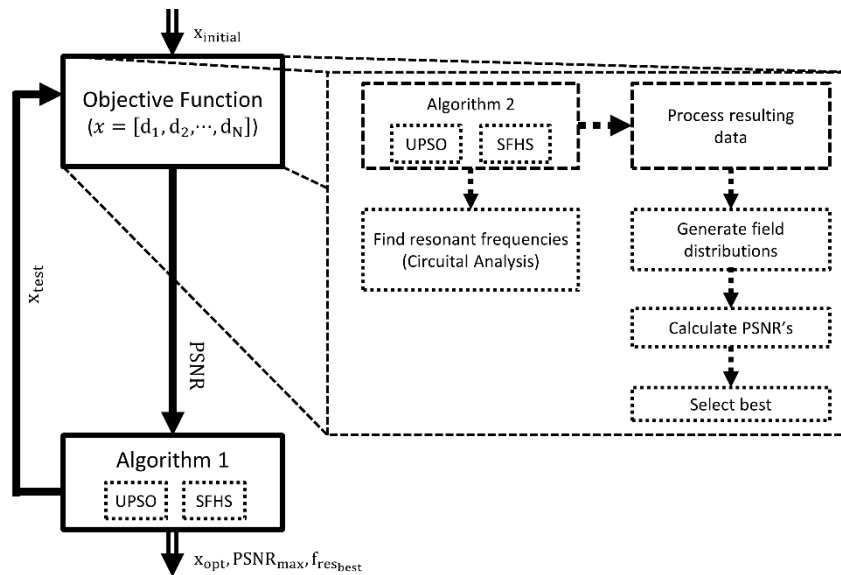


Figure 5-1. Overview of the procedure for merging objective function and optimization algorithm

Nevertheless, and as was mentioned in Chapter 2, each possible design has multiple resonant frequencies, so every evaluation of the objective function requires an internal optimization cycle that finds them. An alternative for doing so, is the procedure followed in [4], where each solution found was added as a penalty factor to the objective function. During this cycle, each frequency must be evaluated in order to estimate the electric field distribution. Then, it must be compared against the desired field distribution, calculating the PSNR between the fields. The best solution (i.e. the frequency that yields the highest PSNR) is selected and sent to the main loop.

5.2 METHODOLOGY

According to the discussion given in Chapter 4, UPSO and SFHS were selected as feasible algorithms for this chapter. Since it was already proved that they perform well, data for standard test functions is not shown. Moreover, there are two optimization loops (i.e. the external one, in charge of optimizing the dimensions; and the internal one, in charge of finding the resonant frequencies of a given test design), and so there appears four possible combinations of algorithms. Moreover, each optimization loop represents an independent problem, so run parameters need not be equal for both of them. Nevertheless, we selected the following common parameters for UPSO: $c_p = 2.05$, $c_g = 2.05$, and $u = 0.5$; and these for SFHS: $HMS = 5$, $HMCR = 0.95$, $PAR = 0.8$, $FW_{sat} = 100$, $FW_{min} = 10^{-12}$, and $C_{FW} = 1$. The remaining parameter of UPSO, i.e. the swarm size, was set to 5 for the external loop and to 15 for the internal one. For SFHS, the particular parameters of the internal loop were: $FW_{max} = 10^8$, and $FW_{ini} = 0.5 \times 10^8$; whilst for the external loop were: $FW_{max} = 1$, and $FW_{ini} = 0.5$.

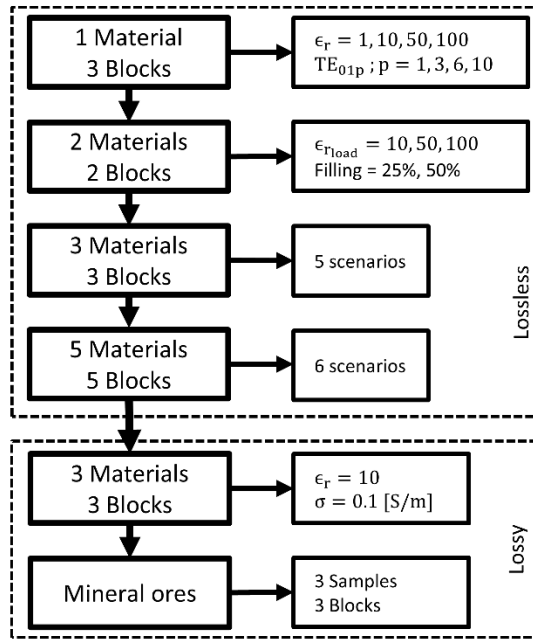


Figure 5-2. Methodology followed throughout this chapter

Figure 5-2 shows an overview of the methodology followed during this chapter. As a first approach, and striving to verify that the optimization algorithms are able to find an appropriate design, simple tests were run, considering only one material. Nonetheless, we split the resonator into three blocks, in order to consider all types of building blocks. Four materials were selected, with $\epsilon_r = 1, 10, 50, \text{ and } 100$. Also, four different TE_{01p} resonating modes were analyzed, with $p = 1, 3, 6, \text{ and } 10$. All combinations of algorithms were tested and their average performance (based on 30 runs) was compared against commercial software (CST). Since there are two optimization loops that must be addressed, it is necessary to establish both search domains. The outer loop (i.e. the length of each block) ranged between 0.2 and 0.6 [m], whilst the inner loop (i.e. the frequency) spanned from 0.05 [GHz], and up to a maximum frequency that depended on the load. This was done to avoid having too many resonant frequencies in some scenarios, and too few in others. Hence, for the first case, i.e. $\epsilon_r = 1$, the maximum frequency was set to 1.5 [GHz]. For $\epsilon_r = 10, \epsilon_r = 50, \text{ and } \epsilon_r = 100$, it was set to 1.0, 0.5, and 0.15 [GHz], respectively.

The second phase of testing dealt with a partially filled cavity of volume $0.1 \times 0.2 \times 1.0 \text{ [m}^3\text{]}$. This means that the resonator was split into two blocks, one with $\epsilon_r = 1$ (i.e. air) and one with a given ϵ_{rload} . In order to generate the desired field distributions, we considered four different sets of relative permittivity (i.e. ϵ_{rload}) and fill percentage. Moreover, we analyzed two different resonant frequencies of the first set. This information is summarized in Table 5-1.

Table 5-1. Scenarios for the second battery of tests

Scenario	$\epsilon_{r_{load}}$	Filling [%]	Frequency [GHz]
1	10	25	0.72
2	10	25	0.89
3	10	50	0.75
4	50	50	0.75
5	100	25	0.81

The third phase of testing related to resonators split into three blocks. The total volume was preserved, and the ideal fields correspond to blocks with the same length. Table 5-2 shows the selected scenarios and it can be seen that the first three are different resonances of the same design. This was done to observe the evolution of the algorithm at different frequencies. All algorithms were tested for the first three scenarios, and the best configuration was defined based on the results reached so far. The selected combination of algorithms was used from this point onward.

Table 5-2. Scenarios for the third battery of tests

Scenario	ϵ_{r_1}	ϵ_{r_2}	ϵ_{r_3}	Frequency [GHz]
1	1	10	1	0.63
2	1	10	1	0.75
3	1	10	1	1.02
4	10	1	10	1.94
5	1	10	20	0.76

The fourth phase of testing referred to resonators split in more than three blocks. The testing scenarios are laid out in Table 5-3. Again, the total volume of the resonator is preserved and all blocks are assumed of the same length. Two frequencies were considered for the first two configurations, striving to observe a change in the precision of our approach.

Table 5-3. Scenarios for resonators split into five blocks

Scenario	ϵ_{r_1}	ϵ_{r_2}	ϵ_{r_3}	ϵ_{r_4}	ϵ_{r_5}	Frequency [GHz]
1	1	10	20	10	1	0.24
2	1	10	20	10	1	0.86
3	10	1	20	10	1	0.26
4	10	1	20	10	1	0.90
5	10	20	1	10	20	0.26
6	10	20	1	10	1	0.26

Afterwards, we move on to the testing lossy materials in a three block resonator. Both of the extreme blocks were made of air and the mid one was made of a material with $\epsilon_r = 10$ and conductivity $\sigma = 0.1$. The selected complex frequency was $f = 0.75 + j0.081$ [GHz]. Then,

we analyzed three of the minerals discussed in Chapter 3, and observed the electric field distribution at five different temperatures (Table 5-4). This time we considered a resonator with a volume of $0.1 \times 0.2 \times 0.5 \text{ [m}^3\text{]}$, split into three networks with identical length. Also, two of the minerals represent samples that reacted strongly under the influence of microwaves (i.e. they roasted), whilst the remaining one represents a sample that exhibited weak interaction.

Table 5-4. Scenarios considered for simulations including minerals

Juan Blanco - S100	T [°C]	24	100	350	640	50
(JB-S100)	ϵ'_r	5.20	5.40	6.10	10.10	7.90
	$\sigma \text{ [S/m]}$	0.10	0.11	0.13	0.14	0.13
M9 - S100	T [°C]	24	100	420	627	50
(M9-S100)	ϵ'_r	6.97	7.05	7.80	6.40	7.77
	$\sigma \text{ [S/m]}$	0.17	0.17	0.19	0.18	0.19
Juan Blanco - S200	T [°C]	24	100	160	246	50
(JB-S200)	ϵ'_r	2.51	3.15	4.30	3.40	2.50
	$\sigma \text{ [S/m]}$	0.01	0.01	0.01	0.01	0.00

5.3 RESULTS

5.3.1 Resonator uniformly filled with a material

According to the methodology discussed in the previous section, the first approach was verifying that the optimization algorithms were able to find appropriate designs. Hence, Figure 5-3 shows the average performance achieved with each combination of UPSO and SFHS, compared against the data yielded by commercial software. It is clear that the commercial software exhibited a decaying performance, achieving PSNR values in the range from about 50 [dB] to almost 20 [dB]. However, all the selected combinations of algorithms exhibited a more stable behavior, with PSNR values above 60 [dB], and in some cases, around 80 [dB].

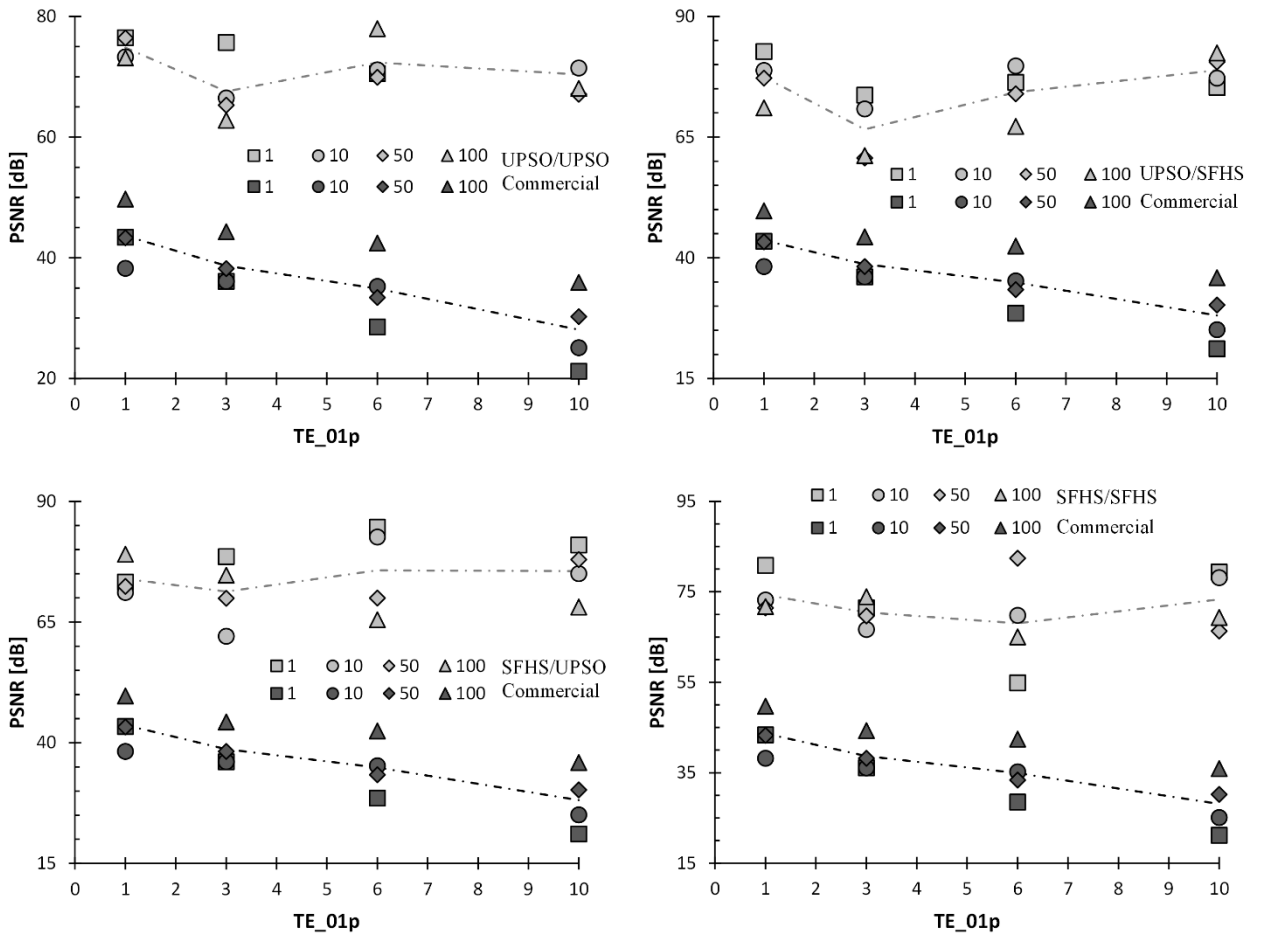


Figure 5-3. Quality of the answers found with all combinations of UPSO and SFHS (average data for 30 runs), compared against the quality of solutions yielded by commercial software

Since all algorithms had a stable performance for different modes, we decided to analyze the influence of the search domain on the quality of the results. Hence, we ran some tests, striving to find an appropriate width for all blocks, such that the dominant mode is excited in the resulting cavity. For starters, we considered that each block could have a length of, maximum, 0.1 [m]. Then, we progressively increased this value up to 1 [m]. As expected, we found that smaller values of the search domain allow higher values of PSNR to be found, even above 100 [dB] (first case). After that, the PSNR begins decaying, reaching values around 80 [dB] for the widest scenario (Figure 5-4).

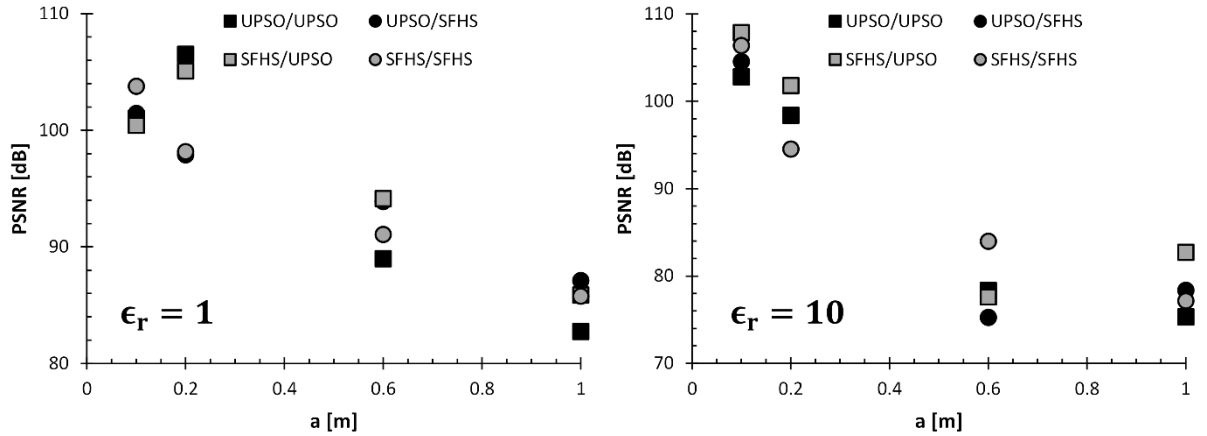


Figure 5-4. Comparison of all algorithms for different widths of search domain, and two scenarios with different relative permittivity (ϵ_r). Average data for 30 runs

5.3.2 Resonator filled with multiple lossless materials

We now migrate to more complex scenarios that include different combinations of materials. We begin by showing the performance of the algorithm when the resonator contains two materials with different dielectric properties. Then, we explore what happens when the number of materials increases to three. At the end of this subsection, we show data for resonators that contain more than three blocks.

5.3.2.1 Resonator with two materials

The first test considered two different resonant frequencies for a resonator 25% filled with a material having $\epsilon_r = 10$. The first frequency is located at 0.72 [GHz], whilst the second one is located at 0.89 [GHz]. Figure 5-5 shows the field distribution for both cases, as reported by the commercial software, by the analytic solution, and by the model used during this dissertation. A comparison of the fields at each frequency reveals that the commercial software yields a PSNR of 33 [dB] and 28 [dB], whilst the model of this dissertation reports values of 27 [dB] and 26 [dB], respectively. Even so, a visual inspection of the fields reveals that the contours yielded by the commercial software are less uniform than those reported by the model we used.

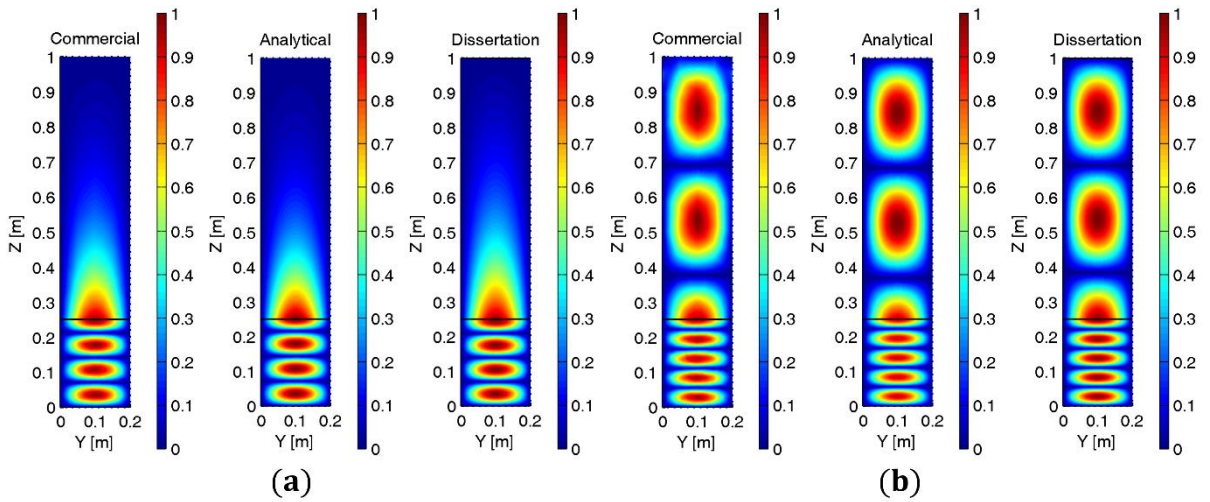


Figure 5-5. Electric field distribution (normalized) for a resonator of volume $0.1 \times 0.2 \times 1.0$ [m³], 25% filled with $\epsilon_r = 10$. Resonant frequency: (a) 0.72 [GHz] (b) 0.89 [GHz]

Increasing the filling to 50% shifts the resonant frequency to 0.75 [GHz]. We also inverted the order of the materials and verified that our algorithm responds appropriately. Figure 5-6 shows the field distribution under these conditions, where the commercial software reached a PSNR of 28 [dB] whilst our model achieved 24 [dB]. A closer look at the field distributions reveal that the commercial software fails to report most of the highest intensity zones (i.e. the center of each loop), but our algorithm does not. Even so, the PSNR value is lower due to the error in the lower half, where $\epsilon_r = 1$.

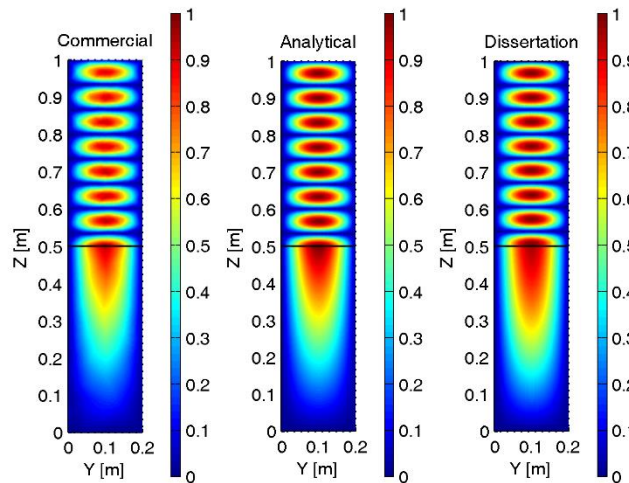


Figure 5-6. Electric field distribution (normalized) for a resonator of volume $0.1 \times 0.2 \times 1.0$ [m³], 50% filled with $\epsilon_r = 10$

When analyzing the effect of materials with higher permittivity, we found that both, commercial software and our model, are able to find similar values of PSNR, but ours yield

a more uniform field distribution. For example, consider a material with $\epsilon_r = 100$ that is used to fill 25% of a resonator. In this case, the commercial software yields a PSNR of 37 [dB] and our model yields 32 [dB]. But, the field distribution of the commercial software is not as uniform as ours (Figure 5-7). Another example is a resonator half-filled with a material having $\epsilon_r = 50$. Here, the nonuniform field distribution is more notorious, but still, the commercial software reports a PSNR of 24 [dB] whilst our model reports a PSNR of 21 [dB] (Figure 5-8).

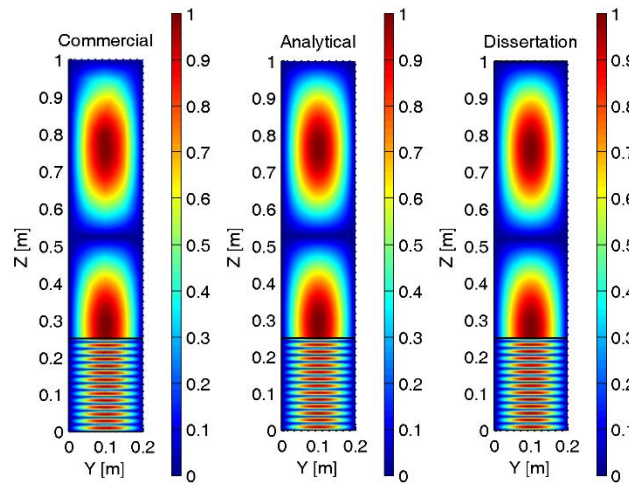


Figure 5-7. Electric field distribution (normalized) for a resonator of volume $0.1 \times 0.2 \times 1.0$ [m³], 25% filled with $\epsilon_r = 100$

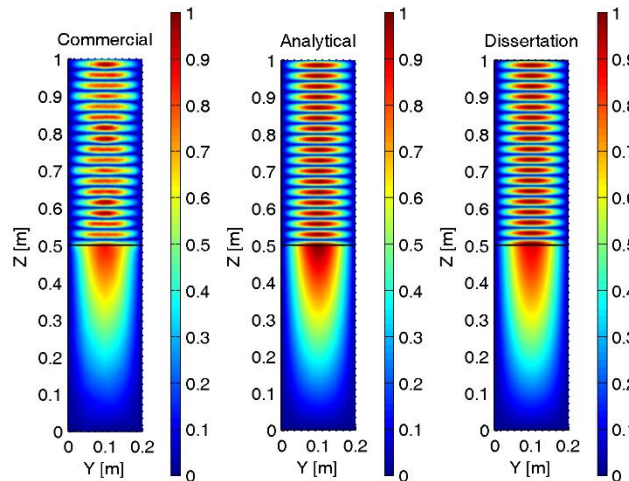


Figure 5-8. Electric field distribution (normalized) for a resonator of volume $0.1 \times 0.2 \times 1.0$ [m³], 50% filled with $\epsilon_r = 50$

Figure 5-9 shows the average \pm standard deviation of running our algorithm 30 times, for each one of the previously mentioned scenarios, and demanding a minimum PSNR of 20 [dB]. In all cases, our algorithm performed appropriately, and sometimes the dispersion was significantly smaller than others. This is due to the fact that the current model (i.e. using the norm) does not provide the same level of accuracy for all resonant frequencies, although it seems that this effect is lessened at higher frequencies.

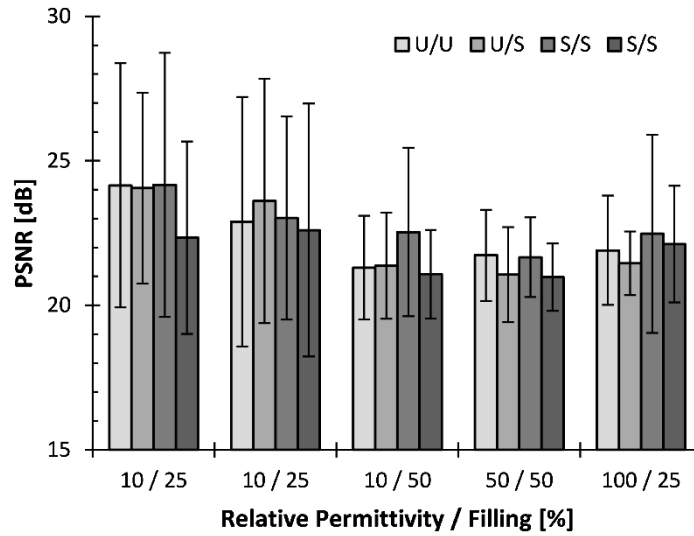


Figure 5-9. PSNR (average \pm standard deviation) found by all algorithms for different scenarios and 30 runs. A minimum PSNR of 20 dB was demanded in all cases

5.3.2.2 Resonator with three materials

We now analyze the performance of the algorithm for configurations with three different materials. Also, throughout this item we select a combination of algorithms that will be used for the remainder of the chapter. It is worth mentioning that even if we show data for symmetric designs, the process followed during the dissertation, and the models provided, can be used for non-symmetric designs.

In order to select the best pair of algorithms, we focus on three different resonant frequencies of a given configuration. In this case, the outer blocks are empty (i.e. $\epsilon_r = 1$ in blocks one and three) and the middle one is made of a material with $\epsilon_r = 10$. We consider the resonances located at 0.63 [GHz], 0.75 [GHz], and 1.02 [GHz], because our model reports different levels of precision at each one of them, and because we want to observe a wider frequency range. Figure 5-10 shows the electric field distribution of the first resonant frequency, and it is clear that our model is not able to fully replicate it, thus reporting a PSNR of just 19 [dB]. Even so, the field distribution in the loaded block is more uniform than that yielded by the commercial software, who reported a PSNR of 34 [dB].

Similarly, Figure 5-11 shows the field distribution for the remaining scenarios, and it is evident that our algorithm outperforms the commercial alternative. In the first case, i.e. at a resonant frequency of 0.75 [GHz], the commercial alternative provides a nonuniform field distribution, and this reflects on a diminished PSNR of 22 [dB]. Our model, on the other hand, reports a more stable field distribution, thus increasing its PSNR up to 23 [dB]. In the remaining case, i.e. at a resonant frequency of 1.02 [GHz], the commercial software preserves its behavior (i.e. nonuniform field distribution), reaching a PSNR of 23 [dB], whilst our alternative is able to increase its PSNR up to 51 [dB].

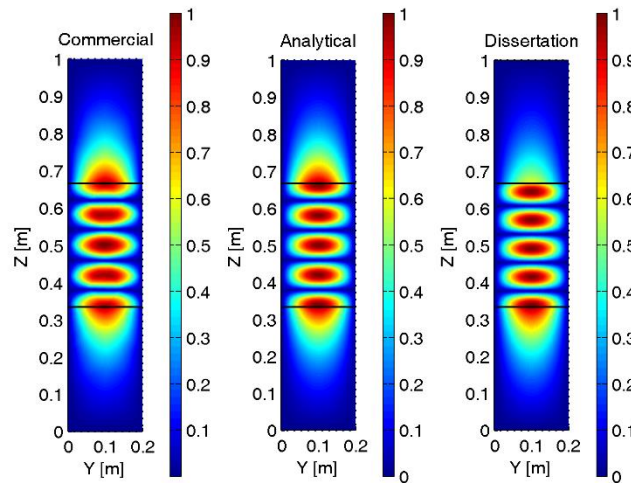


Figure 5-10. Electric field distribution (normalized) for a resonator of volume $0.1 \times 0.2 \times 1.0$ [m³], 33% filled with $\epsilon_r = 10$. Resonant frequency: 0.63 [GHz]

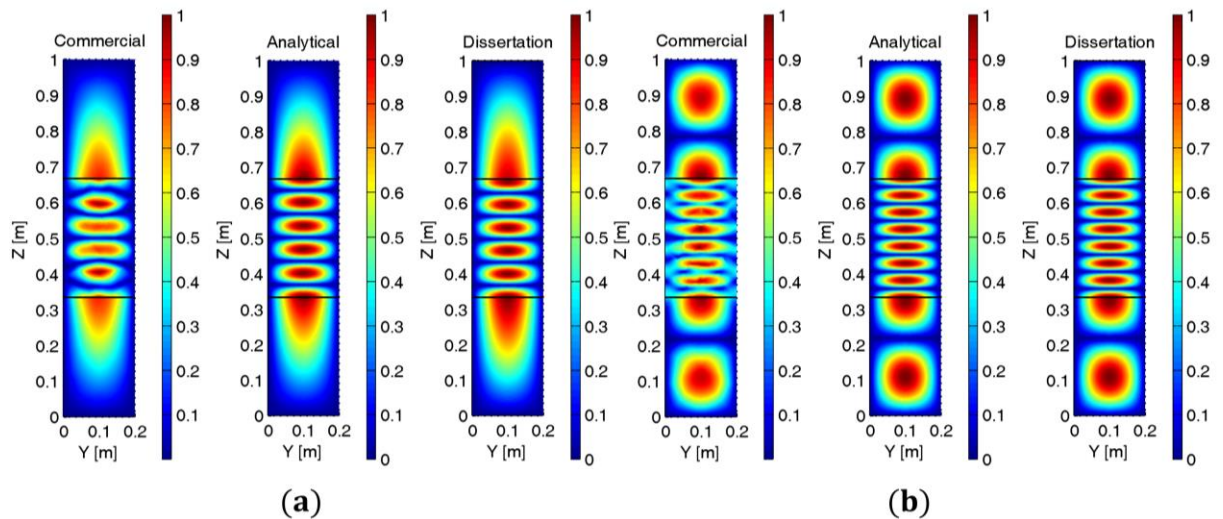


Figure 5-11. Electric field distribution (normalized) for a resonator of volume $0.1 \times 0.2 \times 1.0$ [m³], 33% filled with $\epsilon_r = 10$. Resonant frequency: (a) 0.75 [GHz] (b) 1.02 [GHz]

Based on these three scenarios, we ran tests with all combinations of the algorithms, striving to detect which one of them performed better. Table 5-5 summarizes the average data of 10 runs. During the first two scenarios, UPSO/UPSO and UPSO/SFHS performed similarly, but they both outperformed SFHS/UPSO and SFHS/SFHS. So, the latter two were not tested under the third scenario. The remaining combinations were compared under the more demanding third scenario, requesting a minimum PSNR of 51 [dB]. Both combinations still performed similarly well, but UPSO/SFHS required, in average, 50 less evaluations of the objective function (Table 5-5). As a complimentary test, we calculated the average PSNR of all alternatives, for 10 runs, and across the first 250 function evaluations. It is clear that the evolution of SFHS/UPSO and SFHS/SFHS is slower than that of UPSO/UPSO and UPSO/SFHS (Figure 5-12). Hence, we selected UPSO/SFHS as the best combination of algorithms and as the one that will be used for the remainder of this chapter.

Table 5-5. Statistical data for all combinations of algorithms and the three scenarios of the first design. Average data for 10 runs. Tests for the third scenario were not run with SFHS/UPSO and SFHS/SFHS since the other alternatives outperformed them in the previous stages

Algorithm		First scenario		Second scenario		Third scenario	
		PSNR [dB]	Evaluations	PSNR [dB]	Evaluations	PSNR [dB]	Evaluations
UPSO/UPSO	Avg	21.9	9.0	21.9	32.0	51.6	400.0
	SD	2.5	14.7	0.9	26.5	0.8	138.2
	Max	26.2	45.0	23.5	80.0	53.1	585.0
	Min	19.2	0.0	21.1	5.0	51.0	200.0
UPSO/SFHS	Avg	20.5	10.0	22.6	76.5	52.3	350.0
	SD	1.2	16.7	1.9	71.8	2.0	153.0
	Max	22.5	55.0	26.1	185.0	56.1	595.0
	Min	19.1	0.0	21.1	0.0	51.0	220.0
SFHS/UPSO	Avg	20.4	18.5	21.6	63.0	--	--
	SD	1.4	26.9	0.6	77.9	--	--
	Max	23.8	80.0	23.2	277.0	--	--
	Min	19.1	0.0	21.0	8.0	--	--
SFHS/SFHS	Avg	20.3	46.3	21.7	107.1	--	--
	SD	2.1	49.0	0.7	108.4	--	--
	Max	25.8	122.0	23.5	369.0	--	--
	Min	19.0	0.0	21.0	0.0	--	--

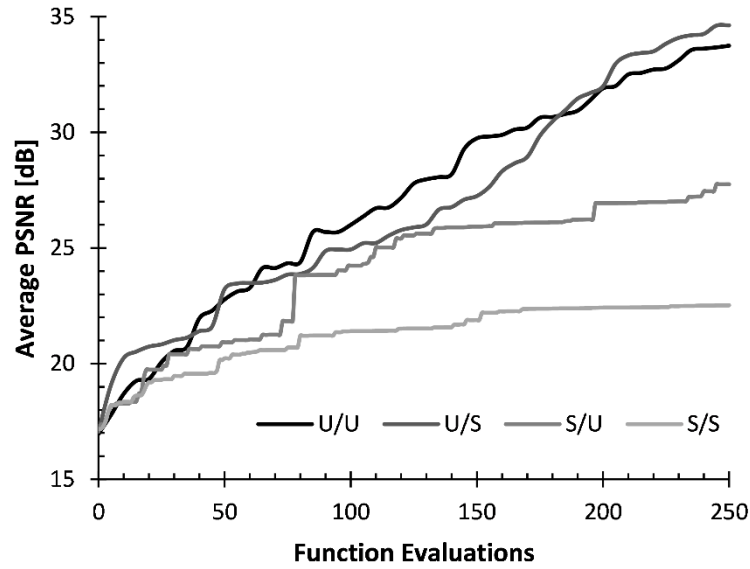


Figure 5-12. First 250 function evaluations for the third scenario, using all combinations of the algorithms. Average data for 10 runs

For the remaining tests we considered a scenario where the outer blocks were made of a material with $\epsilon_r = 10$, whilst the inner one was empty (i.e. $\epsilon_r = 1$), and a scenario with progressively increasing permittivity, such that $\epsilon_r = [1, 10, 20]$. Again, we observe that the field distribution yielded by the commercial software is distorted (Figure 5-13), generating a PSNR of 28 [dB] and 20 [dB] for each scenario. Our model, however, was more stable and reached PSNR values of 31 [dB] and 54 [dB], respectively.

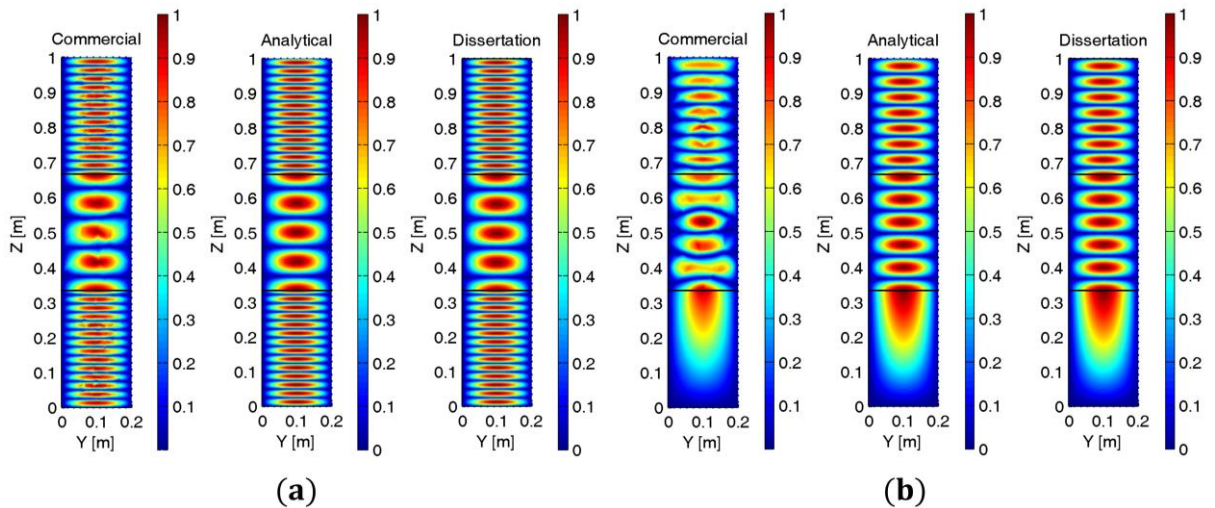


Figure 5-13. Electric field distribution (normalized) for a resonator of volume $0.1 \times 0.2 \times 1.0$ [m³], split into three blocks of the same length. Dielectric properties and resonant frequency: (a) $\epsilon_r = [10 \ 1 \ 10]$, $f = 0.75$ [GHz] (b) $\epsilon_r = [1 \ 10 \ 20]$, $f = 1.02$ [GHz]

Table 5-6 shows the designs found by the selected combination of algorithms, i.e. UPSO/SFHS, and its comparison against the theoretical data. It is clear that whenever the PSNR is above 50 [dB], the design found by the algorithm has virtually no error. Even so, the worst case of the designs shown in Table 5-6 has an error of only a few centimeters.

Table 5-6. Designs found by UPSO/SFHS for each one of the scenarios considered during this testing phase, including the length of each block (L_i), the resonant frequency, and the PSNR. In all cases, a theoretical value of 0.33 [m] was assumed for each block

Relative Permittivity			Theoretical Values Frequency [GHz]	Found Values				PSNR [dB]
ϵ_{r1}	ϵ_{r2}	ϵ_{r3}		L_1 [m]	L_2 [m]	L_3 [m]	Frequency [GHz]	
1	10	1	0.63	0.36	0.36	0.32	0.64	20.50
1	10	1	0.75	0.36	0.31	0.33	0.76	22.58
1	10	1	1.02	0.33	0.33	0.33	1.02	52.32
10	1	10	1.94	0.32	0.32	0.32	2.00	32.90
1	10	20	0.76	0.33	0.33	0.33	0.76	61.85

5.3.2.3 Resonator with more than three blocks

Consider a test design comprised of five blocks of the same length (0.2 [m]), with relative permittivity of 1, 10, 20, 10, and 1, respectively. Figure 5-14 shows the electric field distribution at two different resonant frequencies (0.24 [GHz] and 0.86 [GHz]). In the first case, our model is unable to provide a field distribution as good as the one yielded by commercial software (PSNR of 23 [dB] and 51 [dB], respectively). But, at higher frequencies the opposite happens, and our model yields a field distribution quite similar to the analytical, reaching a PSNR of 31 [dB] as opposed to 19 [dB] yielded by the commercial solution.

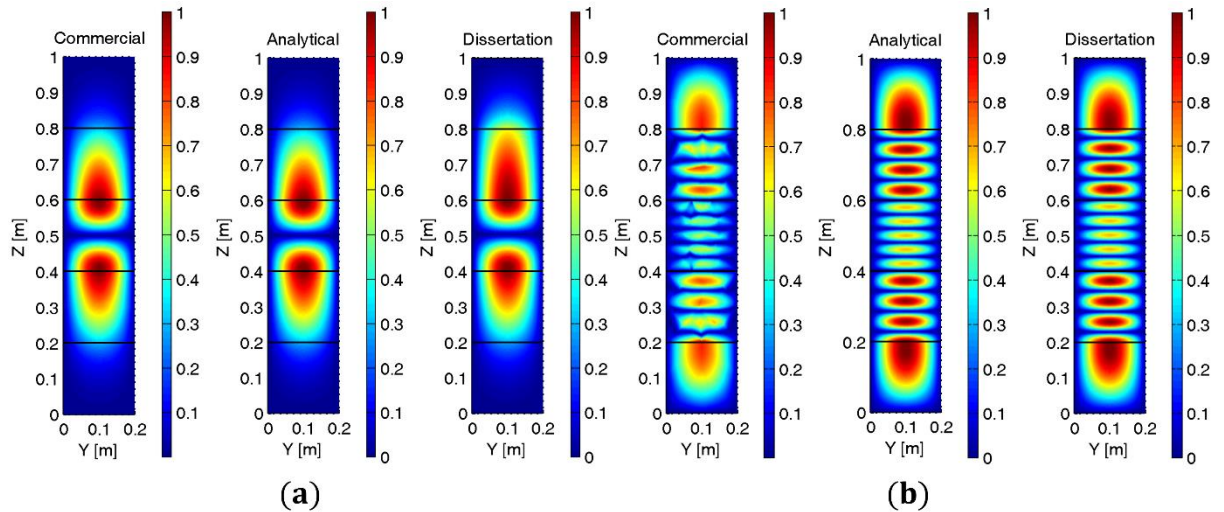


Figure 5-14. Electric field distribution (normalized) for a resonator of volume $0.1 \times 0.2 \times 1.0$ [m³], split into five blocks of the same length. Dielectric properties: $\epsilon_r = [1 \ 10 \ 20 \ 10 \ 1]$. Resonant frequency: (a) $f = 0.24$ [GHz] (b) $f = 0.86$ [GHz]

If the order of materials one and two is exchanged, the resulting resonator is formed by blocks with relative permittivity of 10, 1, 20, 10, and 1, respectively. Using similar resonant frequencies, one arrives at the field distributions shown in Figure 5-15. In this case, the first resonant frequency is located at 0.26 [GHz], and the commercial solution yields a PSNR of 51 [dB] whilst our model yields 34 [dB]. The second resonant frequency shifts to 0.90 [GHz] and the commercial solution is hindered down to 27 [dB] whilst our model improves to 35 [dB]. Moreover, the field distribution provided by the commercial solution is distorted.

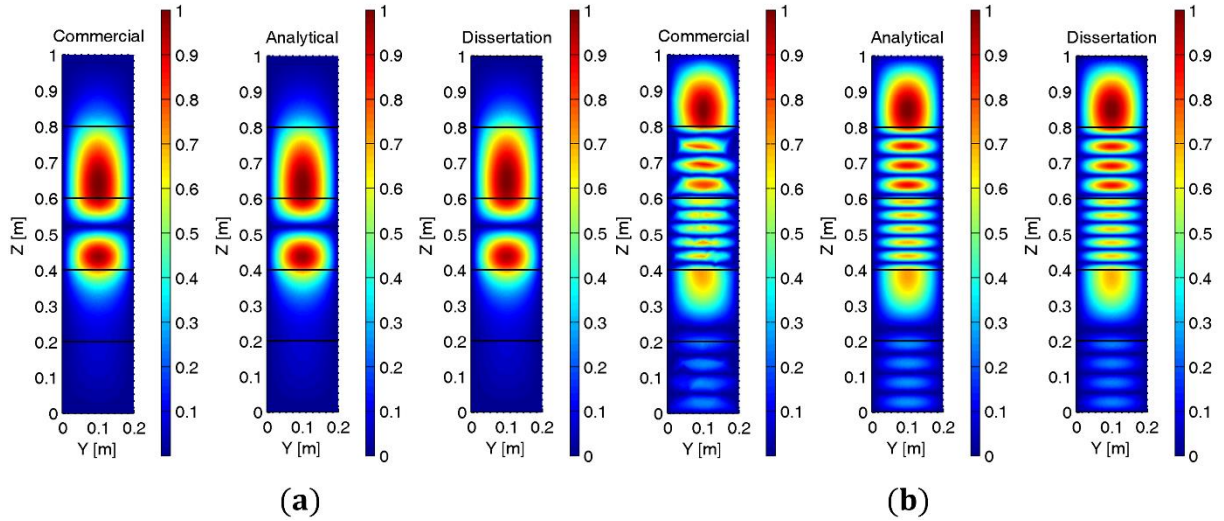


Figure 5-15. Electric field distribution (normalized) for a resonator of volume $0.1 \times 0.2 \times 1.0$ [m³], split into five blocks of the same length. Dielectric properties: $\epsilon_r = [10 \ 1 \ 20 \ 10 \ 1]$. Resonant frequency: (a) $f = 0.26$ [GHz] (b) $f = 0.90$ [GHz]

Finally, we strived to observe the way in which our model behaved under a slight change in the permittivity. Hence, we chose two resonators with common materials for the four first blocks, and a different material for the final blocks. So, the first case is a resonator with relative permittivity of 10, 20, 1, 10, and 20, whilst the second one is a resonator with relative permittivity of 10, 20, 1, 10, and 1. Furthermore, we selected a resonant frequency with weak interaction at this final block (0.26 [GHz]). Figure 5-16 shows the field distribution for both scenarios, where the commercial software was able to achieve a PSNR of 50 [dB]. Our model yielded a PSNR of 36 [dB] in the first case, and of 32 [dB] in the second one. A visual inspection of the field distributions reveal that our model is able to detect the change in permittivity, but it is unable to completely adapt to it. Table 5-7 summarizes the results found with the selected algorithm (i.e. UPSO/SFHS). Even if there is some degree of error, the algorithm was always able to find the length of each block and the resonant frequency for the desired field distributions, with PSNR values over 30 [dB].

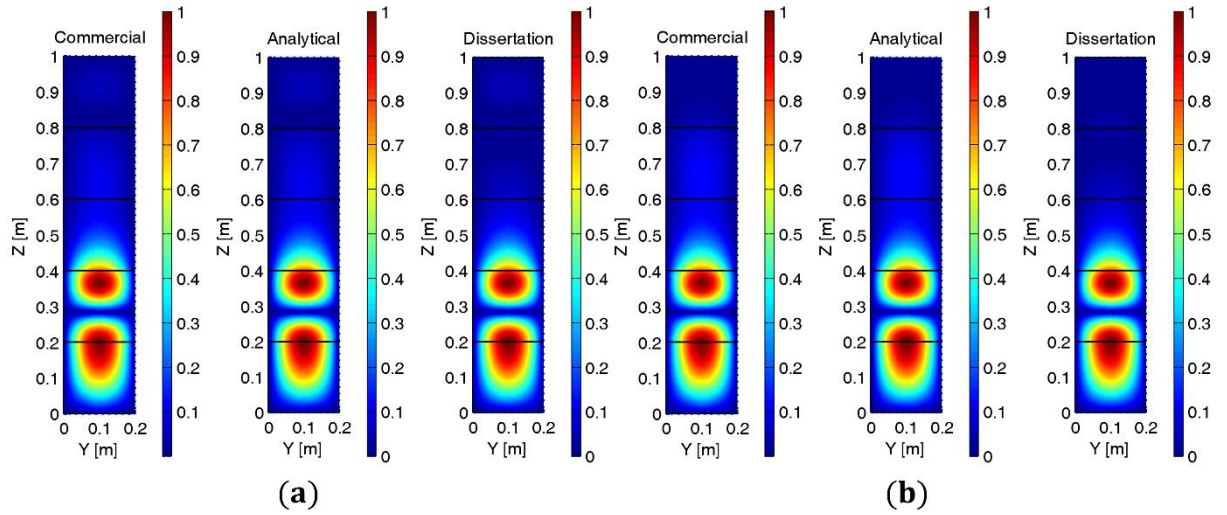


Figure 5-16. Electric field distribution (normalized) for a resonator of volume $0.1 \times 0.2 \times 1.0 \text{ [m}^3\text{]}$, split into five blocks of the same length. Dielectric properties and resonant frequency: (a) $\epsilon_r = [10 \ 20 \ 1 \ 10 \ 20]$, $f = 0.26 \text{ [GHz]}$
 (b) $\epsilon_r = [10 \ 20 \ 1 \ 10 \ 1]$, $f = 0.26 \text{ [GHz]}$

Table 5-7. Designs found by UPSO/SFHS for each one of the scenarios considered during this testing phase, including the length of each block (L_i), the resonant frequency, and the PSNR. In all cases, a theoretical value of 0.20 [m] was assumed for each block

Relative Permittivity		Theoretical Values					Found Values					PSNR [dB]
ϵ_{r_1}	ϵ_{r_2}	ϵ_{r_3}	ϵ_{r_4}	ϵ_{r_5}	Frequency [GHz]	L_1 [m]	L_2 [m]	L_3 [m]	L_4 [m]	L_5 [m]	Frequency [GHz]	
1	10	20	10	1	0.24	0.217	0.186	0.211	0.183	0.218	0.24	32.03
1	10	20	10	1	0.86	0.206	0.204	0.208	0.209	0.207	0.84	32.40
10	1	20	10	1	0.26	0.211	0.205	0.204	0.203	0.214	0.26	41.77
10	1	20	10	1	0.90	0.201	0.194	0.201	0.199	0.196	0.90	35.11
10	20	1	10	20	0.26	0.194	0.194	0.186	0.180	0.220	0.27	39.42
10	20	1	10	1	0.26	0.188	0.199	0.186	0.202	0.203	0.26	32.69

5.3.3 Resonator filled with lossy materials

Figure 5-17 shows the electric field distribution of a sample design, used to verify the proper behavior of the algorithm. In this case, the resonator is 33% filled with a material that has a relative permittivity of 10, and a conductivity of 0.1 [S/m] . Analyzing the solution located at the complex frequency of $0.75+j0.08 \text{ [GHz]}$ reveals that our model is able to provide a better solution than the commercial software, since the former achieved a PSNR of 25 [dB] and the latter only reached 18 [dB] . Running a test with the combined algorithm provided a resonator with block lengths of 0.343 [m] , 0.347 [m] , and 0.327 [m] . Also, it returned a complex frequency of $0.74+j0.09 \text{ [GHz]}$. Hence, our algorithm performs satisfactorily, so we move on to analyzing the field distributions of mineral samples at given temperatures.

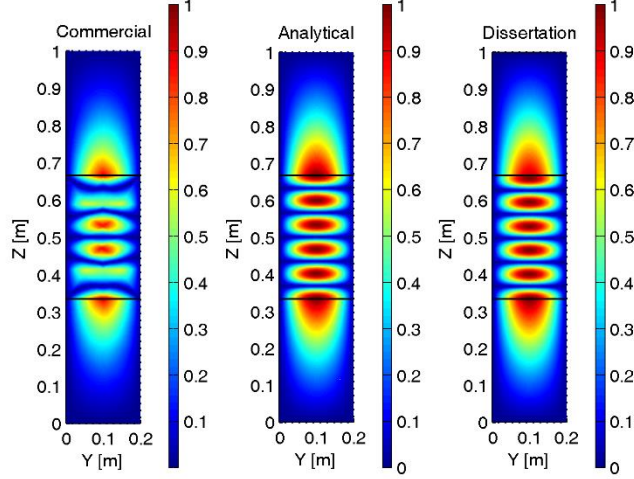


Figure 5-17. Electric field distribution (normalized) for a resonator of volume $0.1 \times 0.2 \times 1.0$ [m³], 33% filled with $\epsilon_r = 10$ and $\sigma = 0.1$. Complex frequency: $0.75+j0.08$ [GHz]

Table 5-8 summarizes the designs found by our algorithm, for three samples of minerals at five different temperatures. During this scenario, the complex frequency was selected striving to preserve the same field distribution, i.e. to excite the same resonant mode inside the cavity. Even so, and due to the wide range of complex permittivity that appears inside the resonator, some values of temperature inhibit the appearance of a given mode. For example, consider Figure 5-18, where the field distribution for each temperature has been plotted and normalized to the maximum of all electric field intensities. Throughout the first three plots, temperature goes from 24 [°C] to 350 [°C] and the relative permittivity and conductivity increase from 5.20 to 6.10, and from 0.10 [S/m] to 0.13 [S/m], respectively (Table 5-8). However, the temperature at the fourth plot increases all the way to 640 [°C], shifting the relative permittivity to 10.10 and the conductivity to 0.14 [S/m]. This makes it impossible to sustain the same field distribution as in the previous plots, and the closest one is shown in the figure. When the temperature drops all the way back to 50 [°C] (fifth plot) the mineral sample has changed internally (i.e. it roasted), and so the dielectric properties are different from the starting ones, making it impossible to sustain the desired field distribution. A comparison between the fields obtained through our algorithm and the ones yielded by the analytical mode, reveal that even if the shape of the field distribution is properly identified, the field intensities is not always obtained properly. This is due to the error level associated to the model, and in some cases is more critical than in others. Also, the PSNR values shown in Figure 5-18 are lower than those shown in Table 5-8, because the field distributions have been normalized to a single value (i.e. the maximum field intensity of all temperatures), instead of normalizing each distribution separately (i.e. using the maximum field intensity at each temperature).

Table 5-8. Designs found by UPSO/SFHS for three mineral samples at different temperatures, including the length of each block (L_i), the real (f') and imaginary (f'') parts of the complex frequency, and the PSNR. In all cases, a theoretical value of 0.166 [m] was assumed for each block

Sample	T [°C]	ϵ_r'	σ [S/m]	Theoretical Values		Found Values					
				f' [GHz]	f'' [GHz]	L_1 [m]	L_2 [m]	L_3 [m]	f' [GHz]	f'' [GHz]	PSNR [dB]
JB-S100	24	5.20	0.10	2.380	0.127	0.168	0.170	0.173	2.334	0.173	26.09
	100	5.40	0.11	2.350	0.136	0.142	0.140	0.141	2.802	0.183	21.32
	350	6.10	0.13	2.240	0.144	0.168	0.162	0.165	2.309	0.192	24.62
	640	10.10	0.14	1.690	0.098	0.166	0.174	0.167	1.605	0.125	25.31
	50	7.90	0.13	2.270	0.118	0.166	0.165	0.165	2.316	0.148	32.10
M9-S100	24	6.97	0.17	2.390	0.174	0.165	0.177	0.162	2.316	0.219	20.18
	100	7.05	0.17	2.380	0.173	0.164	0.172	0.164	2.345	0.217	24.06
	420	7.80	0.19	2.280	0.178	0.164	0.167	0.164	2.318	0.219	29.74
	627	6.40	0.18	2.480	0.192	0.169	0.174	0.170	2.513	0.259	18.11
	50	7.77	0.19	2.280	0.178	0.167	0.166	0.167	2.314	0.220	29.13
JB-S200	24	2.51	0.01	2.340	0.020	0.167	0.166	0.169	2.344	0.036	50.72
	100	3.15	0.01	2.190	0.016	0.168	0.155	0.156	2.335	0.029	22.34
	160	4.30	0.01	2.030	0.008	0.174	0.151	0.173	2.126	0.021	15.75
	246	3.40	0.01	2.150	0.014	0.146	0.148	0.144	2.473	0.026	21.16
	50	2.50	0.00	2.340	0.000	0.180	0.180	0.178	2.194	0.000	46.01

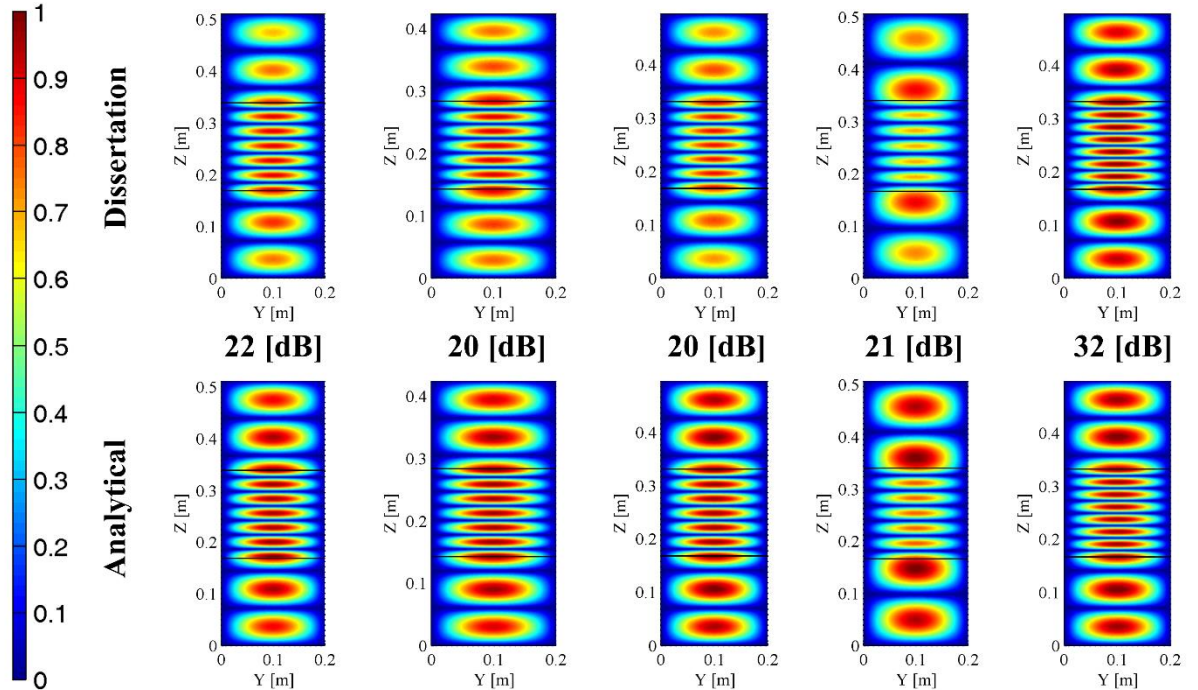


Figure 5-18. Electric field distribution for a resonator of volume $0.1 \times 0.2 \times 0.5$ [m³], 33% filled with a mineral sample of Juan Blanco (Sieve 100) at different temperatures. Values are normalized to the maximum field intensity of all five cases

5.4 FINAL COMMENTS

We have shown different design scenarios throughout this chapter. They spanned from simple resonators, uniformly filled with a given lossless material, up to more complex resonators partially filled with lossy minerals, who alter their dielectric properties with temperature. We used the main results of earlier chapters to find the optimum design under these scenarios. Mathematical models (and, thus, the objective functions) were derived along the lines of Chapter 2 (based on circuit analysis). Dielectric properties of the minerals were extracted from Chapter 3 (based on experimental data). Optimization algorithms were selected from Chapter 4 (based on tests with different strategies). Synergy of this information leads to an automatic design strategy, able to find the optimum length of each material inside a resonator and the operating frequency, such that the electric field distribution matches the one desired by the designer. For lossy materials, this operating frequency becomes complex.

Out of the four possible combinations of algorithms, UPSO/SFHS is best suited to these optimization tasks. This does not imply that the other combinations could not find good answers (Table 5-5), but that UPSO/SFHS did it with less function evaluations (Figure 5-12). We recommend using few particles for UPSO since additional ones imply evaluating the objective function more times per iteration. This requires solving the internal optimization problem (i.e. finding the multiple resonant frequencies) more often, increasing the computational cost.

Alas, not everything is perfect. As such, the precision of the mathematical model needs to be improved. Sometimes, our algorithm found answers that agreed outstandingly with the desired field distribution (PSNR values over 50 [dB]). These answers were even better than those yielded by the commercial software (PSNR values around 20 [dB]), especially at higher frequencies. But, in other cases our algorithm found answers that did not agree so well with the analytic ones (PSNR values around 20 [dB]). They were outperformed by the commercial solution (PSNR values around 30 [dB]), especially at lower frequencies. Still, and even when both PSNR values (i.e. commercial and ours) are similar, our field distributions are more uniform, representing a better solution. So, we recommend using the proposed algorithm for optimizing the design of microwave resonators, and including a metric that takes into account the similarity between the form factors of the fields.

REFERENCES

- [1] C. Balanis, *Advanced Engineering Electromagnetics*, John Wiley & Sons, Inc., New York, 1989.
- [2] R.F. Harrington, *Time-Harmonic Electromagnetic Fields*, John Wiley & Sons, Inc., 1961.
- [3] F.L. Peñaranda-Foix, *Aplicación de la teoría de análisis circuital generalizado a la resolución de problemas de difracción electromagnética*, Ph.D. Thesis, Universidad Politécnica de Valencia, 2001. doi:hdl.handle.net/10251/7121.
- [4] I. Amaya, R. Correa, Finding resonant frequencies of microwave cavities through a Modified Harmony Search algorithm, *Int. J. Bio-Inspired Comput.* In-Press. (2015).

BIBLIOGRAPHY

- Abdel-Rahman, A. B., Montaser, A. M., & Elmikati, H. A. (2012). Design a novel bandpass filter with microstrip resonator loaded capacitors using CFO-HC algorithm. In *The 2nd Middle East Conference on Antennas and Propagation* (pp. 1–6). IEEE. doi:10.1109/MECAP.2012.6618188
- Abril, J. S., & Gomez, J. A. (2012). *Ingeniería Conceptual de un Proceso de Recuperación de Oro con Microondas a Partir de Muestras Provenientes de los Municipios de Vetas y California (Santander)* (Undergraduate Thesis). Universidad Industrial de Santander.
- Agacayak, T., & Koseler, M. (2015). Effect of Microwave Heating on the Leaching of Lateritic Nickel Ore in Perchloric Acid. *Journal of The Chemical Society of Pakistan*, 37(2), 230–235.
- Aghaie, M., Nazari, T., Zolfaghari, a., Minuchehr, a., & Shirani, a. (2013). Investigation of PWR core optimization using harmony search algorithms. *Annals of Nuclear Energy*, 57, 1–15. doi:10.1016/j.anucene.2013.01.046
- Agrawal, D., Cheng, J., Peng, H., Hurt, L., & Cherian, K. (2008). Microwave Energy Applied to Processing of High-Temperature Materials. *American Ceramic Society Bulletin*, 87(3), 39–44.
- Aguirre, R. D., & Botero, W. (2012). *Interacción de las Microondas con Trazas de Oro en Muestras Provenientes del Municipio de Vetas (Santander)* (Undergraduate Thesis). Universidad Industrial de Santander.
- Al-Harashseh, M., Kingman, S., Al-Makhadmah, L., & Hamilton, I. E. (2014). Microwave treatment of electric arc furnace dust with PVC: dielectric characterization and pyrolysis-leaching. *Journal of Hazardous Materials*, 274, 87–97. doi:10.1016/j.jhazmat.2014.03.019
- Al-Harashseh, M., & Kingman, S. W. (2004). Microwave-assisted leaching—a review. *Hydrometallurgy*, 73(3-4), 189–203. doi:10.1016/j.hydromet.2003.10.006
- Alia, O. M., & Mandava, R. (2011). The Variants of the Harmony Search Algorithm: An Overview. *Artificial Intelligence Review*, 36(1), 49–68. doi:10.1007/s10462-010-9201-y
- Amankwah, R. K., Khan, A. U., Pickles, C. A., & Yen, W. T. (2005). Improved Grindability and Gold Liberation by Microwave Pretreatment of a Free-Milling Gold Ore. *Mineral Processing and Extractive Metallurgy*, 114(1), 30–36. doi:10.1179/037195505X28447
- Amankwah, R. K., & Ofori-Sarpong, G. (2011). Microwave Heating of Gold Ores for Enhanced Grindability and Cyanide Amenability. *Minerals Engineering*, 24(6), 541–544. doi:10.1016/j.mineng.2010.12.002

- Amankwah, R. K., & Pickles, C. A. (2009). Microwave roasting of a carbonaceous sulphidic gold concentrate. *Minerals Engineering*, 22(13), 1095–1101. doi:10.1016/j.mineng.2009.02.012
- Amankwah, R., Pickles, C., & Yen, W. (2005). Gold recovery by microwave augmented ashing of waste activated carbon. *Minerals Engineering*, 18(5), 517–526. doi:10.1016/j.mineng.2004.08.015
- Amaya, I., Bernal, D., Garnica, S., Reslen, M., & Correa, R. (2013). Improved Roasting of Some Colombian Gold Ores. *Revista Dyna*, 80(178), 70–77.
- Amaya, I., & Correa, R. (2010). Electromagnetic heating as a way of cutting costs while saving energy: Time evolution. *Revista Ingenierías Universidad de Medellín (Submitted)*, 11(20), 1–28.
- Amaya, I., & Correa, R. (2012). Electromagnetic heating as a way of cutting costs while saving energy: Time evolution. *Revista Ingenierías Universidad de Medellín*, 11(20), 215–226.
- Amaya, I., & Correa, R. (2013). Optimal Design of Multilayer EMAs for Frequencies between 0.85 GHz and 5.4 GHz. *Revista de Ingeniería*, 38, 33–37.
- Amaya, I., & Correa, R. (2015). Finding resonant frequencies of microwave cavities through a Modified Harmony Search algorithm. *International Journal of Bio-Inspired Computation: InPress*.
- Amaya, I., Cruz, J., & Correa, R. (2011). Real Roots of Nonlinear Systems of Equations Through a Metaheuristic Algorithm. *Revista Dyna*, 78(170), 15–23.
- Amaya, I., Cruz, J., & Correa, R. (2012). Solution of the Mathematical Model of a Nonlinear Direct Current Circuit Using Particle Swarm Optimization. *Revista Dyna*, 79(172), 77–84.
- Amaya, I., Cruz, J., & Correa, R. (2014). A modified firefly-inspired algorithm for global computational optimization. *Dyna*, 81(187), 85–90. doi:http://dx.doi.org/10.15446/dyna.v81n187.34594
- Amaya, I., Cruz, J., & Correa, R. (2015). Harmony Search algorithm: a variant with Self-regulated Fretwidth. *Applied Mathematics and Computation*, 266, 1127–1152. doi:10.1016/j.amc.2015.06.040
- Amaya, I., Gómez, L. A., & Correa, R. (2014). Discrete Particle Swarm Optimization in the numerical solution of a system of linear Diophantine equations. *Dyna*, 81(185), 139–144.

- Arias, J., & Mogollón, M. (2013). *Algoritmo de Optimización Gotas de Agua Virtuales Inteligentes Aplicado a la Planeación de Ruta Óptima de un Robot Móvil* (Undergraduate Thesis). Universidad Industrial de Santander.
- Ávila, J., & Navarro, O. (2014). *El Método de Colonia Artificial de Abejas y el Criterio de Mínima Entropía para el Diseño Óptimo de un Disipador de Calor* (Undergraduate Thesis). Universidad Industrial de Santander.
- Balanis, C. (1989). *Advanced Engineering Electromagnetics*. New York: John Wiley & Sons, Inc.
- Barreto, K. (2014). *Evaluación del Método Optimizador de Fuerza Central Frente al Optimizador por Enjambre de Partículas Unificado en la Solución de Ecuaciones No Lineales* (Undergraduate Thesis). Universidad Industrial de Santander.
- Benasla, L., Belmadani, A., & Rahli, M. (2014). Spiral Optimization Algorithm for solving Combined Economic and Emission Dispatch. *International Journal of Electrical Power & Energy Systems*, 62, 163–174. doi:10.1016/j.ijepes.2014.04.037
- Bernal, D., Garnica, S., & Reslen, Y. (2012). *Irradiación con Microondas a Minerales Ricos en Oro en Muestras Provenientes de la Zona del Sur de Bolívar* (Undergraduate Thesis). Universidad Industrial de Santander.
- Binner, E., Mediero-Munoyerro, M., Huddle, T., Kingman, S., Dodds, C., Dimitrakis, G., ... Lester, E. (2014). Factors affecting the microwave coking of coals and the implications on microwave cavity design. *Fuel Processing Technology*, 125, 8–17. doi:10.1016/j.fuproc.2014.03.006
- Birla, S., Wang, S., Tang, J., & Tiwari, G. (2008). Characterization of radio frequency heating of fresh fruits influenced by dielectric properties. *Journal of Food Engineering*, 89(4), 390–398. doi:10.1016/j.jfoodeng.2008.05.021
- Bobicki, E. R., Liu, Q., & Xu, Z. (2014). Microwave heating of ultramafic nickel ores and mineralogical effects. *Minerals Engineering*, 58, 22–25. doi:10.1016/j.mineng.2014.01.003
- Borrell, A., Salvador, M. D., Peñaranda-Foix, F. L., & Cátala-Civera, J. M. (2013). Microwave Sintering of Zirconia Materials: Mechanical and Microstructural Properties. *International Journal of Applied Ceramic Technology*, 10(2), 313–320. doi:10.1111/j.1744-7402.2011.02741.x
- Canos, A. J., Penaranda-Foix, F. L., Catala-Civera, J. M., & Garcia-Banos, B. (2010). Measurement of dielectric properties at high-temperatures in real-time with cylindrical cavity. In *2010 IEEE MTT-S International Microwave Symposium* (pp. 1044–1047). IEEE. doi:10.1109/MWSYM.2010.5515877

Castro, H., & Otero, M. (2014). *El Algoritmo del Murciélago Virtual (Bat Algorithm) como Estrategia para el Diseño Óptimo de Filtros Pasa-Bajas* (Undergraduate Thesis). Universidad Industrial de Santander.

Catalá Civera, J. M., Gutiérrez Cano, J. D., Peñaranda-Foix, F. L., & Garcia-Baños, B. (2011). Portable System for Dielectric Characterization of Materials at Microwave Frequencies. In *13th International Conference on Microwave and RF heating, AMPERE 2011* (pp. 137–140). Toulouse: Ampere.

Celis, J., & Rincón, F. (2013). *Evaluación y Comparación entre los Métodos Newton Raphson y Artificial Bee Colony (ABC) para el Análisis del Flujo de Carga de un Sistema de Potencia* (Undergraduate Thesis). Universidad Industrial de Santander.

Chan, E., Lim, Y., & Chew, Y. (2007). Antioxidant activity of Camellia sinensis leaves and tea from a lowland plantation in Malaysia. *Food Chemistry*, *102*(4), 1214–1222. doi:10.1016/j.foodchem.2006.07.009

Civicioglu, P. (2013). Artificial cooperative search algorithm for numerical optimization problems. *Information Sciences*, *229*, 58–76. doi:10.1016/j.ins.2012.11.013

Clerc, M., & Kennedy, J. (2002). The particle swarm - explosion, stability, and convergence in a multidimensional complex space. *IEEE Transactions on Evolutionary Computation*, *6*(1), 58–73. doi:10.1109/4235.985692

Contreras, J., Amaya, I., & Correa, R. (2014). An improved variant of the conventional Harmony Search algorithm. *Applied Mathematics and Computation*, *227*, 821–830. doi:10.1016/j.amc.2013.11.050

Contreras, J., & Villanueva, C. (2013). *Solución de un Sistema de Ecuaciones No Lineales, Utilizando una Estrategia Basada en el Algoritmo de Harmony Search* (Undergraduate Thesis). Universidad Industrial de Santander.

Correa, R., Amaya, I., & Araque-Herrera, A. (2011). Uso de algoritmos metaheurísticos híbridos para la minimización de entropía en problemas de transferencia de calor en circuitos electrónicos. *Revista Ingeniería Y Universidad*, *15*(2), 403–421.

Cruz, J. (2012). *Solución del Modelo Matemático de un Circuito Electronico D.C. No Lineal Mediante una Estrategia de Optimización* (Undergraduate Thesis). Universidad Industrial de Santander.

Cruz, J., Amaya, I., & Correa, C. (2013). Algoritmo de optimización para el cálculo de múltiples raíces de sistemas de ecuaciones no lineales. *Inge CUC*, *9*(1), 197–208.

- Cruz, J., Amaya, I., & Correa, R. (2012). Solution of the mathematical model of a DC nonlinear electronic circuit using an optimization strategy: Application of the original and unified Particle Swarm Metaheuristics. In *2012 IEEE 4th Colombian Workshop on Circuits and Systems (CWCAS)* (pp. 1–6). IEEE. doi:10.1109/CWCAS.2012.6404080
- Darvekar, M., Ghorpade, B., & Vankar, P. S. (2004). Microwave Assisted Improved Syntheses of Indigoid and Anthraquinoid Dyes. *Asian Journal of Chemistry*, *16*(2), 965–970.
- Dávila, D., & Rutto, A. (2014). *Identificación de Sistemas No Lineales Mediante el Método de Optimización de la Gota de Agua Virtual Inteligente* (Undergraduate Thesis). Universidad Industrial de Santander.
- Davoodnia, A. (2010). Microwave Assisted Synthesis of Fused Benzimidazoles. *Asian Journal of Chemistry*, *22*(2), 1591–1594.
- Díaz, M., & Rueda, M. (2012). *Uso de las Microondas en el Proceso de Recuperación de Trazas de Oro* (Undergraduate Thesis). Universidad Industrial de Santander.
- Eberhart, R., & Kennedy, J. (1995). A new optimizer using particle swarm theory. In *MHS'95. Proceedings of the Sixth International Symposium on Micro Machine and Human Science* (pp. 39–43). IEEE. doi:10.1109/MHS.1995.494215
- Farfán, E., & Fontecha, J. (2013). *Obtención de Las Curvas de Dispersión de Modos Híbridos para Guías de Onda de Sección Transversal Rectangular Parcialmente Llena con un Dieléctrico, Mediante Optimización por Enjambre de Partículas Unificado UPSO* (Undergraduate Thesis). Universidad Industrial de Santander.
- Fister, I., Yang, X.-S., Ljubič, K., Fister, D., & Brest, J. (2014). Towards the novel reasoning among particles in PSO by the use of RDF and SPARQL. *The Scientific World Journal*, *2014*, 1–10. doi:10.1155/2014/121782
- Formato, R. A. (2007). Central force optimization: A new metaheuristic with application in applied. *Progress In Electromagnetics Research, PIER* *77*, 425–491, 2007, 425–491.
- Formato, R. A. (2007). Central Force Optimization: a New Metaheuristic With Applications in Applied Electromagnetics. *Progress In Electromagnetics Research*, *77*, 425–491. doi:10.2528/PIER07082403
- Formato, R. A. (2009). Central force optimisation: a new gradient-like metaheuristic for multidimensional search and optimisation. *International Journal of Bio-Inspired Computation*, *1*(4), 217. doi:10.1504/IJBIC.2009.024721
- Formato, R. A. (2010). Improved CFO Algorithm for Antenna Optimization. *Progress In Electromagnetics Research B, Vol. 19*, 405–425, 2010, 19, 405–425.

Formato, R. A. (2010). Improved CFO Algorithm for Antenna Optimization. *Progress In Electromagnetics Research*, 19, 405–425.

Formato, R. A. (2011a). A novel methodology for antenna design and optimization: Variable Zo, 1–97. Retrieved from <http://arxiv.org/abs/1107.1437>

Formato, R. A. (2011b). Issues in Antenna Optimization - A Monopole Case Study, 1–82. Retrieved from <http://arxiv.org/abs/1103.5629>

Formato, R. A. (2011c). UWB Array Design Using Variable Zo Technology and Central Force Optimization. *ArXiv*, 0901, 1–97. Other Computer Science. Retrieved from <http://arxiv.org/abs/1108.0901>

Gao, W., Liu, S., & Huang, L. (2012a). A global best artificial bee colony algorithm for global optimization. *Journal of Computational and Applied Mathematics*, 236(11), 2741–2753. doi:10.1016/j.cam.2012.01.013

Gao, W., Liu, S., & Huang, L. (2012b). A global best artificial bee colony algorithm for global optimization. *Journal of Computational and Applied Mathematics*, 236(11), 2741–2753. doi:10.1016/j.cam.2012.01.013

Garcia, J., & Corredor, D. (2013). *Algoritmo Híbrido del Simplex con la Estrategia de Optimización de Fuerza Central (CFO) Aplicado a la Solución de Sistemas de Ecuaciones No Lineales* (Undergraduate Thesis). Universidad Industrial de Santander.

Gaviria C., A. C., González, J., & Mora, H. F. (2006). Tostación, empleando microondas, en menas refractarias auríferas y su efecto en la extracción del oro. *Revista Dyna*, 73(150), 29–37.

Geem, Z. W. (2008). Novel derivative of harmony search algorithm for discrete design variables. *Applied Mathematics and Computation*, 199(1), 223–230. doi:10.1016/j.amc.2007.09.049

Geem, Z. W. (2009). *Music-Inspired Harmony Search Algorithm*. (Springer, Ed.) (1 th.). Springer.

Geem, Z. W. (2010). State-of-the-Art in the Structure of Harmony Search Algorithm. In *Recent Advances In Harmony Search Algorithm* (pp. 1–11). Springer Berlin Heidelberg. doi:10.1007/978-3-642-04317-8_1

Geem, Z. W., Fesanghary, M., Choi, J., Saka, M. P., Williams, J. C., Ayvaz, M. T., ... Vasebi, A. (2008). Recent Advances in Harmony Search. In *Advances in Evolutionary Algorithms* (pp. 127–142). InTech. Retrieved from

http://www.intechopen.com/books/advances_in_evolutionary_algorithms/recent_advances_in_harmony_search

Geem, Z. W., & Hwangbo, H. (2006). Application of Harmony Search to Multi-Objective Optimization for Satellite Heat Pipe Design, 2–4.

Geem, Z. W., Kim, J. H., & Loganathan, G. V. (2001). A New Heuristic Optimization Algorithm: Harmony Search. *Simulation*, 76(2), 60–68. doi:10.1177/003754970107600201

Gómez, C., Amaya, I., & Correa, R. (2012). An Alternative Method for the Design of Time-varying Feedback Control Systems. *Revista Dyna*, 79(176), 168–174.

Gómez, C., & Pérez, O. (2012). *Implementación de un Algoritmo de Optimización para Sistemas Discretos Fundamentado en la Técnica de Enjambre de Partículas* (Undergraduate Thesis). Universidad Industrial de Santander.

González, J., & Bayona, C. (2013). *Aplicación del Método de Optimización por Fuerza Central (CFO), al Diseño de un Absorbedor Electromagnético Óptimo* (Undergraduate Thesis). Universidad Industrial de Santander.

González, J. E., Amaya, I., & Correa, R. (2013). Design of an Optimal Multi-layered Electromagnetic Absorber through the Central Force Optimization Algorithm. In *PIERS Proceedings* (Vol. 1, pp. 1082–1086). Stockholm.

Gonzalez, S., & Traslado, O. (2013). *Análisis de la Eficiencia del Algoritmo Harmony Search en la Solución de un Circuito Electrónico No Lineal* (Undergraduate Thesis). Universidad Industrial de Santander.

Granville, V., Kfivanek, M., & Rasson, J. (1994). Simulated Annealing: A Proof of Convergence, 16(6), 652–656.

Green, R. C., Wang, L., & Alam, M. (2012). Training neural networks using Central Force Optimization and Particle Swarm Optimization: Insights and comparisons. *Expert Systems with Applications*, 39(1), 555–563. doi:10.1016/j.eswa.2011.07.046

Green, R. C., Wang, L., Alam, M., & Formato, R. A. (2011). Central Force Optimization on a GPU: A case study in high performance metaheuristics using multiple topologies. In *2011 IEEE Congress of Evolutionary Computation (CEC)* (pp. 550–557). IEEE. doi:10.1109/CEC.2011.5949667

Green, R. C., Wang, L., Alam, M., & Formato, R. a. (2012). Central force optimization on a GPU: a case study in high performance metaheuristics. *The Journal of Supercomputing*, 62(1), 378–398. doi:10.1007/s11227-011-0725-y

- Gu, J., Fan, W., Shimojima, A., & Okubo, T. (2008). Microwave-induced synthesis of highly dispersed gold nanoparticles within the pore channels of mesoporous silica. *Journal of Solid State Chemistry*, *181*(4), 957–963. doi:10.1016/j.jssc.2008.01.039
- Guo, Z., Lei, T., Li, W., Luo, H., Ju, S., Peng, J., & Zhang, L. (2015). Clean utilization of CuCl residue by microwave roasting under the atmosphere of steam and oxygen. *Chemical Engineering and Processing: Process Intensification*, *92*, 67–73. doi:10.1016/j.cep.2015.03.024
- Haddad, O. B., Afshar, A., & Mariño, M. a. (2006). Honey-Bees Mating Optimization (HBMO) Algorithm: A New Heuristic Approach for Water Resources Optimization. *Water Resources Management*, *20*(5), 661–680. doi:10.1007/s11269-005-9001-3
- Han, K., & Kim, J. (2002). Quantum-inspired evolutionary algorithm for a class of combinatorial optimization. *IEEE Transactions on Evolutionary Computation*, *6*(6), 580–593. doi:10.1109/TEVC.2002.804320
- Hansson, L., & Antti, a. (2006). The effect of drying method and temperature level on the hardness of wood. *Journal of Materials Processing Technology*, *171*(3), 467–470. doi:10.1016/j.jmatprotec.2005.08.007
- Hara, K., Hayashi, M., Sato, M., & Nagata, K. (2011). Continuous Pig Iron Making by Microwave Heating with 12.5 kW at 2.45 GHz. *Journal of Microwave Power and Electromagnetic Energy*, *45*(3), 137–147.
- Harrington, R. F. (1961). *Time-Harmonic Electromagnetic Fields*. John Wiley & Sons, Inc.
- Harris, V. G., Geiler, A., Chen, Y., Yoon, S. D., Wu, M., Yang, A., ... Zuo, X. (2009). Recent advances in processing and applications of microwave ferrites. *Journal of Magnetism and Magnetic Materials*, *321*(14), 2035–2047. doi:10.1016/j.jmmm.2009.01.004
- Hascakir, B., & Akin, S. (2010). Recovery of Turkish Oil Shales by Electromagnetic Heating and Determination of the Dielectric Properties of Oil Shales by an Analytical Method. *Energy & Fuels*, *24*(1), 503–509. doi:10.1021/ef900868w
- Hemono, N., Chenu, S., Lebullenger, R., Rocherulle, J., Keryvin, V., & Wattiaux, A. (2010). Microwave synthesis and physical characterization of tin(II) phosphate glasses. *JOURNAL OF MATERIALS SCIENCE*, *45*(11), 2916–2920.
- Hernandez, M. (2013). *Inteligencia Computacional Inspirada en la Cuántica, Aplicada a la Optimización de la Producción de Petróleo en el Modelo de un Pozo Inteligente* (Undergraduate Thesis). Universidad Industrial de Santander.

Hinojosa, A., & Espinosa, K. (2011). *El Método de Enjambre de Partículas y el Criterio de Mínima Entropía en el Diseño Óptimo de un Disipador de Calor* (Tesis de Pregrado). Universidad Industrial de Santander.

Hong, C., & Xing-sheng, G. (2012). Multi-HM Adaptive Harmony Search Algorithm and its Application to Continuous Function Optimization. *Research Journal of Applied Sciences, Engineering and Technology*, 4(2), 100–103.

Horng, M.-H. (2011). Multilevel thresholding selection based on the artificial bee colony algorithm for image segmentation. *Expert Systems with Applications*, 38(11), 13785–13791. doi:10.1016/j.eswa.2011.04.180

Hosseini, H. S. (2011). Principal components analysis by the galaxy-based search algorithm: a novel metaheuristic for continuous optimisation. *International Journal of Computational Science and Engineering*, 6(1/2), 132. doi:10.1504/IJCSE.2011.041221

Hsu, C.-W., Chen, P., & Ting, J.-M. (2013). Microwave-Assisted Hydrothermal Synthesis of TiO₂ Mesoporous Beads Having C and/or N Doping for Use in High Efficiency All-Plastic Flexible Dye-Sensitized Solar Cells. *Journal of the Electrochemical Society*, 160(3), H160–H165. doi:10.1149/2.048303jes

Huang, H., Qin, H., Hao, Z., & Lim, A. (2012). Example-based learning particle swarm optimization for continuous optimization. *Information Sciences*, 182(1), 125–138. doi:10.1016/j.ins.2010.10.018

Huang, Y., Sheng, J., Yang, F., & Hu, Q. (2007). Effect of enzyme inactivation by microwave and oven heating on preservation quality of green tea. *Journal of Food Engineering*, 78(2), 687–692. doi:10.1016/j.jfoodeng.2005.11.007

Huynh-Thu, Q., & Ghanbari, M. (2008). Scope of validity of PSNR in image/video quality assessment. *Electronics Letters*. doi:10.1049/el:20080522

Iwasaki, K., Mashiko, K., Saito, Y., Yoshikawa, N., Todoroki, H., & Taniguchi, S. (2009). Application of Microwave Technique for Dehydration of Sludge Generated in a Stainless Steel Plant. *ISIJ International*, 49(4), 596–601. doi:10.2355/isijinternational.49.596

Jin, J.-M. (2010). Fields and Waves in Rectangular Coordinates. In *Theory and Computation of Electromagnetic Fields* (pp. 152–199). John Wiley & Sons, Inc.

Jurado, D., & Ortiz, M. (2013). *Implementación de un Sistema de Medición y Control de la Temperatura en una Cavidad Electromagnética* (Undergraduate Thesis). Universidad Industrial de Santander.

Kappe, C. O. (2004). Controlled microwave heating in modern organic synthesis. *Angewandte Chemie (International Ed. in English)*, 43(46), 6250–84. doi:10.1002/anie.200400655

Karaboga, D. (2005). *An Idea Based on Honey Bee Swarm for Numerical Optimization* (Technical Report).

Karaboga, D., & Akay, B. (2009). A comparative study of Artificial Bee Colony algorithm. *Applied Mathematics and Computation*, 214(1), 108–132. doi:10.1016/j.amc.2009.03.090

Karaboga, D., & Basturk, B. (2007). A powerful and efficient algorithm for numerical function optimization: artificial bee colony (ABC) algorithm. *Journal of Global Optimization*, 39(3), 459–471. doi:10.1007/s10898-007-9149-x

Karaboga, D., Gorkemli, B., Ozturk, C., & Karaboga, N. (2014). A comprehensive survey: artificial bee colony (ABC) algorithm and applications. *Artificial Intelligence Review*, 42(1), 21–57. doi:10.1007/s10462-012-9328-0

Karaboga, D., Ozturk, C., Karaboga, N., & Gorkemli, B. (2012). Artificial bee colony programming for symbolic regression. *Information Sciences*, 209, 1–15. doi:10.1016/j.ins.2012.05.002

Kattan, A., & Abdullah, R. (2013). A dynamic self-adaptive harmony search algorithm for continuous optimization problems. *Applied Mathematics and Computation*, 219(16), 8542–8567. doi:10.1016/j.amc.2013.02.074

Kaveh, A., & Nasrollahi, A. (2013). Engineering design optimization using a hybrid PSO and HS algorithm. *Asian Journal of Civil Engineering*, 14(2), 201–223.

Kaya, E. (2010). Effect of Microwave Radiation on the Flootation of Copper Sulfide Ores. *Asian Journal of Chemistry*, 22(10), 7874–7882.

Kennedy, J., & Eberhart, R. (1995). Particle Swarm Optimization. In *Proceedings of ICNN'95 - International Conference on Neural Networks* (pp. 1942–1948). Perth, Australia: IEEE. doi:10.1109/ICNN.1995.488968

Kennedy, J., & Eberhart, R. C. (1997). A Discrete Binary Version of the Particle Swarm Algorithm. In *1997 IEEE International Conference on Systems, Man, and Cybernetics. Computational Cybernetics and Simulation* (Vol. 5, pp. 4104–4108). IEEE. doi:10.1109/ICSMC.1997.637339

Kesselring, J. P., & Smith, R. D. (1996). Development of a microwave clothes dryer. *IEEE Transactions on Industry Applications*, 32(1), 47–50. doi:10.1109/28.485811

Kingman, S., Jackson, K., Cumbane, A., Bradshaw, S. M., Rowson, N. A., & Greenwood, R. (2004). Recent developments in microwave-assisted comminution. *International Journal of Mineral Processing*, 74(1-4), 71–83. doi:10.1016/j.minpro.2003.09.006

Kirkpatrick, S., Gelatt, C. D., & Vecchi, M. P. (1983). Optimization by Simulated Annealing. *Science*, 220(4598), 671–680.

Kirksey, M. (2008). Green Technology : Hi-Temperature Microwave Sintering Reduces Energy Use Up to 80 % and Process Time Up to 90 %. *WebWire*. Retrieved from <http://www.webwire.com/ViewPressRel.asp?aId=58548>

Kitchen, H. J., Vallance, S. R., Kennedy, J. L., Tapia-Ruiz, N., Carassiti, L., Harrison, A., ... Gregory, D. H. (2014). Modern microwave methods in solid-state inorganic materials chemistry: from fundamentals to manufacturing. *Chemical Reviews*, 114(2), 1170–206. doi:10.1021/cr4002353

Krishnanand, K. N., & Ghose, D. (2005). Detection of multiple source locations using a glowworm metaphor with applications to collective robotics. In *Proceedings 2005 IEEE Swarm Intelligence Symposium* (pp. 84–91). IEEE. doi:10.1109/SIS.2005.1501606

Kumar, V., Chhabra, J. K., & Kumar, D. (2014). Parameter adaptive harmony search algorithm for unimodal and multimodal optimization problems. *Journal of Computational Science*, 5(2), 144–155. doi:10.1016/j.jocs.2013.12.001

Landa-Torres, I., Manjarres, D., Salcedo-Sanz, S., Del Ser, J., & Gil-Lopez, S. (2013). A multi-objective grouping Harmony Search algorithm for the optimal distribution of 24-hour medical emergency units. *Expert Systems with Applications*, 40(6), 2343–2349. doi:10.1016/j.eswa.2012.10.051

Larhed, M., & Hallberg, A. (2001). Microwave-assisted high-speed chemistry : a new technique in drug discovery. *Drug Discovery Today*, 6(8), 406–416.

Lee, K. S., & Geem, Z. W. (2005). A new meta-heuristic algorithm for continuous engineering optimization: harmony search theory and practice. *Computer Methods in Applied Mechanics and Engineering*, 194(36-38), 3902–3933. doi:10.1016/j.cma.2004.09.007

Li, J., Huang, J., Wu, J., Cao, L., Li, Q., & Yanagisawa, K. (2013). Microwave-assisted growth of WO₃·0.33H₂O micro/nanostructures with enhanced visible light photocatalytic properties. *CrystEngComm*, 15(39), 7904–7913. doi:10.1039/c3ce41005f

Li, Z., Li, J., Zhang, L., Peng, J., Wang, S., Ma, A., & Wang, B. (2015). Response surface optimization of process parameters for removal of F and Cl from zinc oxide fume by microwave roasting. *Transactions of Nonferrous Metals Society of China*, 25(3), 973–980. doi:10.1016/S1003-6326(15)63687-1

Liang, J. J., Qin, A. K., Suganthan, P. N., & Baskar, S. (2006). Comprehensive learning particle swarm optimizer for global optimization of multimodal functions. *IEEE Transactions on Evolutionary Computation*, *10*(3), 281–295. doi:10.1109/TEVC.2005.857610

Liu, H., Zhang, L., Gao, Y., Shen, Y., & Shi, D. (2009). Electromagnetic Wave Absorber Optimal Design Based on Improved Particle Swarm Optimization. *EMC 2009, IEICE*, 797–800.

Lovás, M., Kováčová, M., Dimitrakis, G., Čuvanová, S., Znamenáčková, I., & Jakabský, Š. (2010). Modeling of microwave heating of andesite and minerals. *International Journal of Heat and Mass Transfer*, *53*(17-18), 3387–3393. doi:10.1016/j.ijheatmasstransfer.2010.03.012

M.J., A., & N.I., D. (2010). Design of Multilayer Microwave Broadband Absorbers Using Central Force Optimization. *Progress in Electromagnetics Research B*, *26*, 101–113.

Ma, M., Liang, J., Guo, M., Fan, Y., & Yin, Y. (2011). SAR image segmentation based on Artificial Bee Colony algorithm. *Applied Soft Computing*, *11*(8), 5205–5214. doi:10.1016/j.asoc.2011.05.039

Ma, X., Zhang, M., Min, F., Ge, T., & Cai, C. (2015). Fundamental study on removal of organic sulfur from coal by microwave irradiation. *International Journal of Mineral Processing*, *139*, 31–35. doi:10.1016/j.minpro.2015.04.009

Mahdavi, M., Chehreghani, M. H., Abolhassani, H., & Forsati, R. (2008). Novel meta-heuristic algorithms for clustering web documents. *Applied Mathematics and Computation*, *201*(1-2), 441–451. doi:10.1016/j.amc.2007.12.058

Mahdavi, M., Fesanghary, M., & Damangir, E. (2007). An improved harmony search algorithm for solving optimization problems. *Applied Mathematics and Computation*, *188*(2), 1567–1579. doi:10.1016/j.amc.2006.11.033

Marland, S., Han, B., Merchant, A., & Rowson, N. (2000). The effect of microwave radiation on coal grindability. *Fuel*, *79*(11), 1283–1288. doi:10.1016/S0016-2361(99)00285-9

Meredith, R. (1998). *Engineers' Handbook of Industrial Microwave Heating*. London: The Institution of Electrical Engineers.

Mernik, M., Liu, S.-H., Karaboga, D., & Črepinšek, M. (2015). On clarifying misconceptions when comparing variants of the Artificial Bee Colony Algorithm by offering a new implementation. *Information Sciences*, *291*, 115–127. doi:10.1016/j.ins.2014.08.040

- Metaxas, A. C., & Meredith, R. (1983). *Industrial Microwave Heating*. London: The Institution of Electrical Engineers.
- Milani, G., & Milani, F. (2009). A Numerical Model for the Optimal Vulcanization of 2D Polar Rubber Compounds Using Microwaves. *Macromolecular Theory and Simulations*, 18(6), 336–354. doi:10.1002/mats.200900017
- Miranda, A., & Ruiz, J. (2014). *Implementacion del Algoritmo de Busqueda Gravitacional (GSA) para el Diseño de un Absorbedor Electromagnetico Óptimo* (Undergraduate Thesis). Universidad Industrial de Santander.
- Montaser, A. M., Mahmoud, K. R., & Elmikati, H. A. (2012). B15. Tri-band slotted bow-tie antenna design for RFID reader using hybrid CFO-NM algorithm. In *2012 29th National Radio Science Conference (NRSC)* (pp. 119–126). IEEE. doi:10.1109/NRSC.2012.6208515
- Monzó-Cabrera, J., Catalá-Civera, J. M., Plaza-Gonzalez, P., & Sánchez-Hernández, D. (2004). A Model for Microwave-Assisted Drying of Leather: Development and Validation. *Journal of Microwave Power and Electromagnetic Energy*, 39(1), 53–64.
- Mujumdar, A. S. (2007). *Handbook of industrial drying* (Third Ed.). CRC Press. Retrieved from <http://books.google.com/books?hl=es&lr=&id=uKOGg1vk61MC&pgis=1>
- Nanthakumar, B., Pickles, C., & Kelebek, S. (2007). Microwave Pretreatment of a Double Refractory Gold Ore. *Minerals Engineering*, 20(11), 1109–1119. doi:10.1016/j.mineng.2007.04.003
- Nasir, A. N. K., Tokhi, M. O., Sayidmarie, O., & Raja Ismail, R. M. T. (2013). A novel adaptive spiral dynamic algorithm for global optimization. *2013 13th UK Workshop on Computational Intelligence (UKCI)*, 334–341. doi:10.1109/UKCI.2013.6651325
- Nekooei, K., Farsangi, M. M., Nezamabadi-Pour, H., & Lee, K. Y. (2013). An Improved Multi-Objective Harmony Search for Optimal Placement of DGs in Distribution Systems. *IEEE Transactions on Smart Grid*, 4(1), 557–567. doi:10.1109/TSG.2012.2237420
- Nelson, S. O. (2010). Fundamentals of Dielectric Properties Measurements and Agricultural Applications. *Journal of Microwave Power and Electromagnetic Energy*, 44(2), 98–113.
- Noh, H., Cannon, a., Hesketh, P. J., & Wong, C. P. (2004). Wafer bonding using microwave heating of parylene for MEMS packaging. *2004 Proceedings. 54th Electronic Components and Technology Conference (IEEE Cat. No.04CH37546)*, 924–930. doi:10.1109/ECTC.2004.1319448

- Offermanns, S. (1990). Resonance characteristics of a cavity-operated electrodeless high-pressure microwave discharge system. *IEEE Transactions on Microwave Theory and Techniques*, 38(7), 904–911. doi:10.1109/22.55783
- Ortíz, R., & García, E. (2013). *Diseño de un Absorbedor Electromagnético Multicapa Mediante el Método de la Espiral* (Undergraduate Thesis). Universidad Industrial de Santander.
- Osepchuk, J. M. (1984). A History of Microwave Heating Applications. *IEEE Transactions on Microwave Theory and Techniques*, MTT-32(9), 1200–1224.
- Osepchuk, J. M. (2002). Microwave power applications. *IEEE Transactions on Microwave Theory and Techniques*, 50(3), 975–985.
- Parsopoulos, K. E., & Vrahatis, M. N. (2004). UPSO: A unified particle swarm optimization scheme. *Lecture Series on Computer and Computational Sciences*, 1, 868–873.
- Peltosaari, O., Tanskanen, P., Heikkinen, E.-P., & Fabritius, T. (2015). A \rightarrow Γ \rightarrow B-Phase Transformation of Spodumene With Hybrid Microwave and Conventional Furnaces. *Minerals Engineering*, 1–7. doi:10.1016/j.mineng.2015.04.012
- Peñaranda-Foix, F. L. (2001). *Aplicación de la teoría de análisis circuital generalizado a la resolución de problemas de difracción electromagnética* (Ph.D. Thesis). Universidad Politécnica de Valencia. Retrieved from <http://hdl.handle.net/10251/7121>
- Penaranda-Foix, F. L., & Catala-Civera, J. M. (2010). Circuitual Analysis of Cylindrical Structures Applied to the Electromagnetic Resolution of Resonant Cavities. In *Passive Microwave Components and Antennas* (pp. 141–168). InTech. doi:10.5772/226
- Pérez, O., Amaya, I., & Correa, R. (2013). Numerical solution of certain exponential and non-linear Diophantine systems of equations by using a discrete particle swarm optimization algorithm. *Applied Mathematics and Computation*, 225, 737–746. doi:10.1016/j.amc.2013.10.007
- Petro, E., & Fuentes, R. (2013). *Mantenimiento Preventivo Básico de un Desfibrilador Monofásico Mediante los Métodos de Enjambre de Partículas Mejorado y Colonia Artificial de Abejas* (Undergraduate Thesis). Universidad Industrial de Santander.
- Pickles, C. A. (2004). Microwave Heating Behaviour of Nickeliferous Limonitic Laterite Ores. *Minerals Engineering*, 17(6), 775–784. doi:10.1016/j.mineng.2004.01.007
- Pinzón, C., & Ardila, E. (2013). *Evaluación y Comparación de los Métodos UPSO y Newton Raphson para el Análisis de Flujo de Cargas en un Sistema de Potencia* (Undergraduate Thesis). Universidad Industrial de Santander.

- Pojanavaraphan, T., & Magaraphan, R. (2008). Prevulcanized natural rubber latex/clay aerogel nanocomposites. *European Polymer Journal*, 44(7), 1968–1977. doi:10.1016/j.eurpolymj.2008.04.039
- Portilla, J. (2012). *Solución de las Ecuaciones que Modelan un Circuito No Lineal de Corriente Directa Mediante el Método de Espiral* (Undergraduate Thesis). Universidad Industrial de Santander.
- Qin, G., & Gong, D. (2013). Pretreatment of petroleum refinery wastewater by microwave-enhanced Fe⁰/GAC micro-electrolysis. *Desalination and Water Treatment*, 52(13-15), 2512–2518. doi:10.1080/19443994.2013.811120
- Qubati, G. M., & Dib, N. I. (2010). Microstrip Patch Antenna Optimization Using Modified Central Force Optimization. *Progress In Electromagnetics Research B*, 21, 281–298.
- Ramírez, F., & Roa, O. (2012). *Solución de las Ecuaciones que Describen el Modelo Matemático de un Circuito Electrónico Compuesto de Elementos No Lineales Mediante el Optimizador de Fuerza Central* (Undergraduate Thesis). Universidad Industrial de Santander.
- Ramirez, J., & Osorio, F. (2013). *Algoritmo de Enjambre de Partículas Unificado para la Solución de Ecuaciones Diofánticas Lineales Comúnmente Encontradas en Problemas de Ingeniería Electrónica* (Undergraduate Thesis). Universidad Industrial de Santander.
- Ramos, C. C. O., Souza, A. N., Chiachia, G., Falcão, A. X., & Papa, J. P. (2011). A Novel Algorithm for Feature Selection Using Harmony Search and its Application for Non-Technical Losses Detection. *Computers & Electrical Engineering*, 37(6), 886–894. doi:10.1016/j.compeleceng.2011.09.013
- Rashedi, E., Nezamabadi-pour, H., & Saryazdi, S. (2009). GSA: A Gravitational Search Algorithm. *Information Sciences*, 179(13), 2232–2248. doi:10.1016/j.ins.2009.03.004
- Ratnaweera, A., Halgamuge, S. K., & Watson, H. C. (2004). Self-Organizing Hierarchical Particle Swarm Optimizer With Time-Varying Acceleration Coefficients. *IEEE Transactions on Evolutionary Computation*, 8(3), 240–255. doi:10.1109/TEVC.2004.826071
- Roa, O., Amaya, I., Ramirez, F., & Correa, R. (2012). Solution of nonlinear circuits with the Central Force Optimization algorithm. In *2012 IEEE 4th Colombian Workshop on Circuits and Systems (CWCAS)* (pp. 1–6). Barranquilla: IEEE. doi:10.1109/CWCAS.2012.6404079
- Robinson, J., Binner, E., Saeid, A., Al-Harashseh, M., & Kingman, S. (2014). Microwave processing of Oil Sands and contribution of clay minerals. *Fuel*, 135, 153–161. doi:10.1016/j.fuel.2014.06.057

- Robinson, J., & Rahmat-Samii, Y. (2004). Particle Swarm Optimization in Electromagnetics. *IEEE Transactions on Antennas and Propagation*, 52(2), 397–407. doi:10.1109/TAP.2004.823969
- Rodríguez, A., & Gaona, K. (2014). *Diseño Óptimo de Filtros Electrónicos (Chebyshev) Mediante el Algoritmo de la Luciérnaga Virtual (Firefly)* (Undergraduate Thesis). Universidad Industrial de Santander.
- Salazar, E., & Mora, J. (2011). *Diseño de Absorbedores Electromagnéticos Óptimos Utilizando Optimización por Enjambre de Partículas y Análisis de Intervalos* (Undergraduate Thesis). Universidad Industrial de Santander.
- Salcedo-Sanz, S., Manjarrés, D., Pastor-Sánchez, Á., Del Ser, J., Portilla-Figueras, J. a., & Gil-López, S. (2013). One-way urban traffic reconfiguration using a multi-objective harmony search approach. *Expert Systems with Applications*, 40(9), 3341–3350. doi:10.1016/j.eswa.2012.12.043
- Sanborn, M. R., Wan, S. K., & Bulard, R. (1982). Microwave sterilization of plastic tissue culture vessels for reuse. *Applied and Environmental Microbiology*, 44(4), 960–4. Retrieved from <http://www.ncbi.nlm.nih.gov/pubmed/7149721>
- Shah-Hosseini, H. (2007). Problem solving by Intelligent Water Drops. In *2007 IEEE Congress on Evolutionary Computation* (pp. 3226–3231). Singapore: IEEE. doi:10.1109/CEC.2007.4424885
- Shah-Hosseini, H. (2012). An approach to continuous optimization by the Intelligent Water Drops algorithm. *Procedia - Social and Behavioral Sciences*, 32(2010), 224–229. doi:10.1016/j.sbspro.2012.01.033
- Shaikh, N. F., & Doye, D. D. (2014). A Novel Iris Recognition System Based on Central Force Optimization. *International Journal of Tomography and Simulation*, 27(3), 23–34.
- Sharma, V., Gulati, a, & Ravindranath, S. (2005). Extractability of tea catechins as a function of manufacture procedure and temperature of infusion. *Food Chemistry*, 93(1), 141–148. doi:10.1016/j.foodchem.2004.10.016
- Shi, Y., & Eberhart, R. (n.d.). A modified particle swarm optimizer. *1998 IEEE International Conference on Evolutionary Computation Proceedings. IEEE World Congress on Computational Intelligence (Cat. No.98TH8360)*, 69–73. doi:10.1109/ICEC.1998.699146
- Singh, S., Gupta, D., Jain, V., & Sharma, A. (2015). Microwave Processing of Materials and Applications in Manufacturing Industries: A Review. *Materials and Manufacturing Processes*, 30(1), 37–41. doi:10.1080/10426914.2014.952028

Suarez, J., & Romero, J. (2013). *Solución de las Ecuaciones que Describe el Comportamiento de los Modos Híbridos en una Guía de Onda Rectangular Parcialmente Llena Mediante el Método de Optimización Recocido Simulado (Simulated Annealing)* (Undergraduate Thesis). Universidad Industrial de Santander.

Subramanian, A., Ravi, G., & Arun Gopal, D. (2012). Loss Minimization and Voltage Profile Improvement Incorporating Multiple SVC using PSO Algorithm. *International Journal of Computer Applications*, 46(22), 15–20.

Sun, W., Wang, J., & Chen, J. (2013). Harmony Search Based Optimization GM (1, 1) Model for Power Generation Forecasting. *International Journal on Advances in Information Sciences and Service Sciences*, 5(4), 500–506. doi:10.4156/aiss.vol5.issue4.62

Szeto, W. Y., Wu, Y., & Ho, S. C. (2011). An artificial bee colony algorithm for the capacitated vehicle routing problem. *European Journal of Operational Research*, 215(1), 126–135. doi:10.1016/j.ejor.2011.06.006

Taleizadeh, A. A., Niaki, S. T. A., & Barzinpour, F. (2011). Multiple-buyer multiple-vendor multi-product multi-constraint supply chain problem with stochastic demand and variable lead-time: A harmony search algorithm. *Applied Mathematics and Computation*, 217(22), 9234–9253. doi:10.1016/j.amc.2011.04.001

Tamura, K., & Yasuda, K. (2011a). Primary study of spiral dynamics inspired optimization. *IEEE Transactions on Electrical and Electronic Engineering*, 6(S1), S98–S100. doi:10.1002/tee.20628

Tamura, K., & Yasuda, K. (2011b). Spiral Dynamics Inspired Optimization. *Journal of Advanced Computational Intelligence and Intelligent Informatics*, 15(8), 1116–1122.

Tamura, K., & Yasuda, K. (2011c). Spiral optimization -A new multipoint search method. In *2011 IEEE International Conference on Systems, Man, and Cybernetics* (pp. 1759–1764). IEEE. doi:10.1109/ICSMC.2011.6083926

Tanaka, K., Ann, S., Allen, B., & Kohl, P. A. (2007). Variable Frequency Microwave Curing of Amide-Epoxy Based Polymers. *IEEE Transactions on Components and Packaging Technologies*, 30(3), 472–477.

Teodorovic, D., & Dell'Orco, M. (2005). Bee Colony Optimization - A Cooperative Learning Approach to Complex Transportation Problems. In *Proceedings of the 10th EWGT Meeting*. Poznan.

Teodorovic, D., Lucic, P., Markovic, G., & Dell'Orco, M. (2006). Bee Colony Optimization: Principles and Applications. In *8th Seminar on Neural Network Applications in Electrical*

Engineering (Vol. 00, pp. 151–156). Belgrade, Serbia & Montenegro: IEEE. doi:10.1109/NEUREL.2006.341200

Turkmen, Y., & Kaya, E. (2010). Leaching of Chalcopyrite Concentrate in Sulphuric Acid with the Aid of Mechanical Activation and Microwave Energy. *Asian Journal of Chemistry*, 22(10), 8107–8116.

Valian, E., Tavakoli, S., & Mohanna, S. (2014). An intelligent global harmony search approach to continuous optimization problems. *Applied Mathematics and Computation*, 232, 670–684. doi:10.1016/j.amc.2014.01.086

Vanegas, S., Amaya, I., & Correa, R. (2013). Virtual bat algorithm for the computation of Duhamel ' s Integral applied to structural systems with one degree of freedom. *Revista Ingeniería de Construcción*, 28(3), 278–289.

Vaughan, J. P. (2004). The process mineralogy of gold: The classification of ore types. *Journal of the Minerals, Metals and Materials Society*, 56(7), 46–48. doi:10.1007/s11837-004-0092-8

Verma, H. K., Jain, C., Rathore, A., & Gupta, P. (2012). A Comparative Study of GA, PSO and Big Bang-Big Crunch Optimization Techniques for Optimal Placement of SVC 's. *International Journal of Electronics Communication and Computer Engineering*, 3(3), 263–269.

Visentin, S., Medana, C., Barge, A., Giancotti, V., & Cravotto, G. (2010). Microwave-assisted Maillard reactions for the preparation of advanced glycation end products (AGEs). *Organic & Biomolecular Chemistry*, 8(10), 2473–7. doi:10.1039/c000789g

Vorster, W. (2001). *The Effect of Microwave Radiation on Mineral Processing* (Ph.D. Thesis). *Chemical Engineering*. The University of Birmingham.

Vural, R. A., Bozkurt, U., & Yildirim, T. (2013). Analog active filter component selection with nature inspired metaheuristics. *AEU - International Journal of Electronics and Communications*, 67(3), 197–205. doi:10.1016/j.aeue.2012.07.009

Wang, M., Xian, P., Wang, X., & Li, B. (2015). Extraction of Vanadium from Stone Coal by Microwave Assisted Sulfation Roasting. *JOM*, 67(2), 369–374. doi:10.1007/s11837-014-1215-5

Wang, Y., & Djordjevic, N. (2014). Thermal stress FEM analysis of rock with microwave energy. *International Journal of Mineral Processing*, 130, 74–81. doi:10.1016/j.minpro.2014.05.012

- Whittles, D. (2003). Application of numerical modelling for prediction of the influence of power density on microwave-assisted breakage. *International Journal of Mineral Processing*, 68(1-4), 71–91. doi:10.1016/S0301-7516(02)00049-2
- Wierstra, D., Schaul, T., Peters, J., & Schmidhuber, J. (2008). Natural Evolution Strategies. *2008 IEEE Congress on Evolutionary Computation (IEEE World Congress on Computational Intelligence)*, 3381–3387. doi:10.1109/CEC.2008.4631255
- Willert-Porada, M. (Ed.). (2006). *Advances in Microwave and Radio Frequency Processing*. Processing. Berlin, Heidelberg: Springer Berlin Heidelberg. doi:10.1007/978-3-540-32944-2
- Wolpert, D. H., & Macready, W. G. (1997). No free lunch theorems for optimization. *IEEE Transactions on Evolutionary Computation*, 1(1), 67–82. doi:10.1109/4235.585893
- Yang, X. (2009). Cuckoo Search via Lévy flights. In *2009 World Congress on Nature & Biologically Inspired Computing (NaBIC)* (pp. 210–214). IEEE. doi:10.1109/NABIC.2009.5393690
- Yang, X. (2010a). A New Metaheuristic Bat-Inspired Algorithm. In *International Workshop on Nature Inspired cooperative Strategies for Optimization (NICSO 2010)* (pp. 65–74). Granada: Springer. doi:10.1007/978-3-642-12538-6_6
- Yang, X. (2010b). Firefly Algorithm, Stochastic Test Functions and Design Optimisation. *International Journal of Bio-Inspired Computation*, 2(2), 78–84. Optimization and Control. Retrieved from <http://arxiv.org/abs/1003.1409>
- Yang, X. (2010c). Firefly Algorithms for Multimodal Optimization. *Stochastic Algorithms: Foundations and Applications*, 5792, 169–178. Optimization and Control. Retrieved from <http://arxiv.org/abs/1003.1466>
- Yang, X.-S. (2010a). *Engineering Optimization: An Introduction* (1st ed.). New Jersey: John Wiley & Sons.
- Yang, X.-S. (2010b). *Nature-Inspired Metaheuristic Algorithms* (2nd ed.). Luniver Press Frome. Retrieved from http://books.google.com/books?hl=es&lr=&id=iVB_ETlh4ogC&pgis=1
- Yoshikawa, N., Wang, H., & Taniguchi, S. (2009). Application of Microwave Heating to Reaction between Soda-Lime Glass and Liquid Al for Fabrication of Composite Materials. *MATERIALS TRANSACTIONS*, 50(5), 1174–1178. doi:10.2320/matertrans.MRA2008461
- Zhang, Y., Zou, J., Cheuh, C., Yip, H., & Jen, A. K.-Y. (2012). Significant Improved Performance of Photovoltaic Cells Made from a Partially Fluorinated

Cyclopentadithiophene/Benzothiadiazole Conjugated Polymer. *Macromolecules*, 45(13), 5427–5435. doi:10.1021/ma3009178

Zhao, W., Chen, J., Chang, X., Guo, S., Srinivasakannan, C., Chen, G., & Peng, J. (2014). Effect of microwave irradiation on selective heating behavior and magnetic separation characteristics of Panzhihua ilmenite. *Applied Surface Science*, 300, 171–177. doi:10.1016/j.apsusc.2014.02.038

Zhao, Y., Hou, Y., Cui, Y., Liang, H., & Li, L. (2015). Recovery of Copper from Copper Sulfide Concentrate by Sulfation Roasting. *International Journal of Nonferrous Metallurgy*, 04(02), 9–13. doi:10.4236/ijnm.2015.42002

Zhu, H., Wang, Y., Wang, K., & Chen, Y. (2011). Particle Swarm Optimization (PSO) for the constrained portfolio optimization problem. *Expert Systems with Applications*, 38(8), 10161–10169. doi:10.1016/j.eswa.2011.02.075

APPENDIX

A. ELECTROMAGNETIC MODELLING OF THE RESONATOR

A.1. COMPLETELY FILLED RECTANGULAR RESONATOR

Solving Maxwell equations in rectangular coordinates is perhaps one of the simplest scenarios that can be found. In this sense, the wave function must be of the form $\Psi(x, y, z) = X(x)Y(y)Z(z)$ and the mathematical functions best suited under these conditions are of the form $\sin(k_i i)$, $\cos(k_i i)$ for stationary waves, or of the phasor form $e^{jk_i i}$, $e^{-jk_i i}$ for traveling waves [1]. Here, i can be any of the problem dimensions and each k_i is a separation parameter that must comply with the separation equation $k_x^2 + k_y^2 + k_z^2 = k^2$. Moreover, most problems can be easily separated into a pair of independent solutions along a given axis. For example, an empty waveguide (extending over the z -axis) can be analyzed through a family of electromagnetic modes whose transverse electric field is zero (TE modes) and a family of electromagnetic modes whose transverse magnetic field is zero (TM modes). Should this waveguide be partially filled with a dielectric, the problem would have to be solved through a similar couple of family modes, but this time they would have to be transverse to an appropriate axis (i.e. they should be TE_x and TM_x modes, or TE_y and TM_y modes, depending on the material's location).

The particular case of a rectangular resonator completely filled with a given load (Figure A1-1) implies that the wave is confined to the volume of the resonator. Hence, a standing wave behavior can be assumed along each axis, so the wave function of the TM and TE modes become $\Psi^{TM} = \sin(k_x x) \sin(k_y y) \cos(k_z z)$ and $\Psi^{TE} = \cos(k_x x) \cos(k_y y) \sin(k_z z)$, respectively.

Now, in order to find the separation parameters, boundary conditions must be accounted for. Even so, it is important to first analyze the relation between the electromagnetic field inside the resonator and the elemental wave function. In the case of TM modes, the relation is shown in eq. (A1.1), whilst eq. (A1.2) shows the relation for TE modes.

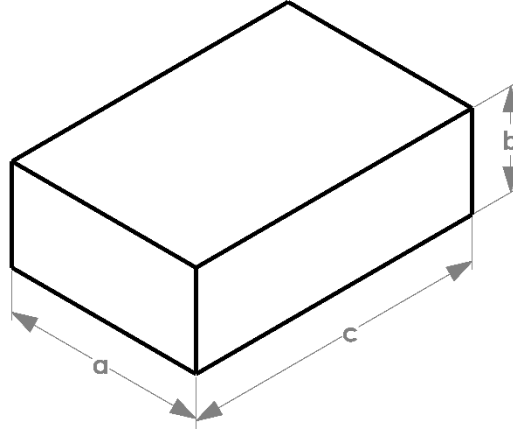


Figure A1-1. General layout of a rectangular resonator

$$E_x = \frac{1}{j\omega\epsilon} \frac{\partial^2 \Psi^{TM}}{\partial x \partial z}, E_y = \frac{1}{j\omega\epsilon} \frac{\partial^2 \Psi^{TM}}{\partial y \partial z}, E_z = \frac{1}{j\omega\epsilon} \left(\frac{\partial^2}{\partial z^2} + k^2 \right) \Psi^{TM}$$

$$H_x = \frac{\partial \Psi^{TM}}{\partial y}, H_y = -\frac{\partial \Psi^{TM}}{\partial x}, H_z = 0$$

(A1.1)

$$E_x = -\frac{\partial \Psi^{TE}}{\partial y}, E_y = \frac{\partial \Psi^{TE}}{\partial x}, E_z = 0$$

$$H_x = \frac{1}{j\omega\mu} \frac{\partial^2 \Psi^{TE}}{\partial x \partial z}, H_y = \frac{1}{j\omega\mu} \frac{\partial^2 \Psi^{TE}}{\partial y \partial z}, H_z = \frac{1}{j\omega\mu} \left(\frac{\partial^2}{\partial z^2} + k^2 \right) \Psi^{TE}$$

(A1.2)

Boundary conditions require that the tangential field at each wall nullifies. Hence, applying this criteria to eqs. (A1.1) and (A1.2) leads to eq. (A1.3), where m, n start at zero for TE modes ($m = n = 0$ excluded), and at one for TM modes. The remaining index, i.e. p , starts at one for TE modes and at zero for TM modes.

$$k_x = \frac{m\pi}{a}, k_y = \frac{n\pi}{b}, k_z = \frac{p\pi}{c}$$

(A1.3)

Using eq. (A1.3) and taking into account that $k^2 = \omega^2 \mu \epsilon$, the separation equation can be solved to find the resonant frequency of each mode, arriving at eq. (A1.4). From this equation, it is evident that the resonant frequencies of a homogenously filled rectangular resonator depend on the geometry, as well as on the electromagnetic properties of the filling. Moreover, materials with higher dielectric constant (and thus, higher ϵ) will exhibit lower resonant frequencies.

$$f_{r_{mnp}} = \frac{1}{2\sqrt{\mu\epsilon}} \sqrt{\left(\frac{m}{a}\right)^2 + \left(\frac{n}{b}\right)^2 + \left(\frac{p}{c}\right)^2}$$

(A1.4)

A.2. FIELD VISUALIZATION

Plotting the electromagnetic field inside the previously analyzed resonator (Figure A1-1) is a rather simple task. The process can be summarized as defining the index of the mode and whether it is TE or TM. Afterwards, the resonant frequency is calculated through eq. (A1.4) and the fields are plotted using eq. (A1.1) and (A1.2) accordingly. However, a more general design scenario implies different materials inside the resonator. Even so, before delving into the electromagnetic analysis of a partially filled resonator, it is convenient to first analyze the way in which the internal fields can be plotted. In the most general case, the resonator can be split into N different blocks (or networks, Figure 2-1), giving rise to different configurations.

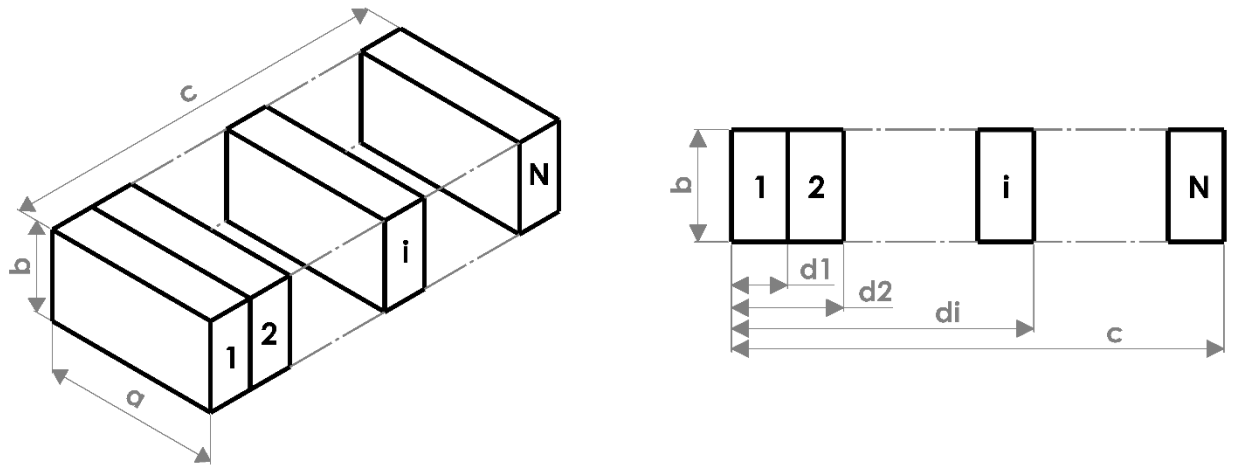


Figure A1-2. Rectangular resonator split into N blocks

A.2.1. Resonator split into two blocks

Assuming there is only one change of material inside the applicator, the total number of blocks equals two. The elemental equations for each region of this scenario are given by eq. (A1.5), and the x -component of the electric field corresponds to eq. (A1.6).

$$\begin{aligned}\Psi_1^{\text{TE}} &= A_1 \cos(k_x x) \cos(k_y y) \sin(k_{z_1} z) \\ \Psi_2^{\text{TE}} &= A_2 \cos(k_x x) \cos(k_y y) \sin(k_{z_2} (c - z))\end{aligned}\quad (\text{A1.5})$$

$$\begin{aligned}E_{x_1}^{\text{TE}} &= A_1 k_y \cos(k_x x) \sin(k_y y) \sin(k_{z_1} z) \\ E_{x_2}^{\text{TE}} &= A_2 k_y \cos(k_x x) \sin(k_y y) \sin(k_{z_2} (c - z))\end{aligned}\quad (\text{A1.6})$$

These equations comply with the boundary conditions on the walls of the cavity. However, continuity of tangential fields at the interface of both materials must be guaranteed, so:

$$\begin{aligned}
E_{x_1}^{\text{TE}}(d_1) &= E_{x_2}^{\text{TE}}(d_1) \\
A_2 &= \frac{A_1 \sin(k_{z_1} d_1)}{\sin(k_{z_2}(c - d_1))}
\end{aligned} \tag{A1.7}$$

Hence, in order to plot the electric field distribution inside the cavity, eq. (A1.6) can be used, assuming any given value for A_1 (e.g. $A_1 = 1$) and calculating A_2 through eq. (A1.7).

A.2.2. Cavity with three blocks

When considering three blocks, the z-component of the wave functions for the first and last block remain the same as in the previous case (since they must comply with boundary conditions). However, the middle block has no restriction of zero field at any of the interfaces, so it is chosen as a sum of a component nullified at the beginning of block one and a component nullified at the end of the last block. Thus, the wave functions are written as shown by eq. (A1.8), and the electric and magnetic fields are as shown by eq. (A1.9) and eq. (A1.10), respectively.

$$\begin{aligned}
\Psi_1^{\text{TE}} &= A_1 \cos(k_x x) \cos(k_y y) \sin(k_{z_1} z) \\
\Psi_2^{\text{TE}} &= \cos(k_x x) \cos(k_y y) \left(A_{2a} \sin(k_{z_2} z) + A_{2b} \sin(k_{z_2}(c - z)) \right)
\end{aligned} \tag{A1.8}$$

$$\begin{aligned}
\Psi_3^{\text{TE}} &= A_3 \cos(k_x x) \cos(k_y y) \sin(k_{z_3}(c - z)) \\
E_{x_1}^{\text{TE}} &= A_1 k_y \cos(k_x x) \sin(k_y y) \sin(k_{z_1} z) \\
E_{x_2}^{\text{TE}} &= k_y \cos(k_x x) \sin(k_y y) \left(A_{2a} \sin(k_{z_2} z) + A_{2b} \sin(k_{z_2}(c - z)) \right)
\end{aligned} \tag{A1.9}$$

$$\begin{aligned}
E_{x_3}^{\text{TE}} &= A_3 k_y \cos(k_x x) \sin(k_y y) \sin(k_{z_3}(c - z)) \\
H_{y_1}^{\text{TE}} &= -\frac{A_1 k_y k_{z_1}}{j\omega\mu_1} \cos(k_x x) \sin(k_y y) \cos(k_{z_1} z) \\
H_{y_2}^{\text{TE}} &= -\frac{k_y k_{z_2}}{j\omega\mu_2} \cos(k_x x) \sin(k_y y) \left(A_{2a} \cos(k_{z_2} z) + A_{2b} \cos(k_{z_2}(c - z)) \right) \\
H_{y_3}^{\text{TE}} &= \frac{A_3 k_y k_{z_3}}{j\omega\mu_3} \cos(k_x x) \sin(k_y y) \cos(k_{z_3}(c - z))
\end{aligned} \tag{A1.10}$$

Applying continuity of tangential fields at the interface yields:

$$A_1 \sin(k_{z_1} d_1) = A_{2a} \sin(k_{z_2} d_1) + A_{2b} \sin(k_{z_2}(c - d_1)) \tag{A1.11}$$

$$A_{2a} \sin(k_{z_2} d_2) + A_{2b} \sin(k_{z_2}(c - d_2)) = A_3 \sin(k_{z_3}(c - d_2)) \tag{A1.12}$$

$$\frac{A_1 k_{z_1}}{\mu_1} \cos(k_{z_1} d_1) = \frac{k_{z_2}}{\mu_2} \left(A_{2a} \cos(k_{z_2} d_1) + A_{2b} \cos(k_{z_2}(c - d_1)) \right) \tag{A1.13}$$

$$-\frac{k_{z_2}}{\mu_2} \left(A_{2a} \cos(k_{z_2} d_2) + A_{2b} \cos(k_{z_2}(c - d_2)) \right) = \frac{A_3 k_{z_3}}{\mu_3} \cos(k_{z_3}(c - d_3)) \tag{A1.14}$$

Solving eq. (A1.11) and eq. (A1.13) for A_{2a} , and after equating, the expression for A_{2b} shown in eq. (A1.15) is obtained. Hence, A_{2a} and A_3 can be calculated through eq. (A1.16) and eq. (A1.17), respectively.

$$A_{2b} = \frac{A_1 \sin(k_{z_1} d_1) - k_k A_1 \cos(k_{z_1} d_1) \tan(k_{z_2} d_1)}{\sin(k_{z_2} (c - d_1)) + \cos(k_{z_2} (c - d_1)) \tan(k_{z_2} d_1)} \quad (\text{A1.15})$$

$$k_k = \frac{\mu_2 k_{z_1}}{\mu_1 k_{z_2}}$$

$$A_{2a} = \frac{A_1 \sin(k_{z_1} d_1) - A_{2b} \sin(k_{z_2} (c - d_1))}{\sin(k_{z_2} d_1)} \quad (\text{A1.16})$$

$$A_3 = \frac{A_{2a} \sin(k_{z_2} d_2) + A_{2b} \sin(k_{z_2} (c - d_2))}{\sin(k_{z_3} (c - d_2))} \quad (\text{A1.17})$$

A.2.3. Cavity with more than three blocks

Assume a resonant cavity split into N blocks, as shown by Figure 2-1, where index i indicates all internal blocks, i.e. $i = [2, N - 1]$. Following the same rationale of the previous case, the wave functions, electric fields, and magnetic fields of the blocks, are given by eqs. (A1.18), (A1.19), and (A1.20), respectively.

$$\begin{aligned} \Psi_1^{\text{TE}} &= A_1 \cos(k_x x) \cos(k_y y) \sin(k_{z_1} z) \\ \Psi_i^{\text{TE}} &= \cos(k_x x) \cos(k_y y) (A_{ia} \sin(k_{z_i} z) + A_{ib} \sin(k_{z_i} (c - z))) \end{aligned} \quad (\text{A1.18})$$

$$\begin{aligned} \Psi_N^{\text{TE}} &= A_N \cos(k_x x) \cos(k_y y) \sin(k_{z_N} (c - z)) \\ E_{x_1}^{\text{TE}} &= A_1 k_y \cos(k_x x) \sin(k_y y) \sin(k_{z_1} z) \\ E_{x_i}^{\text{TE}} &= k_y \cos(k_x x) \sin(k_y y) (A_{ia} \sin(k_{z_i} z) + A_{ib} \sin(k_{z_i} (c - z))) \\ E_{x_N}^{\text{TE}} &= A_N k_y \cos(k_x x) \sin(k_y y) \sin(k_{z_N} (c - z)) \end{aligned} \quad (\text{A1.19})$$

$$\begin{aligned} H_{y_1}^{\text{TE}} &= -\frac{A_1 k_y k_{z_1}}{j\omega\mu_1} \cos(k_x x) \sin(k_y y) \cos(k_{z_1} z) \\ H_{y_i}^{\text{TE}} &= -\frac{k_y k_{z_i}}{j\omega\mu_i} \cos(k_x x) \sin(k_y y) (A_{ia} \cos(k_{z_i} z) + A_{ib} \cos(k_{z_i} (c - z))) \\ H_{y_N}^{\text{TE}} &= \frac{A_N k_y k_{z_N}}{j\omega\mu_N} \cos(k_x x) \sin(k_y y) \cos(k_{z_N} (c - z)) \end{aligned} \quad (\text{A1.20})$$

After solving the system of equations, the amplitude coefficients are found to be:

$$\begin{aligned}
A_{2b} &= \frac{A_1 \sin(k_{z_1} d_1) - k_k A_1 \cos(k_{z_1} d_1) \tan(k_{z_2} d_1)}{\sin(k_{z_2} (c - d_1)) + \cos(k_{z_2} (c - d_1)) \tan(k_{z_2} d_1)} \\
A_{2a} &= \frac{A_1 \sin(k_{z_1} d_1) - A_{2b} \sin(k_{z_2} (c - d_1))}{\sin(k_{z_2} d_1)} \\
k_k &= \frac{\mu_2 k_{z_1}}{\mu_1 k_{z_2}}
\end{aligned} \tag{A1.21}$$

$$\begin{aligned}
A_{ib} &= \frac{A_{(i-1)a} \sin(k_{1_i}) + A_{(i-1)b} \sin(k_{4_i}) - k_{k_i} \tan(k_{2_i}) (A_{(i-1)a} \cos(k_{1_i}) - A_{(i-1)b} \cos(k_{4_i}))}{\sin(k_{3_i}) + \cos(k_{3_i}) \tan(k_{2_i})} \\
A_{ia} &= \frac{A_{(i-1)a} \sin(k_{1_i}) + A_{(i-1)b} \sin(k_{4_i}) - A_{ib} \sin(k_{3_i})}{\sin(k_{2_i})}
\end{aligned} \tag{A1.22}$$

$$\begin{aligned}
k_{k_i} &= \frac{\mu_i k_{z_{i-1}}}{\mu_{i-1} k_{z_i}}, k_{1_i} = k_{z_{i-1}} d_{i-1}, k_{2_i} = k_{z_i} d_{i-1}, k_{3_i} = k_{z_i} (c - d_{i-1}), k_{4_i} = k_{z_{i-1}} (c - d_{i-1}) \\
A_N &= \frac{A_{(N-1)a} \sin(k_{z_{(N-1)}} d_{(N-1)}) + A_{(N-1)b} \sin(k_{z_{(N-1)}} (c - d_{(N-1)}))}{\sin(k_{z_N} (c - d_{(N-1)}))}
\end{aligned} \tag{A1.23}$$

A.3. PARTIALLY FILLED RECTANGULAR RESONATOR

The inclusion of a material (homogeneous and isotropic) with a given permittivity inside the resonator perturbs the resonant frequencies. As an example, consider the plot given in Figure A1-3 where three different materials were selected. It is easily seen that as the layer of material grows thicker, the resonant frequency of a given mode diminishes. The electric field distribution is also affected by this mix of materials inside the resonator, as can be seen in Figure A1-4 and in Figure A1-5, where the electric field distribution of the first and second modes (respectively) is shown for different fill percentages. It is clear that the electric field tends to concentrate on the layer of material with the higher dielectric constant (ϵ_r). However, under this condition (i.e. partial filling) the resonant frequency can no longer be calculated through eq. (A1.4), so a new alternative must be implemented.

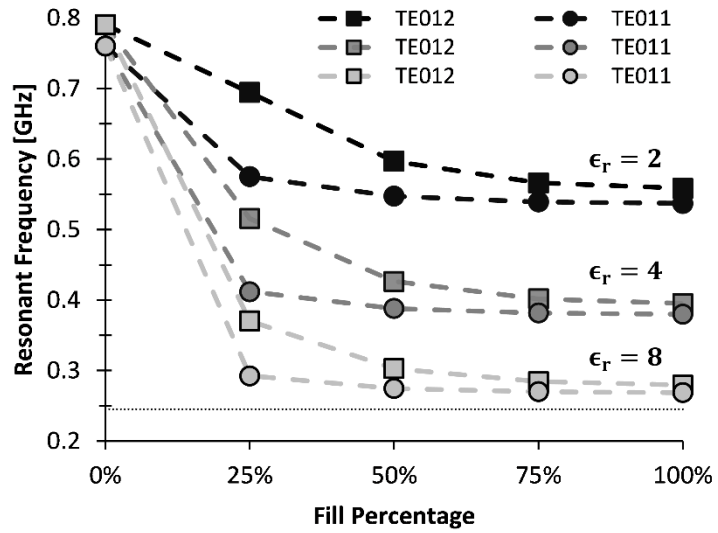


Figure A1-3. Resonant frequency of a partially filled resonator as a function of the fill percentage, for two modes and three different materials. The dotted line represents the standard frequency of 2.45 [GHz] and the volume of the resonator is $0.1 \times 0.2 \times 1.2$ [m³]

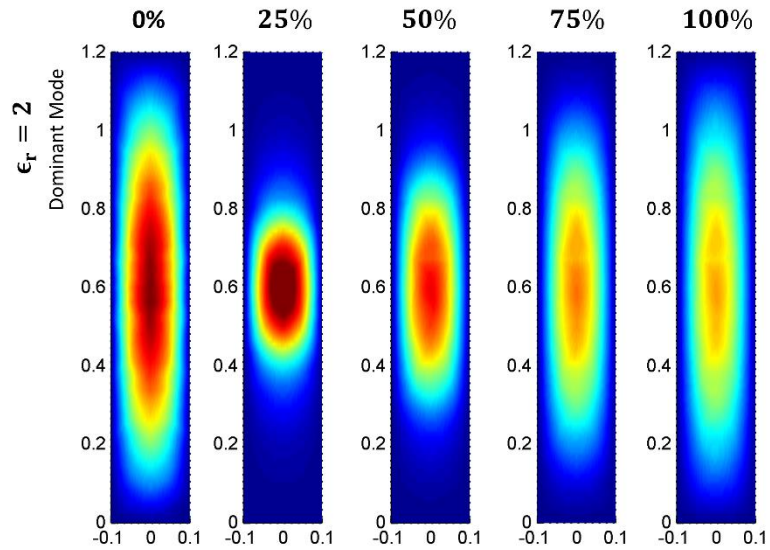


Figure A1-4. Electric field distribution for the dominant mode of a partially filled rectangular resonator. The load is located so symmetry is preserved, i.e. the load is centered about $z = 0.6$

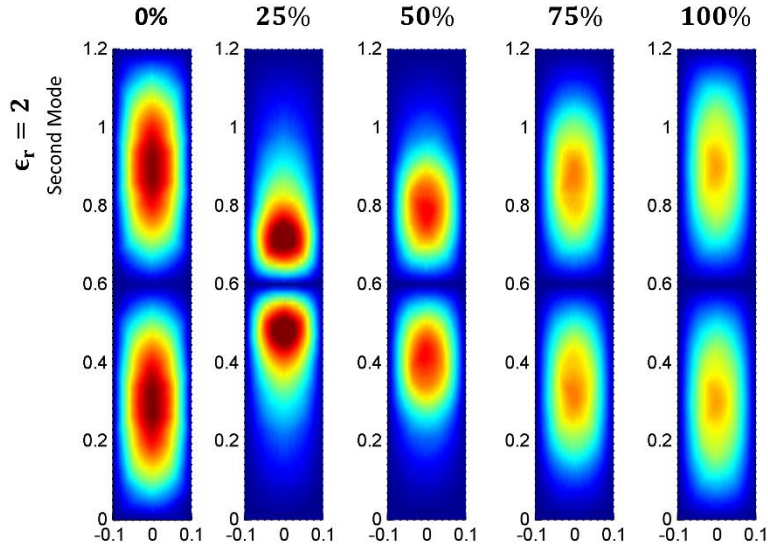


Figure A1-5. Electric field distribution for the second mode of a partially filled rectangular resonator. The load is located so symmetry is preserved, i.e. the load is centered about $z = 0.6$

Circuitual analysis is an approach that can be used for solving an electromagnetic problem by separating it into smaller and easier to analyze structures. Afterwards, these simple networks can be connected and a global behavior can be obtained, which is usually given by its general impedance, admittance or scattering matrices (GIM, GAM and GSM, respectively). Even though the segmentation technique has been around for some time (it was first attributed to Harrington in 1961), it has been widely used up to our days [1,2]. Hence, some comments will be made in the next section regarding circuitual analysis and its relation with this dissertation.

A.4. CIRCUITAL ANALYSIS

Following is a brief analysis, through circuit theory, of different networks (or blocks), so they can be used as building blocks in the analysis of a multi-layered resonator.

A.4.1. Admittance Matrix of the Rectangular resonator

A.4.1.1. Bottom network

Figure A1-6 shows the general layout of a rectangular network with a port located on its top face, i.e. at $z = c$. Hence, this block can be used as the bottom network of a multi-layered design. Since this is not a closed structure (there is one port) the wave function in the z -axis should be assumed as a traveling wave. Thus, $\Psi^{\text{TE}} = \cos(k_x x) \cos(k_y y) (A^+ e^{-\gamma z} + A^- e^{\gamma z})$ can be selected. Moreover, boundary conditions along the x -axis and y -axis imply that $k_x = m\pi/a$ and $k_y = n\pi/b$.

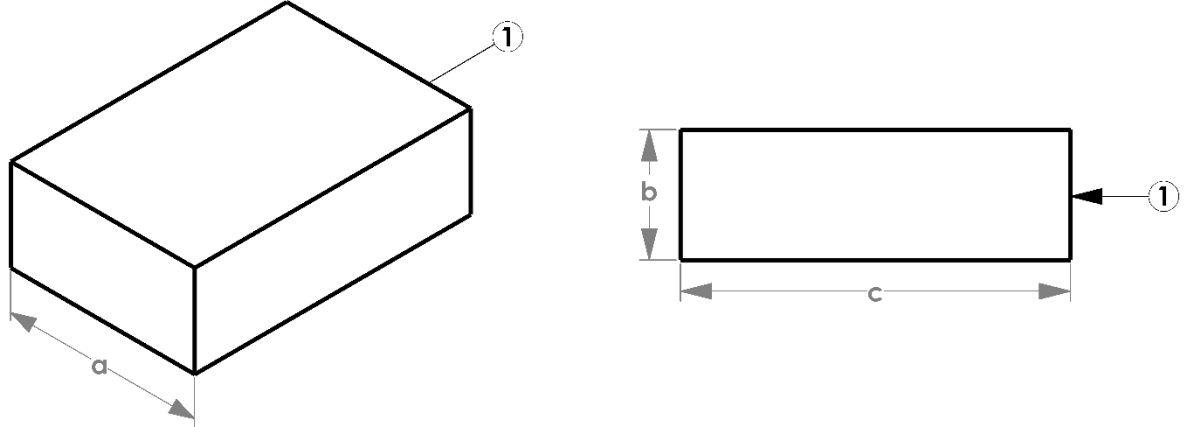


Figure A1-6. General layout of the rectangular network with one port located on its top face ($z = c$)

Applying eq. (A1.2) to the wave function reveals that the electric field along the x -axis is of the form shown by eq. (A1.24), whilst the magnetic field along the y -axis is of the form shown by eq. (A1.25). Now, the boundary condition at the wall in the z -axis, i.e. the wall located at $z = 0$ require that the tangential electric field becomes zero. From eq. (A1.24) it follows that $A^+ = A^-$, so the fields can be rewritten as shown in eq. (A1.26).

$$E_x = k_y \cos(k_x x) \sin(k_y y) (A^+ e^{-\gamma z} + A^- e^{\gamma z}) \quad (\text{A1.24})$$

$$H_y = \frac{k_y \gamma}{j\omega\mu} \cos(k_x x) \sin(k_y y) (A^+ e^{-\gamma z} - A^- e^{\gamma z}) \quad (\text{A1.25})$$

$$E_x = -2A^+ k_y \cos(k_x x) \sin(k_y y) \sinh(\gamma z) \quad (\text{A1.26})$$

$$H_y = 2A^+ \frac{k_y \gamma}{j\omega\mu} \cos(k_x x) \sin(k_y y) \cosh(\gamma z)$$

The internal electric field at the port, i.e. at $z = c$ must be the same as the incident field at the port, so:

$$-2A^+ k_y \cos(k_x x) \sin(k_y y) \sinh(\gamma c) = \sum_{m=0}^{\infty} \alpha_m \sin\left(\frac{2\pi m y}{b}\right) + \beta_m \cos\left(\frac{2\pi m y}{b}\right) \quad (\text{A1.27})$$

Multiplying both sides by $\sin(k_y y)$ and integrating between zero and b leads to eq. (A1.28), where $I_m^s = \int_0^b \sin(k_y y) \sin\left(\frac{2\pi m y}{b}\right) dy$ and $I_m^c = \int_0^b \sin(k_y y) \cos\left(\frac{2\pi m y}{b}\right) dy$. Because of orthogonality, $\int_0^b \sin(k_y y) \sin(k_y y) dy = b/2$, so eq. (A1.28) can be solved in terms of A^+ , yielding eq. (A1.29).

$$-2A^+ k_y \cos(k_x x) \sinh(\gamma c) \int_0^b \sin(k_y y) \sin(k_y y) dy = \sum_{m=0}^{\infty} \alpha_m I_m^s + \beta_m I_m^c \quad (\text{A1.28})$$

$$A^+ = -\frac{1}{bk_y \cos(k_x x) \sinh(\gamma c)} \sum_{m=0}^{\infty} \alpha_m I_m^s + \beta_m I_m^c \quad (\text{A1.29})$$

The magnetic field must also be continuous at the port, so this means that at $z = c$ the internal magnetic field must equal the incident magnetic field, as shown in eq. (A1.30). As in the previous case, this equation can be solved via the orthogonality of trigonometric functions.

$$2A^+ \frac{k_y \gamma}{j\omega\mu} \cos(k_x x) \sin(k_y y) \cosh(\gamma c) = \sum_{q=0}^{\infty} c_q \sin\left(\frac{2\pi q y}{b}\right) + d_q \cos\left(\frac{2\pi q y}{b}\right) \quad (\text{A1.30})$$

In order to obtain c_q , both sides of the equation can be multiplied by $\sin\left(\frac{2\pi q y}{b}\right)$ and then integrated between zero and b , yielding eq. (A1.31), where $I_q^s = \int_0^b \sin(k_y y) \sin\left(\frac{2\pi q y}{b}\right) dy$. For obtaining d_q it is necessary to multiply eq. (A1.30) by $\cos\left(\frac{2\pi q y}{b}\right)$ and integrate over the same domain, yielding eq. (A1.32), where $I_q^c = \int_0^b \sin(k_y y) \cos\left(\frac{2\pi q y}{b}\right) dy$. Thus, after replacing A^+ from eq. (A1.29) the values for c_q, d_q shown in eq. (A1.33) are obtained.

$$4A^+ \frac{k_y \gamma}{j\omega\mu b} \cos(k_x x) \cosh(\gamma c) I_q^s = c_q \quad (\text{A1.31})$$

$$4A^+ \frac{k_y \gamma \chi_q}{j\omega\mu b} \cos(k_x x) \cosh(\gamma c) I_q^c = d_q \quad (\text{A1.32})$$

$$\chi_q = \begin{cases} 1/2 & q = 0 \\ 1 & q > 0 \end{cases}$$

$$c_q = \frac{-4\gamma}{\omega\mu b^2 \tan(j\gamma c)} \frac{1}{I_q^s} \sum_{m=0}^{\infty} \alpha_m I_m^s + \beta_m I_m^c \quad (\text{A1.33})$$

$$d_q = \frac{-4\gamma \chi_q}{\omega\mu b^2 \tan(j\gamma c)} \frac{1}{I_q^c} \sum_{m=0}^{\infty} \alpha_m I_m^s + \beta_m I_m^c$$

Equation (A1.33) can be expressed in matrix form as shown in eq. (2.1), where $Y^{ss}, Y^{sc}, Y^{cs}, Y^{cc}$ are submatrices composed by q, m elements, as shown by eq. (2.2).

$$\begin{bmatrix} c \\ d \end{bmatrix} = [Y] \begin{bmatrix} \alpha \\ \beta \end{bmatrix} = \begin{bmatrix} Y^{ss} & Y^{sc} \\ Y^{cs} & Y^{cc} \end{bmatrix} \begin{bmatrix} \alpha \\ \beta \end{bmatrix} \quad (\text{A1.34})$$

$$\begin{aligned} Y_{qm}^{ss} &= \frac{-4\gamma}{\omega\mu b^2 \tan(j\gamma c)} \frac{1}{I_q^s I_m^s} & Y_{qm}^{sc} &= \frac{-4\gamma}{\omega\mu b^2 \tan(j\gamma c)} \frac{1}{I_q^s I_m^c} \\ Y_{qm}^{cs} &= \frac{-4\gamma \chi_q}{\omega\mu b^2 \tan(j\gamma c)} \frac{1}{I_q^c I_m^s} & Y_{qm}^{cc} &= \frac{-4\gamma \chi_q}{\omega\mu b^2 \tan(j\gamma c)} \frac{1}{I_q^c I_m^c} \end{aligned} \quad (\text{A1.35})$$

It is important to now observe the influence of the integrals over the results. For a given n , they can be calculated as shown in eq. (2.3). Hence, any cross product between sine and cosine components (i.e. $I_q^s I_m^c$ and $I_q^c I_m^s$) yield zero, so $Y^{sc} = Y^{cs} = 0$ for all n . Moreover, $[Y] = [Y^{ss}]$ if $2m = 2q = n$ and $[Y] = [Y^{cc}]$ if n is odd.

$$\begin{aligned}
 I_m^s &= \int_0^b \sin\left(\frac{2\pi m y}{b}\right) \sin\left(\frac{n\pi y}{b}\right) dy = \begin{cases} b/2 & 2m = n \\ 0 & 2m \neq n \end{cases} \\
 I_m^c &= \int_0^b \cos\left(\frac{2\pi m y}{b}\right) \sin\left(\frac{n\pi y}{b}\right) dy = \begin{cases} 0 & 2m = n \text{ OR } n = \text{even} \\ \frac{-2bn}{\pi(4m^2 - n^2)} & n = \text{odd} \end{cases} \\
 I_q^s &= \int_0^b \sin\left(\frac{2\pi q y}{b}\right) \sin\left(\frac{n\pi y}{b}\right) dy = \begin{cases} b/2 & 2q = n \\ 0 & 2q \neq n \end{cases} \\
 I_q^c &= \int_0^b \cos\left(\frac{2\pi q y}{b}\right) \sin\left(\frac{n\pi y}{b}\right) dy = \begin{cases} 0 & 2q = n \text{ OR } n = \text{even} \\ \frac{-2bn}{\pi(4q^2 - n^2)} & n = \text{odd} \end{cases}
 \end{aligned} \tag{A1.36}$$

A.4.1.2. Top network

Figure A1-7 shows the dual case of the previously discussed network. This time, the port is located at $z = 0$ and the electric wall is located at $z = c$. Hence, this network can be used as the top element of a multi-layered design. Following the same procedure as in the previous case, the wave function is $\Psi^{\text{TE}} = \cos(k_x x) \cos(k_y y) (A^+ e^{-\gamma z} + A^- e^{\gamma z})$, with $k_x = m\pi/a$ and $k_y = n\pi/b$. Applying boundary conditions at the wall, leads to $A^- = -A^+ e^{-2\gamma c}$ so the fields can be rewritten as in eq. (A1.37). Applying equivalence of the internal and incident electric fields at the port, eq. (A1.38), and solving for A^+ , leads to eq. (A1.39). Similarly, using the equivalence of the magnetic fields, solving for c_q, d_q and replacing A^+ , leads to eq. (A1.40), where $I_q^s, I_q^c, I_m^s, I_m^c$ are given in eq. (2.3).

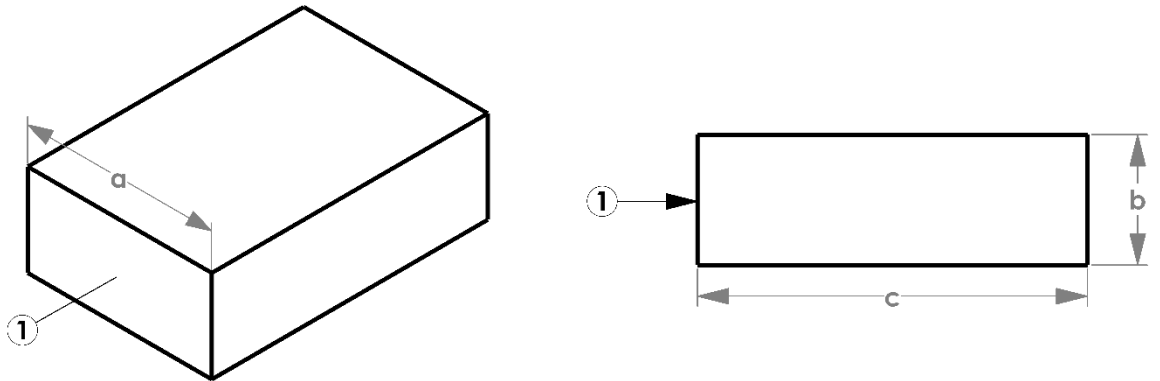


Figure A1-7. General layout of the rectangular network with one port located on its bottom face ($z = 0$)

$$E_x = -2A^+ k_y e^{-\gamma c} \cos(k_x x) \sin(k_y y) \sinh(\gamma(z-c))$$

$$H_y = 2A^+ \frac{k_y \gamma}{j\omega\mu} e^{-\gamma c} \cos(k_x x) \sin(k_y y) \cosh(\gamma(z-c)) \quad (\text{A1.37})$$

$$-2A^+ k_y e^{-\gamma c} \cos(k_x x) \sinh(-\gamma c) \int_0^b \sin(k_y y) \sin(k_y y) dy = \sum_{m=0}^{\infty} \alpha_m I_m^s + \beta_m I_m^c \quad (\text{A1.38})$$

$$A^+ = -\frac{1}{bk_y e^{-\gamma c} \cos(k_x x) \sinh(-\gamma c)} \sum_{m=0}^{\infty} \alpha_m I_m^s + \beta_m I_m^c \quad (\text{A1.39})$$

$$c_q = \frac{4\gamma}{\omega\mu b^2 \tan(j\gamma c)} I_q^s \sum_{m=0}^{\infty} \alpha_m I_m^s + \beta_m I_m^c \quad (\text{A1.40})$$

$$d_q = \frac{4\gamma\chi_q}{\omega\mu b^2 \tan(j\gamma c)} I_q^c \sum_{m=0}^{\infty} \alpha_m I_m^s + \beta_m I_m^c$$

Hence, the elements that compose the admittance matrix of the top network are:

$$Y_{qm}^{ss} = \frac{4\gamma}{\omega\mu b^2 \tan(j\gamma c)} I_q^s I_m^s \quad Y_{qm}^{sc} = 0$$

$$Y_{qm}^{cs} = 0 \quad Y_{qm}^{cc} = \frac{4\gamma\chi_q}{\omega\mu b^2 \tan(j\gamma c)} I_q^c I_m^c \quad (\text{A1.41})$$

A.4.1.3. Middle network

Figure A1-8 shows the case where the network has two ports, one at $z = 0$ and one at $z = c$. This type of network can be used as an intermediate network, and several of them can be used to allow for more complex designs. Since this network is comprised of two ports, its admittance matrix, $[Y]$, is made up of four submatrices, and each one of them contains the four submatrices already discussed, see eq. (2.5).

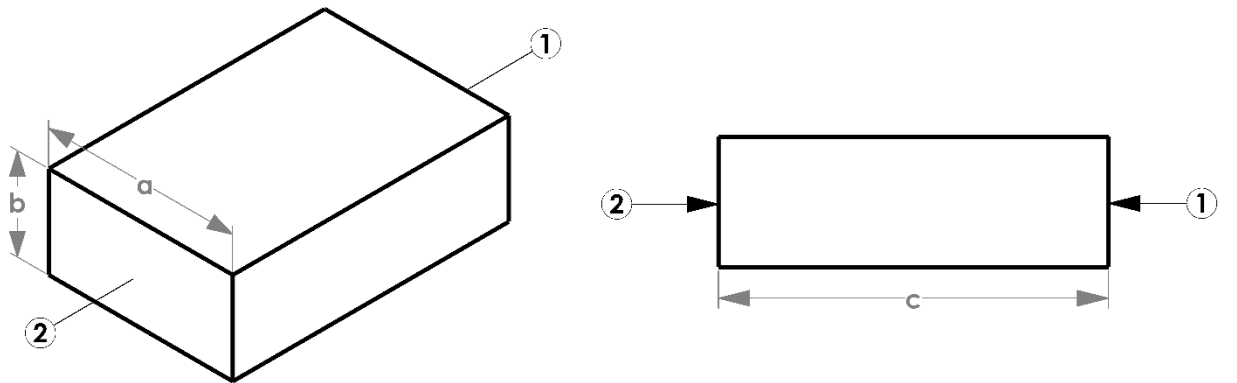


Figure A1-8. General layout of the rectangular network with one port located on its top face ($z = c$) and one port on its bottom face ($z = 0$)

$$[Y] = \begin{bmatrix} [Y_{11}] & [Y_{12}] \\ [Y_{21}] & [Y_{22}] \end{bmatrix} = \begin{bmatrix} \begin{bmatrix} Y^{ss} & Y^{sc} \\ Y^{cs} & Y^{cc} \end{bmatrix}_{11} & \begin{bmatrix} Y^{ss} & Y^{sc} \\ Y^{cs} & Y^{cc} \end{bmatrix}_{12} \\ \begin{bmatrix} Y^{ss} & Y^{sc} \\ Y^{cs} & Y^{cc} \end{bmatrix}_{21} & \begin{bmatrix} Y^{ss} & Y^{sc} \\ Y^{cs} & Y^{cc} \end{bmatrix}_{22} \end{bmatrix} \quad (\text{A1.42})$$

The admittance submatrix of elements $[Y_{11}]$ and $[Y_{22}]$ are the same as for the one port networks, see eq. (2.2) and eq. (2.4), respectively, so it is only required to calculate $[Y_{12}]$ and $[Y_{21}]$. Since the admittance matrix relates the interaction between magnetic and electric field at a given port, each of the remaining submatrices can be calculated in the same fashion as previously discussed. Though, caution must be taken to include the appropriate conditions when equating the internal and incident fields. This means that, for example, calculation of $[Y_{12}]$ implies assuming an incident electric field at port 2 (with port 1 acting as a short circuit) and then including the effect of port 1 via the equivalence of incident and internal magnetic fields. Hence, A^+ is readily available from eq. (A1.39). Specializing the magnetic field from eq. (A1.37) at port 1 ($z = c$), and equating it with an incident magnetic field, yields eq. (A1.43). Solving this equation for c_q, d_q leads to the admittance elements shown in eq. (2.6).

$$2A^+ \frac{k_y \gamma}{j\omega\mu} e^{-\gamma c} \cos(k_x x) \sin(k_y y) = \sum_{q=0}^{\infty} c_q \sin\left(\frac{2\pi q y}{b}\right) + d_q \cos\left(\frac{2\pi q y}{b}\right) \quad (\text{A1.43})$$

$$\begin{bmatrix} Y_{qm}^{ss} = \frac{4\gamma}{\omega\mu b^2} \frac{1}{\sin(j\gamma c)} I_q^s I_m^s & Y_{qm}^{sc} = 0 \\ Y_{qm}^{cs} = 0 & Y_{qm}^{cc} = \frac{4\gamma\chi_q}{\omega\mu b^2} \frac{1}{\sin(j\gamma c)} I_q^c I_m^c \end{bmatrix}_{12} \quad (\text{A1.44})$$

A similar procedure for $[Y_{21}]$ leads to eq. (2.7), where A^+ is given by eq. (A1.29) and the incident magnetic field is analyzed at port 2 (i.e. at $z = 0$).

$$\begin{bmatrix} Y_{qm}^{ss} = \frac{-4\gamma}{\omega\mu b^2} \frac{1}{\sin(j\gamma c)} I_q^s I_m^s & Y_{qm}^{sc} = 0 \\ Y_{qm}^{cs} = 0 & Y_{qm}^{cc} = \frac{-4\gamma\chi_q}{\omega\mu b^2} \frac{1}{\sin(j\gamma c)} I_q^c I_m^c \end{bmatrix}_{21} \quad (\text{A1.45})$$

A.4.2. Transformation of the Admittance Matrix into the Scattering Matrix

The admittance matrix, $\overline{\overline{Y}}$, of a given network represents the ratio between magnetic and electric fields. The scattering matrix, $\overline{\overline{S}}$, relates the behavior of a given electromagnetic wave at each port inside a specific network. Moreover, knowing one of these representations allows mapping the other one. The mathematical procedure is widely explained in literature [2,3], so here it will be just enough to mention that eq. (A1.46) shows how this transformation can be carried out, considering that $\overline{\overline{Y}}_0^{(r)}$ and $\overline{\overline{Y}}_0^{(i)}$ are the reflected and incident components of

the characteristic impedance (eq. (A1.47) and (A1.48), respectively) [1]. This notation assumes that the incident wave travels along the +z-axis, so it is appropriate for the top network (i.e. the one with the port located at $z = 0$). However, in the case of the bottom network (i.e. the one with the port located at $z = c$) the incident wave travels along the $-z$ -axis, so both terms of the characteristic admittance must be multiplied by minus one.

$$\bar{S} = (\bar{Y} + \bar{Y}_0^{(r)})^{-1} \cdot (\bar{Y}_0^{(i)} - \bar{Y}) \quad (\text{A1.46})$$

$$\bar{Y} = (\bar{Y}^{(i)} - \bar{Y}_0^{(r)} \cdot \bar{S})^{-1} \cdot (\bar{I} + \bar{S})$$

$$\bar{Y}_0^{(r)} = \text{diag}\left(\frac{k_z}{\omega\mu}\right) \quad (\text{A1.47})$$

$$\bar{Y}_0^{(i)} = \text{diag}\left(-\frac{k_z}{\omega\mu}\right) \quad (\text{A1.48})$$

A.4.3. Connecting Networks

This process implies two stages: joining the networks and connecting them. The first one creates a matrix with the information from the networks that are being connected. For example, if a two-port network and a one-port network are being connected, the resulting matrix would be of size 3×3 as shown in eq. (A1.49), where $\overline{[S]}_{N1}$ is the scattering matrix of the first network, composed of its corresponding four sub matrices, and \overline{S}_{N2} is the scattering matrix of the one-port network.

$$\overline{S}_{N12} = \begin{bmatrix} \overline{S}_{11} & \overline{S}_{21} & 0 \\ \overline{S}_{12} & \overline{S}_{22} & 0 \\ 0 & 0 & \overline{S}_{N2} \end{bmatrix}_{N1} \quad (\text{A1.49})$$

The second stage, i.e. connecting the networks, operates over the ports and returns a matrix with the equivalent scattering parameters. This new network has two ports less than \overline{S}_{N12} and each one of its elements is obtained through eq. (A1.50), where \overline{S}_{pqN12} represents each element of \overline{S}_{N12} , k, l are the port numbers that are being connected, and p, q are the indexes of \overline{S}_{N12} . Here it is worth mentioning that care must be taken as to avoid the operations where $p, q = k, l$, since these are the ports being connected and thus must not be operated.

$$\begin{aligned} \overline{S}_{pq} &= \overline{S}_{pqN12} \\ &+ \overline{S}_{pl} \cdot \Delta_1 \cdot \Delta_{kl} \cdot (\overline{S}_{kq} + \overline{S}_{kk} \cdot \Delta_{lk} \cdot \overline{S}_{lq}) \\ &+ \overline{S}_{pk} \cdot \Delta_2 \cdot \Delta_{lk} \cdot (\overline{S}_{lq} + \overline{S}_{ll} \cdot \Delta_{kl} \cdot \overline{S}_{kq}) \\ \Delta_1 &= (1 - \Delta_{kl} \cdot \overline{S}_{kk} \cdot \Delta_{lk} \cdot \overline{S}_{ll})^{-1}, \Delta_2 = (1 - \Delta_{lk} \cdot \overline{S}_{ll} \cdot \Delta_{kl} \cdot \overline{S}_{kk})^{-1} \\ \Delta_{kl} &= (1 - \overline{S}_{kl})^{-1}, \Delta_{lk} = (1 - \overline{S}_{lk})^{-1} \end{aligned} \quad (\text{A1.50})$$

A.4.4. Resonant Frequencies

Traditional circuit analysis theory conveys that the resonant frequencies of a given setup are those for which eq. (2.8) is satisfied [3]. This, however, does not require $\overline{\overline{S}}_1$ or $\overline{\overline{S}}_2$ to be the scattering matrix of a single network, so either one of them (or even both) can be the result of connecting several networks. Even so, matrix theory states that if all elements of at least one row or column are zero, then the determinant of a matrix becomes zero. This impacts directly our model, since as will be shown now, for a given n there are always rows or columns full of zero elements.

$$|\det(\overline{\overline{S}}_1 \overline{\overline{S}}_2 - 1)| = 0 \quad (\text{A1.51})$$

Assume we want to analyze the TE_{01p} modes of a given resonator split into two networks. Hence, $m = 0$ and $n = 1$, and the problem is composed of a bottom network (network 1) and a top network (network 2). Based on eq. (2.2) and eq. (2.4), and using the results shown in eq. (2.3), the admittance matrices of both networks become:

$$[Y_{\text{net}_1}] = \begin{bmatrix} [0] & [0] \\ [0] & [Y_{\text{net}_1}^{\text{cc}}] \end{bmatrix}; [Y_{\text{net}_2}] = \begin{bmatrix} [0] & [0] \\ [0] & [Y_{\text{net}_2}^{\text{cc}}] \end{bmatrix} \quad (\text{A1.52})$$

Hence, there is at least one row and one column where all the elements are zero. If we change the mode being analyzed to, e.g. $n = 2$, then the admittance matrices become:

$$[Y_{\text{net}_1}] = \begin{bmatrix} [Y_{\text{net}_1}^{\text{ss}}] & [0] \\ [0] & [0] \end{bmatrix}; [Y_{\text{net}_2}] = \begin{bmatrix} [Y_{\text{net}_2}^{\text{ss}}] & [0] \\ [0] & [0] \end{bmatrix} \quad (\text{A1.53})$$

Again, there are rows and columns filled with zero elements. This behavior repeats itself for the remaining modes, yielding eq. (A1.52) whenever n is odd, and yielding eq. (A1.53) whenever n is even. Hence, eq. (2.8) cannot be used under the scenario we are analyzing in this dissertation (i.e. a single value of n) and another alternative must be sought.

In this research work, we considered that the norm function may provide a valid approach at finding the resonant frequencies. It is illustrated as follows. We analyzed the first ten TE_{01p} modes, calculating the error between the analytic solution and the one yielded by different types of norms. We found that all norms allowed finding the resonant frequencies with error levels below 0.01% (Table 2-1). Even so, the norm that performed better was the 1-norm, so it is the one that will be used during the remainder of this dissertation. The frequency response of this approach is shown in Figure 2-2, where it can be seen that even if not all resonant

frequencies yield a value of zero norm, they do correspond with a local minima of the function and so, this approach can be used.

Table A1-1. Resonant frequencies for the first ten TE_{01p} modes, found through the analytic solution and through three different types of matrix norms

p	1-Norm				2-Norm			Inf-Norm			
	Frequency (GHz)	Frequency (GHz)	Error (kHz)	Error (%)	Frequency (GHz)	Error (kHz)	Error (%)	Frequency (GHz)	Error (kHz)	Error (%)	
1	0.7598	0.7599	28.5440	0.0038	0.7599	28.5450	0.0038	0.7599	28.5450	0.0038	
2	0.7900	0.7900	55.7820	0.0071	0.7900	55.7880	0.0071	0.7900	55.7860	0.0071	
3	0.8380	0.8380	14.1170	0.0017	0.8380	14.8290	0.0018	0.8380	16.6420	0.0020	
4	0.9008	0.9009	101.9200	0.0113	0.9009	101.9200	0.0113	0.9009	101.9300	0.0113	
5	0.9756	0.9755	120.9000	0.0124	0.9755	120.9000	0.0124	0.9755	120.8900	0.0124	
6	1.0599	1.0599	20.6650	0.0019	1.0599	20.9020	0.0020	1.0599	20.0300	0.0019	
7	1.1516	1.1518	146.5200	0.0127	1.1518	146.5300	0.0127	1.1518	146.5200	0.0127	
8	1.2491	1.2490	157.8200	0.0126	1.2490	157.8200	0.0126	1.2490	157.8200	0.0126	
9	1.3511	1.3512	43.8620	0.0032	1.3512	44.6950	0.0033	1.3512	44.8250	0.0033	
10	1.4567	1.4569	163.7700	0.0112	1.4569	163.7800	0.0112	1.4569	163.8300	0.0112	
Average: 85.3900				0.00780	85.5709			0.00782	85.6818		0.00783

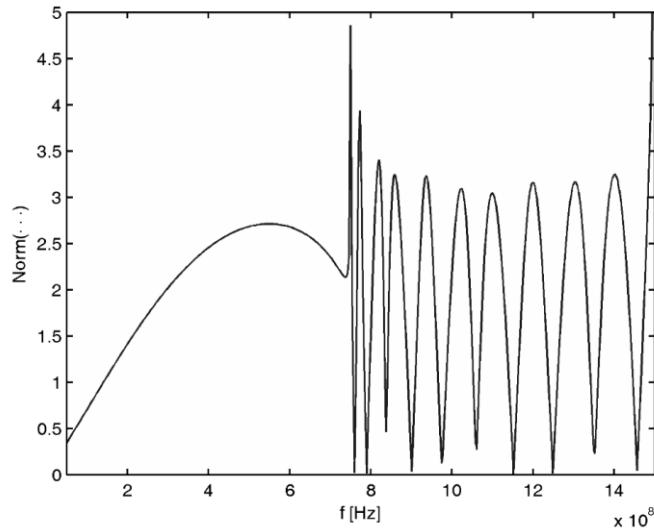


Figure A1-9. Frequency response of circuit analysis considering the 1-norm

A.5. ANALYSIS INVOLVING LOSSY MATERIALS

So far, our analysis has only considered lossless materials. However, a more general case implies that this material may have a complex permittivity, given by $\epsilon^* = \epsilon' - j\sigma/\omega$. This is reflected in the conductivity (σ) of the sample and the equations must be slightly modified.

These include changing the trigonometric functions of the wave function into their hyperbolic counterparts. Also, now $k_x = jm\pi/a$, $k_y = jn\pi/b$ and $k = j\omega\mu(\sigma + j\omega\epsilon')$.

The admittance matrices derived from circuit analysis are then modified in the following way: the bottom network is now ruled by eq. (2.12), the top network is now ruled by eq. (2.13) and the middle networks are now ruled by eq. (2.14). The expressions for each integral are, however, not modified. It is important to note that eq. (2.14) only shows the formulae for A at each port, and that each one of them has a set of associated admittance matrices (i.e. there is a set of $Y^{ss}, Y^{sc}, Y^{cs}, Y^{cc}$ per each A)

$$A = -\frac{4\gamma_z}{j\omega\mu b^2 \tanh(\gamma_z c)} \quad (A1.54)$$

$$Y^{ss} = A I_q^s I_m^s \quad Y^{sc} = 0$$

$$Y^{cs} = 0 \quad Y^{cc} = A \chi_q I_q^c I_m^c$$

$$A = \frac{4\gamma_z}{j\omega\mu b^2 \tanh(\gamma_z c)} \quad (A1.55)$$

$$Y^{ss} = A I_q^s I_m^s \quad Y^{sc} = 0$$

$$Y^{cs} = 0 \quad Y^{cc} = A \chi_q I_q^c I_m^c$$

$$A = \frac{4\gamma_z}{j\omega\mu b^2}$$

$$A_{11} = -\frac{A}{\tanh(\gamma_z c)} \quad A_{12} = \frac{A}{\sinh(\gamma_z c)} \quad (A1.56)$$

$$A_{21} = -\frac{A}{\sinh(\gamma_z c)} \quad A_{22} = \frac{A}{\tanh(\gamma_z c)}$$

The field distribution is also affected by the inclusion of the conductivity. If the resonator is split into two blocks, the amplitude of the second one is given by eq. (A1.57). If it is split into three or more, the amplitude at the second block is given by eq. (A1.58), while the amplitude at the remaining blocks is given by eq. (A1.59) and eq. (A1.60).

$$A_2 = \frac{A_1 \epsilon_2^* \sinh(k_{z_1} d_1)}{\epsilon_1^* \sinh(k_{z_2} (c - d_1))} \quad (A1.57)$$

$$A_{2b} = \frac{A_1 \epsilon_2^* (k_{z_2} \sinh(k_1) - k_{z_1} \tanh(k_2) \cosh(k_1))}{\epsilon_1^* k_{z_2} (\sinh(k_3) + \tanh(k_2) \cosh(k_3))} \quad (A1.58)$$

$$A_{2a} = \frac{A_1 \epsilon_2^* \sinh(k_1) - \epsilon_1^* A_{2b} \sinh(k_3)}{\epsilon_1^* \sinh(k_2)} \quad)$$

$$k_1 = k_{z_1} d_1 \quad k_2 = k_{z_2} d_1 \quad k_3 = k_{z_2} (c - d_1)$$

$$\begin{aligned}
A_{ib} &= \frac{\epsilon_i^* (k_{z_i} Ast_{1_i} - k_{z_{i-1}} \tanh(k_{2_i}) Ast_{2_i})}{\epsilon_{i-1}^* k_{z_i} (\sinh(k_{3_i}) + \tanh(k_{2_i}) \cosh(k_{3_i}))} \\
A_{ia} &= \frac{\epsilon_i^* Ast_{1_i} - \epsilon_{i-1}^* A_{ib} \sinh(k_{3_i})}{\epsilon_{i-1}^* \sinh(k_{2_i})}
\end{aligned} \tag{A1.59}$$

$$k_{1_i} = k_{z_{i-1}} d_{i-1} \quad k_{2_i} = k_{z_i} d_{i-1} \quad k_{3_i} = k_{z_i} (c - d_{i-1}) \quad k_{4_i} = k_{z_{i-1}} (c - d_{i-1})$$

$$\begin{aligned}
Ast_{1_i} &= A_{(i-1)a} \sinh(k_{1_i}) + A_{(i-1)b} \sinh(k_{4_i}) \quad Ast_{2_i} = A_{(i-1)a} \cosh(k_{1_i}) - A_{(i-1)b} \cosh(k_{4_i}) \\
A_N &= \frac{\epsilon_N^* (A_{(N-1)a} \sinh(k_{z_{(N-1)}} d_{(N-1)}) + A_{(N-1)b} \sinh(k_{z_{(N-1)}} (c - d_{(N-1)}))}{\epsilon_{N-1}^* \sinh(k_{z_N} (c - d_{(N-1)}))}
\end{aligned} \tag{A1.60}$$

B. ANALYTIC RESULTS OF THE SAMPLES

This appendix includes the data gathered from the analytic testing of minerals with X-ray diffraction and/or X-ray fluorescence. Only the most significant minerals were analyzed due to budgetary limitations, and fluorescence was only carried out for the as received samples because this test required more ore than it was available after microwave roasting. We begin by showing a comparison of the elemental analysis of the as received samples used for dielectric properties measurement, sorted by atomic number (Table A2.1). Then, we contrast their diffraction results, before and after roasting (Table A2.2 to Table A2.7). Finally, we show the diffraction results for a mineral used during the experimental testing stage, i.e. Juan Blanco sieve: 170 (Table A2.8).

Table A2.1. Elemental analysis of the as received samples used for measuring dielectric properties, sorted by atomic number (Z). JB stands for “Juan Blanco”, IS stands for “Ismael”, CA stands for “Carlos Arias”, CV stands for “Core from El Volcán”, and RS stands for “Rock from Segovia”. The sieve size is given by the letter S and the number next to it

Element	Z	JB S100	JB S200	JB S-200	M9 S100	IS S-170	CA S100	CV S-120	RS S-120
Na	11	--	--	N.Q.	--	--	0.08%	0.10%	--
Mg	12	0.29%	0.32%	0.40%	0.03%	0.48%	0.20%	1.04%	1.90%
Al	13	11.02%	14.38%	13.69%	0.60%	11.15%	2.84%	8.56%	9.10%
Si	14	14.87%	18.57%	17.98%	14.29%	20.26%	23.43%	22.03%	22.56%
P	15	0.09%	0.10%	0.07%	--	0.06%	0.06%	0.04%	0.08%
S	16	10.72%	6.57%	4.27%	23.51%	0.01%	17.11%	0.45%	0.95%
Cl	17	--	--	--	--	--	0.01%	0.02%	0.02%
K	19	5.54%	7.87%	8.94%	0.21%	4.75%	2.04%	7.29%	5.06%
Ca	20	0.08%	0.07%	0.06%	86 ppm	0.03%	0.23%	0.26%	6.46%
Sc	21	--	--	N.Q.	--	--	--	--	--
Ti	22	0.83%	0.83%	0.44%	0.02%	0.20%	0.24%	0.79%	0.42%
V	23	--	--	0.03%	--	--	--	--	--
Cr	24	72 ppm	--	20 ppm	N.Q.	49 ppm	0.01%	0.02%	0.01%
Mn	25	0.06%	0.06%	0.07%	--	0.02%	0.02%	0.47%	0.68%
Fe	26	18.35%	14.03%	9.17%	30.67%	13.09%	24.09%	8.37%	2.06%

Ni	28	53 ppm	44 ppm	39 ppm	35 ppm	21 ppm	50 ppm	0.01%	27 ppm
Cu	29	0.91%	0.47%	0.96%	0.48%	0.06%	0.21%	0.04%	0.02%
Zn	30	3.68%	1.92%	1.89%	0.01%	0.02%	0.54%	0.02%	95 ppm
Ga	31	--	--	--	--	--	--	47 ppm	22 ppm
As	33	5.33%	5.28%	3.59%	0.01%	1.55%	0.06%	0.01%	0.03%
Se	34	--	--	--	N.Q.	--	28 ppm	--	--
Rb	37	0.02%	0.03%	0.05%	--	0.02%	65 ppm	0.04%	0.02%
Sr	38	72 ppm	76 ppm	N.Q.	--	26 ppm	9 ppm	0.01%	0.01%
Y	39	--	--	--	--	--	--	N.Q.	--
Zr	40	0.03%	0.05%	0.07%	11 ppm	0.03%	0.02%	0.08%	0.01%
Nb	41	20 ppm	21 ppm	--	--	--	--	58 ppm	11 ppm
Mo	42	--	--	--	--	--	26 ppm	--	--
Ag	47	0.03%	0.02%	0.03%	85 ppm	--	0.02%	--	--
Cd	48	0.05%	0.03%	0.04%	--	--	--	--	--
Sb	51	0.06%	0.04%	N.Q.	--	0.15%	--	--	--
Te	52	--	--	--	--	--	N.Q.	--	--
Ba	56	0.07%	0.12%	0.14%	--	0.10%	N.Q.	0.17%	0.02%
Hg	80	--	83 ppm	0.01%	--	--	0.08%	--	--
Pb	82	6.50%	5.33%	5.72%	--	0.25%	0.06%	--	39 ppm

Table A2.2. Mineral composition before and after roasting for “Juan Blanco”, sieve: 100 . N.Q.: Not Quantifiable

Compound	Before	After
Quartz (SiO ₂)	18.1%	14.0%
Moscovite (KAl ₂ (Si, Al) ₄ O ₁₀ (OH) ₂)	17.5%	20.1%
Pyrite (FeS ₂)	26.7%	12.8%
Galena (PbS)	<1.0%	<1.0%
Anglesite (Pb(SO ₄))	3.1%	--
Mackinawite (FeS)	2.2%	1.5%
Sphalerite (ZnO)	--	<1.0%
Arsenopyrite (FeAsS)	N.Q.	--

Pyrrhotite ($\text{Fe}_{0.95}\text{S}_{1.05}$)	--	1.4%
Spinel ($\text{Mg}_{1.01}\text{Fe}_{1.77}\text{Al}_{2.22}\text{O}_4$)	--	1.9%
Melanterite ($(\text{Fe}, \text{Cu}, \text{Zn})\text{SO}_4 \cdot 7\text{H}_2\text{O}$)	--	1.9%
Zincocopiatite ($\text{ZnFe}_4(\text{SO}_4)_6(\text{OH})_2 \cdot 18\text{H}_2\text{O}$)	--	N.Q.
Anatase (TiO_2)	--	<1.0%
Others	31.6%	44.3%

Table A2.3. Mineral composition before and after roasting for “Juan Blanco”, sieve: 200 . N.Q.: Not Quantifiable

Compound	Before	After
Quartz (SiO_2)	13.0%	13.4%
Moscovite ($\text{KAl}_2(\text{Si}, \text{Al})_4\text{O}_{10}(\text{OH})_2$)	20.0%	18.0%
Pyrite (FeS_2)	14.2%	11.8%
Galena (PbS)	<1.0%	<1.0%
Anglesite ($\text{Pb}(\text{SO}_4)$)	--	<1.0%
Hematite (Fe_2O_3)	--	1.8%
Sphalerite (ZnO)	1.4%	1.6%
Arsenopyrite (FeAsS)	N.Q.	N.Q.
Alunite ($\text{K}(\text{Al}_3(\text{SO}_4)_2(\text{OH})_6)$)	--	2.4%
Others	51.1%	49.8%

Table A2.4. Mineral composition before and after roasting for “Juan Blanco”, sieve: -200. N.Q.: Not Quantifiable; N.Q.O.: Not Quantified due to preferential orientation of the reflections

Compound	Before	After
Quartz (SiO_2)	3.2%	3.6%
Moscovite ($\text{KAl}_2(\text{Si}, \text{Al})_4\text{O}_{10}(\text{OH})_2$)	N.Q.O.	N.Q.O.
Pyrite (FeS_2)	3.0%	3.0%
Galena (PbS)	<1.0%	<1.0%
Anglesite ($\text{Pb}(\text{SO}_4)$)	2.2%	2.3%
Troilite ($\text{Fe}_{0.94}\text{S}$)	--	N.Q.
Cuprite (Cu_2O)	N.Q.	N.Q.
Arsenopyrite (FeAsS)	N.Q.	N.Q.
Jarosite ($(\text{K}_{0.87}(\text{H}_3\text{O})_{0.13})\text{Fe}_{2.58}(\text{SO}_4)_2$ ($(\text{OH})_{4.74}(\text{H}_2\text{O})_{1.26}$)	4.7%	4.9%
Others	86.9%	86.2%

Table A2.5. Mineral composition before and after roasting for “M9”, sieve: 100 . N.Q.: Not Quantifiable

Compound	Before	After
Quartz (SiO_2)	38.7%	27.1%
Moscovite ($\text{KAl}_2(\text{Si}, \text{Al})_4\text{O}_{10}(\text{OH})_2$)	9.8%	--
Pyrite (FeS_2)	31.2%	25.0%
Pyrrhotite (Fe_7S_8)	--	16.0%

Compound	Before	After
Sphalerite (ZnO)	N.Q.	--
Others	20.3%	31.9%

Table A2.6. Mineral composition before and after roasting for “Carlos Arias”, sieve: 100

Compound	Before	After
Quartz (SiO ₂)	46.1%	47.0%
Moscovite (KAl ₂ (Si, Al) ₄ O ₁₀ (OH) ₂)	10.9%	6.8%
Pyrite (FeS ₂)	17.2%	13.9%
Calcite (Ca(CO ₃))	1.3%	2.0%
Microcline (KAlSi ₃ O ₈)	2.1%	6.9%
Pyrrhotite (Fe _{0.95} S _{1.05})	--	9.1%
Others	22.4%	14.3%

Table A2.7. Mineral composition before and after roasting for “Core from El Volcán”, sieve: -120

Compound	Before	After
Quartz (SiO ₂)	42.0%	41.8%
Moscovite (KAl ₂ (Si, Al) ₄ O ₁₀ (OH) ₂)	20.4%	20.3%
Pyrite (FeS ₂)	<1.0%	--
Orthoclase (K(AlSi _{3.02} O ₈))	8.7%	9.2%
Phlogopite (K(Mg _{2.18} Fe _{0.82})(Al _{1.29} Si _{2.71} O ₁₀ (OH) ₂))	14.5%	14.7%
Others	13.9%	14.0%

Table A2.8. Mineral composition before and after roasting for “Juan Blanco”, sieve: 170

Compound	Before	After
Diaoyudaoite (Na ₂ Al ₂₂ O ₃₄)	3.8%	3.0%
Quartz (SiO ₂)	41.9%	24.6%
Moscovite (KAl ₂ (Si, Al) ₄ O ₁₀ (OH) ₂)	15.9%	--
Pyrite (FeS ₂)	29.1%	--
Magnetite (Fe ₃ O ₄)	0.3%	--
Erdite (NaFeS ₂ ·H ₂ O)	0.2%	--
Arsenolite (As ₄ O ₆)	0.6%	--
Hematite (Fe ₂ O ₃)	--	47.7%
Others	8.2%	24.7%

C. RESULTS OF THE DESIGN OF EXPERIMENTS

Following, four plots and a table are shown for each mineral. These data refer to the results of the design of experiments and to the ANOVA table.

C.1. MINE “JUAN BLANCO” (ASSIGNED TO: BERNAL, D; GARNICA, S; RESLEN, Y)

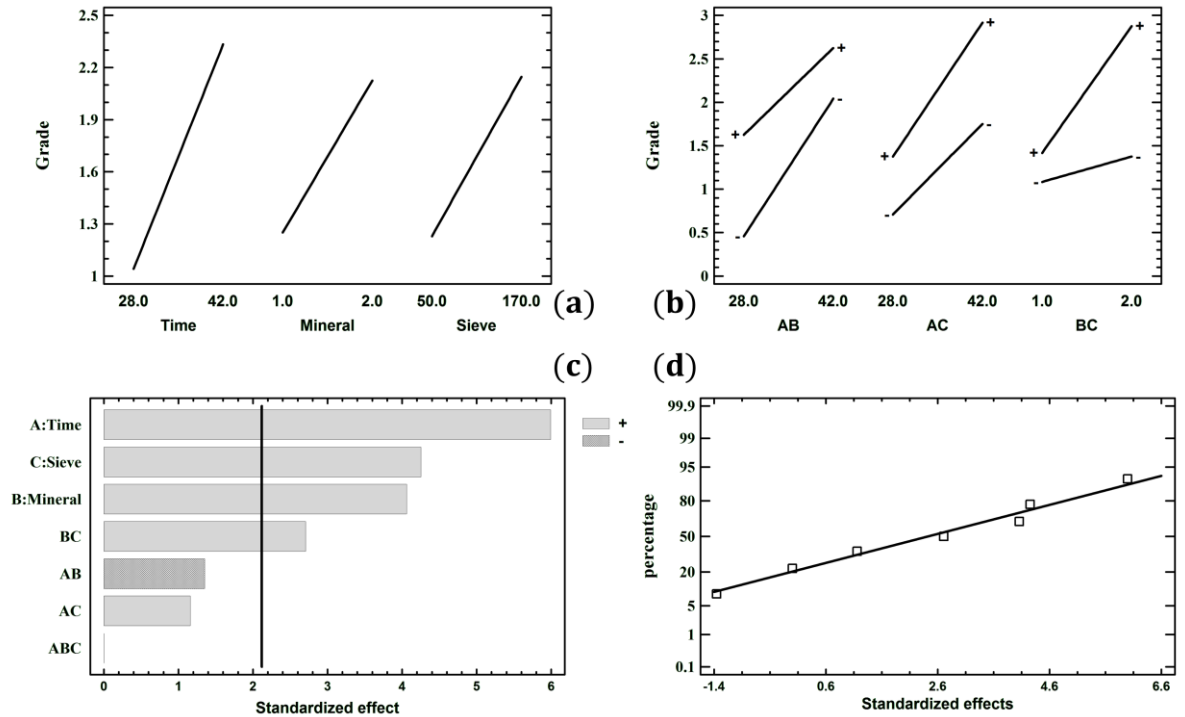


Figure A3-1. Data interpretation for the design of experiments with mine “Juan Blanco”. The following plots are presented: main effects (a), interactions (b), Pareto (c), and normal probability (d)

Table A3.1. ANOVA results for mine “Juan Blanco”

Source	Sum of Squares	Df	Mean Square	F-Ratio	P-Value
A:Time	10.01	1	10.01	35.93	0.0000
B:Mineral	4.59	1	4.59	16.49	0.0009
C:Sieve	5.04	1	5.04	18.09	0.0006
AB	0.51	1	0.51	1.83	0.1947
AC	0.38	1	0.38	1.35	0.2630
BC	2.04	1	2.04	7.33	0.0156
ABC	0.00	1	0.00	0.00	1.0000
Total error	4.46	16	0.28		
Total (corr.)	27.03	23			

C.2. MINE “REINA DE ORO” (ASSIGNED TO: DIAZ, M; RUEDA, M)

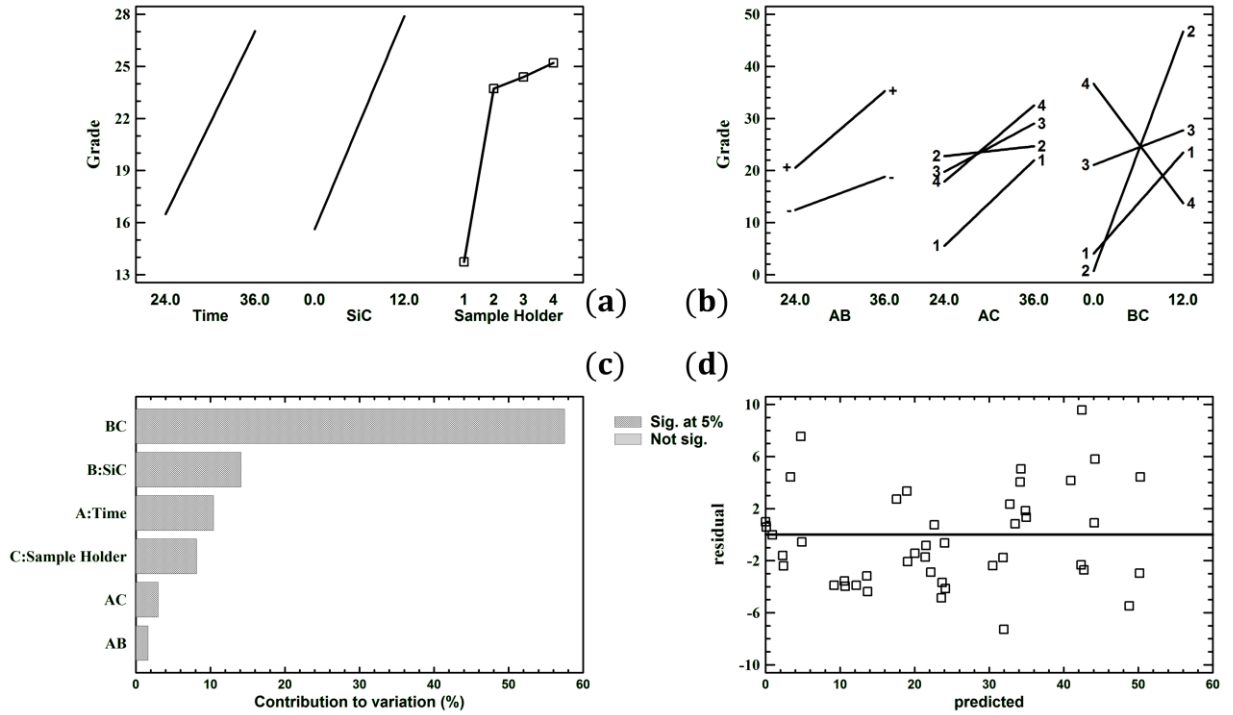


Figure A3-2. Data interpretation for the design of experiments with mine “Reina de Oro”. The following plots are presented: main effects (a), interactions (b), Pareto (c), and residuals (d)

Table A3.2. ANOVA results for mine “Reina de Oro”

Source	Sum of Squares	Df	Mean Square	F-Ratio	P-Value
Blocks	22.23	2	11.11	0.57	0.5735
A:Time (min)	1334.58	1	1334.58	67.89	0.0000
B:SiC (g)	1806.88	1	1806.88	91.92	0.0000
C:Sample Holder	1044.18	3	348.06	17.71	0.0000
AB	209.59	1	209.59	10.66	0.0026
AC	382.23	3	127.41	6.48	0.0014
BC	7371.48	3	2457.16	125.00	0.0000

C.3. MINE “TAJO ABIERTO” (ASSIGNED TO: AGUIRRE, R; BOTERO, W)

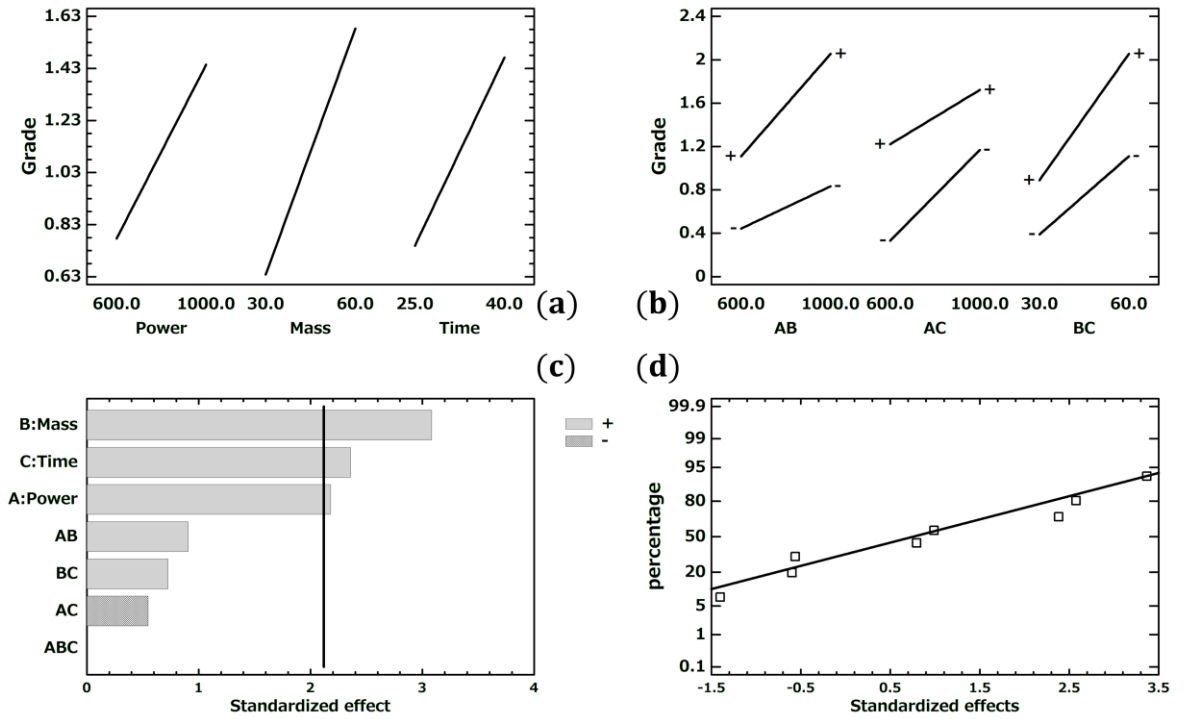


Figure A3-3. Data interpretation for the design of experiments with mine “Tajo Abierto”. The following plots are presented: main effects (a), interactions (b), Pareto (c), and normal probability (d)

Table A3.3. ANOVA results for mine “Tajo Abierto”

Source	Sum of Squares	Df	Mean Square	F-Ratio	P-Value
A:Power	2.67	1	2.67	5.67	0.0310
B:Mass	5.35	1	5.35	11.34	0.0042
C:Time	3.13	1	3.13	6.64	0.0210
AB	0.46	1	0.46	0.98	0.3380
AC	0.17	1	0.17	0.36	0.5591
BC	0.30	1	0.30	0.63	0.4398
ABC	0.00	1	0.00	0.00	0.9979
Total error	7.07	15	0.47		
Total (corr.)	21.09	23			

D. ALGORITHMS BOARDED THROUGHOUT THE DISSERTATION

The algorithms shown below represent nature-inspired iterative strategies to improve a solution during a number of iterations. An extended list is presented here, and it includes all the algorithms tested throughout the dissertation. The easiest and most simple logic for improving a solution through these algorithms is to keep iterating for a fixed number of cycles. However, most often than not, one of two things happen: a valid answer is not found, or it was found a long time ago. In the first case, the process would have to begin anew allowing for more iterations, while in the second scenario the answer could have been achieved with fewer iterations. In both cases, precious computational resources are wasted. Even so, the algorithms are described as originally conceived, but in this dissertation some convergence criteria are implemented, basically analyzing if the error at a given stage is within a tolerable range. Following, a description of all the strategies used during this dissertation is provided:

D.1. ARTIFICIAL BEE COLONY (ABC)

ABC was first proposed in a technical report by Karaboga during 2005 [4], but it was not until 2007 that it was officially presented, when he teamed up with Basturk and published their article in the Journal of Global Optimization [5]. After that, important work has been carried out by these authors [6–8] as well as by others [9–12]. ABC follows the metaphor of honey bees looking for food sources (nectar), and considers three types of bees: onlookers, scouts, and employees (slaves). The first one represents bees currently on hold, waiting to choose a food source. The second one, corresponds to bees randomly navigating the search domain. The final one, relates to bees that are currently exploiting a food source.

The idea behind ABC is that each food source represents a possible (candidate) solution, with a given amount of nectar that depends on its fitness (objective function evaluated at the food source). In each iteration, ABC offers different options to improve a solution, but after a fixed number of iterations without improvement (called “limit”), the source is considered to be exhausted and a scout replaces it with a randomly generated candidate. Improvements can be found by either, the employees or the onlookers, via modification of a candidate using eq. (A4.1), where v_{ij} is the modified solution, x_{ij} is the source position, ϕ_{ij} is a random number between -1 and 1, and where the index j represent a coordinate (dimension) of the solution, while the index k relates to a randomly chosen candidate. This means that each bee searches in the direction of an employee.

$$v_{ij} = x_{ij} + \phi_{ij}(x_{ij} - x_{kj}) \quad (\text{A4.1})$$

Broadly speaking, an iteration of ABC requires that each employed bee perturbs its position, that each onlooker bee positions near a source, and that the employed bee chooses the best coordinates. Thus, a general algorithm can be laid out as:

Algorithm I: Original Artificial Bee Colony

1. Define execution parameters: number of food sources (NS), limit, and maximum number of iterations (NI).
 2. Assign each employed bee to a randomly generated source.
 3. For each employed bee, perturb the source location, following eq. (A4.1) and evaluate its nectar (fitness).
 4. Assign each onlooker bee to a source, based on the probability p_i given in eq. (A4.2), where fit is the fitness.
 5. Repeat step 3 for the onlooker bees.
 6. Check the fitness of the sources and their perturbations. If a source was improved, modify its coordinates and go to step 8. Otherwise, increase the saturation counter of that source and go to step 7.
 7. If the saturation counter exceeds the value in the limit, abandon that source and take one from a scout bee (random generation).
 8. Repeat for NI iterations.
 9. Report results and end the process.
-

$$p_i = \frac{\text{fit}_i}{\sum_{n=1}^{NS} \text{fit}_n} \quad (\text{A4.2})$$

D.2. BAT-INSPIRED ALGORITHM (BA)

BA was proposed by Yang in 2010, and it draws on concepts from Particle Swarm Optimization (PSO) and from Simulated Annealing (SA) [13]. BA strives to replicate the behavior of simplified microbats, assuming they only use echolocation to catch a prey, and considering that they can adjust the frequency and loudness of pulse emission in relation to their distance to prey. At each iteration, BA adjusts the velocity and position of each bat, using the random frequencies given by eq. (A4.3), where β is a uniformly distributed random vector between zero and one. Velocity is updated according to eq. (A4.4), where x^* is the best solution that has been found so far and the index t relates to the current iteration. Position is updated as in PSO, and it is shown in eq. (A4.5).

$$f_i = f_{\min} + \beta(f_{\max} - f_{\min}) \quad (\text{A4.3})$$

$$v_i^t = v_i^{t-1} + f_i(x_i^t - x^*) \quad (\text{A4.4})$$

$$x_i^t = x_i^{t-1} + v_i^t \quad (\text{A4.5})$$

After all bats have relocated, one of them is randomly selected for local improvement. This is achieved through eq. (A4.6), where ϵ is a random number such that $\epsilon \in [-1,1]$, and where A^t is the average loudness of all the bats at the current iteration.

$$x_{\text{new}} = x_{\text{old}} + \epsilon A^t \quad (\text{A4.6})$$

Finally, all that remains is to update the loudness and the pulse emission rate, so a new iteration may begin. As shown in eq. (A4.7), this process requires two constants, α and γ , and it is quite straightforward.

$$A_i^{t+1} = \alpha A_i^t ; r_i^{t+1} = r_i^0 (1 - e^{-\gamma t}) \quad (A4.7)$$

When Yang presented BA, he considered the following parameters: $f_{\min} = 0, f_{\max} = 100$, and $\alpha = \gamma = 0.9$. The general algorithm, thus, can be laid out as:

Algorithm II: Original Bat-Inspired Algorithm

1. Define BA parameters, including the frequency range (f_{\min}, f_{\max}), the pulse rate (r_i), the loudness (A_i) and the constants α, γ .
 2. Randomly initialize the position of each bat and their speed.
 3. Adjust the frequency vector, using eq. (A4.3).
 4. Update the velocity and position of each bat, using eq. (A4.4) and (A4.5) respectively.
 5. Generate a random number. If it is higher than r_i , select a random bat and do a local search using eq. (A4.6).
 6. Generate a new random solution.
 7. Generate a random number. If it is lower than A_i , and the function evaluated at that point, i.e. $f(x_i)$, is better than the current best solution, i.e. $f(x^*)$, store the solution and update r_i and A_i with eq. (A4.7).
 8. Sort the bats and update the current best solution.
 9. Check convergence criteria. If it complies, stop the process. Otherwise, return to step 3.
-

D.3. CENTRAL FORCE OPTIMIZATION (CFO)

CFO was proposed by Formato in 2007 [14], and it was inspired by gravitational kinematics. As opposed to other approaches, the inner logic of CFO is deterministic in nature. This means that if the same starting points and parameters are used, the algorithm will always find the same answer. However, Formato also shows that random starting points can be used. In a general sense, CFO creates a set of probes that fly throughout the search domain, constantly attracting themselves while looking for a maximum. Some of the works related to this algorithm can be found in [15–27].

In CFO, the mass (M) represents the fitness, and the gravitational pull (G) is one of the parameters that, as with other metaheuristics, varies for each problem. However, and as posed by Formato, a value of two seems to provide good results. CFO's evolution is governed by eq. (4.1) and eq. (4.2), where the velocity (V) and the time difference (Δt) can be arbitrarily set to zero and one, respectively, in order to simplify calculations (this also following Formato's suggestion). Therefore, the only two relevant parameters that remain from the physical domain are the position (R) and acceleration (a) of each probe. There are a couple more parameters, i.e. exponents α and β , that usually take a value of two and that do not relate to any physical parameters [28].

$$a_{j-1}^p = G \sum_{\substack{k=1 \\ k \neq p}}^{N_p} U(M_{j-1}^k - M_{j-1}^p) \cdot (M_{j-1}^k - M_{j-1}^p)^\alpha \frac{R_{j-1}^k - R_{j-1}^p}{|R_{j-1}^k - R_{j-1}^p|^\beta} \quad (A4.8)$$

$$R_j^p = R_{j-1}^p + V_{j-1}^p \Delta t + \frac{1}{2} a_{j-1}^p \Delta t^2, \quad j \geq 1 \quad (A4.9)$$

It is important to note that CFO maximizes a problem, as opposed to other metaheuristics. It also forces the probes to remain inside the search domain, using a factor (F_{rep}) that indicates the loss of energy against the boundary. A general algorithm can be written as:

Algorithm III: Original Central Force Optimization

1. Define an initial position, and zero acceleration, for each probe.
 2. Calculate the mass (M) for each probe, and choose the position with the highest M.
 3. Calculate the new position of the probes, R_j^p , using eq. (4.2), and adjust the ones outside the search domain through F_{rep} .
 4. Update M and find the probe with maximum value.
 5. Update the acceleration of each probe, using eq. (4.1).
 6. Evaluate the convergence criteria. If it does not comply, return to 3.
-

D.4. FIREFLY ALGORITHM (FA)

FA was proposed by Yang in 2010 [29,30], and it is based on the attraction of artificial fireflies via the light they emit. Yang considers that any artificial firefly can attract, or be attracted, to any other one (i.e. they are unisex). Also, that the attractiveness is proportional to the brightness, where the latter is affected by the landscape of the objective function [31]. This implies, however, that the only function of light-emission in fireflies is mating, while it could also be used for attracting preys or for intimidating foes, as appears to be the case for real fireflies.

Regarding the algorithm itself, Yang proposes the use of a fixed pair of constants, α and γ . The former relates to the randomness in the movement of an artificial firefly (between zero and one), while the latter relates to the dimming of emitted light as it travels through the search domain (usually between 0.01 and 100). The algorithm can be briefly described as:

Algorithm IV: Original Firefly

1. Initialize fireflies.
 2. Calculate the light emitted by each firefly (i.e. evaluate the objective function for each firefly).
 3. Sort fireflies by light intensity (in ascending order).
 4. Update the position of each firefly (i.e. adjust each firefly according to eq. (4.3) and to the light intensity).
 5. Check for convergence. If it complies, exit. If not, go to step 2.
-

$$\begin{aligned}x_i^{k+1} &= x_i^k(1 - \beta) + x_j^k\beta + \alpha(R_1 - 0.5) \\ \beta &= \beta_0 e^{-\gamma r_{ij}^2}\end{aligned}\tag{A4.10}$$

It is important to point out that in eq. (4.3), subscripts i, j relate to the firefly under analysis, and to the other fireflies, respectively. Also, superscript k relates to the time lapse, β_0 to the attractiveness at distance zero, R_1 is a random number such that $R_1 \in [0,1]$, α and γ are the previously mentioned constants and r_{ij} is the Cartesian distance between fireflies.

D.5. GRAVITATIONAL SEARCH ALGORITHM (GSA)

GSA first appeared in a paper published by Rashedi et al. during 2009, and it is based on the attracting force of masses separated by a distance [32]. GSA revolves around the law of gravitational attraction, assuming a continually evolving universe (i.e. the gravitational constant begins at a given value and then decays). The underlying modeling allows for GSA

to change between exploration and exploitation as the search progresses. At the beginning of the search all masses (i.e. the agents) attract each other, but at the end only one mass attracts the others. In a broad sense, GSA can be described with the following algorithm:

Algorithm V: Original Gravitational Search Algorithm

1. Define GSA parameters: Initial gravitational constant, $G(t_0)$, decrease factor for the gravitational constant, β , force constant, ϵ , and number of agents, N .
 2. Randomly initialize the position of each agent and evaluate their fitness, $fit_j(t)$.
 3. Update the gravitational constant using eq. (A4.11).
 4. Identify the best and worst agents through eq. (A4.12).
 5. Update the mass of all agents, $M_i(t)$, using eq. (A4.13).
 6. Calculate the total force on each direction, $F_i^d(t)$, using eq. (A4.14), where $rand_j$ is a random number between zero and one, and $R_{ij}(t)$ is the Euclidean distance between agents i and j .
 7. Update the acceleration, $a_i^d(t)$, and velocity, $v_i^d(t)$, of each agent using eq. (A4.15), where $rand_i$ is a random number between zero and one.
 8. Update the position of each agent through eq. (A4.16).
 9. Check for convergence. If it complies, exit. If not, go to step 3.
-

$$G(t) = G(t_0) \cdot \left(\frac{t_0}{t}\right)^\beta \quad (A4.11)$$

$$\begin{aligned} best(t) &= \min_{j \in \{1, \dots, N\}} fit_j(t) \\ worst(t) &= \max_{j \in \{1, \dots, N\}} fit_j(t) \end{aligned} \quad (A4.12)$$

$$M_i(t) = \frac{m_i(t)}{\sum_{j=1}^N m_j(t)} \quad (A4.13)$$

$$m_i(t) = \frac{fit_i(t) - worst(t)}{best(t) - worst(t)}$$

$$F_i^d(t) = \sum_{j=1, j \neq i}^N rand_j \cdot F_{ij}^d(t) \quad (A4.14)$$

$$F_{ij}^d(t) = G(t) \frac{M_i(t)M_j(t)}{R_{ij}(t) + \epsilon} (x_j^d(t) - x_i^d(t))$$

$$a_i^d(t) = \frac{F_i^d(t)}{M_i(t)} \quad (A4.15)$$

$$\begin{aligned} v_i^d(t+1) &= rand_i \cdot v_i^d(t) + a_i^d(t) \\ x_i^d(t+1) &= x_i^d(t) + v_i^d(t+1) \end{aligned} \quad (A4.16)$$

D.6. HARMONY SEARCH (HS)

HS was proposed by Geem et al. in 2001, and it is the first approach based on the process that musicians carry out when composing music [33]. The general idea is that in a similar fashion that a musician uses his knowledge of music for composing melodies, HS uses the knowledge of solutions stored in its memory in tandem with some random alterations (akin to improvisation), to find a good solution. One of the special things about HS is that it improves the candidate solution (x') one coordinate at a time (x'_i), using a rather simple equation. Since its creation, HS has been continuously used by its creators [33–39] as well as by other authors [40–54]. The procedure can be described as follows:

Algorithm VI: Original Harmony Search (HS)

1. Define the execution parameters: memory size (HMS), memory considering rate (HMCR, usually performs better for values between 0.8 and 0.9), pitch adjusting rate (PAR, usually performs better for values around 0.1), and maximum number of iterations (NI).
 2. Generate a random initial matrix, HM, of size $HMS \times N$, where N represents the number of dimensions.
 3. Generate a random number. If it is lower than HMCR, go to step 4. Otherwise, take a random value from the search domain and go to step 6.
 4. Pick the value located at a random row of HM, and at the column corresponding to the component being updated.
 5. Generate a random number. If it is lower than PAR, adjust the pitch using eq. (4.4), where r is a random number in the interval $[-1,1]$.
 6. Repeat steps 3 to 5 for the remaining dimensions.
 7. Evaluate the new candidate solution. If it is better than the worst solution stored in HM, replace it and discard the worst.
 8. Repeat for NI iterations.
 9. Report results and end the process.
-

$$x'_i = x_i + r \cdot BW \quad (A4.17)$$

D.7. INTELLIGENT WATER DROPS (IWD)

IWD was first presented by Shah-Hosseini during an IEEE congress in 2007 and it followed the logic of water drops flowing through a river while dragging the underlying soil [55]. IWD was meant, however, for combinatorial optimization problems, such as the traveling salesman problem (TSP), so in 2012 Shah-Hosseini presented a continuous version [56]. This time, each component of the search domain is discretized into a number of valid points (bits) that allow for a given precision. The original approach (i.e. discrete solution) is then used to assign a value to each bit, and a normalization from the resulting binary number to the search domain is carried out. The algorithm treats each possible value of the bits, k, as a different path with its own soil values. A general algorithm can be laid out as:

Algorithm VII: Original Intelligent Water Drops (IWD)

1. Define the execution parameters: number of IWDs (N_{IWD}), number of bits (default value: $N_{bit} = 32$), initial soil (default value: 5000), minimum and maximum soil (default values: $soil_{min} = 2000$ and $soil_{max} = 1000$), number of mutations (default value: $N_{mut} = 100$), and maximum number of iterations (NI).
 2. Generate an empty matrix for each IWD, of size $M \times N_{bit}$, where M represents the number of dimensions.
 3. Select an edge for the first bit of each IWD, i.e. assign the bit a value of zero or one, based on the probability given by eq. (A4.18), where $f(soil(e_{i,i+1}(k)))$ is given by eq. (A4.19), $g(soil(e_{i,i+1}(k)))$ is given by eq. (A4.20), and k is zero or one and represents an independent path for each possible solution.
 4. Update the local soil of the edges, through eq. (A4.21), and of the IWD, through eq. (A4.22), where $\Delta_{soil} = 0.001$.
 5. Repeat steps 3 and 4 for the remaining bits.
 6. Transform each generated solution into their decimal equivalent, and evaluate them.
 7. Apply mutation-based local search N_{mut} times for each solution, i.e. randomly select an edge and replace it by its opposite if it improves the solution.
-

-
8. Identify the best solution of the current iteration, T^{IB} .
 9. Update the global soil, using eq. (A4.23), where $T_{soil}(e_{i,i+1}(k))$ is given by eq. (A4.24).
 10. Go to step 2 and repeat for NI iterations.
 11. Report results and end the process.
-

$$P^{IWD}(e_{i,i+1}(k)) = \frac{f(\text{soil}(e_{i,i+1}(k)))}{\sum_{l=0}^1 f(\text{soil}(e_{i,i+1}(l)))} \quad (\text{A4.18})$$

$$f(\text{soil}(e_{i,i+1}(k))) = \frac{1}{0.0001 + g(\text{soil}(e_{i,i+1}(k)))} \quad (\text{A4.19})$$

$$g(\text{soil}(e_{i,i+1}(k))) = \begin{cases} \text{soil}(e_{i,i+1}(k)) & \min \text{soil}(e_{i,i+1}(0:1)) \geq 0 \\ \text{soil}(e_{i,i+1}(k)) - \min \text{soil}(e_{i,i+1}(0:1)) & \text{otherwise} \end{cases} \quad (\text{A4.20})$$

$$\text{soil}(e_{i,i+1}(k)) = 1.1 \cdot \text{soil}(e_{i,i+1}(k)) - 0.01 \cdot \Delta_{soil} \quad (\text{A4.21})$$

$$\text{soil}^{IWD} = \text{soil}^{IWD} + \Delta_{soil} \quad (\text{A4.22})$$

$$\text{soil}(e_{i,i+1}(k)) = \min(\max(T_{soil}(e_{i,i+1}(k)), \text{soil}_{\min}), \text{soil}_{\max}) \quad (\text{A4.23})$$

$$T_{soil}(e_{i,i+1}(k)) = 1.1 \cdot \text{soil}(e_{i,i+1}(k)) - 0.01 \cdot \frac{\text{soil}_{IB}^{IWD}}{M \cdot N_{bit}} \quad (\text{A4.24})$$

D.8. PARTICLE SWARM OPTIMIZATION (PSO)

PSO may have been the strategy that revolutionized optimization approaches and that ignited the spark in bio-inspired computation developments. This technique, proposed by Eberhart and Kennedy almost two decades ago, mimics the collaborative intelligence exhibited by swarms when looking for sources of food [57,58]. PSO was not the first approach based on naturally occurring processes, but it has certainly inspired a great deal of work throughout the years [44,59–75]. Broadly speaking, PSO generates a swarm that transverse the search domain, communicating the best solutions found by each particle and working together to find a minimum. A general layout of its algorithm can be given as:

Algorithm VIII: Original Particle Swarm Optimization

1. Assign a random initial position and zero speed for each particle.
 2. Evaluate the objective function, f , and calculate the best position each particle has found, P_{Best_i} , and the best position of all the swarm G_{Best} .
 3. Update position and speed for each particle with eq. (4.5) and (4.6), where i, j represent pointers for each position and time step, respectively; X is a particle's position, V its speed, w an inertia factor to limit the effect of its previous speed, C_1, C_2 are the self and swarm trust factors (default value: $C_1, C_2 = 2.05$), and R_1, R_2 are random numbers (uniformly distributed) between zero and one.
 4. Evaluate the objective function.
 5. Compare, for each particle, the evaluated value and P_{Best_i} . If it is lower, then update P_{Best_i} .
 6. Select the best particle and compare it to G_{Best} . If it is lower, then update G_{Best} .
 7. Compare G_{Best} with convergence criteria. If it does not comply, return to 3.
-

$$X_i^{j+1} = X_i^j + V_i^{j+1} \quad (\text{A4.25})$$

$$V_i^{j+1} = wV_i^j + C_1R_1(P_{\text{Best}_i} - X_i^j) + C_2R_2(G_{\text{Best}} - X_i^j) \quad (\text{A4.26})$$

D.9. QUANTUM-INSPIRED EVOLUTIONARY ALGORITHM (QEA)

QEA was proposed by Han and Kim in 2002, and it is based on concepts from quantum computation [76]. QEA uses a search agent based on a probabilistic representation, known as a Q-bit, composed of a string of Q-bits representing a binary solution. Thus, each element of the string has a probability α_i^2 of being zero and a probability β_i^2 of being one. In this strategy, a Q-gate guides the solution towards a single state, and it represents a rotation matrix. A general algorithm can be laid out as:

Algorithm IX: Original Quantum-Inspired Evolutionary Algorithm

1. Define the number of search agents, n , and the length of each string, m .
 2. Initialize each Q-bit: assign $\alpha_i = \beta_i = 1/\sqrt{2}$ for each q_j , where $i = 1, 2, \dots, m$ and $j = 1, 2, \dots, n$.
 3. Generate the n binary solutions and store them in P : for each solution, generate m random numbers and assign a value of zero if the number is lower than α_i (otherwise assign a value of one).
 4. Copy the solutions stored in P to B .
 5. Calculate the fitness of each solution stored in P .
 6. Generate a new set of n binary solutions, as in step 3.
 7. Calculate the fitness of each solution stored in P .
 8. Update the probabilities of each Q-bit, using eq. (A4.27), where the angle is given by eq. (A4.28).
 9. Compare each solution stored in P with the ones stored in B . If one solution in P is better, move it to B .
 10. Find the best solution stored in B and copy it to b if it is better than the one already there.
 11. If migration is enabled, copy b into all solutions of B (global migration) or just into some (local migration).
 12. Return to step 6 and repeat until convergence criteria is achieved.
-

$$\begin{bmatrix} \alpha_i \\ \beta_i \end{bmatrix} = \begin{bmatrix} \cos(\Delta\theta_i) & -\sin(\Delta\theta_i) \\ \sin(\Delta\theta_i) & \cos(\Delta\theta_i) \end{bmatrix} \begin{bmatrix} \alpha_i \\ \beta_i \end{bmatrix} \quad (\text{A4.27})$$

$$\Delta\theta_i = \begin{cases} 0.01\pi & x_i = 0 \wedge b_i = 1 \wedge f(x) < f(b) \\ -0.01\pi & x_i = 1 \wedge b_i = 0 \wedge f(x) < f(b) \\ 0 & \text{otherwise} \end{cases} \quad (\text{A4.28})$$

D.10. SIMULATED ANNEALING (SA)

SA was presented by Kirkpatrick et al. back in 1983, and it is one of the oldest modern optimization techniques [77]. An interesting fact about SA is that proofs of convergence have been published, such as the one by Granville et al. [78]. Unfortunately, SA only deals with one solution at the time (i.e. one agent) and that could be considered as a disadvantage.

SA mimics the cooling process of a hot metal, from a high temperature and up to a thermal equilibrium with the environment. The fitness of the objective function represents the energy level of a solution, so $E_i = f(x_i)$, and the probability of accepting a new solution follows Metropolis criterion, eq. (A4.29), where T is the current temperature, and k is Boltzmann's constant.

$$P(E_{i+1}) = \min\left(1, e^{-\frac{\Delta E}{kT}}\right) \quad (A4.29)$$

$$\Delta E = E_{i+1} - E_i$$

A general algorithm can be described as:

Algorithm X: Original Simulated Annealing

1. Define starting temperature, T_0 , the number of design points, n , and the temperature reduction factor, c .
 2. Choose a random starting solution, x_1 , and calculate its energy, E_1 .
 3. Choose a random point near the solution, x_{i+1} , and calculate its energy, E_{i+1} .
 4. Determine whether or not to accept the new solution, based on the probability given in eq. (A4.29).
 5. Repeat steps 3 and 4 for n iterations.
 6. Decrease temperature using c .
 7. Return to step 3 and repeat until convergence criteria is achieved.
-

D.11. SPIRAL OPTIMIZATION (SO)

SO was proposed by Tamura and Yasuda in 2011, mimicking the path followed by a given number of logarithmic spirals [79,80]. Akin to an eagle stalking a prey, each spiral closes in on the minimum through inward traveling loops, changing their target (convergence point) each time a spiral detects a better solution. SO requires defining the rotation angle, θ (default value: $\pi/2$), and the distance rate, r (default value can be either 0.95 or 0.99), at each step. The combination of these two effects (i.e. changing the convergence point and the free definition of rotation angle and distances) may generate paths that resemble anything but a logarithmic spiral, even though the mathematical model is appropriate. Some of the recent work related to SO can be found in [81,82] and a general algorithm can be defined as:

Algorithm XI: Original Spiral Optimization

1. Define the number of spirals, m , as well as r and θ .
 2. Assign a random initial position inside the search domain.
 3. Find the starting convergence point, x^* , such as $f(x^*) = \min(f(x^1), f(x^2), \dots, f(x^m))$.
 4. Update position of each spiral, x^k , using eq. (4.7) and eq. (4.8), where t indicates the current iteration, I_n is the identity matrix, and the index n represents the number of dimensions of the problem. Each element of the rotation matrix, $R^n(\theta)$, is given by eq. (4.9), where $a_{i,j}$ is the corresponding element of the identity matrix.
 5. Evaluate the objective function.
 6. Update the convergence point, x^* .
 7. Compare with convergence criteria. If it does not comply, return to 4.
-

$$x^k(t+1) = S_n(r, \theta) \cdot x^k(t) - (S_n(r, \theta) - I_n) \cdot x^* \quad (A4.30)$$

$$S_n(r, \theta) = r \cdot R^n(\theta) = r \prod_{i=1}^{n-1} \prod_{j=1}^i R_{n-i, n+1-j}^n(\theta_{n-i, n+1-j}) \quad (A4.31)$$

$$y_{p,q} = \begin{cases} \cos \theta_{i,j} & p = i \wedge q = i \\ -\sin \theta_{i,j} & p = i \wedge q = j \\ \sin \theta_{i,j} & p = j \wedge q = i \\ \cos \theta_{i,j} & p = j \wedge q = j \\ a_{i,j} & \text{otherwise} \end{cases} \quad (A4.32)$$

D.12. UNIFIED PARTICLE SWARM OPTIMIZATION (UPSO)

UPSO was proposed by Parsopoulos and Vrahatis in 2004 and appeared as a strain of PSO variants [83]. However, we include it in this section since we are leaving the next one just for the modifications proposed during this dissertation. This modification defines a local and global behavior for each particle of the swarm (L_p, G_p respectively), calculated through eq. (4.10) and eq. (4.11), where χ stands for the constriction factor. Default values of $c_p = c_g = 2.05$ are commonly used. Afterwards, the data is merged into a single update of velocity—eq. (4.12)—via the unification factor (default value: $u = 0.5$). The position of each particle, however, is updated in the same fashion as in PSO, i.e. through eq. (4.13).

$$L_p^{t+1} = \chi \cdot [V_p^t + c_p r_3 (P_p - X_p^t) + c_g r_4 (P_{gp} - X_p^t)] \quad (\text{A4.33})$$

$$G_p^{t+1} = \chi \cdot [V_p^t + c_p r_1 (P_p - X_p^t) + c_g r_2 (P_g - X_p^t)] \quad (\text{A4.34})$$

$$V_p^{t+1} = (1 - u) \cdot L_p^{t+1} + u \cdot G_p^{t+1} \quad (\text{A4.35})$$

$$X_p^{t+1} = X_p^{t+1} + V_p^{t+1} \quad (\text{A4.36})$$

A general algorithm can be laid out as:

Algorithm XII: Unified Particle Swarm Optimization

1. Define UPSO parameters, including the size of the swarm (Ψ).
 2. Randomly initialize the position of each particle and their speed.
 3. Evaluate each candidate solution, and determine the best coordinate of each particle (P_p), of each neighbourhood (P_{gp}), and of all the swarm (P_g).
 4. Update the velocity and position of each particle, using eq. (4.12) and eq. (4.13), respectively.
 5. Evaluate each new position and update P_p, P_{gp}, P_g .
 6. Check convergence criteria. If it complies, stop the process. Otherwise, return to step 4.
-

E. ANALYSIS OF HYBRID MODES IN A PARTIALLY-FILLED WAVEGUIDE

Homogeneously filled rectangular waveguides can be easily studied by analytical means, since the problem can be decoupled into transverse electric (TE) and transverse magnetic (TM) modes, where the electric or magnetic fields are zero in the traveling direction, respectively. However, if there is a discontinuity (i.e. change of material), perpendicular to wave propagation, the solution cannot be decoupled and both, electric and magnetic field in the traveling direction, become non-zero. Therefore, hybrid modes appear. They are known as HE and EH modes, depending on whether the magnetic or electric field dominates near cutoff, respectively [84]. Solving Maxwell's equations for EH and HE modes now imply finding roots for eq. (A5.1) and eq. (A5.2), respectively.

$$\frac{\mu_1}{k_{1y}} \tan(k_{1y}h) = -\frac{\mu_2}{k_{2y}} \tan(k_{2y}(b-h))$$

$$k_x^2 + k_{1y}^2 + k_z^2 = k_1^2 = \omega^2 \mu_1 \epsilon_1 \quad (\text{A5.1})$$

$$k_x^2 + k_{2y}^2 + k_z^2 = k_2^2 = \omega^2 \mu_2 \epsilon_2$$

$$\frac{k_{1y}}{\epsilon_1} \tan(k_{1y}h) = -\frac{k_{2y}}{\epsilon_2} \tan(k_{2y}(b-h))$$

$$k_x^2 + k_{1y}^2 + k_z^2 = k_1^2 = \omega^2 \mu_1 \epsilon_1 \quad (\text{A5.2})$$

$$k_x^2 + k_{2y}^2 + k_z^2 = k_2^2 = \omega^2 \mu_2 \epsilon_2$$

Two studies were carried out on this regard: the one of Farfán and Fontecha [85], and the one of Suarez and Romero [86]. The first team used UPSO and the second one used SA, but both focused on replicating the dispersion curves in a half-filled rectangular waveguide. The general procedure followed in both cases was:

1. Define an operating mode: choose indices m and n and whether it is HE or EH.
2. Find the cutoff frequency of the chosen mode: use the optimization algorithm to solve either eq. (A5.1) or eq. (A5.2), with $k_z = 0$ and $k_x = \frac{m\pi}{a}$, where a is the length in the x-direction.
3. Make a frequency sweep and preserve the mode: increase the frequency, use the optimization algorithm to find a similar propagation constant, and repeat until all frequencies are done.
4. Repeat for the remaining modes.

Table A5-1 shows sample data for finding a propagation constant above the resonant frequency, focusing on the required number of iterations and possible fitness with UPSO and SA. For more details, please refer to the full reports of each study. Both strategies allowed for good results, but UPSO only required a small fraction of iterations. Moreover, SA and UPSO allowed an appropriate reconstruction of the dispersion curves (Figure A5-1).

Table A5-1. Sample data of the required number of iterations and fitness yielded by UPSO and SA

Mode	Iterations		Fitness	
	UPSO	SA	UPSO	SA
EH01	72	1067	4.50E-15	1.65E-24
EH11	107	1669	4.97E-15	3.26E-26
EH21	49	2270	1.13E-15	8.96E-24
EH31	4	2247	2.34E-15	8.97E-26

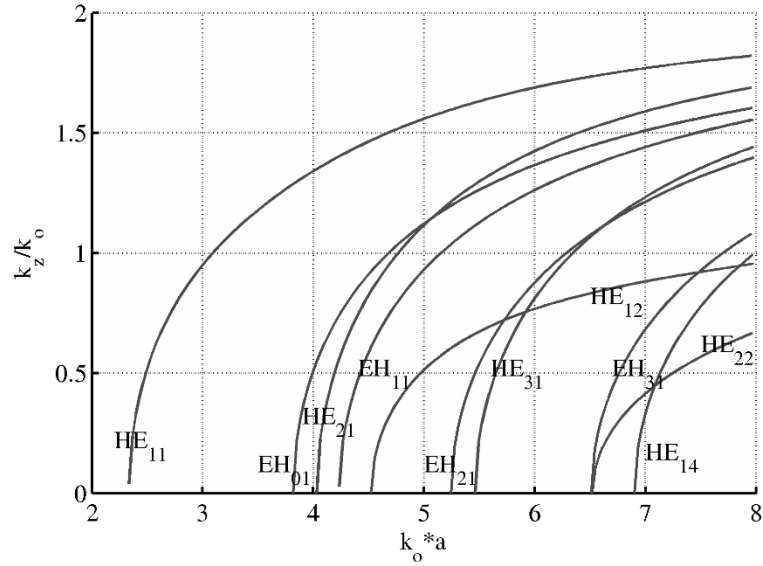


Figure A5-1. Dispersion curves generated by UPSO and SA for the half-filled rectangular waveguide

References

- [1] R.F. Harrington, *Time-Harmonic Electromagnetic Fields*, John Wiley & Sons, Inc., 1961.
- [2] F.L. Penaranda-Foix, J.M. Catala-Civera, *Circuit Analysis of Cylindrical Structures Applied to the Electromagnetic Resolution of Resonant Cavities*, in: *Passiv. Microw. Components Antennas*, InTech, 2010: pp. 141–168. doi:10.5772/226.
- [3] F.L. Peñaranda-Foix, *Aplicación de la teoría de análisis circuital generalizado a la resolución de problemas de difracción electromagnética*, Ph.D. Thesis, Universidad Politécnica de Valencia, 2001. doi:hdl.handle.net/10251/7121.
- [4] D. Karaboga, *An Idea Based on Honey Bee Swarm for Numerical Optimization*, 2005.
- [5] D. Karaboga, B. Basturk, A powerful and efficient algorithm for numerical function optimization: artificial bee colony (ABC) algorithm, *J. Glob. Optim.* 39 (2007) 459–471. doi:10.1007/s10898-007-9149-x.
- [6] D. Karaboga, B. Gorkemli, C. Ozturk, N. Karaboga, A comprehensive survey: artificial bee colony (ABC) algorithm and applications, *Artif. Intell. Rev.* 42 (2014) 21–57. doi:10.1007/s10462-012-9328-0.
- [7] D. Karaboga, B. Akay, A comparative study of Artificial Bee Colony algorithm, *Appl. Math. Comput.* 214 (2009) 108–132. doi:10.1016/j.amc.2009.03.090.
- [8] D. Karaboga, C. Ozturk, N. Karaboga, B. Gorkemli, Artificial bee colony programming for symbolic regression, *Inf. Sci. (Ny)*. 209 (2012) 1–15. doi:10.1016/j.ins.2012.05.002.
- [9] W. Gao, S. Liu, L. Huang, A global best artificial bee colony algorithm for global optimization, *J. Comput. Appl. Math.* 236 (2012) 2741–2753. doi:10.1016/j.cam.2012.01.013.
- [10] W.Y. Szeto, Y. Wu, S.C. Ho, An artificial bee colony algorithm for the capacitated vehicle routing problem, *Eur. J. Oper. Res.* 215 (2011) 126–135. doi:10.1016/j.ejor.2011.06.006.
- [11] M.-H. Horng, Multilevel thresholding selection based on the artificial bee colony algorithm for image segmentation, *Expert Syst. Appl.* 38 (2011) 13785–13791. doi:10.1016/j.eswa.2011.04.180.

- [12] M. Ma, J. Liang, M. Guo, Y. Fan, Y. Yin, SAR image segmentation based on Artificial Bee Colony algorithm, *Appl. Soft Comput.* 11 (2011) 5205–5214. doi:10.1016/j.asoc.2011.05.039.
- [13] X. Yang, A New Metaheuristic Bat-Inspired Algorithm, in: *Int. Work. Nat. Inspired Coop. Strateg. Optim. (NICSO 2010)*, Springer, Granada, 2010: pp. 65–74. doi:10.1007/978-3-642-12538-6_6.
- [14] R.A. Formato, Central Force Optimization: a New Metaheuristic With Applications in Applied Electromagnetics, *Prog. Electromagn. Res.* 77 (2007) 425–491. doi:10.2528/PIER07082403.
- [15] R.C. Green, L. Wang, M. Alam, Training neural networks using Central Force Optimization and Particle Swarm Optimization: Insights and comparisons, *Expert Syst. Appl.* 39 (2012) 555–563. doi:10.1016/j.eswa.2011.07.046.
- [16] R.C. Green, L. Wang, M. Alam, R. a. Formato, Central force optimization on a GPU: a case study in high performance metaheuristics, *J. Supercomput.* 62 (2012) 378–398. doi:10.1007/s11227-011-0725-y.
- [17] N.F. Shaikh, D.D. Doye, A Novel Iris Recognition System Based on Central Force Optimization, *Int. J. Tomogr. Simul.* 27 (2014) 23–34.
- [18] R.A. Formato, Central force optimisation: a new gradient-like metaheuristic for multidimensional search and optimisation, *Int. J. Bio-Inspired Comput.* 1 (2009) 217. doi:10.1504/IJBIC.2009.024721.
- [19] A.M. Montaser, K.R. Mahmoud, H.A. Elmikati, B15. Tri-band slotted bow-tie antenna design for RFID reader using hybrid CFO-NM algorithm, in: *2012 29th Natl. Radio Sci. Conf., IEEE*, 2012: pp. 119–126. doi:10.1109/NRSC.2012.6208515.
- [20] A.B. Abdel-Rahman, A.M. Montaser, H.A. Elmikati, Design a novel bandpass filter with microstrip resonator loaded capacitors using CFO-HC algorithm, in: *2nd Middle East Conf. Antennas Propag., IEEE*, 2012: pp. 1–6. doi:10.1109/MECAP.2012.6618188.
- [21] G.M. Qubati, N.I. Dib, Microstrip Patch Antenna Optimization Using Modified Central Force Optimization, *Prog. Electromagn. Res. B.* 21 (2010) 281–298.
- [22] R.A. Formato, Improved CFO Algorithm for Antenna Optimization, *Prog. Electromagn. Res. B*, Vol. 19, 405–425, 2010. 19 (2010) 405–425.
- [23] A. M.J., D. N.I., Design of Multilayer Microwave Broadband Absorbers Using Central Force Optimization, *Prog. Electromagn. Res. B.* 26 (2010) 101–113.

- [24] R.A. Formato, UWB Array Design Using Variable Zo Technology and Central Force Optimization, ArXiv. 0901 (2011) 1–97. <http://arxiv.org/abs/1108.0901> (accessed September 16, 2014).
- [25] R.A. Formato, A novel methodology for antenna design and optimization: Variable Zo, (2011) 1–97. <http://arxiv.org/abs/1107.1437> (accessed December 21, 2011).
- [26] R.A. Formato, Issues in Antenna Optimization - A Monopole Case Study, (2011) 1–82. <http://arxiv.org/abs/1103.5629> (accessed December 21, 2011).
- [27] R.C. Green, L. Wang, M. Alam, R.A. Formato, Central Force Optimization on a GPU: A case study in high performance metaheuristics using multiple topologies, in: 2011 IEEE Congr. Evol. Comput., IEEE, 2011: pp. 550–557. doi:10.1109/CEC.2011.5949667.
- [28] R.A. Formato, Improved CFO Algorithm for Antenna Optimization, Prog. Electromagn. Res. 19 (2010) 405–425.
- [29] X. Yang, Firefly Algorithm, Stochastic Test Functions and Design Optimisation, Int. J. Bio-Inspired Comput. 2 (2010) 78–84. <http://arxiv.org/abs/1003.1409> (accessed September 21, 2012).
- [30] X.-S. Yang, Engineering Optimization: An Introduction, 1st ed., John Wiley & Sons, New Jersey, 2010.
- [31] X. Yang, Firefly Algorithms for Multimodal Optimization, Stoch. Algorithms Found. Appl. 5792 (2010) 169–178. <http://arxiv.org/abs/1003.1466> (accessed August 17, 2012).
- [32] E. Rashedi, H. Nezamabadi-pour, S. Saryazdi, GSA: A Gravitational Search Algorithm, Inf. Sci. (Ny). 179 (2009) 2232–2248. doi:10.1016/j.ins.2009.03.004.
- [33] Z.W. Geem, J.H. Kim, G.V. Loganathan, A New Heuristic Optimization Algorithm: Harmony Search, Simulation. 76 (2001) 60–68. doi:10.1177/003754970107600201.
- [34] Z.W. Geem, State-of-the-Art in the Structure of Harmony Search Algorithm, in: Recent Adv. Harmon. Search Algorithm, Springer Berlin Heidelberg, 2010: pp. 1–11. doi:10.1007/978-3-642-04317-8_1.
- [35] Z.W. Geem, Music-Inspired Harmony Search Algorithm, 1 th, Springer, 2009.
- [36] Z.W. Geem, Novel derivative of harmony search algorithm for discrete design variables, Appl. Math. Comput. 199 (2008) 223–230. doi:10.1016/j.amc.2007.09.049.

- [37] Z.W. Geem, M. Fesanghary, J. Choi, M.P. Saka, J.C. Williams, M.T. Ayvaz, et al., Recent Advances in Harmony Search, in: *Adv. Evol. Algorithms*, InTech, 2008: pp. 127–142.
http://www.intechopen.com/books/advances_in_evolutionary_algorithms/recent_advances_in_harmony_searc.
- [38] Z.W. Geem, H. Hwangbo, Application of Harmony Search to Multi-Objective Optimization for Satellite Heat Pipe Design, (2006) 2–4.
- [39] K.S. Lee, Z.W. Geem, A new meta-heuristic algorithm for continuous engineering optimization: harmony search theory and practice, *Comput. Methods Appl. Mech. Eng.* 194 (2005) 3902–3933. doi:10.1016/j.cma.2004.09.007.
- [40] M. Aghaie, T. Nazari, a. Zolfaghari, a. Minucheher, a. Shirani, Investigation of PWR core optimization using harmony search algorithms, *Ann. Nucl. Energy.* 57 (2013) 1–15. doi:10.1016/j.anucene.2013.01.046.
- [41] O.M. Alia, R. Mandava, The Variants of the Harmony Search Algorithm: An Overview, *Artif. Intell. Rev.* 36 (2011) 49–68. doi:10.1007/s10462-010-9201-y.
- [42] J. Contreras, I. Amaya, R. Correa, An improved variant of the conventional Harmony Search algorithm, *Appl. Math. Comput.* 227 (2014) 821–830. doi:10.1016/j.amc.2013.11.050.
- [43] C. Hong, G. Xing-sheng, Multi-HM Adaptive Harmony Search Algorithm and its Application to Continuous Function Optimization, *Res. J. Appl. Sci. Eng. Technol.* 4 (2012) 100–103.
- [44] A. Kaveh, A. Nasrollahi, Engineering design optimization using a hybrid PSO and HS algorithm, *Asian J. Civ. Eng.* 14 (2013) 201–223.
- [45] I. Landa-Torres, D. Manjarres, S. Salcedo-Sanz, J. Del Ser, S. Gil-Lopez, A multi-objective grouping Harmony Search algorithm for the optimal distribution of 24-hour medical emergency units, *Expert Syst. Appl.* 40 (2013) 2343–2349. doi:10.1016/j.eswa.2012.10.051.
- [46] M. Mahdavi, M.H. Chehreghani, H. Abolhassani, R. Forsati, Novel meta-heuristic algorithms for clustering web documents, *Appl. Math. Comput.* 201 (2008) 441–451. doi:10.1016/j.amc.2007.12.058.
- [47] M. Mahdavi, M. Fesanghary, E. Damangir, An improved harmony search algorithm for solving optimization problems, *Appl. Math. Comput.* 188 (2007) 1567–1579. doi:10.1016/j.amc.2006.11.033.

- [48] K. Nekooei, M.M. Farsangi, H. Nezamabadi-Pour, K.Y. Lee, An Improved Multi-Objective Harmony Search for Optimal Placement of DGs in Distribution Systems, *IEEE Trans. Smart Grid*. 4 (2013) 557–567. doi:10.1109/TSG.2012.2237420.
- [49] C.C.O. Ramos, A.N. Souza, G. Chiachia, A.X. Falcão, J.P. Papa, A Novel Algorithm for Feature Selection Using Harmony Search and its Application for Non-Technical Losses Detection, *Comput. Electr. Eng.* 37 (2011) 886–894. doi:10.1016/j.compeleceng.2011.09.013.
- [50] S. Salcedo-Sanz, D. Manjarrés, Á. Pastor-Sánchez, J. Del Ser, J. a. Portilla-Figueras, S. Gil-López, One-way urban traffic reconfiguration using a multi-objective harmony search approach, *Expert Syst. Appl.* 40 (2013) 3341–3350. doi:10.1016/j.eswa.2012.12.043.
- [51] W. Sun, J. Wang, J. Chen, Harmony Search Based Optimization GM (1, 1) Model for Power Generation Forecasting, *Int. J. Adv. Inf. Sci. Serv. Sci.* 5 (2013) 500–506. doi:10.4156/aiss.vol5.issue4.62.
- [52] A.A. Taleizadeh, S.T.A. Niaki, F. Barzinpour, Multiple-buyer multiple-vendor multi-product multi-constraint supply chain problem with stochastic demand and variable lead-time: A harmony search algorithm, *Appl. Math. Comput.* 217 (2011) 9234–9253. doi:10.1016/j.amc.2011.04.001.
- [53] E. Valian, S. Tavakoli, S. Mohanna, An intelligent global harmony search approach to continuous optimization problems, *Appl. Math. Comput.* 232 (2014) 670–684. doi:10.1016/j.amc.2014.01.086.
- [54] R.A. Vural, U. Bozkurt, T. Yildirim, Analog active filter component selection with nature inspired metaheuristics, *AEU - Int. J. Electron. Commun.* 67 (2013) 197–205. doi:10.1016/j.aeue.2012.07.009.
- [55] H. Shah-Hosseini, Problem solving by Intelligent Water Drops, in: 2007 IEEE Congr. Evol. Comput., IEEE, Singapore, 2007: pp. 3226–3231. doi:10.1109/CEC.2007.4424885.
- [56] H. Shah-Hosseini, An approach to continuous optimization by the Intelligent Water Drops algorithm, *Procedia - Soc. Behav. Sci.* 32 (2012) 224–229. doi:10.1016/j.sbspro.2012.01.033.
- [57] J. Kennedy, R. Eberhart, Particle Swarm Optimization, in: Proc. ICNN'95 - Int. Conf. Neural Networks, IEEE, Perth, Australia, 1995: pp. 1942–1948. doi:10.1109/ICNN.1995.488968.

- [58] R. Eberhart, J. Kennedy, A new optimizer using particle swarm theory, in: MHS'95. Proc. Sixth Int. Symp. Micro Mach. Hum. Sci., IEEE, 1995: pp. 39–43. doi:10.1109/MHS.1995.494215.
- [59] I. Amaya, L.A. Gómez, R. Correa, Discrete Particle Swarm Optimization in the numerical solution of a system of linear Diophantine equations, *Dyna*. 81 (2014) 139–144.
- [60] I. Amaya, J. Cruz, R. Correa, Solution of the Mathematical Model of a Nonlinear Direct Current Circuit Using Particle Swarm Optimization, *Dyna*. 79 (2012) 77–84.
- [61] I. Amaya, J. Cruz, R. Correa, Real Roots of Nonlinear Systems of Equations Through a Metaheuristic Algorithm, *Dyna*. 78 (2011) 15–23.
- [62] O. Pérez, I. Amaya, R. Correa, Numerical solution of certain exponential and non-linear Diophantine systems of equations by using a discrete particle swarm optimization algorithm, *Appl. Math. Comput.* 225 (2013) 737–746. doi:10.1016/j.amc.2013.10.007.
- [63] J. Cruz, I. Amaya, C. Correa, Algoritmo de optimización para el cálculo de múltiples raíces de sistemas de ecuaciones no lineales, *Inge CUC*. 9 (2013) 197–208.
- [64] J. Cruz, I. Amaya, R. Correa, Solution of the mathematical model of a DC nonlinear electronic circuit using an optimization strategy: Application of the original and unified Particle Swarm Metaheuristics, in: 2012 IEEE 4th Colomb. Work. Circuits Syst., IEEE, 2012: pp. 1–6. doi:10.1109/CWCAS.2012.6404080.
- [65] C. Gómez, I. Amaya, R. Correa, An Alternative Method for the Design of Time-varying Feedback Control Systems, *Dyna*. 79 (2012) 168–174.
- [66] H. Zhu, Y. Wang, K. Wang, Y. Chen, Particle Swarm Optimization (PSO) for the constrained portfolio optimization problem, *Expert Syst. Appl.* 38 (2011) 10161–10169. doi:10.1016/j.eswa.2011.02.075.
- [67] A. Subramanian, G. Ravi, D. Arun Gopal, Loss Minimization and Voltage Profile Improvement Incorporating Multiple SVC using PSO Algorithm, *Int. J. Comput. Appl.* 46 (2012) 15–20.
- [68] H.K. Verma, C. Jain, A. Rathore, P. Gupta, A Comparative Study of GA, PSO and Big Bang-Big Crunch Optimization Techniques for Optimal Placement of SVC 's, *Int. J. Electron. Commun. Comput. Eng.* 3 (2012) 263–269.

- [69] I. Fister, X.-S. Yang, K. Ljubič, D. Fister, J. Brest, Towards the novel reasoning among particles in PSO by the use of RDF and SPARQL., *Sci. World J.* 2014 (2014) 1–10. doi:10.1155/2014/121782.
- [70] J.J. Liang, A.K. Qin, P.N. Suganthan, S. Baskar, Comprehensive learning particle swarm optimizer for global optimization of multimodal functions, *IEEE Trans. Evol. Comput.* 10 (2006) 281–295. doi:10.1109/TEVC.2005.857610.
- [71] A. Ratnaweera, S.K. Halgamuge, H.C. Watson, Self-Organizing Hierarchical Particle Swarm Optimizer With Time-Varying Acceleration Coefficients, *IEEE Trans. Evol. Comput.* 8 (2004) 240–255. doi:10.1109/TEVC.2004.826071.
- [72] J. Robinson, Y. Rahmat-Samii, Particle Swarm Optimization in Electromagnetics, *IEEE Trans. Antennas Propag.* 52 (2004) 397–407. doi:10.1109/TAP.2004.823969.
- [73] Y. Shi, R. Eberhart, A modified particle swarm optimizer, 1998 IEEE Int. Conf. Evol. Comput. Proceedings. IEEE World Congr. Comput. Intell. (Cat. No.98TH8360). (n.d.) 69–73. doi:10.1109/ICEC.1998.699146.
- [74] M. Clerc, J. Kennedy, The particle swarm - explosion, stability, and convergence in a multidimensional complex space, *IEEE Trans. Evol. Comput.* 6 (2002) 58–73. doi:10.1109/4235.985692.
- [75] J. Kennedy, R.C. Eberhart, A Discrete Binary Version of the Particle Swarm Algorithm, in: 1997 IEEE Int. Conf. Syst. Man, Cybern. Comput. Cybern. Simul., IEEE, 1997: pp. 4104–4108. doi:10.1109/ICSMC.1997.637339.
- [76] K. Han, J. Kim, Quantum-inspired evolutionary algorithm for a class of combinatorial optimization, *IEEE Trans. Evol. Comput.* 6 (2002) 580–593. doi:10.1109/TEVC.2002.804320.
- [77] S. Kirkpatrick, C.D. Gelatt, M.P. Vecchi, Optimization by Simulated Annealing, *Science* (80-.). 220 (1983) 671–680.
- [78] V. Granville, M. Kfivanek, J. Rasson, Simulated Annealing: A Proof of Convergence, 16 (1994) 652–656.
- [79] K. Tamura, K. Yasuda, Primary study of spiral dynamics inspired optimization, *IEEJ Trans. Electr. Electron. Eng.* 6 (2011) S98–S100. doi:10.1002/tee.20628.
- [80] K. Tamura, K. Yasuda, Spiral optimization -A new multipoint search method, in: 2011 IEEE Int. Conf. Syst. Man, Cybern., IEEE, 2011: pp. 1759–1764. doi:10.1109/ICSMC.2011.6083926.

- [81] L. Benasla, A. Belmadani, M. Rahli, Spiral Optimization Algorithm for solving Combined Economic and Emission Dispatch, *Int. J. Electr. Power Energy Syst.* 62 (2014) 163–174. doi:10.1016/j.ijepes.2014.04.037.
- [82] A.N.K. Nasir, M.O. Tokhi, O. Sayidmarie, R.M.T. Raja Ismail, A novel adaptive spiral dynamic algorithm for global optimization, 2013 13th UK Work. Comput. Intell. (2013) 334–341. doi:10.1109/UKCI.2013.6651325.
- [83] K.E. Parsopoulos, M.N. Vrahatis, UPSO: A unified particle swarm optimization scheme, *Lect. Ser. Comput. Comput. Sci.* 1 (2004) 868–873.
- [84] J.-M. Jin, *Fields and Waves in Rectangular Coordinates*, in: *Theory Comput. Electromagn. Fields*, John Wiley & Sons, Inc., 2010: pp. 152–199.
- [85] E. Farfán, J. Fontecha, Obtención de Las Curvas de Dispersión de Modos Híbridos para Guías de Onda de Sección Transversal Rectangular Parcialmente Llena con un Dieléctrico, Mediante Optimización por Enjambre de Partículas Unificado UPSO, Undergraduate Thesis, Universidad Industrial de Santander, 2013.
- [86] J. Suarez, J. Romero, Solución de las Ecuaciones que Describe el Comportamiento de los Modos Híbridos en una Guía de Onda Rectangular Parcialmente Llena Mediante el Método de Optimización Recocido Simulado (Simulated Annealing), Undergraduate Thesis, Universidad Industrial de Santander, 2013.